Linear and Nonlinear Components

of the

Human Multifocal Electroretinogram

in Normals and in Glaucoma

Thesis submitted by

Andrew Philip Bartholomew

Hetherington

for the degree of

Doctor of Philosophy

to

City University

Department of Optometry and Vision Science

in

December, 1998

Contents

4

Acknowledgements.

I owe an enormous debt of gratitude to Professor Geoffrey Arden and Dr Janet Wolf. Without their advice and tireless patience this thesis could not possibly have been written. I must also thank Professor Arden for critically reading the manuscript.

Mireia Pacheco-Cutillas MCOptom. assisted me in recruiting the normal subjects.

I must thank Vaegan for the DTL fibre.

A huge number of people gave up their time to sit as subjects for me, these acknowledgements would not be complete without them. Martin Bull must be particularly mentioned.

I would like to thank all the postgraduates of this department, past and present, for making my three years at City so enjoyable.

And finally, the ULCC, for so many great times.

als ich kan

Declaration.

I grant powers of discretion to the Librarian of City University to allow this thesis to be copied in whole or in part without reference to me. This permission covers only single copies made for study purposes, and is subject to the normal conditions of acknowledgement.

Thesis Abstract.

Aim.

To investigate the retinal origins of the linear and nonlinear components of the human multifocal electroretinogram.

Method.

Linear and nonlinear multifocal electroretinograms of human subjects were recorded with the VERIS system. Normal subjects (n=34) with an age range of 26-76 years were studied, and subjects with glaucoma (n=23). The temporal and spatial characteristics of VERIS responses were analysed. Comparisons were formed between VERIS responses and published data on retinal neurone densities. The affects of ageing and of primary open angle glaucoma on VERIS responses were studied.

Results.

a-Wave amplitude (linear response) shows close similarity with cone densities in the central retina, but not above 3 degrees. Temporal analysis of second order kernel slices reveals that three corneal positive components and one corneal negative component contribute to the nonlinear response. A close approximation of the nonlinear response can be achieved using Gaussian functions modelled on these four components. A further component of the nonlinear response may be extracted using the method of Sutter and Bearse (1995, 1999). The amplitude of the a- and b-waves are unaffected by ageing ($P>0.05$), except in the central retina (<1.55 degrees). The latency of the a- and b-waves increase with ageing at every eccentricity at between 0.05 and 0.10 ms/year ($P<0.05$). The amplitude of the nonlinear response is unaffected by ageing, but above 6.5 degrees the latency decreases at 0.05-0.06 ms/year. Glaucoma causes a reduction in the amplitude of a positive component of the nonlinear response ($P<0.05$) in scotomatous areas of retina only, whilst the linear response is everywhere unchanged. ROC curves indicate that VERIS is as efficient as the PERG at discriminating between scotomatous and normal retina.

Conclusions.

The a-wave contains a significant cone response, but at eccentricities>3 degrees other responses intrude. Cone function in ageing may be reduced due to impaired phagocytotic reactions. Age related changes in the nonlinear response may be associated with an achromatic component that is only present in peripheral responses and has an enhanced susceptibility to degeneration. Alterations to the outer retina in glaucoma do not register in the linear response. The nonlinear response contains a component rooted in inner retinal neurone function, but VERIS may not be capable of detecting neurone loss in glaucoma that is hidden using standard perimetric methods.

17

Introduction.

The Visually Evoked Response Imaging System is a unique approach to recording electroretinograms. VERIS is new, only seven years have passed since the algorithm on which VERIS runs was first published (Sutter, 1991). Since that time research into human visual function using VERIS has grown and VERIS is now in clinical use.

VERIS has singular attributes: it is able to simultaneously acquire the electroretinographic responses of many adjacent retinal regions, and separate the responses into their linear and nonlinear components, and do this quickly. This thesis is concerned with uncovering the retinal origins of VERIS responses, which are uncertain because a rather eccentric stimulus is employed that is dissimilar to others used in electroretinography.

A discussion of previous work on electroretinography is given in Chapter 1. The mathematics that lie behind VERIS are presented in Chapter 2, under the broader title of Signal Analysis. I have attempted to explain binary orthogonal transforms in the context of the more familiar analogue Fourier Series. To my knowledge, no other explanation puts VERIS in this context. The mathematics are not at all straightforward, I hope this approach helps. The discussion moves on to kernel analysis, an appreciation of which is vital if the rest of the thesis is to be understood.

Setting up VERIS presents some unique problems, described and discussed in Chapter 3. The solutions that I have found probably

reflect my engineering background. Several approaches are taken to investigating the retinal origins of VERIS responses, they are covered in Chapters 4 and 5. Conclusions are drawn from the temporal and spatial characteristics of VERIS responses, from comparisons between VERIS responses and published data on retinal neurone densities and from the affects of ageing and of primary open angle glaucoma on VERIS responses.

1. Anatomical and Physiological Background to the Electroretinogram.

1.1 Anatomy and Physiology of the Eye and Retina

The eye is a slightly asymmetrical sphere with an approximate sagittal diameter of 24 to 25mm and a transverse diameter of 24mm (Williams, 1995). A cross-sectional view shows three layers: The external layer is fibrous and is termed the sclera, except at its most anterior part where the layer is formed by the transparent cornea; the intermediate vascular layer is formed by the iris, the ciliary body and the choroid; the internal nervous layer is called the retina. The eye may be divided into two segments that are separated by the lens.
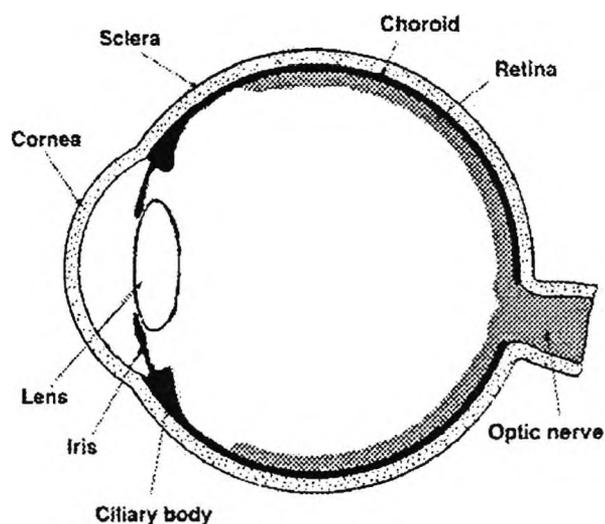
Figure 1-1 Sagittal section of the eye showing the three layers. (Kolb et al. 1997)

21

1.1.1 Macroscopic Appearance of the Retina.

The retina is the light-sensitive neural stratum of the eye. The retina is thin, being thickest (0.56mm) near the optic disk but thinner at the fovea of the macula and in the periphery. At the optic disk the retina is continuous with the optic nerve. Near the centre of the retina is an oval area called the macula lutea, which has a central depression, the fovea centralis. Many of the light-sensitive cells are concentrated in the fovea, where visual acuity is correspondingly high. There are no light-sensitive cells in the optic disk, which is therefore insensitive to light and termed the blind spot.

1.1.2 Microstructure of the Retina.

The retina contains a variety of cell types. They include light-sensitive photoreceptors (rods and cones), bipolar cells and ganglion cells. Also present are interneurons, horizontal, amacrine and interplexiform cells. The retina also contains neuroglia and a vascular system.

The retina is most clearly understood as a special part of the brain, dedicated to the detection and analysis of visual information. This account will consider the retina without the context of its central nervous connections, but the organisation of the retina must always be seen as an integral part of the much larger visual apparatus present in the thalamus, cortex and central nervous system.

1.1.2.1 Retinal laminae.

Ten retinal laminae or layers are distinguished, where distinctive components of retinal cells are clustered together to form continuous strata.   Conventionally, those laminae nearest to the choroid are termed 'outer' and the laminae positioned towards the anterior segment of the eye are termed 'inner'.   The laminae, from outermost to innermost, are:

Lamina 1: Pigment epithelium: a layer of simple, cuboidal epithelium.   The cells of the pigment epithelium contain processes (termed apical processes) that penetrate the second lamina.

Lamina 2: Rod and cone processes: photoreceptor outer segments and the outer part of the inner segments.

Lamina 3: External limiting lamina: this layer consists of junctions between Müller cells and photoreceptors.

Lamina 4: Outer nuclear layer: several tiers of rod and cone cell bodies.

Lamina 5: Outer plexiform layer: synaptic interactions occur here between the cells inhabiting the neighbouring laminae.

Lamina 6: Inner nuclear layer: a layer comprised of three nuclear strata: horizontal cell soma form the outermost zone, bipolar cell soma rest in the middle, and Müller cell nuclei, some amacrine cells and interplexiform cells, the innermost zone.

Lamina 7: Inner plexiform layer: synaptic contacts occur in the inner plexiform layer, as in lamina 5, but this lamina can be subdivided into three more strata depending on which cells are making contact: OFF bipolar, ganglion and amacrine cells in the outer, 'OFF', stratum; ON bipolar, ganglion and amacrine cells in

23

the middle, 'ON', stratum; whilst rod bipolars synapse with 'displaced' amacrine cells in the inner, 'rod', stratum.

Lamina 8: Ganglion cell layer. this layer contains not only ganglion cell bodies, but also the cell bodies of 'displaced' amacrine cells.

Lamina 9: Nerve fibre layer. the nerve fibre layer contains the unmyelinated axons of retinal ganglion cells, and the soma and processes of astrocytes which ensheath the nerve fibres.

Lamina 10: Internal limiting lamina: a glial boundary between the retina and the vitreous, formed by the end feet of Müller cells.

The thickness of the layers vary throughout the retina. Exceptionally, in the fovea, where the retina is thinnest, only the two outermost laminae are present.

1.1.3 Cells of the Retina.

1.1.3.1 Retinal pigment epithelium cells.

Retinal pigment epithelium cells carry out a range of activities vital to vision. They phagocytose discarded pieces of photoreceptor outer segment membrane. The epithelium acts as an antireflective device, reducing the amount of light that is reflected back into the photoreceptor layer. The epithelium forms an important blood-retinal barrier between the retina and the vascular system of the choroid and guards the special ionic environment of the retina (Williams, 1995).

1.1.3.2 Photoreceptors - structure.

Photoreceptor cells can be either rods or cones. Rods and cones have a similar organisation, although details differ. Both cells are long and radially orientated with a light sensitive portion, called the outer segment, that is in contact with the apical processes of the pigment epithelium at the distal end. In both cells the outer segment is linked to an inner segment by a short cilium. In the case of rod photoreceptors the inner and outer segments are thinner and more cylindrical than in the cone photoreceptor, where the segments are wider and tapered. The cell body is attached to the inner segment by direct juxtaposition in cones and by an outer fibre in rods. Rod cells make synaptic contact with adjacent cells via a rod spherule, cone cells via a cone pedicle. Spherule and pedicle are connected to cell body by a narrow process called the internal fibre. In the fovea, where the adjacent cells are displaced from the photoreceptor, the internal fibres are elongated and almost horizontally layered, and are termed the fibres of Henle. (Williams, 1995)

1.1.3.3 Photoreceptors - synaptic contacts.

Rod spherules form synaptic junctions with bipolar cells and horizontal cells and, via gap junctions, with the spherules of other rods and the pedicles of other cones. Each rod spherule synapses with one or more rod bipolar cell dendrites and two horizontal cell axons. This arrangement allows complex synaptic interactions, entailing excitatory and inhibitory influences, to occur between the three types of cell.

Cone pedicles are more complex. In the monkey there are 20-30 invaginations containing a cone ON bipolar and two flanking horizontal cell dendrites. In addition there are many synaptic contacts with cone OFF bipolar cells. Each pedicle may be connected to two midget bipolar cells and up to fifteen diffuse bipolars. Lateral interactions between cones can occur via the gap junctions between pedicles. In the fovea each cone photoreceptor may contact six to twelve pedicles, in the periphery contact is usually made between cone and rod cells. The function of cone to cone gap junctions is not well understood, but rod to cone junctions would allow rods to signal through the inhibitory cone pathway (Williams, 1995).

1.1.3.4 Photoreceptors - function and distribution.

Rod cells provide high monochrome sensitivity to light at a wide range of intensities whereas cone cells are responsible for high spatial resolution colour vision in good lighting conditions. Cone cells are all one of three types according to their maximum spectral sensitivity: red or L, green or M and Blue or S; where L, M and S refer to the wavelength, Long, Medium or Short, of the light to which they are maximally sensitive. (Wiliams 1995)

The total number of rods in the human retina has been estimated at 110-125 million and cones 6.3-6.8 million (Osterberg, 1935). In the fovea the rods are absent but the cones are at their densest. Here the cones achieve a spacing of 2-3μm, or about 147,000 cones per mm^2 (Osterberg, 1935). Cone density diminishes rapidly away from the macula, dropping to 2000-5000/mm^2 at the periphery.

26

Rods are almost the reverse of cones in their distribution, rising from zero at the fovea to a peak density of 160,000/mm^2 at an eccentricity of 10^0 then falling off to about 30,000/mm^2 in the periphery, about ten times more numerous than cones (Osterberg, 1935). This distribution accords well with the phenomena of photopic (cone) and rod (photopic) vision in different parts of the retina. S-cones are slightly larger than L- or M-cones, they form less than a fifth of the total cone population and are absent from the fovea.

1.1.3.5 Bipolar cells - rod bipolars.

Numerically, rod bipolars, bipolar cells with rod inputs, dominate bipolar cells with cone inputs, just as rod photoreceptors dominate cone photoreceptors in the human retina. Rod bipolar dendritic terminals end one to each rod spherule. In the central retina each rod bipolars contacts 15-20 rods, whereas in the periphery each rod bipolar contacts 40-50 rods. Rod bipolar axons do not contact ganglion cells directly but synapse onto amacrine AII cells. All rod bipolars are ON bipolars and so respond to a hyperpolarising rod input with a sign inverting depolarisation (Boycott and Wassle, 1991).

1.1.3.6 Bipolar cells - cone bipolars.

Cone bipolars, bipolar cells that synapse onto cone photoreceptors, can be classified into three groups: midget, blue cone and diffuse.

Midget bipolars are only seen in primates.   They are small cells with a small dendritic tree that is narrow in circumference and contacts only one L- or M-cone pedicle.   At the other pole of the cell the axon synapses with a single ganglion cell and various amacrine cells.   Midget bipolars may be either sign inverting or conserving.   Sign inverting midget bipolar cells respond to cone hyperpolarisation with a depolarising ON response, sign conserving cells respond with an OFF response; each cone will synapse with one ON and one OFF midget bipolar cell (Nelson et al. 1978). Because, at the fovea, the midget bipolar cell is part of a one-to-one channel from one cone to one ganglion cell it is thought to be part of a system that mediates high spatial resolution.

Blue (or sometimes S-cone) bipolars synapse with S-cones.   Blue cone bipolars form a unitary pathway between S-cones and S-cone ganglion cells (Kolb et al. 1997).   Blue cone bipolars are of the ON, sign inverting, variety.

Diffuse bipolar cells are larger than midget bipolars, and are connected to 5-7 bipolar cells in the central retina and 12-14 bipolar cells in the periphery, regardless of cone wavelength specificity. They are thought to signal luminosity.   Their receptive fields are larger than midget bipolar cells and consequently have lower spatial discrimination.   There are six morphologically distinct classes of diffuse bipolar cell, three of them are ON type and three are OFF type.

1.1.3.7 Horizontal cells.

Horizontal cells are inhibitory interneurons. They make synaptic contact with bipolar cells and photoreceptors at rod spherules and cone pedicles, and via gap junctions with each other. The receptive field of horizontal cells is smallest in the centre of the retina, each cell contacting 6 cones, but larger in the periphery where 46 cones may be contacted. Three types of horizontal cell may be distinguished, they are termed HI, HII and HIII. HI cells have a small, bushy dendritic fields, about 15 microns in diameter in the fovea and about 90 microns in diameter in the periphery (Polyak, 1957). HII cells have more spidery dendritic fields than HI cells. HIII cells are very similar in appearance to HI cells but are everywhere 30% bigger in dendritic field size (Kolb et al. 1992).

Horizontal cells create inhibitory surrounds: when a point of light depolarises an ON bipolar, horizontal cell dendrites cause inhibition at the edge of the illuminated area which sharpens contrast and maximises spatial resolution. Some horizontal cells appear to exhibit colour opponency so that, via feed-forward onto bipolar cells, spectrally opponent surrounds can be generated (Ammermuller and Kolb, 1995). A spot of, say, L-wave light falling onto the retina causes inhibition in the M- and S-pathways around the L-cone.

HI cells contact L- and M-cones primarily, but make some contact with some S-cones in their dendritic fields. HII cells contact S-cones with large dendrites, leaving lesser terminals to contact L- and M-cones. HIII cells make contact with L- and M-cones only,

and seemingly avoid S-cones within their dendritic fields (Ammermuller and Kolb, 1995, Kolb et al. 1992) .

1.1.3.8 Amacrine cells.

Amacrine cells serve to integrate, modulate and interpose a temporal domain to the visual message presented to the ganglion cell (Kolb et al. 1997). Amacrine cells are unique in the retina because their dendrites function as axons and dendrites, and can make incoming and outgoing synapses. Amacrine cells are classified into different types on morphological characteristics of dendritic spread and stratification within the inner plexiform layer. Many varieties of amacrine cell are monostratified, restricted to a single stratum, while others are bi- or tristratified. When an amacrine cell passes through all the strata of the inner plexiform layer it is called diffuse. The most studied amacrine cell is the AII amacrine cell, a narrow field bistratified amacrine cell. The signals coming into an AII cell are rod dominated. The receptive field of the cell is circular, rod inputs from the centre cause a depolarising ON response whereas rod inputs from the edge of the AII receptive field cause a hyperpolarising OFF response (Nelson, 1982). Rod bipolars do not make direct contact with ganglion cells, they only do so via amacrine cells. Other amacrine cells include the A2 narrow field, cone pathway amacrine cell, which may have a role in generating the antagonistic surrounds of bipolar cells (Kolb and Nelson, 1984). The A8 amacrine cell is involved, at least in the cat, in midget cone pathways (Nelson and Kolb, 1983). The A17 amacrine cell has inputs from rod cells and has a very large dendritic field. The A17 probably plays a role in converging rod

signal from large areas of the retina to amplify them at very low light intensities (Kolb et al. 1997). A19 (cone driven) and A20 (rod driven via AII amacrines) are two similar cells that are probably involved in transferring fast messages from one area of the retina to another (Freed et al. 1996). Along with A22 (a cone system amacrine cell), A19, A20 may be responsible for the proximal negative response (Burkhardt, 1970) (q.v. 1.2.8, p73).

1.1.3.9 Ganglion cells.

Ganglion cells are the final stage in the retinal signal pathway, and they relay retinal neuronal signals to neurons in the CNS. Ganglion cell bodies form a single stratum in most of the retina; exceptionally, in the macular area they are ranked about 6-8 rows deep and in the fovea they are virtually absent (Bron et al. 1997). Ganglion cells are classified into various types according to their dendritic pattern and electrophysiological reaction. Considerable species differences exist but here a description based on the primate retina will be used.

Most ganglion cells are either midget or parasol. Through the optic nerve midget cells project to the parvocellular layers of the lateral geniculate nucleus and parasol cells to the magnocellular layers, so parasol cells are sometimes termed M cells and midget cells, P cells. Both these classes of cell have subclasses: ON cells that respond to the onset of illumination in their receptive field centres and OFF cells which respond when the illumination ceases. The dendrites of ON and OFF cells spread to make contact in the

appropriate ON and OFF layers of the inner plexiform layer (refer Section 1.1.2.1).

Midget ganglion cells make contact with a single midget cone bipolar cell, they become active (ON) or inactive (OFF) when a single L or M cone is illuminated and can mediate high acuity colour vision (Polyak, 1957). Most midget ganglion cells can be divided according to their chromatic response (Gouras, 1968). Midget ganglion cells form a non-overlapping mosaic covering the retina, accounting for 80-95% of all ganglion cells (Williams, 1995).

Parasol ganglion cells are less numerous than midget ganglion cells, forming only about 10% of all ganglion cells, but are 3-5 times bigger (Polyak, 1957). They receive information from diffuse cone bipolars and, via AII amacrine cells, of rod bipolars. Parasol ganglion cells have extended receptive fields gathering inputs from many photoreceptors. Both ON and OFF parasols ganglion cells exist (Polyak, 1957).

Bistratified ganglion cells have terminals in both ON and OFF strata of the inner plexiform layer. They probably contact blue cone photoreceptors via blue cone bipolars, although they have a much larger receptive field than midget bipolars.

The axons of retinal ganglion cells converge on the optic disk and form the nerve fibre layer. From the nasal half of the retina the axons converge in a simple radial pattern. From the macula the axons pass straight to the optic disk. The fibres from ganglion cells that lie temporal to the macula swerve circumferentially above

and below the macula to reach the disk. Axons of retinal ganglion cells are unmyelinated until they reach the optic disk, an optical advantage as myelin is refractile, the myelin sheath commences as the axons enter the optic disk to become the optic nerve.

1.1.3.10 Retinal glial cells.

Müller cells are the principal glial cells of the retina. They form architectural support structures stretching radially across the thickness of the retina and forming the outer and inner limiting membranes. Müller cells are radially orientated. Their bodies are in the inner nuclear layer and project processes in both directions. Müller cell processes envelop neurons in the retina so that neurons are only allowed direct contact at their synapses. Müller cell functions include the supply of end-products of anaerobic metabolism to fuel aerobic metabolism in neurons, they absorb neuronal waste products, protect neurones from exposure to excess neurotransmitters and are involved in the control of homeostasis (particularly with respect to potassium ions). Müller cells are covered in more detail in Section 1.2.3. Two other types of glial cells exist in the retina: astrocytes and microglia. Astrocytes probably provide glucose to the neurons. Trauma transforms microglia which become macrophagic.

1.1.4 Retinal Circulation.

The retina receives its blood supply from two quite distinct sources, the blood vessels of the choroid and the branches of the central retinal artery. The central retinal artery enters the optic nerve and

travels to the optic nerve head where it divides into two equal
branches. The two branches are termed superior and inferior and
they both then bifurcate into nasal and temporal branches. Each of
these four blood vessels serves one corresponding quadrant of the
retina. Corresponding veins unite to form the central retina vein,
although the courses of the veins do not correspond exactly to that
of the arteries. The capillaries branching from the central retinal
artery do not pass beyond the outer nuclear layer and so do not
supply the photoreceptors. Photoreceptor cells must instead rely
on choroidal circulation, transmitted via retinal pigment epithelium
cells, for oxygen supply and other nutritive functions of the
circulation.
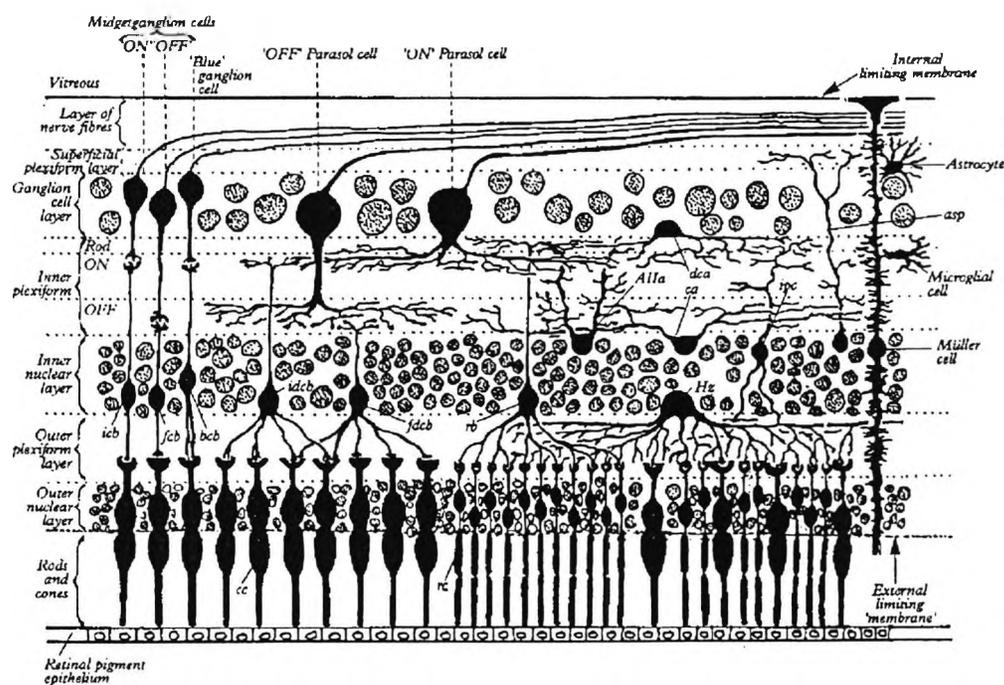
*Figure 1-2 shows the appearance, location and interconnection of many
retinal neurons. Photoreceptors are indicated by rc: rod and rb: cone;
horizontal cells by Hz; bipolar cells by rb: rod, icb: ON midget, fcb: OFF
midget, idcb: ON diffuse, fdcb: OFF diffuse, bcb: blue cone; amacrine cells by
AII: AII amacrine, ca: A17 amacrine, dca: displaced amacrine cell. (Williams,
1995).*

1.2 Components of the Electroretinogram.

When an electrode, such as a length of silver-silver chloride wire, is positioned on the corneal surface of the eye and a second (reference) electrode is placed elsewhere on the head, voltage changes between the electrodes are recorded each time the eye is stimulated with a flash of light. These voltage changes are field potentials and they represent the summed activity of whole populations of cells and cell types. The field potential recorded from the eye is called an electroretinogram (ERG). The ERG is a complex wave form consisting of three major waves and several minor ones. The first wave is a negative deflection at the cornea with respect to reference electrode and is conventionally termed the a-wave. The second, or b-, wave is a positive deflection at the cornea. In a retina dominated by rods the third wave to be seen is the c-wave, which is positive in sign. The c-wave is not usually prominent in ERGs elicited from cone dominated retinas. A prominent potential can be observed at the cessation of stimulus, called the d-wave. In rod dominated retinas the d-wave is a negative deflection, in duplex retinas the d-wave is larger, faster and more complex.

The ERG has generally been held to be the composite result of several underlying components. In view of the complex appearance of the ERG and the equally complex structure of the retina, the electrical summation of current flows differing in sign, strength and latency would offer a reasonable explanation of the ERG in terms of simpler components.

1.2.1 Granit's Analysis of the Electroretinogram.

One of the first analyses that attempted to understand the ERG in terms of its underlying components was carried out by Granit (1933). Granit observed that it is possible to resolve a complex curve, like the ERG, in many ways. He suggested splitting the curve into its components by biological means. An organ like the retina, where cells have become differentiated for specific purposes, may show selective sensitivity or resistance to certain agents. A given agent may act upon one cell type in a different manner to another and allow the response from the two types to be separated. It is only necessary to find an agent and a preparation that is stable and yet sufficiently sensitive to allow analysis.

1.2.1.1 The ERG consists of three 'processes'.

Granit found that a small amount of ether, delivered to a cat by inhalation, was sufficient to remove a positive potential from the corneal recorded ERG of about the latency and amplitude of the c-wave. The component removed in this fashion was termed Process I (PI). Granit found that at very low levels of illumination the ERG consisted of only a b-wave, and that the b-wave could be removed from the ERG by a medium dosage of ether. Granit identified a second Process, PII, which was responsible for the b-wave. The negative waveform that remained after ether had removed PI and PII was termed Process III (PIII). The a-wave seemed to be a similar shape and latency as the rising phase of PIII, so the a-wave was attributed to PIII. Yet further increase in the admitted ether had the effect of removing the ERG all-together.
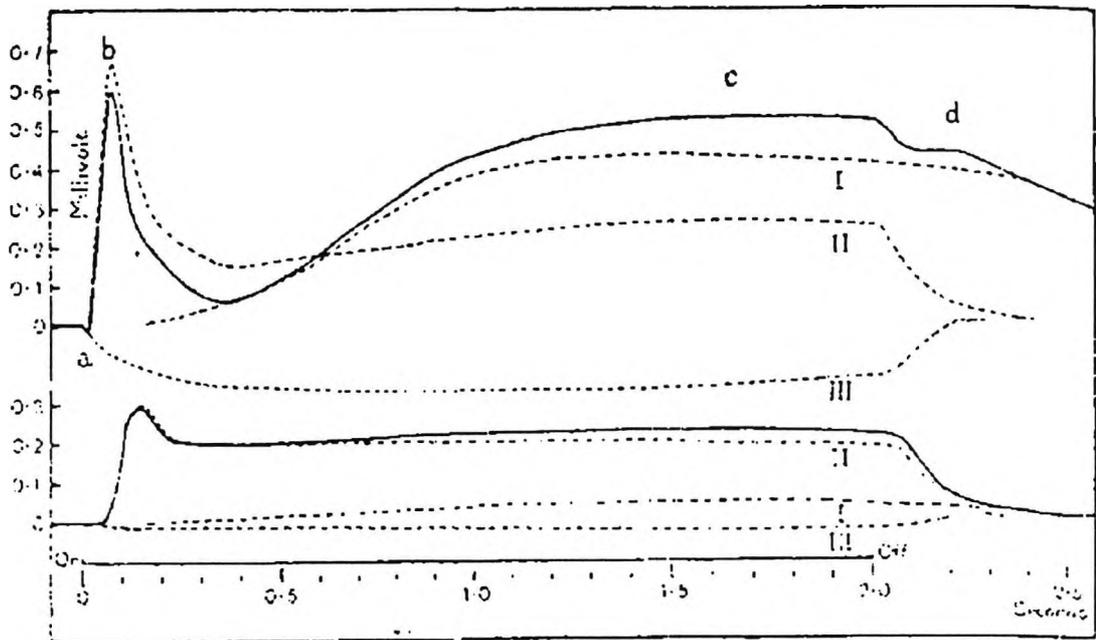
Figure 1-3   Granit's three components of the 'retinal action potential' are illustrated here as broken lines with the electroretinogram, solid lines, at two retinal intensities, 14mL (above) and 0.14mL (below).   (Granit, 1933)

1.2.2 Microelectrodes and the electroretinogram.

Granit's technique for isolating components within the ERG was limited by the ability of the agent to discriminate between cells types.   In Granit's experiments, ether could have been acting upon the cells of many structures within the retina.   Neither was it possible to know which cells were being affected.   Attention therefore concentrated on microelectrode technique, that is, on responses recorded from electrodes placed inside the retina or inside the cells themselves.   Microelectrodes offered promising new techniques for analysing the ERG and determining the origin of its components.

37

1.2.2.1 PII consists of two components.

Granit (1933) observed that reducing the incident luminance caused PII to become isolated. Using new, more sensitive recording methods Brown and Wiesel (1961a) found that stimulus intensity could be reduced sufficiently to abolish the b-wave without abolishing PII itself. The remaining component had a time course similar to a d.c. current pulse and so was termed the d.c. component. The application of xylocaine seemed to abolish the b-wave without affecting the d.c. component or the c-wave. Brown and Wiesel (1961a) concluded that the b-wave and the d.c. component are generated by different mechanisms but both contribute to PII.

1.2.2.2 The ERG as a function of depth

Microelectrodes enabled Brown and Wiesel (1961b) to study the amplitude of the ERG waves as a function of depth. An electrode was pushed into the retina until it penetrated Bruch's membrane. The electrode was then withdrawn in steps and ERG's recorded at each halt. The amplitude maxima for the a- and c-wave were found to be close to the retinal side of the pigment epithelium. The amplitude maxima of the b-wave was found to be halfway through the retina in the region of the inner nuclear layer. These results divide the ERG into responses generated at two distinctly different retinal levels.

1.2.2.3 The a- and c-wave have different origins.

There is strong evidence that the a- and c-waves are not only
generated by separate mechanisms, but arise from two different
cell types. Noell (1954) showed that sodium iodate selectively
reduces the c-wave, correlated this with selective destruction of the
pigment epithelium, and was the first to conclude that the c-wave is
generated by cells of the pigment epithelium. This was confirmed
by Yamashita (1959) and others who did not record the c-wave
when working on the isolated retinas of cold blooded animals. In
the cat, an intracellular response has been obtained which shows a
time course similar to that of the c-wave (Brown and Wiesel,
1961b). This response was only found when the microelectrode
penetrated the pigment epithelium-Bruch's membrane complex.
The response appeared in conjunction with a large d.c. shift,
presumably representing the membrane potential of a cell. It
seemed likely that this response was the c-wave which did, indeed,
arise from within the cells of the retinal pigment epithelium. In the
same experiment the a-wave appeared to have a maximum
amplitude near the retinal side of the pigment epithelium but is
readily recorded from isolated retinas. It was concluded that the a-
wave must be a response from of the photoreceptors (Brown and
Wiesel, 1961b).

1.2.2.4 PIII and the a-wave are the receptor potential.

Brown and Watanabe (1962) used two new techniques to isolate
ERG components. Firstly, they compared ERGs elicited from the
fovea of the cynomolgus monkey retina to ERGs taken from the

periphery. They reasoned that the difference in the ERG would reflect the diverging morphology of these two areas. An ERG recorded from the foveal pit should contain components generated by cone outer segments and Henle's fibres, whereas one recorded more peripherally could contain components from Müller, bipolar, horizontal, ganglon and amacrine cells. So any component generated by cells proximal to the receptors should be greatly reduced or even absent in the fovea, while components generated by the receptors themselves should be unaffected or larger. The other method was to selectively clamp the retinal circulation without affecting the choroidal circulation. Because retinal circulation extends only to the outer margin of the inner nuclear layer, and terminates sharply at that level, it has been thought that in the monkey retina the ganglion cells and the cells of the inner nuclear layer are supported primarily by retinal circulation (Polyak, 1957). Since there is no retinal circulation in the fovea it is thought that photoreceptors satisfy their metabolic demands from the choroidal circulation (Polyak, 1957). These views have been supported by the histological effect of clamping the retinal circulation, which causes severe degeneration of the ganglionic and inner nuclear layers (Noell, 1954). Clamping the retinal circulation was expected to abolish those components not generated in the receptor layer or the retinal pigment epithelium.

Recording from the peripheral retina, clamping the retinal circulation nearly abolished the b-wave. The b-wave must therefore be generated by cells proximal to the photoreceptors, as had been suspected. When recording from the fovea, clamping the retinal circulation left a pure cone receptor potential, consisting

40

of a rapid rise followed by a slight fall to a well maintained plateau that lasted until light offset. In the periphery, the response after clamping consisted of a quick rise at light onset to a level that was well maintained during stimulation but which decayed in two distinct stages at light offset. An initial rapid fall, probably due to the cones, was followed by a much slower decay, assumed to be from the rods. Brown therefore identified these waveforms as receptor potentials. The peripheral receptor potential consisted of a rapidly decaying cone response superimposed on a slowly decaying rod response. The similarity between the shape of the receptor potential and the shape of Granit's PIII identified PIII as the receptor potential.

1.2.2.5 The relationship of the electroretinogram to single, quantal events.

The relationship between the threshold of the various ERG waves and intensity was studied by Cone (1963). By measuring incident luminance in quantal units, Cone was able to deduce the relationship of the b-wave to incident light at very low luminance levels. Working on the (almost) pure rod retina of the rat, Cone found that the b-wave could be observed if at least one rod in 200 absorbed a quantum. Cone found that the near threshold response is produced by absorption of a single quanta of light in a small proportion of rods. The b-wave threshold occurs when enough rods absorb one quantum each to produce a b-wave comparable to the background noise. The relationship between b-wave amplitude and luminance stays linear until about one rod in

41

20 in excited, when the amplitude becomes proportional to the log of the luminance as it is at higher intensities.

As the b-wave becomes non-linear at an intensity where only a small proportion of the rods absorb even one quanta and never more than one, the source of the b-wave must be a cell which monitors a large group of rods. Cone excluded the photoreceptors as a source of the b-wave and suggested the cells of the inner nuclear layer as possible candidates. If the source of the b-wave was the bipolar cell then Cone's electrophysiological data could be able to predict the number of rod cells that synapse on each bipolar cell. Cone suggested 7 to 10 rods per bipolar cell (based on a simple model) which compared favourably with histological studies that have suggested that each bipolar cells monitors around 4 to 12 rods.

Ashmore and Falk extended this analysis by measuring the absolute sensitivity of bipolar cells in the almost pure rod retina of the dogfish, *Scyliorhinus canicula* (1976). Ashmore and Falk found that the dynamic voltage gain, measured as the ratio of flash sensitivity in the bipolar cell to the flash sensitivity in rods, was about 50. Ashmore and Falk assumed that the bipolar cell linearly summed the transmitter-modulated conductance increments contributed by the pre-synaptic cells. They also observed that the contribution may not depend explicitly on rod-bipolar cell convergence if the fractional contribution by each pre-synaptic cell is not equal. This situation might arise if the pre-synaptic cells were not composed exclusively of rods but included, for example, horizontal cells.

42

1.2.2.6 The early receptor potential.

Brown and Murakami (1964) have shown that with a very bright flash of very short (~20μs) duration a small wave can be seen which precedes the a-wave. Initially this wave could only be seen by intraretinal recording, but was soon seen in corneal recordings too. The wave was recorded from cynomolgus monkey but not from the night monkey or the cat. This suggested that the new response was more readily recorded from cone than from rod photoreceptors. The new potential was clearly a receptor potential as it was developed in the same part of the retina as PIII. Brown and Murakami termed the new potential the early receptor potential and re-designated the receptor potential as the late receptor potential (see Figure 1-4). The early receptor potential had no latency and proved to be very resistant to anoxia. Hodgkin and O'Bryan (1977) have shown that the early receptor potential was triggered by isomerisation of the photopigment and generated in the conduction mechanism which carries activity from the outer receptor segment to the terminal of the receptor.

Figure 1-4   Time course of the early RP (early receptor potential) and late RP (a-wave) at two different sweep speeds. (Brown and Murakami, 1964)

43
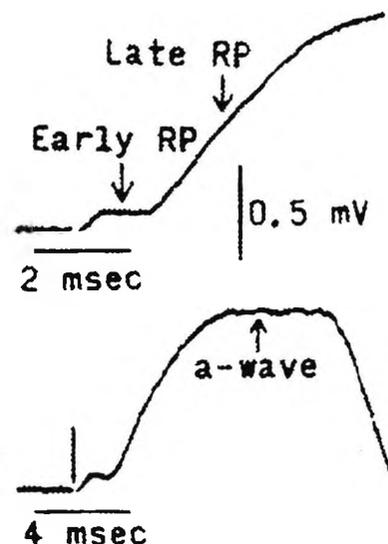
1.2.2.7 Electroretinogram components are generated by dipoles.

It has been proposed that the components of the electroretinogram must be generated by a dipole that is radially orientated through the retina. This would create a polarity inversion between distal and proximal ends of the retina. In the case of the photoreceptors, a polarity inversion has been recorded by many observers (see, for example, Murakami and Kaneko (1966)), as the a-wave is negative then the negative pole of the photoreceptor dipole must be closer to the retinal surface than the positive end.

The locally recorded b-wave has also been shown to invert polarity as the retina is penetrated. Since the b-wave is positive when recorded by conventional methods the positive dipole must be in the proximal retina and the negative end in the distal retina. However, possibly because the proximal end of the dipole is so close to the vitreous humour, the dipole has been hard to detect. Arden and Brown (1965) replaced the vitreous humour in the cat eye with heavy oil, which sank and became closely apposed to the retinal surface. An electrode was then inserted and because oil is non-conducting all the responses recorded were local responses, any current generated at remote sites could not flow to the site of the microelectrode. It was then found that the (local) b-wave did invert polarity during penetration. The maximum negativity was recorded at the outer margin of the inner nuclear layer and the maximum positivity was recorded at the inner margin of the inner plexiform layer. These findings indicated that the cells which generate the b-wave must be radially orientated through the retina, and must extend from the outer margin of the inner nuclear layer to

the inner margin of the inner plexiform layer.   Bipolar cells are the only cells to possess these two characteristics, so Arden and Brown suggested that bipolar cells were the source of the b-wave.
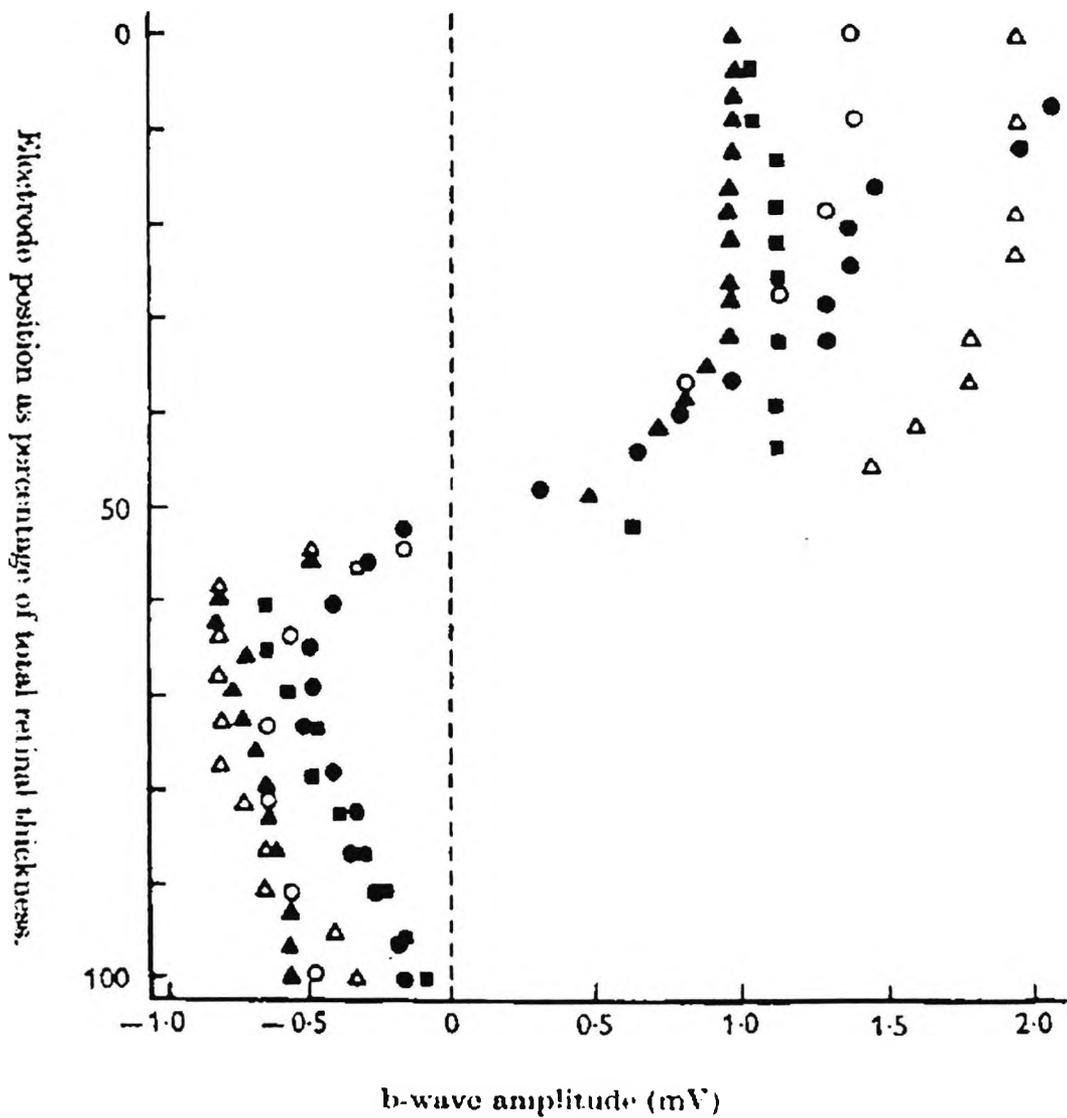
Figure 1-5   Amplitude of the b-wave as a function of retinal electrode depth. Five separate electrode penetrations are presented.   The presence of a dipole is clearly indicated by the inversion in polarity of the response.   (Arden and Brown, 1965)

1.2.3 Müller cell responses and the electroretinogram.

Miller and Dowling (1970) studied the light-response of the neurones in the mudpuppy retina in an attempt to locate the source of the b-wave.   Miller and Dowling found that all the neurones in the retina responded faster than the b-wave.   Miller and Dowling then recorded intra-cellular responses from the Müller cell.

1.2.3.1 The Müller cell response.

Miller and Dowling found that Müller cells produced a depolarisation in response to light.   Miller and Dowling claimed that the Müller cell response was similar to the b-wave, although in fact the Müller cell response at high intensities were sustained whereas the b-wave response were not.   Müller cells proved to have no centre-surround organisation and had a much larger receptive field than the bipolar cell.   Müller cells had no 'a-wave' type response.   Müller cell responses were recorded from nearly all retinal depths and electron micrographs confirmed that mudpuppy Müller cells span the retina from ganglion cell layer to outer nuclear layer.

1.2.3.2 The spatial properties of extracellular currents.

The spatial properties of Müller cells and Müller cell responses led to interest in the distribution of extracellular currents within the retina.   Faber ((1969), cited by (Dowling, 1987)) carried out a second spatial derivative analyses of the voltage depth profile corrected for variation in retinal resistance.   From these data Faber was able to plot the distribution of sources and sinks of extracellular

b-wave currents in the rabbit retina. Faber concluded that the main sink for the b-wave current lies in the outer plexiform layer, but that the current sources were both distal and proximal to that site. The proximal source extended all the way to the inner limiting membrane.

1.2.3.3 The spatial properties of $[K^+]_o$ sources and sinks.

Several laboratories (Dick and Miller, 1978; Kline et al. 1978; Karwoski and Proenza, 1982) have studied the distribution of $[K^+]_o$ within the retina using K^+ specific electrodes. It appears that the locations of the two current sinks correspond closely to the locations of light evoked $[K^+]_o$ increases, with one increase located in the outer plexiform layer and a second in the distal part of the inner plexiform layer. The two $[K^+]_o$ increases have distinct time courses and these too mimic the time courses of the b-wave current sources found by Faber (1969). The outer plexiform increase is more transient whereas the inner plexiform increase is sustained.

Newman (1980) suggested that the Müller cells are responsible for the flow of $[K^+]_o$ within the retina. He proposed a model in which the Müller cells buffer the light induced fluctuations in extracellular K^+. Light induced increases in K^+ in the outer plexiform layer and inner plexiform layer cause currents to flow into the Müller cell in these regions. Most of this current then exits from the highly permeable end-foot region of the Müller cell at the inner limiting membrane. Newman believed that the dipole created by a current flowing through the Müller cells was responsible for the b-wave.

47

1.2.3.4 Müller cell responses do not cause the b-wave.

Arden and Brown's study (1965) had not found the large b-wave current source at the retinal surface that Newman's thesis would imply. Furthermore, Xu and Karwoski (1994a; 1994b) have shown that Ba^{2+} ions do not abolish the b-wave even though they are known to block the K^+ channels in Müller cells. Hanitzsch et al. (1996) have found that $MgCl_2$ nearly abolishes the b-wave but actually enlarges the distal light-induced $[K^+]_o$ increase. The light induced transretinal $[K^+]_o$ fluxes do not correlate with the b-wave and so Müller cells cannot be a major contributor to the ERG b-wave.

1.2.4 Vertebrate photoreceptors and the electroretinogram.

1.2.4.1 Cone photoreceptor response in the carp.

The first convincing intracellular recordings from vertebrate photoreceptors were obtained by Tomita (1967; 1970). Working on the cone dominated retina of the carp, the technique involved jolting the retina at very high acceleration towards an advancing micropipette-electrode. When the micropipette had penetrated a photoreceptor membrane the response to a light input was recorded. He made the finding that when the cell was illuminated, it hyperpolarised, making the cell membrane potential more negative. When the wavelength of the incident light was scanned through the visible spectrum, Tomita observed that the response from the penetrated cone photoreceptor could be observed to fall

48

into anyone of three distinct classes. The most commonly observed response had a peak amplitude of response at 611nm. This so-called R-type response counted for three quarters of the cones penetrated and was therefor supposed to be the most populous cone type in the carp retina. The next most common cone type had a B-type response, with a peak at 462nm. The G-type cone, 529nm, had the smallest population.

1.2.4.2 Rod photoreceptor response in Gekko gekko.

Gekko have large rods that are suitable for micropipette recording, Toyoda (1969) studied their response in isolated retina. Successful penetration of photoreceptor outer segments was achieved using Tomita's jolting technique. Location of the pipette tip was confirmed using dye marking, and dye was found in the outer segments of receptors and not the inner segments. The sign of the response to light was always identical to that found by Tomita in the carp, a hyperpolarisation.

1.2.4.3 Hyperpolarisation and membrane resistance.

The question these results posed was whether the hyperpolarisation is related to an increase or a decrease in the cell membrane resistance. To resolve this issue Toyoda (1969) measured the change in membrane resistance before, during and after light stimuli using a Wheatstone bridge. A train of square current pulses was injected through a current limiter (resistance) and a micropipette electrode into the cell outer segment. This current was balanced with another train of square wave pulses of

opposite polarity and variable amplitude that were applied to a reference electrode, sited on the retina outer margin, through a second current limiter. Toyoda observed that the onset of illumination caused a bridge imbalance that indicated a rise in membrane resistance. The increase in membrane resistance depended on light intensity, becoming larger as intensity was increased. Toyoda then applied an extrinsic hyperpolarising current to the cell. The effect of such a current on the membrane resistance was compared with the resistance increase due to illumination. The passive change in membrane potential caused by the current did not change the bridge balance. However a considerable imbalance was caused by light even when the potential changed had been reduced by the concurrent extrinsic current. This clearly showed that the increase in membrane resistance caused by exposure to light is not a secondary effect of the hyperpolarisation, but a phenomenon directly related to the membrane process that caused hyperpolarisation.

1.2.4.4 The ionic mechanisms of the receptor potential.

It still remained to be shown how the membrane potential is altered by light incident on the photoreceptors. Toyoda (1969) suggested that membrane resistance changed in light because the movement of ions which occur in darkness was suppressed. The increase in membrane resistance might be due to an influx of cations or an efflux of anions. Exactly which ions were involved, was the purpose of Sillman's study (Sillman et al. 1969).

1.2.4.5 Sodium, potassium and chloride ions and the receptor potential.

Working on isolated frog retinas, Sillman isolated the receptor potential by applying aspartate to the retina to abolish all post-synaptic responses.   Replacing the sodium in the extracellular fluid with lithium resulted in the disappearance of the receptor potential. The effect was reversible, if the lithium was replaced with sodium then the receptor potential returned.   Apparently the lithium had no toxic effect.   Sillman tried using a range of sodium concentrations and found that the amplitude of the receptor potential increased in direct proportion to the logarithm of the sodium concentration. Sillman concluded that the photocurrent was carried by sodium.

1.2.4.6 The dark current and the photocurrent.

Hagins, et al. (1970) studied the interstitial voltages, currents and resistances of the receptor layer of the isolated rat retina with arrays of micropipette electrodes inserted under direct visual observation by infrared microscopy.   In a source-sink analysis they established the existence of a dark current within the extracellular space. Hagins et al. found that in darkness a steady current flowed into the rod outer segment.   It was balanced by an equal outward flow of current along the remainder of the rod.   The sign of the dark current underwent a sharp transition at the inner-segment/outer-segment junction.   Penn and Hagins (1972) showed that flashes of light brought about a transient reduction in the dark current.   The photocurrent had a waveform that resembled PIII and the a-wave.

51

Penn and Hagins suggested that that the photocurrent was the suppression of the dark-current. Lamb et al. confirmed the findings of Hagins et al. (1970) when they showed that the outer segment plasma membrane is the site of photocurrent initiation: local outer segment illumination causes local photocurrents.

Figure 1-6 The dark current in a schematic diagram of a rod. Light activated rhdopsin Rh* closes Na+ channels and decreases the flow of Na+. (Lamb, 1996)
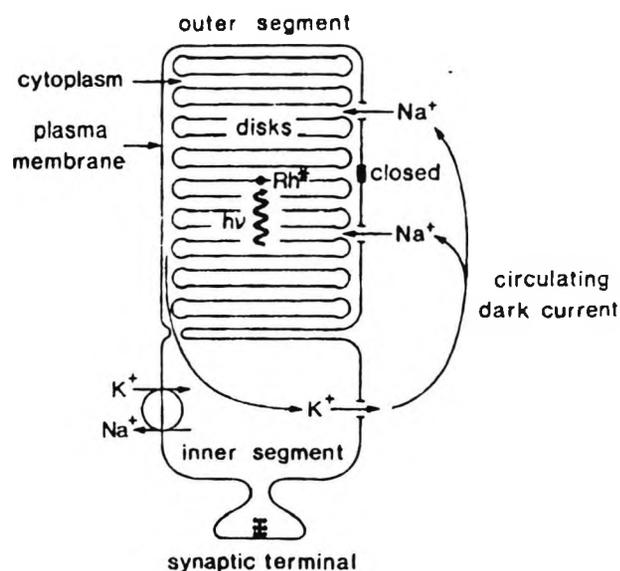
1.2.4.7 Modelling the rod photoresponse.

Fuortes and Hodgkin (1964) had suggested that the photoresponse at low flash intensities could be approximated by the output of a chain of low-pass filters. At low intensities Penn and Hagins (1972) found that four cascaded, low-pass filters produced the best fit with experimentally recorded data. The time to peak response, t_p, was linked with the number of filters in the cascade by $t_p=\tau(n-1)$, where n is the number of filters and τ is the time constant of the filters. Penn and Hagins suggested that four filters would accurately model the time course of the response.

At flash intensities above 30 photons absorbed per rod the peak amplitude becomes less than would be calculated by the simple proportionality indicated by the low-pass filter cascade. For the response at high intensities Penn and Hagins suggested that a hyperbolic, amplitude-limiting function of the form:

$$R(t) = \frac{I}{I + K_a} R_{max}$$

Equation 1-1

should be included, where I is intensity and K_a is the value of I when $R(t) = R_{max}/2$. Naka and Rushton (1967) had already suggested an equation of this form for modelling S-potentials in fish.

Baylor et al. (1984) also proposed a two-phase model. The kinetics of the response was modelled with the impulse response of a Poisson filter, as suggested by Baylor et al. (1974) and Fuortes and Hodgkin (1964). It took the form

$$r^*(t) = \left[(t/t_p) \cdot e^{(1-(t/t_p))} \right]^{(n-1)}$$

Equation 1-2

where $r^*(t)$ is the impulse response of the rod and t is the instantaneous time, t_p is the time to peak response, n is the number of stages in the filter which Baylor et al. suggested was 6.

Baylor et al. modelled the dependence of rod response amplitude on intensity of light input with a saturating exponential function, as suggested by Lamb et al. (1981):

$$R(t) = \left[1 - e^{-I(\ln 2/k_a)}\right] R_{max}$$

where I is intensity and K_a=I when response R at time t is R_{max}, half the saturated value of R at peak amplitude, as before.

Using either of these equations the rod response can be summarised in terms of n, R_{max}, K_a and t_p. Both models yield very similar results (Hood and Birch, 1990a). Baylor et al. found K_a=20-40 isomerisations(i)/rod/flash whilst Penn and Hagins found K_a=30-50 i/rod/flash. Baylor et al. found t_p=190msec to Penn and Hagins' t_p=173msec. The difference in time course is related to the different number of stages in the filter models used by the two groups.

1.2.4.8 Rhodopsin and the second messenger.

The stack of disk membranes in the rod outer segment contain the photo-sensitive protein rhodopsin (Rh). But the response of a cell to illumination is the reduction of the circulating dark current and this is brought about by the closure of Na^+ selective ions channels in the plasma membrane. Baylor and Fuortes (1970) proposed that light led to the release into the cytoplasm of a substance that closed membrane channels. In the rod photoreceptor the disk and the plasma membrane are completely separate from each other,

and hence the diffusion of a messenger substance across the intervening region must be postulated. Baylor, Hodgkin and Lamb (1974) found quantitative evidence for a messenger that was produced in direct proportion to light intensity and suggested that this messenger blocks ion channels in the outer segment.

1.2.4.9 Calcium is not the second messenger.

The hypothesis that calcium is the internal messenger was proposed by Yoshikami and Hagins (1970). A solid role for proposing calcium existed at the time: it was believed to play a key role as an intracellular messenger in muscle; it was believed to be the signalling agent responsible for triggering synaptic vessel fusion; it was thought to play the role of internal messenger in a variety of cellular processes. Evidence accumulated that calcium was the second messenger in vertebrate rod transduction. Changes in external calcium and light have similar affects on the dark current; the affects of altered external calcium on photovoltages are consistent with the notion that the immediate effect of altered external calcium is on membrane conductance; the affects of external calcium on the dark current are greatly enhanced by agents that increase the action of calcium inside the outer segment; injection of calcium hyperpolarises the rod membrane; infusion of calcium decreases the light sensitivity of rods; light causes an increase in extracellular calcium which graded with light intensity and follow photocurrent kinetics (Pugh and Cobbs, 1986).

However, more recent reports have refuted the calcium hypothesis. Infusion of calcium into isolated rods does not increase light sensitivity and free calcium in the outer segment actually decreases during light response; there is no observable change in the conductance of excised membrane patches that is exclusively gated by calcium (Pugh and Cobbs, 1986). It would appear that although calcium has a role to play in phototransduction it is not operating as a second messenger.

1.2.4.10 The role of cyclic GMP.

Fesenko found that cyclic GMP directly opens channels in the outer segment of rod photoreceptors (Fesenko et al. 1985). A piece of outer segment membrane was removed using the patch-clamp method. The current carried by various cations and anions passing through the channels in the patch was measured when the intracellular surface was exposed to calcium and cyclic GMP. Fesenko was able to show that the channels affected by cyclic GMP were selective to cations, and more selective to sodium than any other, whilst calcium was inaffective. He postulated that when light strikes the outer segment cation-specific channels in the membrane are closed. It followed that light must be causing the cyclic GMP levels in the outer segment to fall and that cyclic GMP must be the second messenger.

1.2.4.11 The transduction cascade.

The transduction cascade, a cascade of reactions that leads from the activation of Rhodopsin in the disks by light to the closure of

sodium channels in the plasma membrane, has now been established. The transduction cascade has been variously reviewed (Pugh and Cobbs, 1986; Lamb, 1986; Stryer, 1986) and is summarised here.

Rhodopsin (Rh), a pro-enzyme, is photo-isomerized to an active form Rh* by light. Rh* diffuses laterally in the disk membrane until it contacts a second protein, a trimer, variously called T, the G-protein or transducin. T becomes able to exchange GDP for GTP and Rh* then dissociates into $T\alpha$ and $T\beta\gamma$, and is free to interact with further molecules of T until it becomes inactivated. Activated T (T_αGTP) switches on phosphodiesterase, PDE, by overcoming an inhibitory constraint. Phosphodiesterase quickly allows the hydrolysis of cytoplasmic cyclic GMP. In darkness the total concentration of cyclic GMP in the outer segment is about 70μM but most of this is bound and the affective concentration is about 5-10μM (Lamb, 1986). At this concentration cyclic GMP holds the plasma membrane channels open, permitting the dark current of mainly Na^+ plus a small fraction of calcium ions to enter and depolarise the cell. The hydrolysis of cyclic GMP in the light channels to close, reducing the circulating current and thereby hyperpolarising the cell.
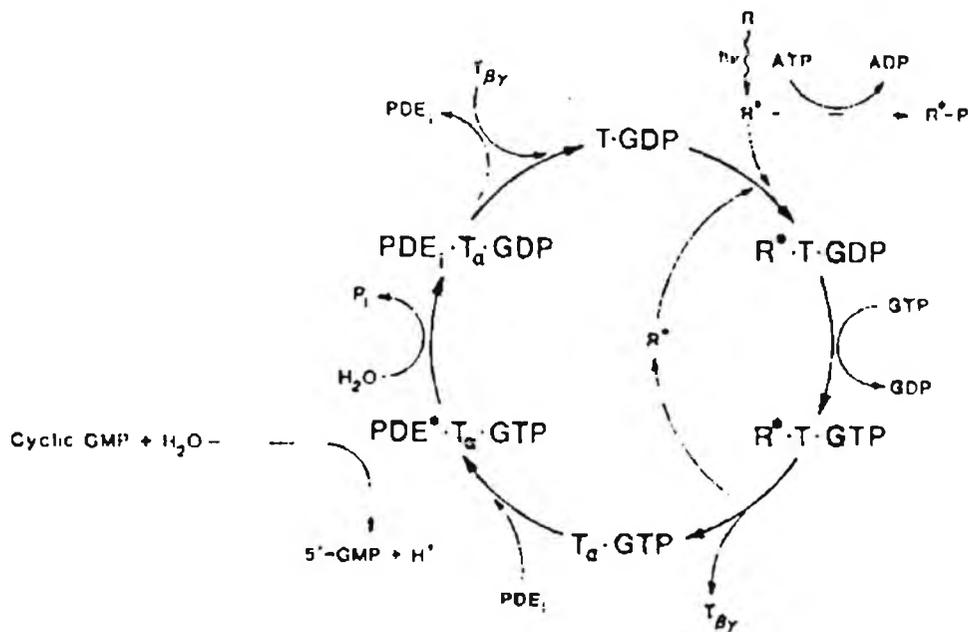
Figure 1-7   Light activated transducin cycle - the phototransduction cascade.
(Stryer, 1986)

This cascade of reactions acts to amplify the charge separation caused by each quanta of light.   One photopigment molecule can activate 500 transducin molecules and each transducin, 100 phosphodiesterase molecules.   Each phosphodiesterase molecule can hydrolysise 2,000 cyclic GMP molecules.   Amplification is of the order of 10^6 to 10^8.   The absorption of one quanta of light will cause the closure of many Na^+ channels and a significant reduction of Na^+ current across the cell membrane.

1.2.4.12 Phototransduction as a model of the rod photoreceptor response.

Attention has concentrated on explicitly modelling the activation steps of the G-protein cascade.   The two stage model, as laid out by either Penn and Hagins (1972) or Baylor et al. (1984), is not a model of the biophysical processes that are at work during

58

phototransduction.   There is no physical basis for the parameters R_{max}, K_a, t_p and n and so it is harder to associate a change in one of the parameters with a change in the physiological function of the photoreceptors. Lamb and Pugh (1992) have shown that each of the five steps in the G-protein cascade of rod photoreceptors can be predicted:

Activation step	Variable	Modelled as
Rh* production	Rh*(t)	$Rh^*(t) = \Phi\left[1 - \exp\left(-t/t_R\right)\right], \quad t > t_R$
G* production	G*(t)	$G^*(t) = \Phi v_{RG}\left(t - t_{RG}\right), \quad t > t_{RG}$
PDE* production	PDE*(t)	$PDE^*(t) = \Phi v_{RP}\left(t - t_{RGP}\right), \quad t > t_{RGP}$
cGMP hydrolysis	cG(t)	$\dfrac{cG(t)}{cG_{dark}} = \exp\left[-1/2\,\Phi\beta_{sub}\left(t - t_{RGP}\right)^2\right], \quad t > t_{RGP}$
cGMP channel closure	F(t)	$F(t) = \left[\dfrac{cG(t)}{cG_{dark}}\right]^n = e\left[-\dfrac{1}{2}\Phi A\left(t - t_{eff}\right)^2\right], \quad t > t_{eff}$

where

Φ = number of photoisomerisations

$_R$ = delay in production of Rh*   (s)

$t_{RG} = t_R$ + delay in production of G*   (s)

$t_{RGP} = t_{RG}$ + delay in production of PDE*   (s)

t_{eff} = total affective time delay (see below)   (s)

v_{RG} = rate of production of G* by a single Rh*   (s^{-1})

v_{RP} = rate of production of PDE* by a single Rh*   (s^{-1})

β_{sub} = rate constant of a single catalytic subunit of PDE (s^{-1})

A = amplification constant

F(t) is the fraction of circulating current (dark current) as a function of time.   The normalised rod photoresponse is R(t)=1-F(t)   The

model describes the photo response in terms of the number of photoisomerisations and two composite parameters of transduction: an amplification constant and a time delay. The affective time delay is the delay in phototransduction and represents the sum of the delays t_R, t_{RG} and t_{RGP} together with delays associated with the rate of diffusion of cGMP and the closure time of the channel.

Breton et al. (1994) used Lamb and Pugh's analysis to model the rod a-wave. Their model assumed that the normalised rod a-wave, $a(t)/a_{max}$, is equal to the normalised rod photo response, $R(t)$. So now:

$$1 - \left[\frac{a(t)}{a_{max}} \right] = F(t) = \exp\left[-\frac{1}{2} \Phi A(t - t_{eff})^2 \right]$$

Equation 1-4

This equation proved to be a good fit to experimentally recorded dark-adapted (rod driven) ERGs. The equation predicts that each member of the family of responses $1-[a(t)/a_{max}]$ should trace out a delayed gaussian function of time (see Figure 1-8). Breton et al. found that the parameter A was constant up to $\Phi \approx 30,000$ photoisomerisations per rod and that t_{eff} in human rods did not exceed 1 ms.

Figure 1-8   Normalised a-wave responses (thick lines) show a good fit to the gaussian function given in Equation 1-4 (dotted lines) (Breton et al. 1994).

60
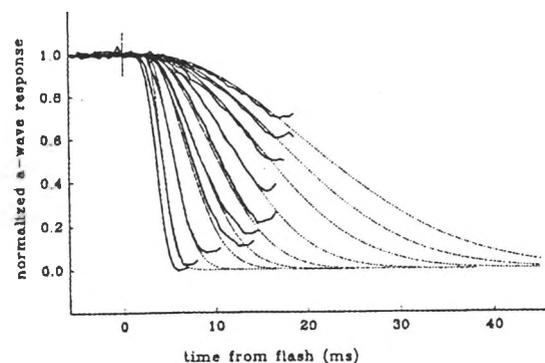
1.2.5 Bipolar cells and the electroretinogram.

The b-wave was associated with bipolar cell activity by Arden and
Brown (1965).   Bipolar cells can be either ON (depolarising) or
OFF (hyperpolarising).   The relative population of each type of
bipolar cell will depend on whether the retina is, in Granit's
terminology, E-type or I-type.   Excitatory, E-type, retinas have only
ON bipolar cells and rod photoreceptors (Smith et al. 1986;
Dacheux and Raviola, 1986).   Inhibitory, I-type, retinas have ON
and OFF bipolar cells and cone photoreceptors (Evers and Gouras,
1986).   I-type retinas exhibit a d-wave.   I-type retinas may have
ON and OFF bipolar cells for all the cone systems present (Smith III
et al. 1989) or only some (Evers and Gouras, 1986).   Most retinas
are duplex showing some mixture of both rod and cone activity and
consequently combine both E- and I- type ERGs.   In duplex retinas
it is possible to separate E- and I-type responses by using stimuli
that favour either rod or cone responses.   Rod responses can be
emphasised by dark-adapting the retina and using dim stimuli that
minimally excite cone photoreceptors.   Cone responses can be
emphasised by light adapted the retina and by using rapidly
alternating sinusoidal (or square-wave) stimuli that minimally excite
rod photoreceptors (Bush and Sieving, 1996).

1.2.5.1 The isolation of classes of cells with pharmacological agents.

Specific neurotransmitter agonists and antagonists have highly
selective affects on specific classes of retinal neurons.   Use of
these drugs serially or in combination permits a differential analysis

of the neuronal basis of ERG generation. APB (2-amino-4-phosphonobutyrate) selectively blocks the light responsiveness of ON bipolar cells while leaving horizontal and OFF bipolar cell responses undiminished (Slaughter and Miller, 1981). PDA (*cis* 2,3-piperidine-dicarboxylic acid) (Slaughter and Miller, 1983a; Slaughter and Miller, 1985) and KYN (kynurenic acid) (Coleman et al. 1986) strongly suppress synaptic transmission from photoreceptors to horizontal and OFF bipolar cells and all transmissions to third order neurons although they do not diminish the response of the ON bipolars. GLY (glycine) suppress the light response of third order neurones by causing them to hyperpolarise (Miller et al. 1981). NMA (*N*-methyl-DL-aspartate, sometimes NMDLA) strongly suppresses the light response of third order neurones by a depolarising block (Slaughter and Miller, 1983b).

Figure 1-9 Summary diagram in which the elimination of cellular light responses by a drug is portrayed by shading the affected elements of the retinal network. (Stockton and Slaughter, 1989)

62
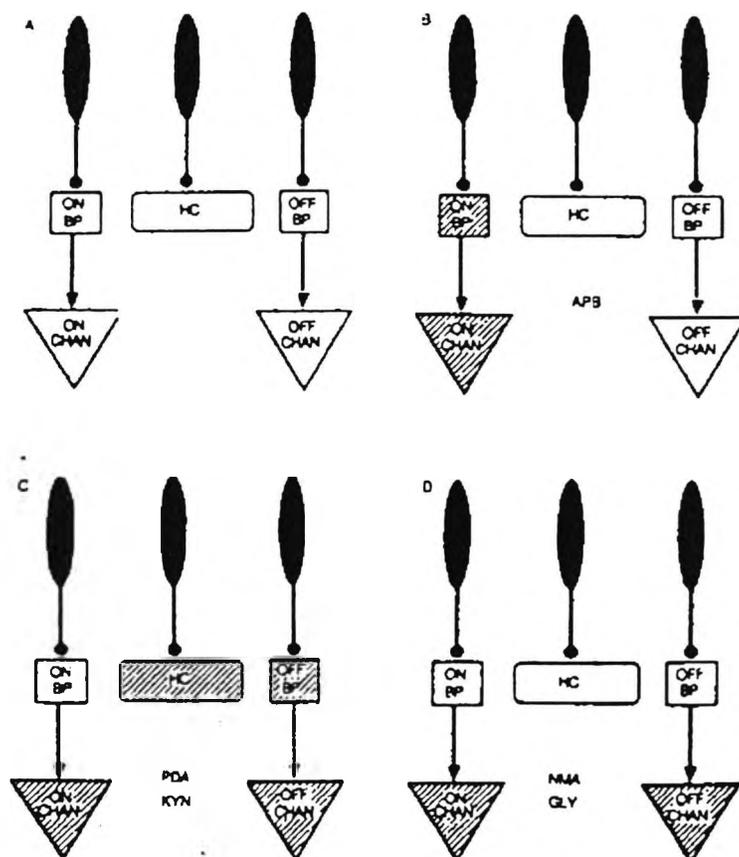
1.2.5.2 ON bipolar cell activity causes the b-wave.

APB blocks the b-wave in the E-type retina of the rabbit and the I-type response of the light adapted macaque monkey retina (Knapp and Schiller, 1984). The I-type retina of the mudpuppy and the tiger salamander also loose their b-wave after application of APB (Stockton and Slaughter, 1989). The b-wave can be isolated from the ERG by subtracting responses before and after APB. In tiger salamander I-type retina, the isolated b-wave is similar in form to the waveform of the ON bipolar neuron (Gurevitch and Slaughter, 1993), and can be correlated dynamically to the ON bipolar neuron response (Tian and Slaughter, 1995). These results indicate that in retinas with or without OFF bipolar cells the b-wave is caused by ON bipolar cell depolarisation.

1.2.5.3 OFF bipolar cell activity causes the d-wave.

The d-wave (off response) of I-type retinas was not abolished by APB in primates (Knapp and Schiller, 1984) or amphibia (Stockton and Slaughter, 1989). The d-wave was abolished by PDA and KYN in amphibia (Stockton and Slaughter, 1989). The d-wave would appear to derive from OFF bipolar cell activity.

1.2.5.4 The d-wave as a diagnostic tool.

Sieving (1993) has shown that the OFF-response can be used as a diagnostic tool. Using long (150ms) stimulus flashes Sieving separated the ON from the OFF responses. Sieving found that some clinical conditions resembled the ERGs recorded in monkeys

after the ON or OFF pathway had been blocked with KYN. Patients with cone or cone-rod dystrophies had abnormal OFF responses whereas those with rod-cone dystrophies did not. Sieving suggested that cone and cone-rod dystrophy was caused by a defect in the cone OFF pathway.

1.2.5.5 A contribution to the b-wave from OFF bipolar cells and horizontal cells.

Working on the I-type response of light adapted primate retinas, Sieving et al. (1994) isolated the ON bipolar cell response by subtracting the ERG response after application of APB from a response recorded immediately before. The ON bipolar cell response consisted of a rapid rise at light onset followed by a fall to a plateau that is maintained during the light flash and a second fall to baseline at light offset (C1 in Figure 1-10). But if OFF bipolar/horizontal cell responses had already been suppressed with a combination of PDA and KYN then the difference in response before and after the application of APB was very different, consisting of a very rapid rise at light onset followed by a maintained plateau for the duration of the light flash and a rapid fall at light offset (D2 in Figure 1-10). As the two ON bipolar cell responses were different it was clear that the presence of OFF bipolar/horizontal cells activity critically affected the contribution of ON bipolar cells to the ERG. Sieving et al. proposed a push-pull model in which ON bipolar cells are required for b-wave production but that OFF bipolar and horizontal cell activity limits amplitude and controls the shape of the b-wave.

64
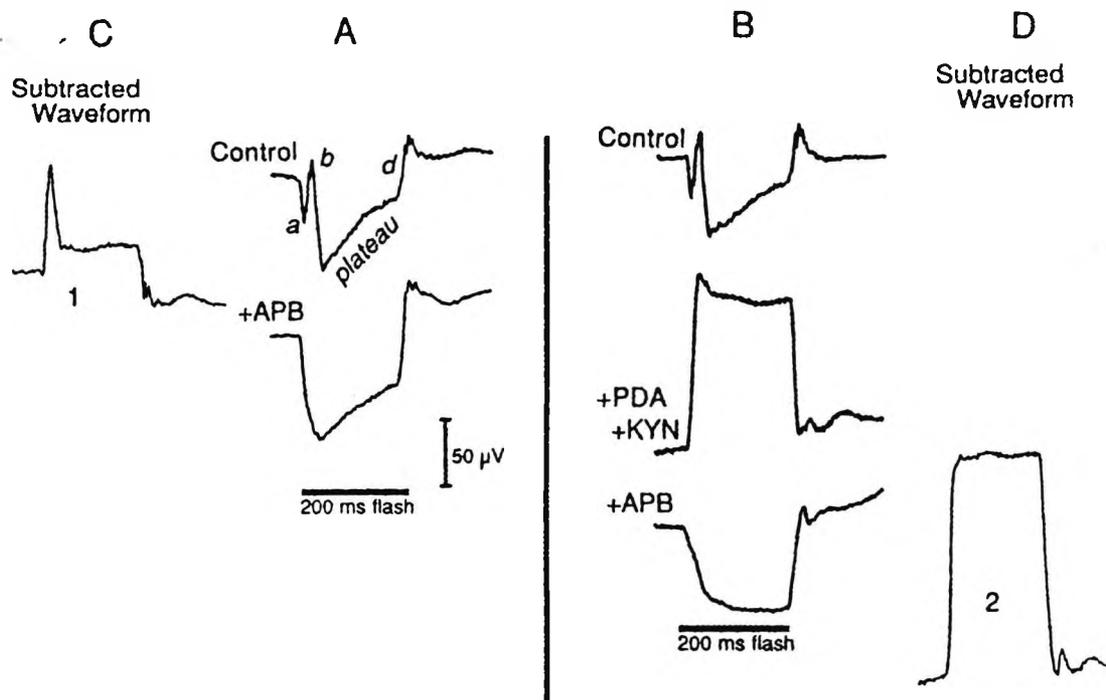
Figure 1-10   Photopic ERG of light adapted monkey during sequential administration of APB and PDA+KDY.   The ON bipolar cell response is isolated by subtracting the response recorded after the application of APB from the response recorded immediately before.   In column A, APB is applied and the subtracted waveform, isolated ON bipolar cell response, is number 1 in column C.   In column B, application of PDA+KDY precedes APB, and the subtracted waveform is number 2 in column D.   As C1 is not identical to D2 then the response of OFF bipolar cells and horizontal cells must affect the response of ON bipolar cells.   (Adapted from Sieving et al., 1994)

1.2.5.6 A contribution to the a-wave from OFF bipolar cells and horizontal cells.

Brown and Watanabe's earlier experiments in clamping retinal circulation (q.v.,(Brown and Watanabe, 1962)) did not exclude the possibility of a post-receptoral contribution to the a-wave from hyperpolarising second order neurons, i.e. OFF bipolar cells and horizontal cells.   Such a possibility was the purpose of Bush and Sieving studies (Bush and Sieving, 1994; Bush and Sieving,

65

1996b). Working on light adapted, primate I-type retinas, they found that the application of PDA, to block hyperpolarising second order neuron activity, completely removed all the negative parts of the ERG, resulting in an entirely positive waveform. Bush and Sieving claimed that this supported the notion of post receptoral contribution to the a-wave from hyperpolarising second order neurons because blocking hyperpolarising neuron activity changed the shape of the ERG.

When APB was introduced with the PDA the waveform obtained was very similar to the cone receptor potential found by Brown and Watanabe (1962). As the combination of PDA and APB will block the activity of all second order neurons Sieving et al. confirmed that Brown and Watanabe had isolated a potential derived from the receptors. However, this receptor potential was slower and considerably smaller than the a-wave. The a-wave was being formed from a sum of two components: a photoreceptor component and a hyperpolarising second order neuron component. By varying the luminance and using PDA and APB to block second order neuron activity Bush and Sieving were able to separate the effect of these two components. As the luminance was increased from the photopic threshold level a PDA-sensitive component to the a-wave could be seen to increase and then saturate at about 4 log td. The increase in a-wave amplitude after this luminance level was attributed to cone photoreceptor response.

Bush and Sieving later showed that, in the same preparation, the 33Hz flicker ERG, hitherto thought to be a direct cone response, was almost completely removed by the application of APB and PDA

66

(Bush and Sieving, 1996a). This result could be achieved with stimuli of both high and low photopic intensities. Bush and Sieving were able to locate the photopic flicker ERG firmly in the fast phasic responses of second order neurons.

1.2.5.7 Bipolar cell intrusion into the a-wave and models of the photoreceptor response.

Models of human photoreceptor activity must start with the ERG a-wave. However, depending on the stimulus conditions, the a-wave may not produced solely by the photoreceptors as the ON and OFF bipolar cell responses can both intrude on the a-wave, it is not even clear at what latency this could occur. b-Wave, ON bipolar activity, is generally avoided by using on the leading edge of the a-wave, up to its first inflection. At some time after this point b-wave intrusion must be assumed to occur.

The possibility that an OFF bipolar cell response contributes to the a-wave might be removed by adopting stimulus conditions that favour a response from the rods, because rods do not synapse with OFF bipolar cells. Hood and Birch (1990b; 1990a) have isolated the rod driven ERG from the cone driven ERG by recording two ERGs, one with long wavelength and another with short wavelength light, and subtracting the former from the later to achieve what they claim to be a pure rod driven ERG. They confirmed their result by recording from a blue-cone monochromat. As blue cones make little contribution to the a-wave, a blue-cone monochromat should have pure rod-driven ERGs without the need for the subtraction procedure. Hood and Birch found that the parameters of the model

where the same for the blue-cone monochromat as for normal observers whose rod-driven ERGs have been isolated with the subtraction procedure. However, rods may synapse with cones and if they do so a purely rod driven response may contain an element of OFF bipolar activity. Hood and Birch's result could conceivably be compromised by a response from OFF bipolar cells.

Cone responses can be obtained with stimulus flashes of very short duration. Hood and Birch (1995) have modelled the cone response using the two stage model outlined in Section 1.2.4.7. An alteration in the time constant was all that was required to use the same model for both rod and cone responses. This result must be treated with caution. OFF bipolar cell contribution to the response can be assumed with a fair degree of certainty. Beyond not using the a-wave after its first inflection, no attempt was made to eliminate a bipolar cell contribution.

1.2.5.8 The transduction cascade as a model for the bipolar cell response.

The Lamb and Pugh (1992) model of rod response provided no way for the photocurrent to return to its resting value and the Breton et al. (1994) a-wave model is therefore only appropriate to the very initial segment of the response. When (t-t_{eff}) is small the Gaussian function in a(t), above, can be approximated by:

$$a(t) = a_{max} A\Phi(t - t_{eff})^2$$

Equation 1-5

The existence of the exponent 2 in this equation is due to the existence of three processes (production of Rh*, production of G* and the hydrolysis of cGMP) that each introduce one integrating step into the cascade of biochemical reactions (Robson and Frishman, 1995). In general, if the response of the system involves s integration steps then:

$$a_s(t) = (a_{max}A)' \, \Phi(t - t_{eff})^{s-1}$$

<p align="right">Equation 1-6</p>

Robson and Frishman (1995) have shown that the pharmacologically isolated, rod-driven PII of the cat can be accurately modelled by a formula of this form with s=6. Other authors (Nawy and Jahr, 1990) have shown that the ON bipolar cell contains a G-protein second messenger system that is activated by the binding of the transmitter. Robson and Frishman suggested that the activation of the messenger and the cascade that leads to the depolarisation of the bipolar cell will bring about the introduction of three further integration steps in the response. Robson and Frishman found that the time course of the PII response had a delay t_{eff} slightly longer than that of the photoreceptor itself and associated this with the extra delay due to the diffusion of the transmitter across the synapse. This result has significant repercussions. If the kinetics of PII can be explained on the basis of the recorded PII signal and results from the electrical affects of the G-protein cascade then there is no place for the stages of temporal integration that would be introduced by the mediation of PII current by Müller cells, as some have suggested (Robson and Frishman, 1995).

1.2.5.9 The transduction cascade as a model for the early part of the ERG.

Robson and Frishman (1996) have combined the two transduction cascade models of a- and b-wave responses (in 1.2.4.12 and 1.2.5.8 above) to produce a single model for the early part of the ERG. Robson and Frishman found that this produced an accurate model of the rod driven ERG up to the first zero-crossing point but only after inner retinal, third order neuron components had been eliminated, either with pharmacological agents or with a steady adapting background. So, models of the rod and bipolar cell responses have provided evidence for the existence of a contribution to the ERG from third order retinal neurons.

1.2.6 Transgenic mice and the electroretinogram.

It is now possible to breed mice whose genetic makeup have been artificially altered. For example, genes responsible for expressing a particular receptor type can be removed, creating mice whose retina lack a particular response. Such mice can be used to isolate the ERG components associated with the absent response.

Masu et al. (1995) generated knockout mice with a targeted disruption of the mGluR6 gene. The mGluR6 gene is responsible for expressing the receptor subtype 6, found in ON bipolar cells. Mice without the mGluR6 gene will possess a specific deficit in the ON response in visual transmission. Mice without the mGluR6 gene showed a loss of ON responses but no changes in the projection of optic fibres into the brain. Despite the absence of an

70

ON pathway the mGluR6-deficient mice showed visual behaviour responses similar to control mice. Masu et al. concluded that the OFF response must provide an important means for transmitting visual information.

Peachey et al. (1997) have studied the functional consequences of horizontal cell-specific degeneration induced by the expression of SV40 tumour antigens in the retina of transgenic mice. Peachey et al. found that the dark adapted a-wave was not different from control mice but that the b-wave was markedly reduced. They ascribed this result to disturbance in the columnar orientation of bipolar cell bodies caused by the mutated gene rather than the loss of horizontal cells, which would have the result of removing a small potential of negative polarity.

1.2.7 The oscillatory potentials.

Cobb and Morton (1954) were the first to describe a series of 4 to 6 wavelets superimposed on the ascending slope of the conventional electroretinogram. These wavelets were dubbed oscillatory potentials (OPs). The exact number of oscillatory potentials recorded, and if they are recorded at all, depends on the level of light adaption of the retina. Various techniques have been used to achieve an optimal state of light adaption; they all use conditioning flashes or controlled background intensity, to manipulate the degree of retinal adaption (Speros and Price, 1981). OPs have been recorded from a variety of animals: rabbit, carp, turtle, cat, guinea pig, pigeon, mouse, bullfrog, tortoise, mudpuppy and primate (Speros and Price, 1981).

1.2.7.1 Oscillatory potentials arise in the proximal retina

Brown (1968) found that the occlusion of the retina artery in monkey resulted in the disappearance of the OPs. If the OPs depend on retinal circulation then they cannot originate in the photoreceptors or horizontal cells. Ogden (1973) recorded the laminar profile of voltages of the OPs in primate retina. Ogden found that the site of origin of the OPs was separate from that of the b-wave. The maximum amplitude of the first three OPs was at the level of the inner plexiform layer and Ogden suggested that elements in the neuropil layer could be involved in the generation of these potentials.

1.2.7.2 The oscillatory potentials are generated by a feedback system.

Wachtmeister and Dowling investigating the depth profile of OPs in the mudpuppy retina (1978), found that intraretinal OPs reverse their polarity with retinal depth in the inner retina, and suggested that OPs reflect a radial flow of current. During electrode penetration the first OP reversed first and the others followed in sequence, which suggests a different origin for each of the potentials. If the neuronal events generating the first OP occur earlier in time than the events generating the later OPs then the chain of events that underlie OP generation starts in the proximal retina and travels distally. Wachtmeister and Dowling suggested that one explanation for such a series of radial loops would be a feedback system.

Heynen et al. (1985) investigated the depth profile of OPs in primate retina. In contrast with Wachtmeister and Dowling's results, Heynen et al. found that the depth profiles of all the OPs were the same. Ogden, quoted above, had found no evidence of sign reversal of intra-retinal response, so there may be a difference between the retinas of primates and cold-blooded animals, like the mudpuppy. Heynen et al. suggested that OPs could arise from interplexiform cells, and if so, then OPs reflect the feedback control function over the centripetal flow of information within the retina.

1.2.8 The scotopic threshold response.

The scotopic threshold response (STR) has been extensively studied in the papers by Sieving, Frishman and Steinberg, (1986), Frishman and Steinberg (1989), Frishman and Sieving (1995) and Sieving (1995). The STR is the dark-adapted response of the retina to threshold stimuli and has been shown in cats, monkeys and humans. The STR consists of a graded negative potential which arises after a long latent period at the onset of illumination that is too weak to evoke any other ERG component. The STR maintains amplitude during illumination and decays back toward the baseline at stimulus offset without an off-response.

Penetrating micro-electrode studies showed that the STR has its maximum amplitude in the proximal retina, and therefore has a quite different source than the scotopic PII. The authors suggested that the STR represents an extracellular voltage arising from proximal retinal neurons, and that the STR depended on the neuronal activity in a low-threshold rod-driven circuit, which differs

73

from the higher-threshold rod-driven circuit from which PII originates. The distinction between the STR and PII therefore underlines the existence of two sites of adaption in cats, primates and humans, because the intensity which alters the sensitivity of the STR is about one fifth of the intensity required to produce any adaptive change in the b-wave. The STR is not abolished by optic nerve section and therefore does not depend on retinal ganglion cell activity.

1.2.9 The pattern electroretinogram.

Riggs at al. (1964) have shown that it is possible to record an ERG when the stimulus consists of a pattern that oscillates between two luminance levels so that each point on the retina is alternately exposed to light and darkness while the total light flux remains constant. An ERG elicited in such a way is called a Pattern ERG or PERG. There are several ways of constructing patterned stimuli. Spatially, the pattern can consist of gratings (bars) or checks (squares). Temporally, the pattern can 'reverse', i.e. bright and darks areas interchange and both checks have the same mean intensity, or the pattern can appear and disappear, so that the two sets of areas are equal in luminance over half the stimulus cycle. The luminance alterations can occur as a square wave, or sinusoidaly.

1.2.9.1 Sources of the PERG.

Spekreijse et al. (1973) have suggested that a patterned stimulus will give a zero ERG if the retina is a purely linear system, because

the response to the two sets of checks will cancel. But if the response to the modulation of the two sets of checks is distorted by nonlinearities in the luminance response then patterned stimulus may yield a luminance response. Spekreijse et al. (1973) have shown that the ERG to a pattern stimulus consists almost entirely of the nonlinear part of the luminance response and does not contain a spatial contrast component. The lack of such a component in the PERG would imply that the PERG has its source in the same retinal structures that produce the flash ERG, but this notion has been challenged. Arden and Vaegan (1982; 1983) have found that the response to a patterned stimulus, changing between L_{max} and L_{min}, is larger than the mean of the responses to a luminance change between $L_{max}/2$ and L_{max}, and $L_{min}/2$ and L_{min}, where that change in illumination is spatially uniform. This result is consistent with the idea that lateral interactions help generate the PERG, but it does not mean that luminance response cannot be produced by patterned stimuli or that pattern and uniform-field ERG's are separate phenomenon.

1.2.9.2 Clinical and experimental evidence that the PERG is generated in the inner retina.

Maffei and Fiorentini (1981) have shown that the PERG elicited from a cat is abolished after the optic nerve has been sectioned. The flash ERG remained unaltered, as did the PERG is the fellow eye. This result strongly suggested that the PERG had its roots, at least in part, in the ganglion cells of the inner retina. Maffei and Fiorentini repeated this result in the monkey (1985) and showed in

post hoc histological examination that the ganglion cells had indeed degenerated after optic nerve section.

Arden and Vaegan (1982) have found that the PERG was reduced in amblyopia, at least when measured as a ratio with the less affected fellow eye. It is well established that flash and focal ERG are unaffected in human amblyopes so it would appear that the PERG is being generated, at least in part, within different retinal structures than the ERG. The PERG was reduced in cases of multiple sclerosis, optic neuritis and glaucoma (Arden et al. 1982), these are all conditions associated with ganglion cell degradation. The same authors found that PERG amplitudes were reduced in optic atrophy, where the disease is limited to the optic nerve. This is strong evidence that the PERG is partly produced in the ganglion cell layer.

Histological examination of patients with Alzheimer's disease have revealed a significant loss of retinal ganglion cells, particularly larger ones (Berninger and Arden, 1988). The negative component of the PERG of patients with Alzheimer's disease are reduced (Berninger and Arden, 1988).

1.2.9.3 Spatial selectivity and tuning in the PERG.

Ganglion cells exhibit strong centre-surround receptive field organisation and lateral inhibition. A response dependant on the ganglion cell layer should exhibit spatial tuning; i.e., in addition to attenuation at higher and lower spatial frequencies there should exist an intermediate frequency which elicits a maximal response.

Spatial tuning has been hard to show in the PERG due to masking of the pattern component by the non-pattern dependant luminance component. However, Arden and Vaegan, (1983), Odom et al. (1982), Korth et al. (1985) and Hess and Baker (1984) have all found that, for a stimulus centred at the fovea, the PERG was maximal when the grating had a spatial frequency of 4 cycles per degree (cpd) of visual angle. Hess and Baker also found that the spatial frequency of the bandpass was smaller in the periphery - at 15 degrees eccentricity the maximal response was at 0.8 cpd and at 34 degrees, 0.4 cpd elicited maximal response.

1.2.9.4 Separation of the PERG into luminance and pattern components.

Drasdo et al. (1987) and Thompson and Drasdo (1987) have separated the PERG into two components, the pattern specific response (PSR) and the retinal illuminance response (RIR). At high spatial frequencies the RIR is reduced due to optical degradation of the fine stimulus details and the PSR dominates the PERG. At very low spatial frequencies the pattern consists of a single check alternating between on and off, the pattern ERG is now a uniform-field flash ERG, and the RIR dominates the PERG so that the PERG is identical to the uniform-field, flash ERG. Drasdo et al. calculated the RIR at higher spatial frequencies from lower spatial frequency RIR attenuated by the contrast reduction due to optical degradation of the eye. The PSR could then be calculated as the difference between the PERG and the (extrapolated) RIR. The PSR was maximal at around 4 cpd, confirming earlier results. Drasdo et al. later showed that the

amplitude of the PSR, as a function of eccentricity, mimicked ganglion cell receptive field diameter, (Drasdo et al. 1990). The spatial variation in the amplitude of the RIR closely followed variation in the thickness of the inner nuclear layer.

Figure 1-11
Hypothetical tuning curve
of the PERG resulting
of the PERG resulting
from summation of a
retinal illuminance
response (RIS) and
pattern specific
response(PSR).
(Drasdo et al. 1987)
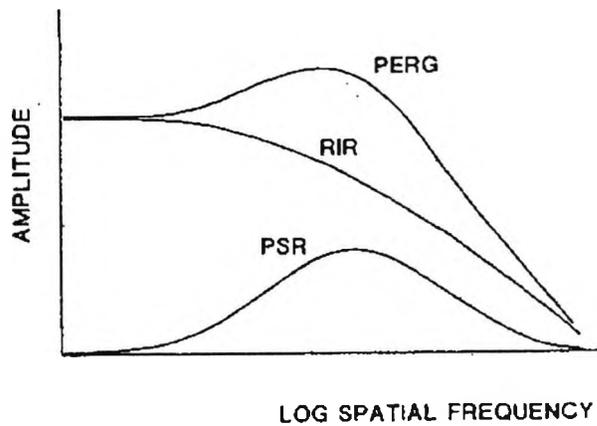
2. Signal Analysis of Electroretinographic Responses.

The previous chapter considered the electroretinogram as an electrophysiological response that arises in the retina to light stimulus. This chapter will treat the electroretinogram as a electrical signal. Initially, two general concepts in signal analysis must be discussed - signal averaging and cross-correlation. Then this chapter will discuss how linear and nonlinear electroretinograms may be extracted from the corneal response. The mathematics that underlie the separation of linear and nonlinear signals are complicated, but must be dealt with initially. The commonly adopted analogue method of nonlinear analysis, using sinusoids, will be covered before the specific case of the binary nonlinear analysis used in the Visual Evoked Response Imaging System, VERIS. VERIS is capable of multiple input analysis; this explanation will consider the single input case first, before discussing the importance of multiple input analysis and explaining how this can be actualised. The literature on nonlinear analysis of the ERG will be discussed.

2.1 Signal Averaging.

The response of the retina to even a bright flash of light is very small: no more than about ½ millivolt. The contamination of the response with background electrical signals, called noise, is a serious problem in ERG technique. In the worst case the ratio of signal to noise can be so small that it is impossible to see a retinal response in the recorded signal at all. A method of noise reduction commonly used in ERG technique is signal averaging. In signal

averaging the input signal is repeated many times and the response to each input is averaged with the response to all the earlier inputs. Provided that the noise is uncorrelated between successive responses, the noise will average out to a constant level which reflects its mean value. ERGs are suited to signal averaging because responses to successive stimuli are theoretically identical. If the noise is completely uncorrelated with the signal then the improvement in signal to noise ratio may be estimated. The variance of a sum of uncorrelated random signals is equal to the sum of their individual variances (Lynn, 1982). If n versions of the noisy response are summed, the signal is increased by n, the noise variance is increased by n and the standard deviation of the noise increases by √n. The ratio of signal amplitude to noise standard deviation is therefore increased by √n. VERIS presents each stimulus many times in the course of one recording, permitting significant signal averaging.

If the noise is correlated with the response or the stimulus, for example, if the noise contains strictly periodic components, such as pick up from the mains-supply frequency (and the stimulus is locked to the mains in some way e.g. by display on a monitor), then the increase in signal to noise ratio will be reduced. VERIS avoids this problem by making the stimulus appear at irregular instants, so that the periodic noise is uncorrelated between stimulus presentations.

2.2 Cross-correlation.

A cross-correlation function relates two signals in terms of their shared signal properties (amplitude and phase), over some given . duration. Complicated patterns of stimulus presentation can be correlated with their response using well understood mathematical algorithms. Cross-correlation is a specific case of the more general principle of convolution. Convolution is more computationally intensive in the amplitude domain than in the frequency domain (these terms will be explained in Section 2.3.1). It is therefore common to transform both the input stimulus and the output response into the frequency domain before performing the convolution and then back transforming the output into the amplitude domain. VERIS uses a novel method of cross-correlation which will be discussed below.

2.3 Orthogonal Transforms.

In three dimensional space any three dimensional vector can be represented as a sum of three orthogonal unit vectors, each parallel to the Cartesian co-ordinate axes. The set of three orthogonal unit vectors is said to be complete because it spans the three dimensional vector. A two dimensional system of unit vectors would be termed incomplete to represent the three dimensional system. Many other examples of orthogonal sets exist, one example is sine-cosine functions (Section 2.3.1), another is binary Walsh functions (Section 2.3.2). Functions that convert between two orthogonal sets are called orthogonal transforms. VERIS uses a technique in which the input and output are both orthogonal to

81

each other. Cross-correlation can then be achieved by the application of one orthogonal transform between in the input stimulus and output response.

2.3.1 Fourier Series and Fourier Transforms.

In 1822 Fourier showed that any periodic function can be represented as a sum of sine and cosine functions. The series of sine and cosine functions is now termed the Fourier series. The Fourier series of a signal $x(t)$ is expressed:

$$x(t) = a_o + \sum_{n=1}^{\infty} a_n \cos(n\omega_o t) + \sum_{n=1}^{\infty} b_n \sin(n\omega_o t)$$

Equation 2-1

where ω_o is the fundamental angular frequency which is related to the period T of $x(t)$ by the formula $T=2\pi/\omega_o$. The first term in the series, a_o, is invariant in time, in electrical signals it is termed the dc response. The terms in n=1 are called the fundamental or first harmonic of the Fourier series. The terms in n=2,3,4 etc. are called the second, third, fourth etc. harmonics. The Fourier series of some signals will posses only sine or cosine terms. Signals that can be expressed solely in terms of the cosine function (all the b_n terms will be zero) are called even. Series that are odd can be expressed in terms of the sine function, and all the a_n terms will be zero. The Fourier series may be an infinite one, where power exists in every harmonic up to infinity, but some signals can be exactly expressed with a Fourier series of a limited number of terms.

82

2.3.1.1 Fourier series example: The square wave.

The Fourier series of a square wave, consists of an infinite series of sinusoidal functions.
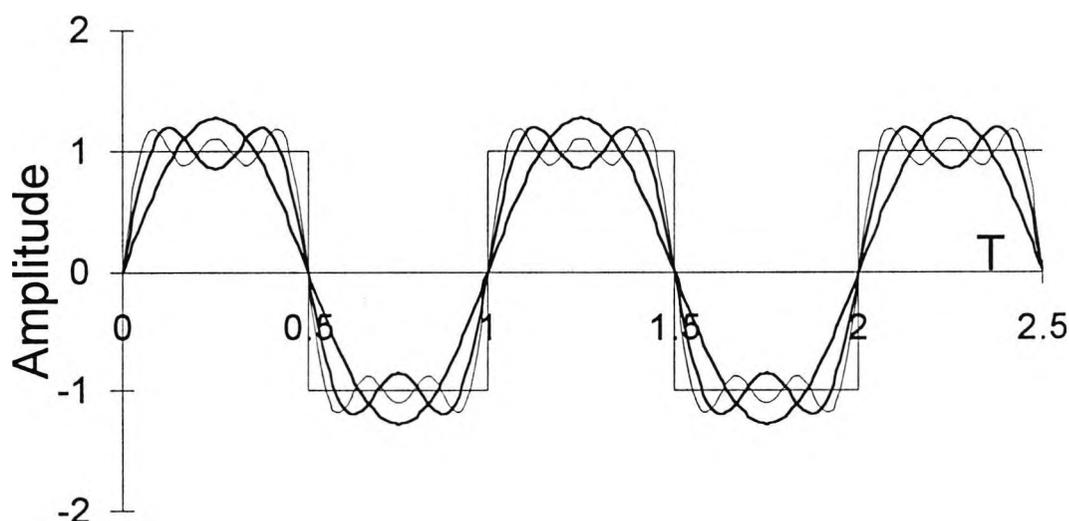
Figure 2-1.   The cumulative sum of the first three terms of a truncated Fourier series of a square wave, and the square wave which they are summing to approximate.

Figure 2-1 shows how a square wave can be constructed from a series of sine waves.   The average value of the square wave is zero so a_0=0.   Only sine waves are necessary in this Fourier Series because the square wave is odd.   The Fourier series of this square wave is:

$$f(t) = \frac{4}{n\pi} \sum_{n=1}^{n=\infty} \sin(n\omega_0 t)$$

Equation 2-2

Only the first three terms of the series, that is:

$$f(t) = \frac{4}{\pi}\left\{\sin(\omega t) + \frac{1}{3}\sin(3\omega t) + \frac{1}{5}\sin(5\omega t)\right\}$$

Equation 2-3

have been illustrated in Figure 2-1.

The Fourier series of a square wave, shown in Equation 2-2, is an orthogonal set because it spans (precisely describes) the square wave. However, the Fourier series shown in Equation 2-3 and illustrated in Figure 2-1 is an incomplete orthogonal set because only the first three terms have been used.

2.3.1.2 *The Fourier transform.*

Any signal can be expressed as a Fourier series, and a Fourier series can be specified by its Fourier transform. The Fourier transform is a mathematical operation that transforms an input signal into its Fourier series components. The Fourier transform applied to a signal in the amplitude domain transforms it into the frequency domain. A back-transform is also possible, that re-converts a signal defined in the frequency domain to its amplitude domain form. All Fourier transforms are orthogonal transforms, because they convert between two orthogonal sets.

2.3.1.3 *The fast Fourier transform.*

If the raw signal is obtained by discontinuous sampling, for example by a digital system, then an alternative Fourier transform exists, called the discrete Fourier transform (DFT). Direct solution of the DFT is highly computationally intensive and a very large number of operations have to be performed, but fortunately an alternative to the DFT exists, called the fast Fourier transform (FFT), which is computationally much more compact. The FFT requires only $n.\log_2(n)$ mathematical operations, each a complex multiplication or addition, for a signal composed of n discrete values. The FFT achieves its reduction in the number of computations by using decimation. In decimation the DFT of two shorter sequences, one containing the even-numbered positions in n and the other the odd-numbered positions, are calculated separately. Decimation relies on n, the number of samples, being divisible by 2.

2.3.2 The Walsh Series and Walsh-Hadamard Transforms.

Walsh functions form an ordered set of waveforms taking values +1 and -1. They are the binary analogues of sinusoidal functions.

Figure 2 shows the first 8 terms of the Walsh series and their sinusoidal harmonic analogues. The first term in the Walsh series is related to the DC term in the Fourier series. Subsequent terms are related to the odd (sine) and then even (cosine) terms of the Fourier series. The Walsh series therefore form a binary analogue of the Fourier series and, in the limit, the Walsh and Fourier series representations are identical (Beauchamp, 1975).
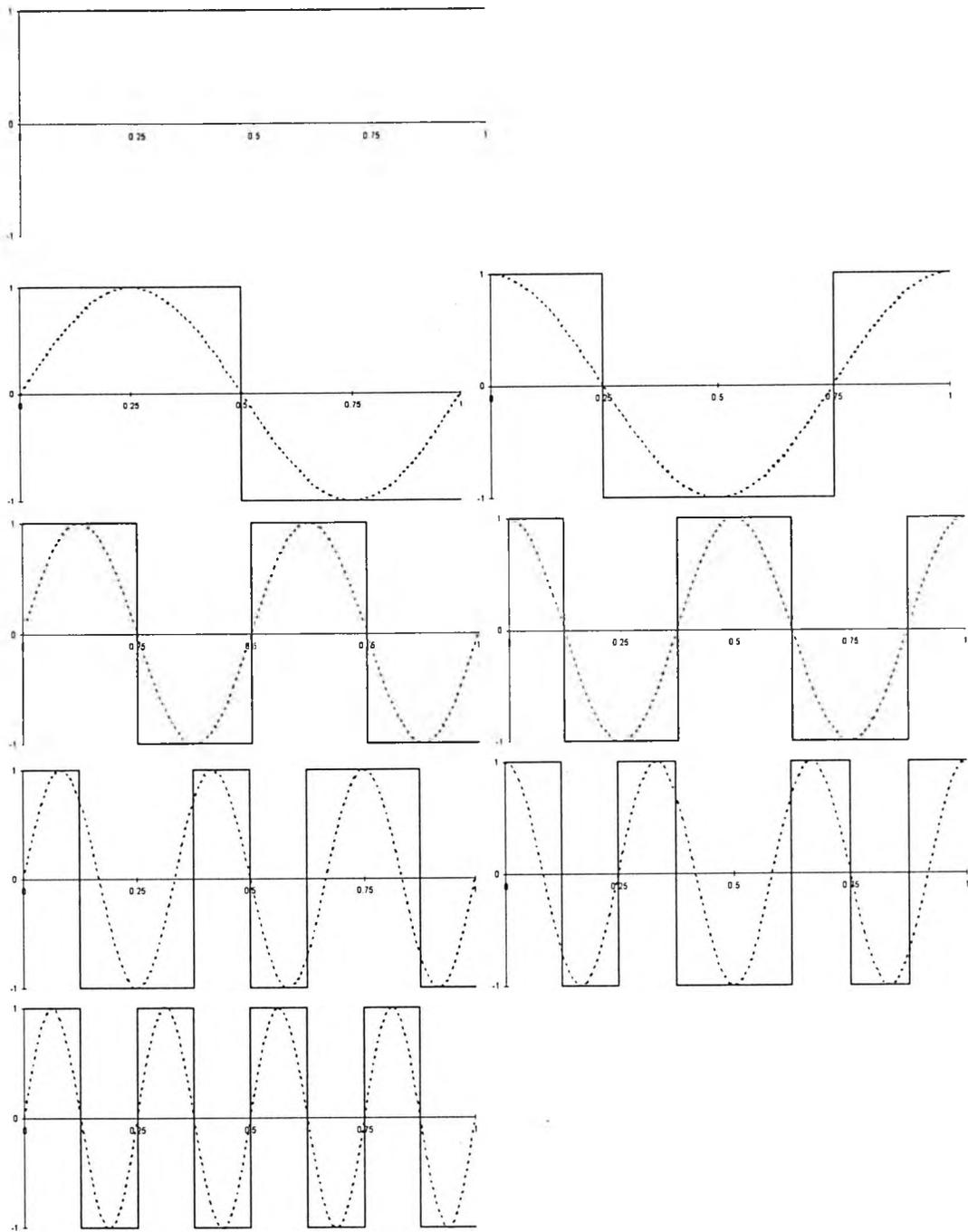
Figure 2-2.   The first eight terms of the Walsh series showing their
relationship with the Fourier series harmonics.

2.3.2.1 Walsh-Hadamard transforms.

Transforms performed on Walsh series are termed Walsh-Hadamard transforms (WHT). As the inputs are binary the transform is made up of +1's and -1's, and since the required computations are only additions and subtractions, this simplification in computation greatly speeds up computer calculation of the Walsh transform. There are several methods of ordering the Walsh series. Reordering a Walsh series is equivalent to reordering the terms in a Fourier series. One particular ordering, Hadamard ordering, and its transform, the Hadamard ordered WHT $(WHT)_h$, will be discussed here because it forms the basis of the transform performed by VERIS. The Hadamard ordered matrix can be easily calculated by computer. For Hadamard matrices of order 2^n, the element in row x column y is defined as the parity of the bitwise logic AND of x and y. So the location row 5, column 6 (or (101,110) in binary) contains -1 as logic 101 AND 110 = 001 which has parity -1. The entire Hadamard ordered matrix for the example n=3 is given here: (+ and - replace +1 and -1 for clarity)

$$
H(n)=
\begin{bmatrix}
+ & + & + & + & + & + & + & + \\
+ & - & + & - & + & - & + & - \\
+ & + & - & - & + & + & - & - \\
+ & - & - & + & + & - & - & + \\
+ & + & + & + & - & - & - & - \\
+ & - & + & - & - & + & - & + \\
+ & + & - & - & - & - & + & + \\
+ & - & - & + & - & + & + & -
\end{bmatrix}
$$

Figure 2-3. *The Walsh series of Figure 2-2 in Hadamard ordering and matrix form. Note that + indicates +1 and - indicates -1.*

Observe in this matrix an array of 2X2 matrices of the form: $\begin{bmatrix} + & + \\ + & - \end{bmatrix}$.

This 2x2 matrix can be used to construct any higher order 2^n matrix by a simple inversion; this feature of Hadamard ordered matrices enables rapid decimation and makes possible the Fast Hadamard ordered Walsh Hadamard Transform $(FWHT)_h$ (Ahmed and Rao, 1975).

If the inputs and responses are each placed in a matrix, then cross-correlation using a Hadamard array of inputs would involve a $(FWHT)_h$ on the matrix of inputs, a $(FWHT)_h$ on a matrix of responses, convolution (matrix multiplication) of the two transformed matrices and a back $(FWHT)_h$ to achieve the cross-correlation in the amplitude domain. However, Sutter (1991) has shown that an alternative and much faster computational technique, that requires only one $(FWHT)_h$, is possible when the input stimulus matrix is formed from an m-sequence. M-sequences will be considered in Section 2.3.3. First the orthogonality of Hadamard matrices must be discussed.

2.3.2.2 Hadamard matrices as orthogonal transforms.

All Walsh functions are orthogonal functions, so the $(FWHT)_h$ is an orthogonal transform. Hadamard ordered matrices have two properties which are utilised by VERIS.

1) For any matrix $AA^{-1}=I$ (just as $a.a^{-1}=1$), but as H, the Hadamard ordered matrix, is orthogonal $H^T=H^{-1}$, so $HH^T=I$. As H is also symmetrical so then $H^T=H$ and $HH=I$. So for:

$$H \cdot \vec{B} = \vec{R}$$

Equation 2-4

a solution of the form:

$$\vec{B} = H^{-1} \cdot \vec{R} = H^T \cdot \vec{R} = H \cdot \vec{R}$$

Equation 2-5

is possible, where **H** denotes the input, $\vec{R}$ the response vector, and $\vec{B}$ the vector of the coefficients of a system of linear equations that describes $\vec{R}$'s response to **H**. Calculating $\vec{B}$ from **H** and $\vec{R}$ is simply a matter of performing one matrix multiplication, a simple and rapid computation for a computer to do. What is more, **H** is its own inverse, so from knowledge of **H** and $\vec{B}$, $\vec{R}$ can be calculated by exactly the same operation. The operation of **H** on $\vec{B}$ or $\vec{R}$ is an orthogonal transform that converts between the coefficients that describe the response and the response itself.

2) Any two Hadamard matrices, H_1 and H_2 are said to be equivalent if:

$$H_2 = P_r^T H_1 P_c$$

Equation 2-6

where P_r and P_c are the permutation matrices of the rows and columns respectively. The operation of the permutation matrices on H_1 is simply to reorder the rows. Equivalent Hadamard matrices are therefore identical except for the order of their rows.

89

It follows from the above two properties that a matrix of the same equivalence class as a Hadamard matrix can be used to form an orthogonal transform just by the application of three matrix multiplications, that is: multiplication of the input matrix with the permutation matrix, multiplication of this outcome with the response vector, followed by multiplication with a second permutation matrix.

2.3.3 m-Sequences.

m-Sequences are a specific example of a class of sequences termed pseudo random binary sequences (PSBR). PSBRs are not truly random sequences, because they are defined by a pre-determined algorithm, and are therefore deterministic. However, PSBRs offer certain advantages over random sequences, particularly in the speed and ease of their calculation. m-Sequences can be generated very simply by using a feedback shift register. If the register has N stages, then the entire sequence will consist of 2^N-1 characters. Feedback shift registers will be explained in Section 2.3.3.1. Sutter (1991) has shown that a matrix filled with bits derived from an m-sequences is equivalent to a Hadamard-ordered matrix. The second property of Hadamard matrices, quoted in Equation 2-6, means that this matrix can be used to compute a Hadamard Ordered, Fast Walsh Hadamard Transform $((FWHT)_h)$. The $(FWHT)_h$ must be preceded and followed by the multiplication of the m-sequence matrix with a permutation matrix, but these do not add significantly to the computation times (Sutter, 1991).

2.3.3.1 Generating m-sequences.

m-Sequences can be generated with feedback shift registers. In VERIS this register is called the generating register. An m-sequence of length 2^N-1 can be generated from a register of length N. The register is N bits deep. The register is initialised with a 1 in the least significant bit position and 0 everywhere else (0....01). The tap word is crucial to m-sequence generation. The tap word is an N digit binary number whose 1's indicate which register stages will be tapped. The contents of the register stages given by the tap number, are summed modulo 2, then the register is shifted right one stage and the new number is fed back into the now vacant, most left-hand, stage. The m-sequence is formed from the 0 or 1 in the left-hand, most significant bit at each shift.

Generating register example: For N=3, and tap word=3, (011 in binary), the m-sequence will be generated in the following manner:

generating register contents: 001

take bits 1 and 2 in the generating register (as given by the tap word: 011) and sum modulo 2 to get 1, shift the generating register one step to the right and place the new number in the most significant bit:

generating register contents: 100

take bits 1 and 2 and sum modulo 2 to get 0, shift the generating register one step to the right and place the new number in the most significant bit:

generating register contents: 010

take bits 1 and 2 and sum modulo 2 to get 1, shift the generating register one step to the right and place the new number in the most significant bit:

generating register contents: $\underline{1}$01

subsequent stages are

generating register contents: $\underline{1}$10

Figure 2-4. The generating register configuration for the case tap word=3

generating register contents: $\underline{1}$11

generating register contents: $\underline{0}$11

So the 2^3-1=7 numbers in the m-sequence are: 0101110 (the underlined numbers above).

2.3.3.2 *The tap register.*

Equivalency between the m-sequence matrix and the Hadamard matrix requires two permutation matrices.   The first is calculated from the generating register (Sutter, 1991), the second requires a new register termed, in VERIS, the tap register.   The tap register is initiated with a 1 in the least significant bit (i.e. right justified) position and shifted left.   The overflow of the register is added modulo 2 to the stages where the generating register has its feedback taps (refer Figure 2-5).

Tap register example: For N=3, and tap word=3, $(011)_2$, the m-sequence will be generated in the following manner:

tap register contents: $\underline{0}$01

shift the tap register one step to the **_left_** and sum the overflow modulo 2 with the contents of the tap register at bits 1 and 2, as given by the tap word:

tap register contents: <u>0</u>10

shift the tap register one step to the left and sum the output modulo 2 with the contents of the register at bits 1 and 2:

tap register contents: <u>1</u>00

shift the tap register one step to the left and sum the output modulo 2 with the contents of the register at bits 1 and 2:

tap register contents: <u>0</u>11

subsequent stages are

tap register contents: <u>1</u>10

tap register contents: <u>1</u>11

tap register contents: <u>1</u>01

Figure 2-5. *Tap register configuration for the case tap word=3*

So the $2^3-1=7$ numbers in the sequence are 0010111 (the underlined numbers above).
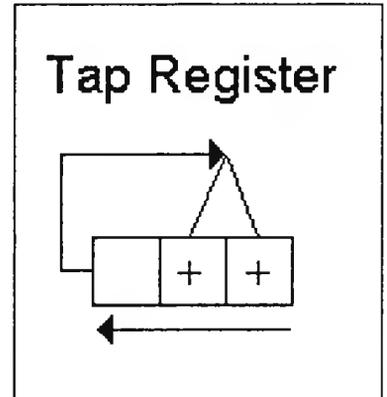
2.4 Kernel Analysis and Functionals.

The relationship between input and output of a simple, linear system contained within a black box can be described by a function. The terms of the function will depend on the nature of the elements within the black box. However, a function is not sufficient to describe the retina because the retina possesses memory. A functional must be employed.

2.4.1 Functionals.

Functionals have been described by Hadamard as 'functions that depend on other functions'. Volterra (1938) has formally defined the functional as: 'a quantity R is a functional of the function x(t) in the interval (a,b) when it depends on all the values taken by x(t) in the interval (a,b); or alternatively when a law is given by which for every function x(t) defined within (a,b) there can be made to correspond one and only one quantity R, perfectly determined'. This functional can be written:

$$R = R\left[\overset{b}{\underset{a}{x(t)}} \right]$$

Equation 2-7

Or, if no ambiguity arises:

$$R = R\left[x(t) \right]$$

Equation 2-8

In the specific case of the retina the response at some time t will be a function of all the stimuli presented to the retina from t -m to t where m is the memory of the retina. The response R at time t_0 is therefore a function of m variables:

$$R_{t_0} = R\left[\overset{t}{\underset{t-m}{x(t)}} \right]$$

Equation 2-9

or in a system with discrete, rather than continuous, variables:

$$R_{t_0} = R(X_{t-m}, X_{(t-m)+1}, X_{(t-m)+2}, \cdots, X_t)$$

Equation 2-10

When studying retinal responses the input window is equal to the memory of the retina; that is, the duration over which the response is of interest, which must be known.

2.4.1.1 Power series of functionals.

Any function can be described as a linear combination of a complete set of familiar functions. One such family of functions is the power series and a specific example of a power series is the Taylor series. Consider a function $W=W(z)$, the Taylor series about some point $z=z_0$ is

$$W(z) = A^{(0)} + A^{(1)}(z - z_0) + A^{(2)}(z - z_0)^2 + \cdots + A^{(n)}(z - z_0)^n$$
$$= \sum_{n=0}^{\infty} A^{(n)}(z - z_0)^n$$

Equation 2-11

Where $A^{(n)}$ indicates the nth value, not the nth power, of A. The solution of all the n coefficients of A in this polynomial will yield an equation which describes $W(z)$ exactly. Practically, an exact solution is not possible because this in an infinite series, but the solution of the coefficients up to (say) the fifth term will yield an approximation of $W(z)$ of the fifth order.

The Taylor series has a functional analogue called the Volterra series. Consider the functional R=R[x(t)], the Volterra series expansion is:

$$R[x(t)] = K^{(0)} + K^{(1)}[x(t_0 - t)]^1 + K^{(2)}[x(t_0 - t)]^2 + \cdots + K^{(n)}[x(t_0 - t)]^n$$

$$= \sum_{n=1}^{\infty} K^{(n)}[x(t_0 - t)]^n$$

Equation 2-12

The coefficients K in this power series are called Volterra kernels (Volterra, 1938). In VERIS, the fact that the complete Volterra series is not attainable does not constitute a problem since it is sufficient to derive a truncated power series that spans the non-zero Volterra series coefficients present in the response.

2.4.2 Kernels.

The Volterra series expansion of Equation 2-10, for a response R at some time j, is:

$$R_j = K^0 + \sum_{i_1=0}^{m} K_{i_1}^{(1)} x_{j-i_1}$$

$$+ \sum_{i_1=0}^{m} \sum_{i_2=0}^{m} K_{i_1,i_2}^{(2)} x_{j-i_1} x_{j-i_2}$$

$$+ \sum_{i_1=0}^{m} \sum_{i_2=0}^{m} \sum_{i_3=0}^{m} K_{i_1,i_2,i_3}^{(3)} x_{j-i_1} x_{j-i_2} x_{j-i_3}$$

$$+ \cdots$$

Equation 2-13

where there are i inputs in the input window at time j. The kernels can be determined experimentally by testing the system with

96

different values of the input x. For each configuration of x within the input window a response amplitude $R(X_0, \ldots X_m)$ is measured. To cover the set of all possible responses the input window, termed k, must be of at least equal length to the system memory, m. The system of equations that can be represented as:

$$\mathbf{X} \cdot \vec{K} = \vec{R}$$

Equation 2-14

where $\vec{K}$ is a vector containing the kernel elements of all orders, **X** is a matrix containing the test input configurations, and $\vec{R}$ a vector containing the corresponding response amplitudes.

2.4.2.1 Binary kernels.

If the inputs are restricted to binary values +1 and -1 then the number of terms in Equation 2-14 that can be solved are reduced. To illustrate this consider a third-order system in which the input window size and memory are both equal to 3. Equation 2-13 becomes:

$$
\begin{aligned}
R_j = K^0 &+ \sum_{i_1=0}^{3} K_{i_1}^{(1)} x_{j-i_1} \\
&+ \sum_{i_1=0}^{3} \sum_{i_2=0}^{3} K_{i_1,i_2}^{(2)} x_{j-i_1} x_{j-i_2} \\
&+ \sum_{i_1=0}^{3} \sum_{i_2=0}^{3} \sum_{i_3=0}^{3} K_{i_1,i_2,i_3}^{(3)} x_{j-i_1} x_{j-i_2} x_{j-i_3}
\end{aligned}
$$

Equation 2-15

Now, if the input configuration is $(x_{i1}, x_{i2}, x_{i3})=(-c, c, -c)$ then Equation 2-15 yields:

$$R(-c, c, -c) = \{K^{(0)} + c^2 K_{1,1}^{(2)} + c^2 K_{2,2}^{(2)} + c^2 K_{3,3}^{(2)}\}$$
$$- \{cK_1^{(1)} + c^3 K_{1,1,1}^{(3)} + c^3 K_{1,2,2}^{(3)} + c^3 K_{1,3,3}^{(3)}\}$$
$$+ \{cK_2^{(1)} + c^3 K_{2,1,1}^{(3)} + c^3 K_{2,2,2}^{(3)} + c^3 K_{2,3,3}^{(3)}\}$$
$$- \{cK_3^{(1)} + c^3 K_{3,1,1}^{(3)} + c^3 K_{3,2,2}^{(3)} + c^3 K_{3,3,3}^{(3)}\}$$
$$- \{c^2 K_{1,2}^{(2)}\} - \{c^2 K_{2,3}^{(2)}\} + \{c^2 K_{1,3}^{(2)}\} + \{c^3 K_{1,2,3}^{(3)}\}$$

Equation 2-16

The terms in the curly brackets always have the same sign irrespective of the sign of the terms in the input. Second order kernels whose indices are the same (i.e. are the product of the same x_i) will always be +1 and third order kernels that have two indices the same will take the sign of the third indices.

1) $K^{(2)}_{1,1}$ $K^{(2)}_{2,2}$ $K^{(2)}_{3,3}$ will be +1;

2) $K^{(3)}_{1,1,1}$ $K^{(3)}_{1,2,2}$ and $K^{(3)}_{1,3,3}$ will take the sign of x_1;

3) $K^{(3)}_{2,1,1}$ $K^{(3)}_{2,2,2}$ and $K^{(3)}_{2,3,3}$ will take the sign of x_2;

4) $K^{(3)}_{3,1,1}$ $K^{(3)}_{3,2,2}$ and $K^{(3)}_{3,3,3}$ will take the sign of x_3;

The system of equations resulting from a complete binary test can be solved for the values of the curly brackets in Equation 2-16 but not the terms contained within them, so the binary test is unable to distinguish the Volterra kernel elements within each bracket. Now define a binary kernel B so that kernels can be grouped with others of the same sign.

e.g.: $B^{(0)} = K^{(0)} + K^{(2)}_{1,1} + K^{(2)}_{2,2} + K^{(2)}_{3,3}$

$B^{(1)}_2 = K^{(1)}_2 + K^{(3)}_{2,1,1} + K^{(3)}_{2,2,2} + K^{(3)}_{2,3,3}$

etc.

Equation 2-16 reduces to:

$$R(-c, c, -c) = B^{(0)} - B^{(1)}_1 + B^{(1)}_2 - B^{(2)}_{1,2} - B^1_3 - B^{(2)}_{2,3} + B^{(2)}_{1,3} + B^{(3)}_{1,2,3}$$

Equation 2-17

There are $8 = 2^3$ different terms to solve.

Now:

$$R_j = B^0 + \sum_{i_1=0}^{3} B^{(1)}_{i_1} x_{j-i_1}$$

$$+ \sum_{i_1=0}^{3} \sum_{i_2=0}^{3} B^{(2)}_{i_1,i_2} x_{j-i_1} x_{j-i_2}$$

$$+ \sum_{i_1=0}^{3} \sum_{i_2=0}^{3} \sum_{i_3=0}^{3} B^{(3)}_{i_1,i_2} x_{j-i_1} x_{j-i_2} x_{j-i_3}$$

Equation 2-18

for this third order system, or more generally:

$$\vec{X} \cdot \vec{B} = \vec{R}$$

Equation 2-19

where $\vec{B}$ is a vector containing the kernel elements of all orders, **X** is a matrix containing the test input configurations, and $\vec{R}$ a vector containing the corresponding response amplitudes. Each test

configuration in the input window contributes one equation for determining one binary kernel.

2.4.2.2 *Slices of the Binary Kernels.*

Each x_i is a slice of the kernel. The slices represent a cut through the kernel time domain. Each cut is parallel to the main diagonal. Figure 2-6 illustrates the first three slices of the second order kernel:

The first slice represents the situation when one stimuli follows another with no time lag between them. The second slice has a time lag of one time bin between the two stimuli, etc. At the main diagonal the two stimuli would have to appear simultaneously, this is only possible with non-binary stimuli. The kernel slice at the leading diagonal is the kernels K_{11}, K_{22}, K_{33} that the binary approach cannot solve (see (1) in Section 2.4.2.1). The significance of this will be considered in due course.

2.4.3 Calculation of Binary Kernels using Hadamard ordering.

Consider again the example of a third order system. The input matrix **X** will consist of $3^2=8$ rows and columns. The test configuration in the input window gives the column number after substituting 0 for 1 and 1 for -1. So, from the earlier example (Equation 2-16, page 98), $(-c,c,-c)=(-1,1,-1)$ gives column 5 after substitution, as $(101)_2=5$. The binary kernels give the rows from their slice delay patterns: e.g. binary kernel $B^{(2)}_{1,2}$ has delay pattern (011) as the stimuli are in the first and second time bins of the input

100
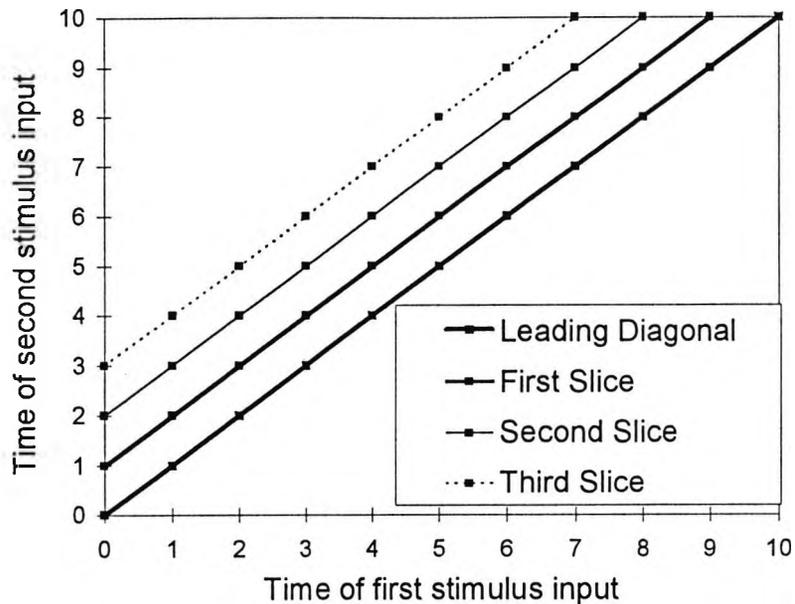
Figure 2-6. The first three slices through the second order kernel, and the leading diagonal. Two stimuli are required to generate the second order kernel and the lag between them gives the slice. As the stimuli are binary they cannot be coincident in time so the kernel slice indicated by the leading diagonal cannot be calculated.

window, $(011)_2 = 3$ so binary kernel $B^{(2)}_{1,2}$ gives row 3. The elements in the matrix are calculated from the bitwise logic AND of the rows and columns, as shown in Section 2.3.2.1. The construction of the entire matrix from the test input and binary kernel delay patterns is illustrated here:

$$X =$$

Kernel	Test / Slice	0 000	1 001	2 010	3 011	4 100	5 101	6 110	7 111
$B^{(0)}$	000	+	+	+	+	+	+	+	+
$B_1^{(1)}$	001	+	−	+	−	+	−	+	−
$B_2^{(1)}$	010	+	+	−	−	+	+	−	−
$B_{1,2}^{(2)}$	011	+	−	−	+	+	−	−	+
B_3^1	100	+	+	+	+	−	−	−	−
$B_{1,3}^{(2)}$	101	+	−	+	−	−	+	−	+
$B_{3,2}^{(2)}$	110	+	+	−	−	−	−	+	+
$B_{1,2,3}^{(3)}$	111	+	−	−	+	−	+	+	−

Equation 2-20

X is now a Hadamard ordered Walsh matrix, and can be transformed using the Hadamard ordered fast Walsh-Hadamard transform $(FWHT)_h$ (refer Section 2.3.2.1), clearly the $(FWHT)_h$ is not dependent on the size of the input window, 3 in this example.

Recall that $X \cdot \vec{B} = \vec{R}$ (Equation 2-19). A solution of this equation, given knowledge of the response vector R and input matrix ensemble X, will be of the form $\vec{B} = X^{-1} \cdot \vec{R}$. Now recall Property 2 of the Hadamard matrix from Section 2.3.2.2 which states that $\vec{B} = X^{-1} \cdot \vec{R} = X^T \cdot \vec{R} = X \cdot \vec{R}$. Computing the binary kernel elements, given knowledge of the response vector R and input matrix ensemble X can now be reduced to a single $(FWHT)_h$.

2.4.3.1 Binary kernel procedure using Hadamard ordering.

1. Choose a window length, k, and generate a random stimulus sequence of length 2^k. Record the response and insert the sampled voltages values into an array of size 2^k. Each value is

added to the contents of the array at the address formed from the elements in the window when the responses is recorded. Example: if the stimulus in the input window at time t is 101 (for k=3) then the response R_t is placed in array address $(101)_2=5$. As the same stimulus may occur more than once it is necessary to count the number of times each binary address is used and divide the contents at the end by this number (that is, signal averaging, see Section 2.1).

2. Apply a Hadamard ordered, Fast Walsh Hadamard Transform $(FWHT)_h$ to the array.

3. The binary kernels are found in the transformed array at the addresses formed from their delay patterns. The number of 1's in the address is equal to the order, the spacing between the 1's gives the slice. Example: Second order kernel, first slice can be found at array address $3=(011)_2$ for k=3.

2.4.4 Calculation of Binary Kernels using m-Sequencing.

In the analysis in the preceding Section the test input configurations are chosen at random. But when test inputs are random, complete testing of the system can only be achieved by significant over-testing. It can be shown that if 2^k data points are recorded, for a window of length k, only about 63% of the locations in the array could be expected to be filled. In order to fill 95% of the array the test would have to be three times as long and there would be considerable redundancy as many of the configurations in the input window would be tested more than once (Sutter, 1992). It is clearly beneficial to reduce testing times as much as possible, in the retina the assumption of time invariance may only be valid for relatively

103

brief periods and the clinical environment does not lend itself to lengthy testing protocols.

An ideal input would test the system completely and without redundancy. This requires a binary sequence of length 2^k, where k is the window length, with the property that the content of a window of k consecutive elements assumes a unique configuration for each of the possible 2k shifts of the window along the cycle (Sutter, 1992). Such complete sequences do exists and one specific example is the m-sequence.

m-Sequences have been described in Section 2.3.3, what remains to be explained is how this is applied in VERIS.

2.4.4.1 Binary kernel procedure using m-sequencing.

1. Choose a window length, k, and initiate an m-sequence. The temporal modulation of the stimulus is derived from the first of the k stages in the m-sequence generating register. The recorded data point is stored in an array address specified by the contents of the generating register at the time the response is recorded. The same stimulus may occur more than once so it is necessary to count the number of times each binary address is used and divide the contents at the end by this number. (See 2.4.3.1, **1**.) This step is equivalent to multiplying the permutation matrix, P_c with the Hadamard matrix as described in Section 2.3.2.2., property **2** (Sutter, 1991).
2. Perform a $(FWHT)_h$ on the entire data array.

3. Initialise another shift register, called the tap register. Cross-correlation between the recorded digitised signal and the m-sequence used for stimulation is read from the binary array addresses specified by consecutive tap register configurations. This step is analogous to multiplying the transformed matrix with the second permutation matrix $\mathbf{P_r}^T$ as described in Section 2.3.2.2., property **2** (Sutter, 1991; Sutter, 1992).

2.4.4.2 Calculating the first order binary kernel.

The binary kernels are the solution of Equation 2-17 and Equation 2-18. The first order kernel is the linear response, where the test has consisted of a single input in the input window (that is, where the Generating Register has a 1 in the most right hand location and 0's everywhere else). It is calculated as the difference between the case when the input window goes from 0, no stimulus, to 1, stimulus on, and when it stays at 0, no stimulus. The derivation of the first kernel response is illustrated in Figure 2-7 for the case of a window length of three.
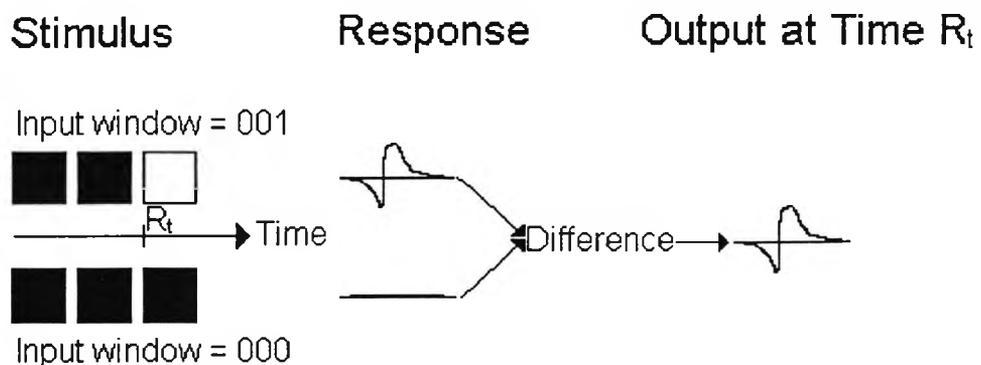
Figure 2-7. The derivation of the first kernel for the case of a window length of three. The response is the difference between the case when the input window goes from black to white and the case when it does not.

105

2.4.4.3 Calculating higher order binary kernels.

The second order kernels are calculated from all the cases where there are two inputs in the input window, and is the difference between the measured two-input response and the response predicted assuming nonlinearity, as illustrated in Figure 2-8.
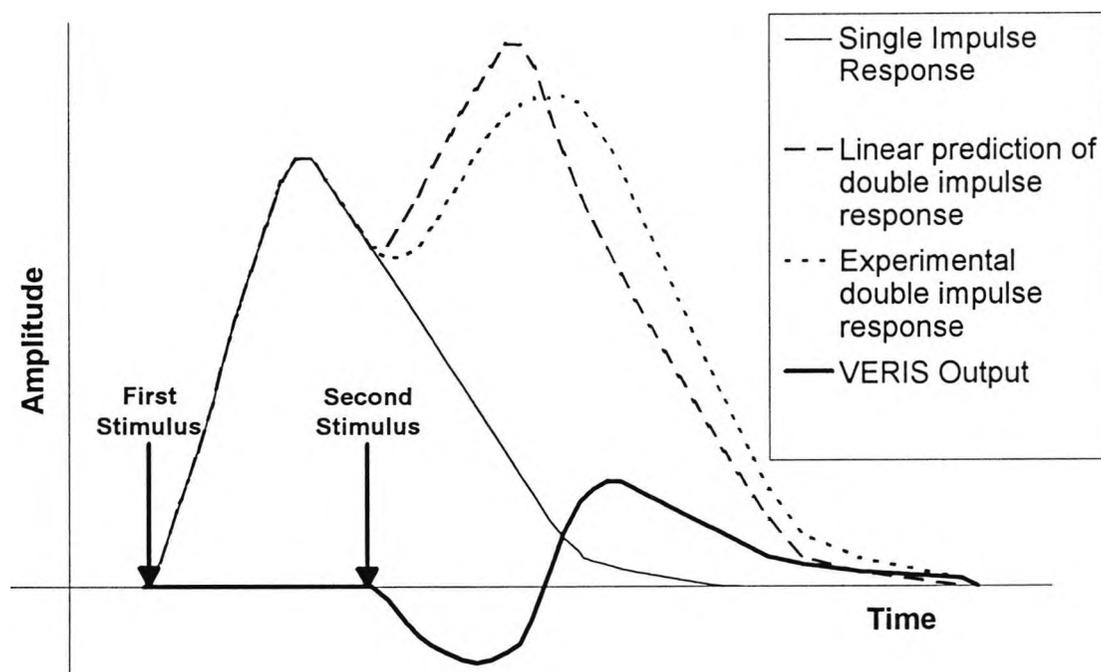
Figure 2-8. The second order kernel is the difference between the predicted double impulse response assuming linearity and the measured double impulse response. The time between the two stimuli gives the slice.

The slices of the binary kernel are given from the delay pattern of the inputs in the input window, so that the first slice has two inputs immediately juxtaposed in time, the second has two inputs with one time bin between them, the third slice has two inputs with two time bins between them, and so on. For example, a second order kernel is calculated as follows. The difference in response to a single input in each of the two input configurations is given a weighting of +1. The difference in response between two inputs in

the configuration and no inputs is given a weight of -1. The mean
of these two weighted differences is the output. Figure 2-9 shows
the calculation of the first slice of the second kernel, that is where
the input configuration is (011), for the case of a window length of
three.
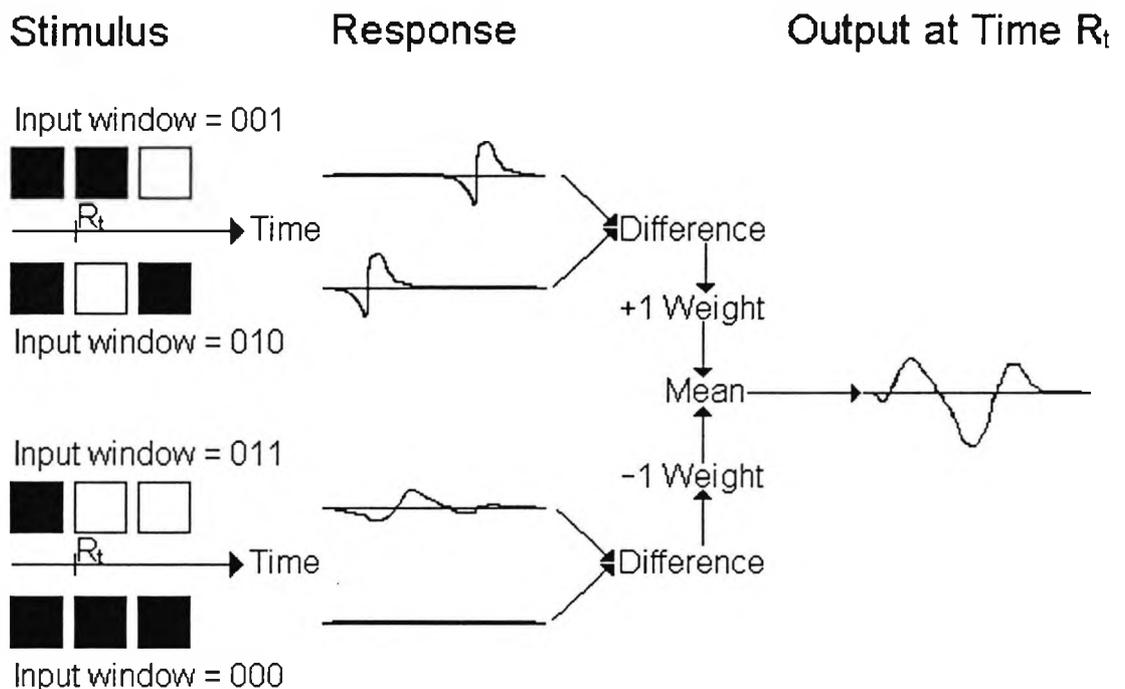
*Figure 2-9. Calculating the first slice of the second kernel for the case of a
window length of three. The difference between the response to the two
impulses presented separately is given a +1 weight. The difference between
the response to the double impulse and the response to no impulse is given a
-1 weight. The output is the mean of the two, weighted waveforms.*

2.5 Multiple Input Systems.

The visual system is a multiple input system where every receptor in the retina represents an input (if not an output). The lateral interaction between receptors and receptor channels is an integral part of the visual process. A knowledge of the topography of the mechanisms of lateral interaction are vital to an understanding of the processes that lead to integration of the visual scene and to visual recognition. VERIS is capable of multiple input analysis and can perform this simultaneously with nonlinear analysis.

2.5.1 Volterra Kernels and Multiple Inputs.

The testing of a system with multiple inputs is no different from testing a system with one (spatially) large input window that is the union of all the smaller input windows (Sutter, 1992). Consider a two input system where r and s are the window sizes of the two inputs, the Volterra expansion is:

$$R_t = K^{(0)} + \sum_{i=1}^{r} K_i^{(10)} x_i \qquad + \sum_{i=1}^{s} K_i^{(10)} y_i$$

$$+ \sum_{i=1}^{r} \sum_{j=1}^{r} K_{i,j}^{(20)} x_i x_j \quad + \sum_{i=1}^{r} \sum_{j=1}^{s} K_i^{(11)} x_i y_j \qquad + \sum_{j=1}^{s} \sum_{j=1}^{s} K_i^{(02)} x_i y_i$$

$$+ \sum_{i=1}^{r} \sum_{i=1}^{r} \sum_{k=1}^{r} K_{i,j,k}^{(30)} x_i x_j x_k + \sum_{i=1}^{r} \sum_{j=1}^{r} \sum_{i=1}^{s} K_i^{(11)} x_i x_j y_k + \cdots$$

Equation 2-21

The kernels of the multiple input expansion are simply segments of the kernels on the single input expansion in Equation 2-13 and can be computed by the same cross-correlation technique utilised in the

single input system described above..   The correspondence between Volterra kernels and binary kernels shown in Section 2.4.2.1 can be extended to the multiple input case.   As for the single input case, the binary kernel slices on the main diagonal cannot be extracted.

The choice of test configuration is even more important when there are many inputs.   With an increasing number of inputs the number of nonzero kernels that need to be spanned to complete the test can quickly approach the maximum number of data points that can be recorded in a given recording time.   Relying on chance to cover the test configurations for all the inputs could produce a test that would dwarf the age of the universe (Sutter, 1992).   m-Sequences therefore offer the best choice of test configuration for the multiple input experiment as all the nonzero kernels for all the inputs can be spanned completely and without redundancy.   The length of test required to cover all the nonzero kernels for all the inputs, for a given window length, can be determined exactly beforehand.

2.5.2 Overlap.

If the m-sequence is not chosen carefully then the cross-correlation procedure will confuse the kernels and create cross-talk between the inputs.   Segments of the kernels from one input will appear in the cross-correlation cycle of another input.   This is termed overlap.   The m-sequence must be carefully selected to avoid overlap between the inputs.   The method used by VERIS to select find the appropriate m-sequences involves checking each m-sequence in turn. For each m-sequence fill the input array with a

constant and perform the (FWHT)$_h$. Then sequentially extract each nonzero kernel slice for each input. Replace this kernel slice with zeroes. If any of the extracted kernel slices contain a stretch of zeroes then there has been an overlap. Repeat this for each m-sequence. When an m-sequence is found for which there is no overlap between nonzero kernel slices, orthogonality between kernels is guaranteed and the kernels for all the inputs can be computed exactly and without redundancy.

2.5.3 Generation of Stimuli.

Multiple input m-sequence stimuli can be generated in real time, as for single input experiments. It is simple to generate evenly spaced lags between each input. If the number of inputs is a power of two then the stimulus for each input can be generated from one m-sequence by a process of decimation (Sutter, 1992). So for a system with four inputs first digit will go to the first input, the second to the second input, the third to the third and the fourth digit to the fourth input. The fifth digit will go to the input that received the first, the sixth to the digit that received the second and so on; the ninth digit will then go to the first input etc. In this way each of the inputs receives the same m-sequence, the lag between each input is the same and all the inputs remain orthogonal to each other.

110

2.5.4 Noise Considerations and Artefact Removal.

Contamination of the response can be due to two sources. One source is noise (almost always a sinusoid with a fundamental at 50Hz and with higher harmonics but conceivably random) from nearby electrical installations. Another source of noise is discrete noise that is located non-randomly in the response and is chiefly due to blinks and eye movements.

2.5.4.1 Random noise.

Contamination of the recorded response due to random noise will be spread equally over the response vector. The contents of the response vector will be the sum of signal and noise vectors. The $(FWHT)_h$ is a linear transform and will preserve the RMS of the noise. The $(FWHT)_h$ will act on the signal and noise vectors independently and preserve their power. After the response vector has been transformed into the kernel vector the noise will be spread equally throughout the kernels whilst the signal power will be contained in just a few kernels. The higher the degree of nonlinearity in the system, the larger are the number of kernels that are of interest. A large number of kernels will require a longer data set to detect the signal from the noise. A longer data set will repeat stimulus configurations. Each time a stimulus configuration is repeated it is placed in the same address in the response array and a count is kept of the number of repeats that have occurred. The final response is divided by the number of repeats to achieve an average response. This is no more than signal averaging and has been considered in Section 2.1. Each time the stimulus is

111

repeated the signal to noise ratio increases by a factor of $\sqrt{2}$. A longer m-sequence length will have more stimulus repeats and more averaging and so an increased signal to noise ratio.

2.5.4.2 Discrete Noise.

In traditional electroretinogram recordings artefacts in contaminated sections of recordings are excised. However, in a deterministic system, a complete record of the response over the stimulation cycle is needed to perform the cross-correlation and calculate the kernels, so excising sections of response is not an option. Another technique for artefact removal is possible, relying on three aspects of VERIS recordings. Firstly, the artefacts are localised in the raw data whilst the response is localised in the kernel domain; secondly, most of the kernels are zero and contain no ERG; thirdly, the $(FWHT)_h$ can be performed backwards as well as forwards. The procedure is as follows: Take the data in the kernel domain and set all the slices that contain no ERG to zero (these kernels must be stipulated beforehand). Back transform all the kernels into the raw data, and a proportion of the artefact voltages should now have gone, but the signal should be largely unchanged (the zeroed slices had no ERG in the first place). The artefacts in the original data can be detected by comparison with the back transformed data. Contaminated sections of response in the original data can then be replaced with the new data. The replacement is based on a section of data from which an artefact has been (partially) removed: it is not an average nor an estimation based on any part of the data other than the section that was contaminated.

2.6 Nonlinear Components of the Electroretinogram.

Flicker electroretinograms, evoked by sinusoidally modulating stimuli, have been studied to improve our understanding of the retinal processes underlying the generation of the electroretinogram by analysing the nonlinear components of the responses they evoke.   The frequencies contained in the sine wave stimuli will be unaltered by a linear system but a nonlinear system will introduce higher harmonics and/or sub-harmonics to the output.   The power contained the additional frequencies is contributed by the nonlinearity.

2.6.1 Nonlinearities evoked by Pattern and Uniform Field Stimuli.

Both the flicker ERG and the PERG contain nonlinear components, but are they derived from the same retinal source?

Porciatti (1987) has shown that in cases of retinal ischemia the second harmonic of both the uniform field flicker ERG (at 20Hz) and the PERG were reduced.   However, in optic atrophy and optic neuritis the second harmonic of the flicker response was unchanged, whereas the PERG was clearly affected.   Porciatti suggested that these results indicated that the sources of the nonlinearities in the flicker ERG and PERG were partly separate and partly shared.

Porciatti's conclusion has been supported by Baker et al. (1988) in their current-source density analysis.   Baker et al. found that the arrangement of current sources and sinks in the PERG was similar,

113

but not identical, to that of the uniform field second harmonic. The PERG had a prominent source-sink pair in the ganglion cell layer, whereas the uniform field flicker nonlinear response was located partly in the photoreceptor layer and partly in the region of the inner plexiform layer/ganglion cell layer.

2.6.2 Nonlinearities - A systems analytic approach.

It is possible to model the retinal circuitry that affects the uniform-field flicker ERG in terms of a circuit of electronic rectifiers and filters. Responses to different flicker rates can be modelled by filters that can be low pass, band pass or high pass. For example, the phenomenon of flicker-fusion, in which above a critical frequency a flickering stimulus becomes a fully uniform and continuous sensation (Cline et al. 1997), indicates the existence of a low pass filter somewhere in the visual system. In the systems analytic approach nonlinearities within the retina are modelled either as compressive or rectifying. Compressive nonlinearities place a limitation to the dynamic range of the response, for example, the Naka-Rushton function. Rectifying nonlinearities, for example, the response of an ON bipolar cell to a hyperpolarising photoreceptor can be modelled as a half wave rectifier, and the response of an ensemble of ON and OFF bipolar as a full wave rectifier, are nonlinearities that are active even for small signals. Circuits of filters and rectifiers can be constructed to model the retina, based on the characteristics of the linear and nonlinear responses recorded at a range of flicker rates and depths. The model may consist of elements in series (as cascades) or in parallel.

114

Odom et al. (1992) has modelled the retinal response with three parallel series of filters and rectifiers. At low frequency (>10Hz) a low pass filter is sufficient to model the response. At intermediate frequencies (~20Hz, and therefore above cone threshold) the response could be modelled with a bandpass filter followed by a rectifying nonlinearity. Higher frequencies (~40Hz) could be modelled as a high pass filter in series with a rectifying nonlinearity. Burns et al. (1992) have found that at high flicker rates (~100Hz), similar to those used in VERIS, the nonlinearities are most closely modelled by a rectification type nonlinearity. However, the possibility of compressive nonlinearities cannot be dismissed: Shuang et al. (1995) have identified a compressive nonlinearity in the outer retina.

2.6.3 Kernel analysis of the flash ERG and PERG.

Kernel analysis of the ERG and PERG, using VERIS, has been undertaken. Vaegan and Sutter (1990) have confirmed that the ERG has power in only a limited number of kernels (refer Section 2.4.1.1). The PERG has a symmetrical, even stimulus and has no response in odd kernels, so the PERG first, third, fifth etc. order kernels are flat. The flash ERG has an odd stimulus and has power in every kernel. However, the power in both the flash ERG and PERG is mostly in lower order kernel responses and falls off rapidly as the nonlinearity, viz. the kernel order, increases. Sutter and Vaegan (1990) found that the flash ERG has no detectable power in kernels higher then the third and the PERG has no detectable power in kernels higher than the second. The authors established that the flash ERG second kernel does not derive from

the same source as the PERG second kernel because the two waveforms are different shapes.

Sutter and Vaegan have studied the relative contributions to slices of the second order kernel of the pattern and luminance components of the PERG (Sutter and Vaegan, 1990). The authors have found that the first slice of the second kernel varies with check size while the second and subsequent slices do not. The response in the second and subsequent slices could be eliminated entirely by subtracting them from the same slice of the second kernel of the flash ERG, leaving a pure pattern specific response. This suggested that a pattern specific component, with virtually no memory, contributes to the first slice whilst that the local luminance response is found in all slices (Sutter and Vaegan, 1990). This result is of great interest clinically. The second kernel slices of both flash ERG and PERG could be extracted very quickly and the pattern specific component isolated by a simple subtraction.

Kondo et al. (1998) inserted filler frames in the VERIS stimulus to slow down the linear response of the flash ERG and separate the OFF response from the a-/b-wave complex of the ON response. They found that the response density of all the components (a- and b-wave and OFF response) decreased with increasing retinal eccentricity, but that the ratio of OFF/b-wave and OFF/a-wave increased towards the periphery. Kondo et al. thought that this may reflect a change in photopic retinal circuitry with increasing retinal eccentricities, and suggested that these results might even imply rod contribution to peripheral responses.

Hood et al. (1997), studying the flash ERG, have compared the first positive peak of the VERIS linear response to the b-wave of a 'traditional' photopic electroretinographic recording, elicited with flashes in a Ganzfield dome. Hood et al. found that after inserting black filler frames into the m-sequence to slow down the stimulus rate the positive deflection of the VERIS linear response and the b-wave of a photopic electroretinogram covaried in amplitude and latency with changes in background and increment stimulus luminance. Hood et al. interpreted this result as indicating that the neural substrates that are responsible for generating the b-wave also give rise to the first positive peak of the VERIS linear response.

An identical conclusion has been reached by Horiguchi et al. (1998) using synapse blocking agents (see 1.2.5.1) on rabbit, they found that APB (which blocks ON bipolar response) reduced the b-wave of the photopic electroretinogram and the first positive deflection of the first kernel response. PDA (which blocks OFF bipolar cell response) reduced the a-wave of the photopic electroretinogram and the first negative response of the first kernel response. The implication of these results, and those of Hood and Kondo discussed above, is that the a- and b-wave of the photopic electroretinogram have similar origins as the first two deflections of the first kernel.

Horiguchi et al (1998) also studied the effect of synapse blocking drugs on the second order kernel. GABA and glycine, which have been shown to suppress oscillatory potentials (see Section 1.2.7), had the effect of diminishing the amplitude, but not the shape of the

response.   This result might imply that the second kernel shares its source with oscillatory potentials, which are thought to arise in the inner retina (see Section 1.2.7.1).   APB and PDA also reduced second kernel responses, suggesting that normal outer retinal function is required for normal second order kernels to be evoked.

3. Installing VERIS.

This chapter will cover the issues involved in installing VERIS.
VERIS ran on a Macintosh Centris 650 computer which contained a
customised video card producing patterns on a 21in monitor,
termed the stimulus monitor.   The computer possessed the usual
peripherals: monitor, keyboard, mouse and printer.   The ERG was
amplified and filtered in an isolated differential amplifier, and the
amplifier output signal fed to an analogue-to-digital converter (ADC)
in the computer via a shielded cable.   The amplifier was powered
by a regulated power-supply.   Computer, monitors, printer and
amplifier power-supply were all powered from the mains via a surge
protecting and filtering extension cable.
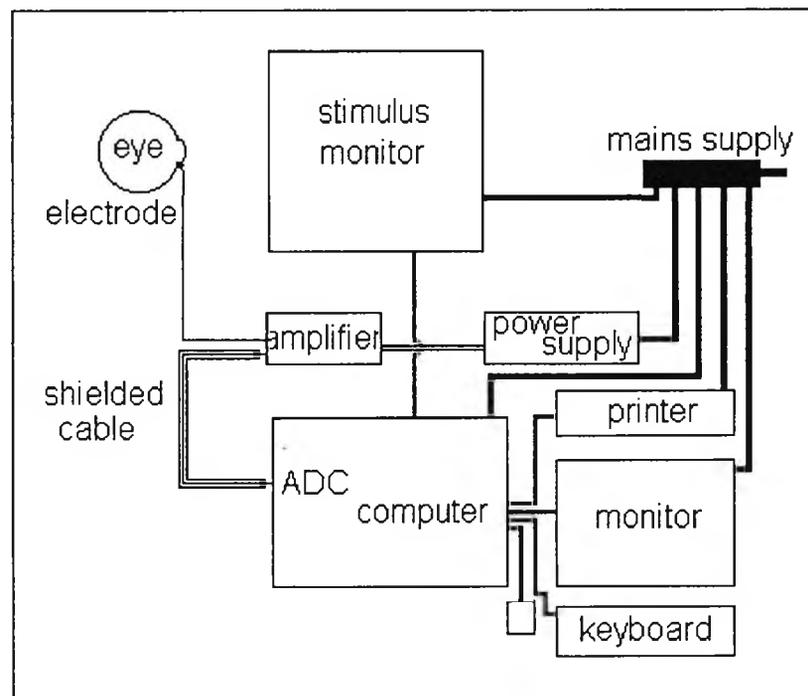
*Figure 3-1   Schematic illustration of the hardware utilised by VERIS.   Only
the active electrode is illustrated, although in practice three (earth, active and
reference) are used.*

3.1 Hardware Devices to Enhance Signal-to-Noise Ratio.

This section will consider the hardware devices that were used to maximise the signal-to-noise ratio before the signal was registered and software manipulation became an option.   Methods to enhance the signal-to-noise ratio that can be implemented in software were covered in the previous chapter.   The largest source of noise, in terms of amplitude, is interference from mains power lines, which is characterised by a fixed 50Hz periodicity.

3.1.1 The Amplifier.

The amplifier used in these experiments was an isolated, differential amplifier (Hogg, 1998).   Isolated amplifiers ensure that the subject cannot be electrically connected to the mains via the amplifier power supply under any circumstances.   Differential amplifiers use operational amplifiers in a circuit with three inputs (active, reference and ground) and two outputs (amplified signal and ground).   The circuit amplified the difference between the active and reference inputs whilst rejecting any signal that was common to both.   The ground input was connected to an electrode placed on the subjects forehead to create a reference level of 0 volts.   The active input carried the voltage measured at the cornea whilst the reference input carried the voltage measured the outer canthus.   When the voltage change between the two inputs was the same in magnitude and time the output voltage gain was less than one, when the voltage change between the inputs was different the gain was about 100,000.

3.1.2 Faraday Cage.

Op-amps failed to remove all the 50Hz contamination of the corneal signal. A more robust method was used to physically shield the electrode wires from the mains interference. The concept of shielding is based on the Faraday ice pail experiment, that demonstrates that there is no charge on the inside of a closed, hollow conductor. Extending this concept to shields requires that the walls be of such thickness and electrical conductivity that there is no leakage of field through the shield-wall (Thornton, 1991). The Faraday cage dramatically increased the signal-noise-ratio of the signal, particularly for noise in the 50Hz region.

3.1.2.1 Design and Construction of the Faraday cage.

The aim of the Faraday cage was to divide the laboratory into two parts, one containing the source of the noise and the other the receiver (Thornton, 1991). Some of the noise sources could be surmised, for example mains power points and the stimulus monitor, but the full complexity of the loci of noise sources around the lab was unknown. The option was taken to shield the subject, electrodes, electrode wires, and amplifier from the rest of the room, leaving a hole in the shield through which the stimulus monitor could be viewed.

The dimensions of the Faraday cage were: depth=915mm, breadth=760mm, height=1750mm, permitting enough space inside the shielded area for an adjustable chair and a frame to support a chin-rest. The chin-rest and the window in the Faraday cage for

121

the stimulus monitor set the viewing distance at 40cm. The
Faraday cage was constructed from a frame made of hollow,
square-section, plastic coated mild steel tubing, slotted into
preformed corner pieces that provided rigidity (trade name
'Speedframe', supplied by Duval Products, London, UK). The ideal
shielding material for a Faraday cage is continuous sheets of a low
resistivity metal, like copper (Thornton, 1991). However, the
Faraday cage was small and it was feared that such an enclosed,
dark space might induce feelings of claustrophobia in the subjects.
Instead, a twofold approach to the shielding material was taken.
On the two sides that faced the wall the shield was formed from
3mm thick copper sheet. The shield on the other sides was
formed from of ¼ inch galvanised steel mesh. On the roof, floor
and one side that faced into the room one layer of mesh was used.
One the side that faced the computer and peripherals, a potential
source of noise, the shield was reinforced with a second layer of
mesh. In both cases, the shielding material was fastened onto the
frame with self-tapping steel screws. The mesh enabled the
experimenter to watch the subject whilst an experiment was in
progress, and it allowed light to enter and air to circulate through
the cage. One mesh-side was penetrated by a square hole
through which the stimulus could be viewed. The hole was the
same dimension as the stimulus monitor. The stimulus monitor
screen was placed in the vertical plane of the mesh so that the
stimulus filled as much of the subjects visual field as possible while
keeping the monitor, a significant source of noise, outside the
screened area. Another mesh-side formed a hinged door. The
chin-rest was supported on a cradle suspended from the roof of the
Faraday cage. The chin-rest was adjustable so that the subject's

head could be supported in comfort, encouraging them to concentration and fixate steadily. The amplifier was placed on the chin-rest.
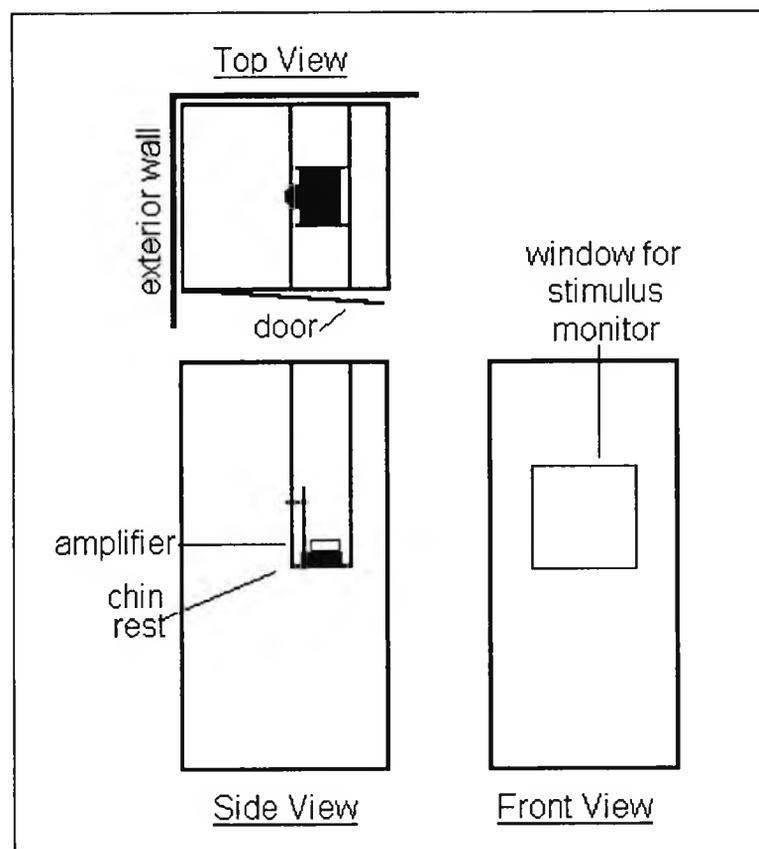
Figure 3-2   The Faraday cage showing the chin-rest and amplifier in situ.

Change in noise response due to Faraday cage
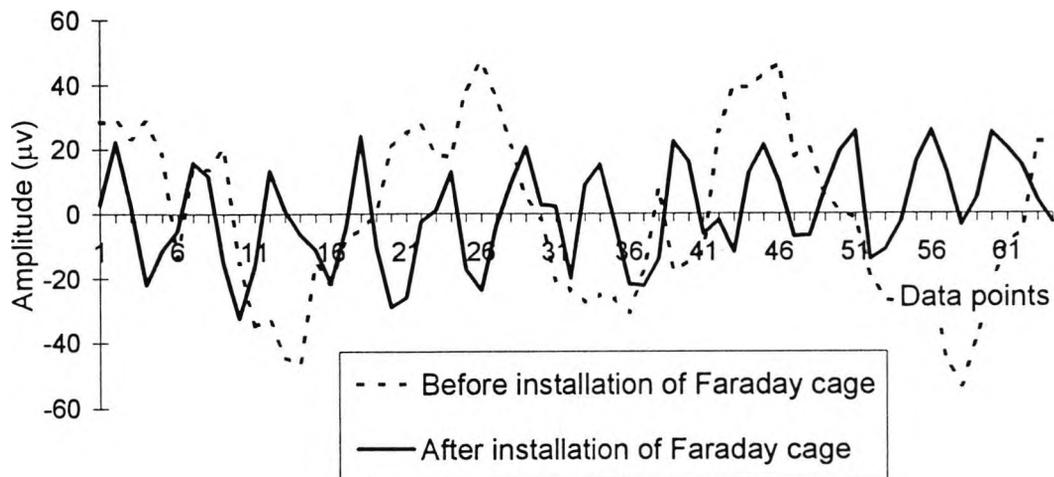
Figure 3-3. These responses were obtained with 10KΩ resistors placed across the amplifier terminals to achieve a pure noise response, without any corneal signal. The Faraday cage completely removed a low frequency component at about 50Hz but left a smaller amplitude component at about 240Hz which may have arisen in the fluorescent lighting. Abscissa scale is data points where one data point = 0.83ms. Ordinate scale is in microvolts, the magnitude of the resistance across the amplifier terminals does not match the physiological conditions, so the amplitude of these responses bore no relation to the amplitude of the noise in an electroretinographic recording.

3.2 Pharmacological Aids to Enhance Signal-to-Noise Ratio.

Drugs may be used which, although not directly affecting the signal to noise ratio, have the effect of increasing the signal power or decreasing the noise power. The drugs complement the hardware and software based approaches already considered.

3.2.1 Pupil Dilation.

The signal-to-noise ratio can be improved by increasing the diameter of the pupil. A larger pupil will admit more light and evoke an increased response from the retina.

3.2.1.1 Choice of Mydriatic.

Many mydriatics are available. These experiments required a preparation that would act quickly for a relatively short duration - no more than 20 minutes of mydriasis were required. Tropicamide is dispensed in 0.5% or 1% w/v, and in convenient, preservative free, single use capsules, called minims. Tropicamide 0.5% was chosen for use in these experiments: it takes about 20 minutes to act and lasts for 2 to 3 hours. The pigment cells in the iris bind with the mydriatic and if there are many pigment cells the action of the drug may be lessened, so in black and Afro-Caribbean subjects another mydriatic was required. Phenylephrine hydrochloride is a mydriatic with a more considerable effect than tropicamide 0.5%. In the case of well-pigmented subjects both drugs were instilled.

3.2.2 Corneal Anaesthesia.

The importance of blink-artefact free recordings has been discussed in 2.5.4. The signal-to-noise ratio may be improved by reducing the number of blinks and the amplitude of their artefact in the response, by the use of a topical corneal anaesthetic. A popular anaesthetic termed benoxinate 0.4% was used. Benoxinate 0.4% has a duration of effect of 20 minutes from a few

seconds after instillation. The anaesthetic could be instilled moments before the experiment begun and lasted almost exactly as long.

3.3 Electrodes.

Two different kinds of electrode were used in these experiments. The skin electrode was used as reference and ground electrode (see Section 3.1.1). The corneal electrode was placed on the cornea to measure the difference in potential between the cornea and the skin.

3.3.1 Skin Electrodes.

The skin electrodes used were 8mm silver-silver chloride (Ag-AgCl) cup-shaped disks. First, the skin local to the electrode position was cleaned with an abrading paste. Then a small volume of a water-based conducting gel was placed between the skin and the electrode. Finally, the electrode was pushed onto the skin and held in place with 'micropore' tape. A small hole was present in the centre of the cup, so that when the electrode was pushed onto the skin the excess gel vacated the electrode site through the hole, rather than around the edge of the disk, and forced the tape away from the skin and skin-electrode. If the ohmic impedance between the two electrodes was greater than $5K\Omega$ the electrodes were removed and re-placed.

126

3.3.2 The Corneal Electrode.

The choice of corneal electrode will have a considerable influence on ERG amplitude and between-test repeatability, and on the appearance of artefacts due to blinking. Electrode materials, size and surface contact geometry all influence the recorded response.

3.3.2.1 Overview of Corneal Electrodes Available.

Many types of corneal electrode are available, but three, the Burian-Allen, gold-foil and DTL, are the most popular. The Burian-Allen electrode is a contact-lens electrode. The contact lens is mounted in a speculum and sits directly on the cornea. The contact lens must be sterilised between use. The gold-leaf electrode (Arden et al. 1979) is a thin, oblong piece of insulating mylar, coated with gold on one side. The electrode is hooked over the lower lid with the insulated side against the lid. One end is suspended into the lower conjunctival sac to anchor the electrode, the other end makes electrical contact with the cornea through a saline bridge at the limbal-scleral junction. The DTL (Dawson, Trick and Litzkow) electrode (Dawson et al. 1979) consists of a fine filament of Ag-AgCl coated nylon. The filament is draped across the cornea and, like the gold-foil electrode, electrical contact is achieved through a saline bridge on the limbal-scleral junction.

3.3.2.2 Factors Affecting Corneal Electrode Choice.

Several papers have compared different electrode types in terms of ERG amplitude, repeatability and subject comfort. The ERG

recorded from the Burian-Allen electrode was larger than the gold-foil (Gjotterberg, 1986; Esakowitz et al. 1993) and larger than the DTL (Esakowitz et al. 1993) in both photopic and scotopic conditions (Esakowitz et al. 1993), although the latency was constant between electrodes (Gjotterberg, 1986; Esakowitz et al. 1993; Hennessy and Vaegan, 1995). The DTL electrode had less inter-session variability than any other type (Hennessy and Vaegan, 1995). The DTL electrode was considered the most comfortable by the subjects (Esakowitz et al. 1993) and more comfortable than the gold foil (personal experience). DTL electrodes could be constructed cheaply in the laboratory and be disposed after each use. Contact lens electrodes involved a prohibitive one-off capital cost to purchase and must then be sterilised between uses. DTL electrodes were elected for use because they had almost the best response amplitude, were reliable, were comfortable to wear and offered the facility of being constructed in-house.

3.3.2.3 Constructing DTL electrodes.

Dawson, Trick and Litzkov (Dawson et al. 1979) used DTL electrodes in which only one end of DTL fibre was fixed to the patient's canthus, at the junction with the electrode lead, whilst the other end was placed over the cornea. The disadvantage of this design rests in the extremely low mass of the DTL fibre, which sometimes slipped into the sub-conjunctival sac (where the ERG potential is smaller) and sometimes wandered from the eye all together, but always required considerable dexterity and patience to handle. Riemslag has improved the design by using a Y-shaped electrode lead. The DTL fibre is suspended across the two short

ends of the 'Y'. In these experiments the electrode was secured to the patient by double-sided adhesive pads placed on the canthi. Electrode leads were constructed from a metre length of 2mm insulated wire, with a 2mm jack soldered to one end and two 10cm . lengths of 2mm wire soldered to the other, so forming the Y-shape. A 3mm length of tinned wire was left at the two short ends of the 'Y'.

A jig for constructing the electrodes was formed from a foam strip with a 2.5cm^2 cross-section and with 2, 0.5cm deep incisions right across the strip about 3cm apart. The two short ends of the Y-shaped electrode leads were pushed into the slits in the jig, leaving the tinned ends protruding from the strip.   The distance between the slits gave the size of the electrode (the distance across the top of the 'Y'), which had to match as closely as possible the inter-canthus distance of the subject (see Figure 3-4).   In practice, it was convenient to construct several electrodes of different sizes simultaneously, by having many slits cut in the jig.   The DTL fibre was anchored to one end to the jig with adhesive tape, enabling some tension to be maintained whilst the fibre was woven twice around the tinned, electrode lead ends.   A drop of silver conductive paint (supplied by R.S.) was applied to the DTL fibre/electrode lead junction to form a solid and conducting join.   The electrodes were left to dry for 24hrs, before the DTL fibre between the electrodes was cut away.   Figure 3-4 shows three finished electrodes in a jig.
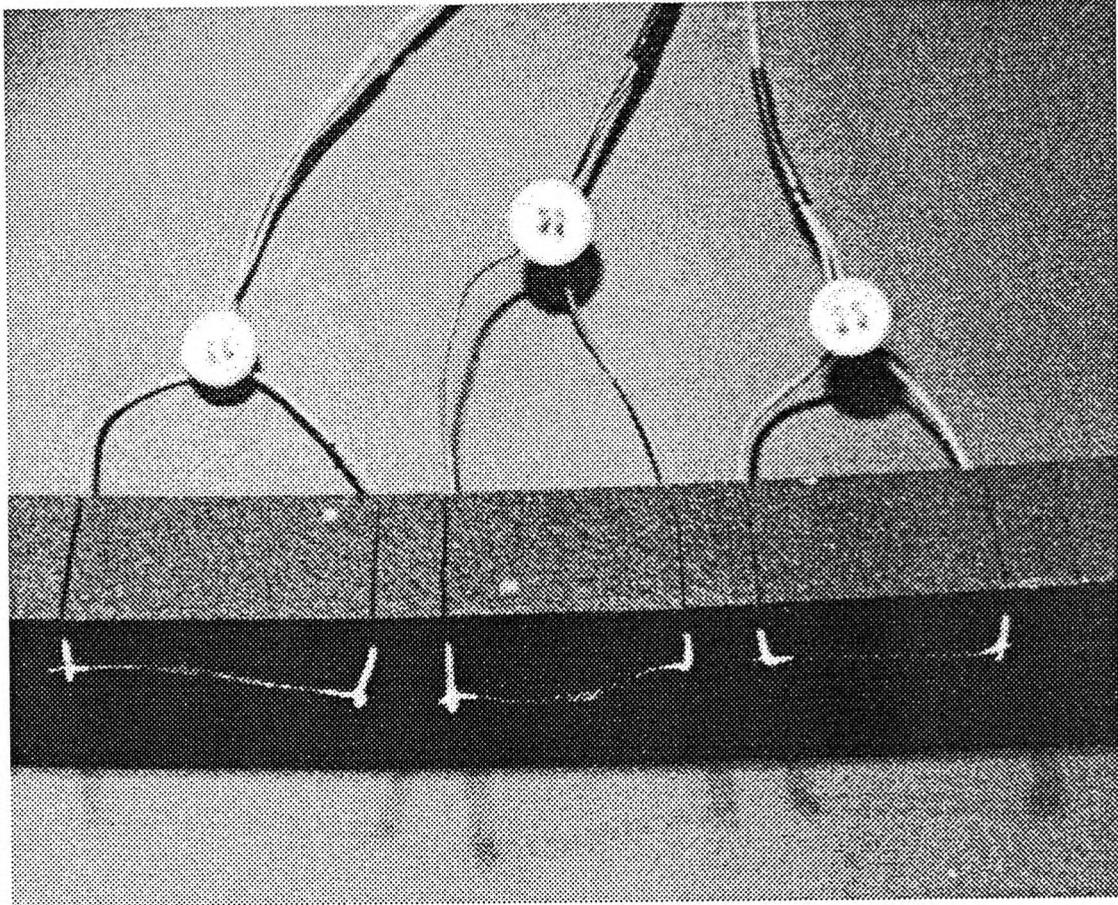
Figure 3-4   Three DTL electrodes mounted in a jig.   Distance between incisions in the jig gives electrode 'size'.   Several electrodes could be constructed simultaneously in the jig, and stored there until required.

3.4 Recording Parameters.

3.4.1 Stimulus Configuration.

VERIS is supplied with a choice of stimulus configurations that are intended for electroretinography, and all consist of an array of hexagons.   Each hexagon evokes a response from a focal patch of retina.   A distinction is made between the number of hexagons in the stimulus and the number of inputs for which VERIS can extract the responses.   The number of inputs must be a power of four and must be higher than or equal to the number of hexagons, if overlap is to be avoided (see 2.5.2).

3.4.1.1 Number of hexagons.

A stimulus composed of many hexagons that evoke a separable response will allow spatial resolution of retinal function.   The greater the number of hexagons, the smaller the projected retinal area of each hexagon and hence the smaller the electroretinographic response.   A stimulus configuration with fewer hexagons therefore has better signal-to-noise ratio characteristics but provides a coarser resolution of the topography of retinal responses.   VERIS stimulus configurations have either 61, 103 or 241 hexagons.   The 103 hexagon stimulus was chosen as it produced a sufficient signal-to-noise ratio for details in the ERG to be perceived, whilst tiling the retina more finely than most static perimeters.

3.4.1.2 Stimulus tile scaling.

VERIS tile configurations are an array of hexagons that are either scaled or unscaled. Unscaled arrays have hexagons all the same size, whereas scaled arrays (see Figure 3-5) have hexagons in the centre of the visual field scaled down compared to hexagons at the edge. Larger hexagons at the edge of the visual field evoke a response from a larger patch of the peripheral retina than central hexagons evoke from the macula. There are fewer neurones in the periphery than in the macula so the signal response and the signal-to-noise ratio from this region are smaller (Drasdo et al. 1987). By scaling the hexagons the stimulus causes a more equal number of neurones to be excited and the variations in signal-to-noise ratio to be evened out across the visual field.
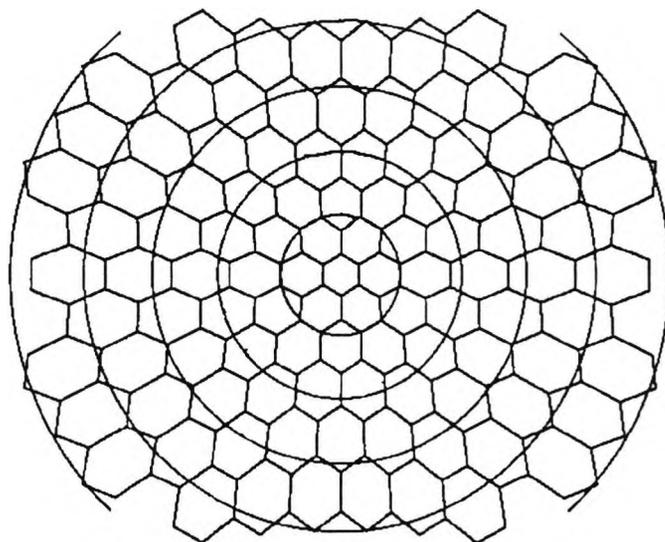
Figure 3-5   The stimulus configuration used in all the experiments consists of 103 hexagons scale so that peripheral hexagons stimulate larger areas of retina than central ones.   The response per unit area is smaller in the periphery so this stimulus helps to reduce the difference in signal-to-noise ratio between responses from the various areas of retina.   The central hex covers the fovea. Lines of equal eccentricity are shown at 5° intervals.

132

3.4.1.3 Fixation target.

If the results evoked with multiple input stimuli are to be meaningful the subject must preserve fixation.   VERIS allows some choice in   . fixation target - crosses, circles and squares of any colour can be used, and may be positioned on any part of the stimulus monitor screen.   These experiments used a red cross placed in the centre of the central hex as the fixation target.   It was found that a red cross stood out clearly from the hexagon, whether it happened to be ON or OFF.   With good acuity individual pixels could be identified in the pattern of the fixation target.

3.4.2 Stimulus Rate.

The VERIS software uses a computer monitor to provide the stimulus.   Computer monitors offer the ability to manipulate a pattern very rapidly, permitting many m-sequence inputs to be controlled simultaneously.   The frame rate is the frequency at which the entire monitor screen in redrawn.   VERIS software demands that the monitor frame rate be set equal to, or a submultiple of, the stimulus rate, the rate at which the m-sequence moves through its successive steps.   In these experiments the frame rate was equal to the stimulus rate (see Section 3.4.6.3). The stimulus monitor had variable frame rate and could be driven at a wide range of frequencies, but the video card supplied with VERIS was limited to a frame rate of either 67 or 75Hz.   A stimulus rate of 75Hz was chosen as the m-sequence step rate to achieve as short a test duration as possible.

3.4.3 Stimulus Contrast.

The largest electroretinographic signals are achieved with high contrast stimuli.   In VERIS the stimulus is binary and has only two levels, ON or OFF, with corresponding luminances I_{ON} and I_{OFF}.   In this case contrast may be defined as:

$$\text{Contrast} = \frac{I_{ON} - I_{OFF}}{I_{ON} + I_{OFF}}$$

Equation 3-1

where luminance is the intensive property of the emitted light flux per unit of projected area and is measured in candela per metre-squared.

3.4.3.1 Monitor gun settings.

The VERIS program allows control over the brightness of each of the guns (RGB) of the monitor.   A photometer was used to find the settings that gave the maximum luminance output from the monitor when the stimulus was ON.   The internal values for brightest good white were: R=63172, G=65535, B=64208.   At these settings and with the monitor settings (see 3.4.3.2) at maximum the monitor luminance output was 173cd/m^2.

3.4.3.2 Monitor 'brightness' and 'contrast'.

The stimulus monitor was equipped with controls termed 'brightness' and 'contrast', although the words do not correspond to

134

the conventional definitions. The 'brightness' control set the output of the guns when the input from the computer is zero. The 'contrast' control set the gain on the gun output, and thus the maximum luminance available (Mollon and Baker, 1995). Some interaction between the two controls was observed. Monitor settings had to be found that gave maximum ON luminance at minimum OFF luminance to achieve the highest contrast possible. The luminance output of the monitor at a range of 'contrast' settings with the 'brightness' setting on 'full' were measured.

Monitor 'Contrast'	ON luminance cd/m^2	OFF luminance cd/m^2	Measured Contrast
1=max	173	6.7	93%
2/3	139	0.5	99%
1/3	78	0.1	99%

Table 3-1   The ON and OFF luminance at three monitor 'contrast' settings. Monitor 'contrast' is the contrast setting on the stimulus monitor as a proportion of its maximum setting.   The measured contrast is the actual contrast of the monitor output as calculated using Equation 3-1.

The 'contrast' setting that offered the highest measured contrast with the highest ON luminance was 2/3 and so that the ON luminance output was 139cd/m^2 and the OFF luminance output was 0.4cd/m^2. These settings were used in all the experiments.

3.4.3.3 Monitor Calibration.

The monitor was recalibrated every 6 weeks, during those episodes of the three year research period where VERIS was being used.

Calibration involved turning the monitor 'contrast' to its highest value and then reducing the 'contrast' until the ON luminance of the centre hexagon was 139.0±0.4cd/m^2. The m-sequence was then advanced until the centre hexagon was OFF and the luminance was measured again. If the contrast was now 99.0±0.4% the calibration was completed, if the 'contrast' had to be adjusted again, the m-sequence was then advanced to a position where the centre hex was ON and the luminance was measured again. The procedure was repeated until the ON luminance was 139±0.4cd/m^2 and the contrast was 99±0.4%, permitting an OFF luminance in the range 0.4-1.0cd/m^2.

3.4.4 Filters.

Filters attenuate components of the signal whose frequencies are above (low pass filters) or below (high pass filters) a particular threshold, or within a small wave band (band-stop filters). These experiments used two filters to bandpass the frequency content of the human corneal ERG (Asi et al. 1992). The high pass filter was a simple RC filter (6dB/octave) at 0.7Hz, the low pass filter was a two pole Bessel filter (6dB/octave) at 120Hz (Hogg, 1998).

3.4.5 Sampling Rate.

The sampling rate is the frequency with which the incoming analogue corneal signal is converted into digital values by the ADC card. VERIS allows the sampling rate to be set as a proportion of the frame rate, at either 1, 2, 4, 8, or 16 samples per frame. Any continuous signal may be recovered from its sampled version as

136

long as the sampling frequency is at least twice the highest frequency of interest in the signal. At the frame rate of 75Hz, 16 samples per frame led to a sampling rate of 1.2kHz, which allowed resolution of all electroretinogram components up to 600Hz, comfortably beyond the upper limit of the frequency content of the human corneal ERG (Asi et al. 1992).

3.4.6 m-Sequence Parameters.

The m-sequence parameters are several and interrelated. They are set on the VERIS software and influence the window length.

3.4.6.1 m-Sequence Length.

The m-sequence length determines the duration of the test and so governs the amount of signal-averaging performed. The longest m-sequence that VERIS offers is 2^{16}-1. A long m-sequence is undesirable, because it leads to extended testing times, but the 2^{16}-1 m-sequence was chosen for these experiments in order to maximise the signal-to-noise ratio. 2^{16}-1 m-sequence steps at 13.3ms per step gives a base test time of 14.56 minutes, although the actual test time was slightly longer than this (see Section 3.4.6.4).

3.4.6.2 Number of kernels and inputs.

The limit on the number of kernels of interest was set to 3 (both even and odd numbered kernels) based on the evidence in Sutter

and Vaegan (1990) that there is no power above the third order kernel or the second slice.

The number of inputs had to be a power of four, to enable the decimation of the m-sequence among the inputs whilst maintaining orthogonality (see 2.5.3), and had to be at least equal to the actual number of inputs in the stimulus array, which was 103 (see Section 3.4.1.1). Therefore, the number of inputs had to be 128. With these parameters the window length was 10 m-sequence steps, or 133ms at 13.3ms per step.

3.4.6.3 m-Sequence frames

VERIS permits the introduction of frames within each m-sequence step. A single ON step could be replaced by two ON frames, for example, or by an ON OFF ON pattern. Each additional frame increases the test duration, so the ON OFF ON stimulus pattern would lead to a test three times as long. As the m-sequence length chosen had already created a long test, it was not possible to extend the test further with additional m-sequence frames.

3.4.6.4 Tap word.

The VERIS software includes a programme for testing each tap word (see 2.3.3) to find which, if any, is suitable for the chosen recording parameters. Running the programme for the parameters laid down above found 6 tap words that did not have overlap (see 2.5.2). Although any and all of these tap words would have brought about the same test and the same results, the same tap

138

word was used for all the experiments. Tap word number 224611 was chosen at random from the 6 candidate tap words.

3.4.7 Segments and Pre-Exposure m-Steps.

It is impossible to expect a subject to refrain from blinking for the entire duration of a 14.56 minute test, so VERIS breaks up the test into segments. Between each segment there is a is paus to give the subject a rest from concentration and a chance to blink. Each segment begins with pre-exposure m-steps, in which random ONs and OFFs start stimulating the retina, before a short section of m-sequence from the end of the previous section is used to adapt the retina to the light level at which the previous segment ended. Then the new segment m-sequence starts and recording commences. The number of pre-exposure m-steps must be kept as small as possible, as they increase test-time. The number of segments is dependent on the duration that the subject can refrain from blinking, but each segment increases test time so the use of very short segments is counter-productive. 34 pre-exposure m-steps, more than 3 input windows, were used in these experiments, allowing 453ms for any transients to subside. The pre-exposure m-steps increase the testing time by 453ms per segment. The number of segments varied slightly between subjects but was always between 30 and 35. Generally, a larger number of shorter segments were used in older subjects whose tolerance to extended periods without blinking, and whose concentration spans, were shorter. The pre-exposure m-steps increased the test duration to 15-16 minutes.

3.5 An Example Data Set.

Each test generates a large volume of data. A typical 15.6 minute test, sampled 1,200 times per second, creates about 1123K data samples. After the cross-correlation, each data set consists of four separate arrays of responses: that is, the first order kernel, two slices of the second order kernel and one slice of the third order kernel. Each array contains 103 responses, so there are 412 responses in total. Each response is an electroretinogram that is associated with one hexagon in the stimulus array and the unique consequence of neuronal activity in one patch of retina. Every ERG consists of one window that is 10 m-sequence steps long and sampled 16 times per step, so there are 160 sampled data points per ERG and about 66K data points in the entire data set. The number of data points is reduced because many data points are only associated with the kernels and kernel slices that have no power and are being discarded. The cross-correlation cycle itself does not discard data points. The following figures illustrate the response arrays of a typical normal using the recording parameters given above, only the first 100ms of response are shown.

1st Order Kernel
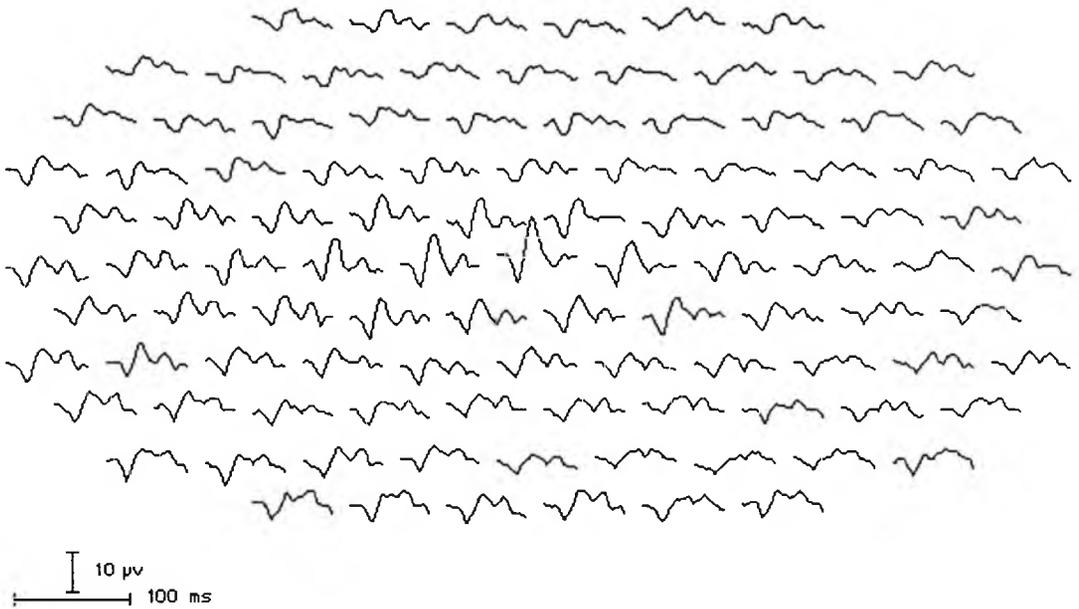
Figure 3-6   Array of 103 ERGs of the first order kernel of a normal.

2nd Order Kernel, 1st Slice
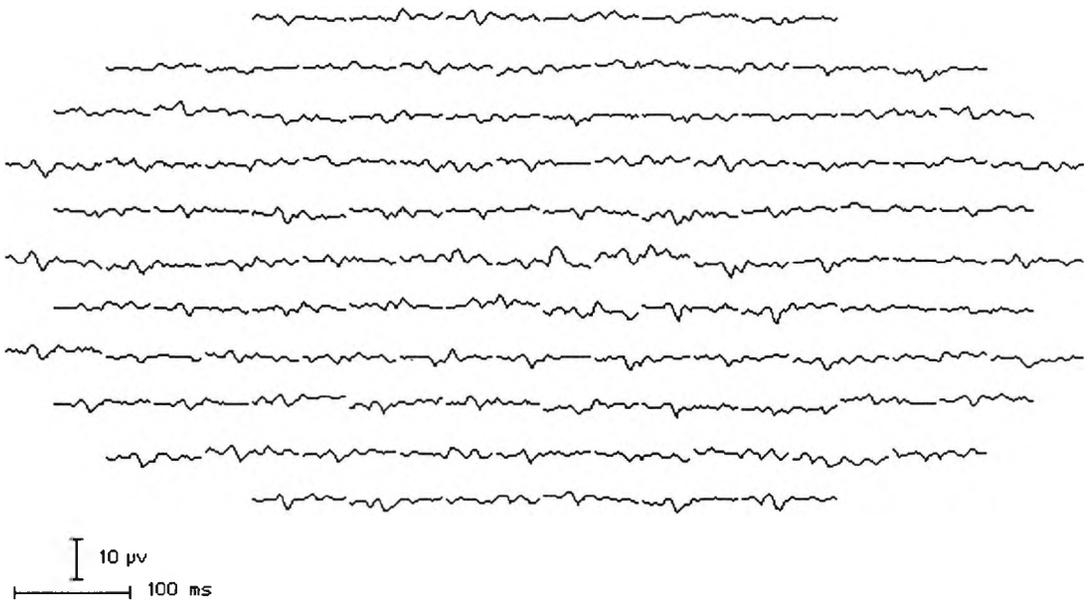
Figure 3-7   Array of 103 ERGs of the first slice of the second kernel of a normal.   The first slice of the second order kernel uses two binary stimuli with no OFF stimuli between them, in an ON ON pattern.

141

2nd Order Kernel, 2nd Slice

10 µv

100 ms
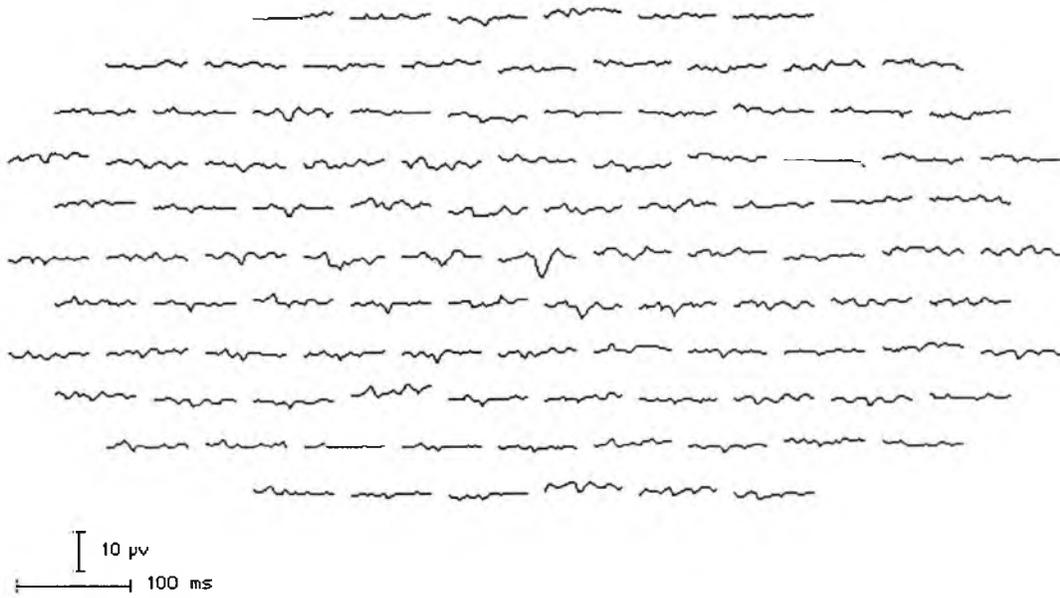
Figure 3-8 Array of 103 ERGs of the second slice of the second kernel of a normal. The second slice of the second order kernel uses two binary stimuli with one OFF stimulus between them, in an ON OFF ON pattern.

3rd Order Kernel, Slice 1,1

10 µv

100 ms
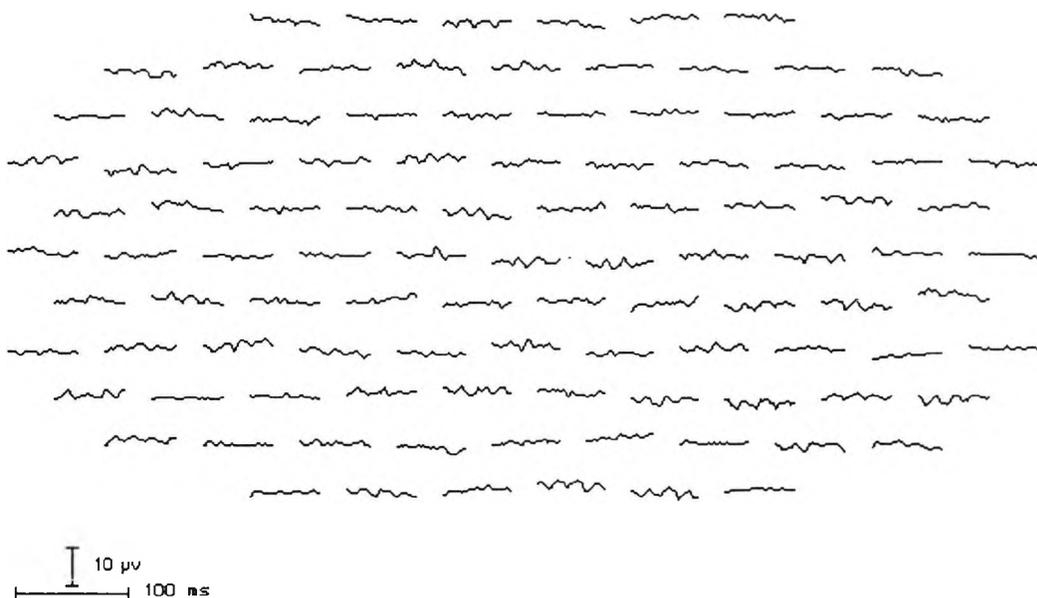
Figure 3-9 Array of 103 ERGs of slice 1,1 of the third order kernel. Slice 1,1 indicates that the three binary stimuli are presented with no OFFs between them, in an ON ON ON pattern.

142

4. Components of the Linear and Nonlinear Electroretinograms, and Changes Due to Ageing.

4.1 Components of the Linear Response.

Figure 4-1 shows 5 repeated VERIS linear responses of a young, normal experienced subject. In this section these responses have been analysed to investigate the topographical variation in the linear response. The raw response waveforms have a tendency to drift from the baseline by a variable amount so each waveform was 'zeroed' to the baseline by averaging the first ten data points, where the retinal response must be zero, and subtracting this number from each data point in the waveform. The responses from each hexagon were then divided by the retinal area of that hexagon to produce a response scaled to pV/micron^2, that allowed direct comparison of responses from different hexagon sizes.
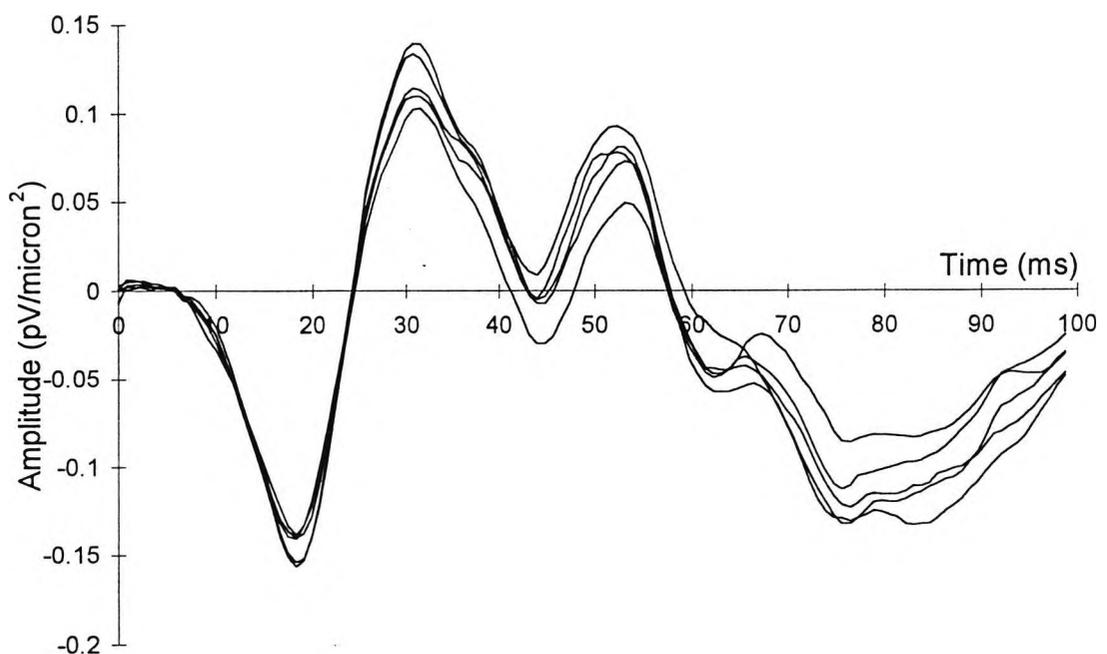
Figure 4-1 Five responses, each the mean of all 103 hexes, of a young normal experienced observer.

4.1.1.1 Components of the linear response: results.

The responses from hexagons lying in five eccentricities have been averaged (see Figure 4-2), and plotted with the response of the central hexagon to examine the topographical variation of response (see Figure 4-3).   Positive deflections at the cornea are registered as positive deflections in the waveform.   The shape of the response at each of the six eccentricities consists of an early negative deflection that is followed by a positive deflection in a fashion that is very similar to the a-wave/b-wave complex of the photopic electroretinogram.   These two deflections are followed by a smaller positive-negative deflection complex, termed T1 and P1 in Figure 4-3.   No OFF response is identifiable in Figure 4-3, almost certainly because the stimulus is too brief (Sieving, 1993). Inspection of Figure 4-3 shows that the amplitude of the a-wave, b-wave, T1 and P1 all decrease as the eccentricity increases.   The relationship between latency and eccentricity, however, is more complicated.   Figure 4-3 shows that the latency of the features in the responses of the centre and first annulus of the retina (≤ 2.8 degrees) behave in a quite differently to the latencies of the features of responses evoked at or above 6.5 degrees.   In the centre the latency of the a-wave and T1 both decrease with eccentricity, but the latency is constant in the periphery.   The latency of the b-wave increases with eccentricity in both central and peripheral areas, but a marked discontinuity is apparent between the two sets of responses.   The latency of P1 decreases with respect to increasing eccentricity in the centre but increases again the periphery.
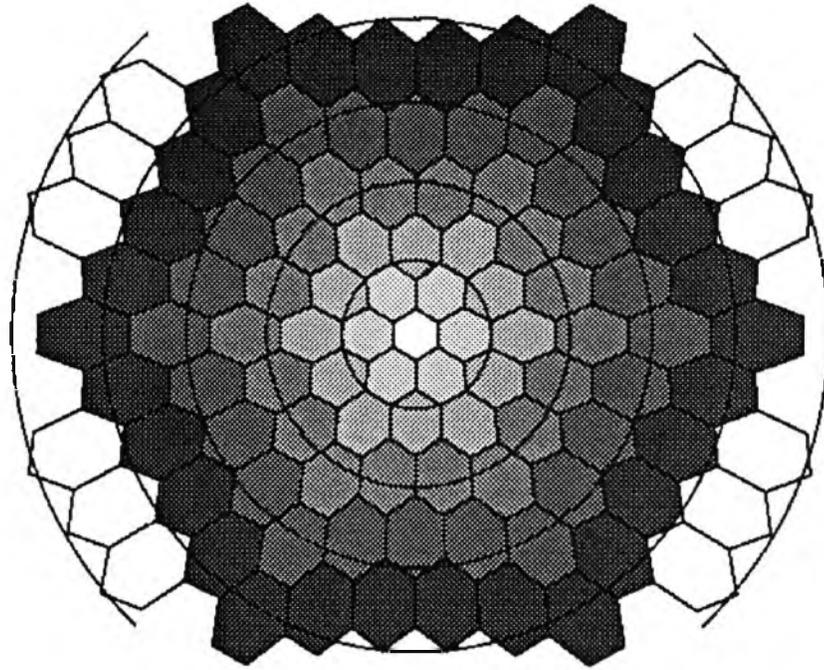
Figure 4-2   The hexagonal array, shading indicates the five concentric annuli from which the five average responses were calculated.   Isoeccentricity contours at 5 degrees radius.
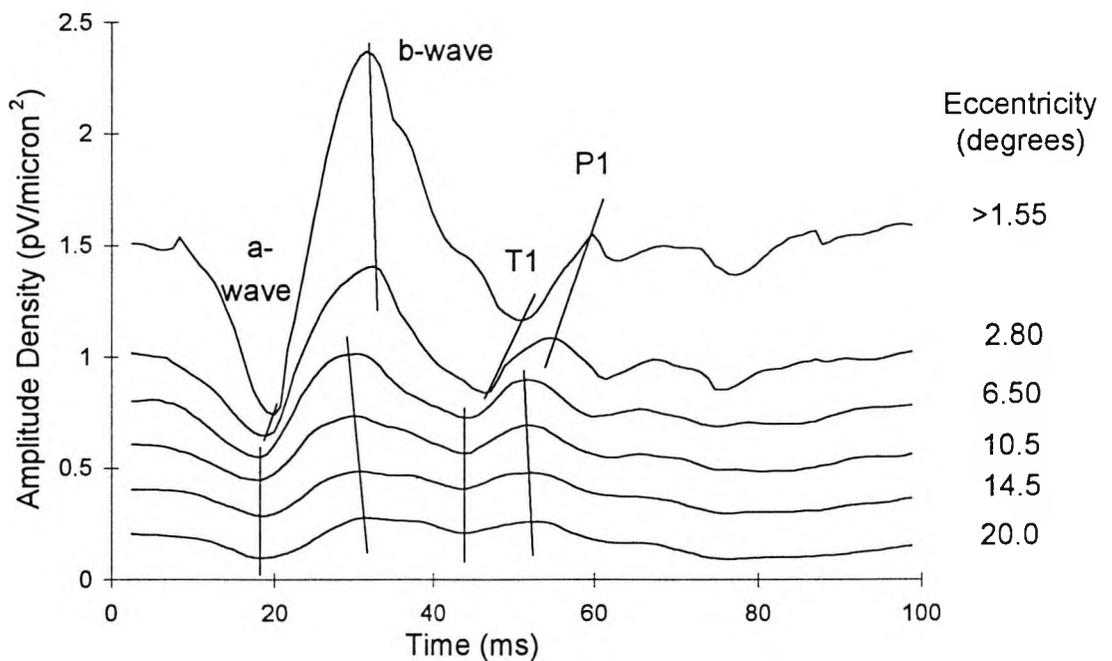
Figure 4-3   The scaled linear response of the central hexagon (>1.5 degrees, top) and five annuli (2.80, 6.50, 10.5, 14.5, 20.0 degrees ,top - bottom).   The amplitude of the response becomes smaller at greater eccentricities, and the shape of the response waveform also appears to vary across the retina.   The vertical and oblique bars, drawn by eye, are explained in the text.

145

4.1.1.2 Components of the linear response: the a-wave.

Bush et al. (1996a) have shown that the 40Hz flicker electroretinogram is almost entirely a bipolar cell response and contains only a very small contribution from the photoreceptors (see 1.2.5.6). Although the flicker electroretinogram is a steady-state response and is qualitatively different from the fast, transient, impulse response that VERIS evokes, it is interesting to enquire whether the a-wave that VERIS evokes is rooted in the photoreceptors, or in other neurones. One approach to answering this question involves forming a comparison between cone population density and scaled a-wave amplitude.

The responses of hexagons lying on the horizontal and vertical mid-lines were selected (Figure 4-4), so that a direct comparison of response amplitude could be made with the figures for cone population density given by Curcio et al. (1990). Figure 4-5 and Figure 4-6 illustrate these responses. Figure 4-7 shows the scaled absolute a-wave amplitude plotted against cone density for these two cross-sections. A quantitative comparison of electroretinographic response and histologically acquired cell densities is not possible. In Figure 4-7 the electroretinographic response have been scaled to the cone density for the central response. This allows a qualitative comparison of the change in electrophysiological response with cone density at a range of eccentricities. The a-wave amplitude function is subject to inter-individual variation. The effect of any such variability has been reduced by using the same subject for all five test runs.
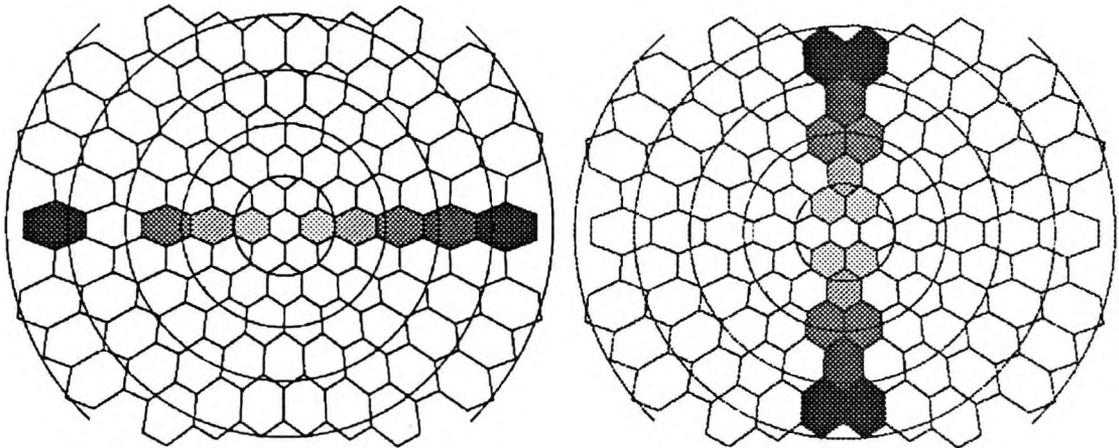
Figure 4-4 The hexagonal array, shading indicates the hexagons used to calculate the response at five eccentricities for the horizontal (left) and vertical (right) cross-sections.   Isoeccentricity contours at five degree intervals, the eccentricity of each hexagon was calculated as its midpoint.   Where two hexagons are shaded the mean of those hexagons was used. The eye is a right eye, so the gap in the horizontal cross-section section is due to the optic nerve head.
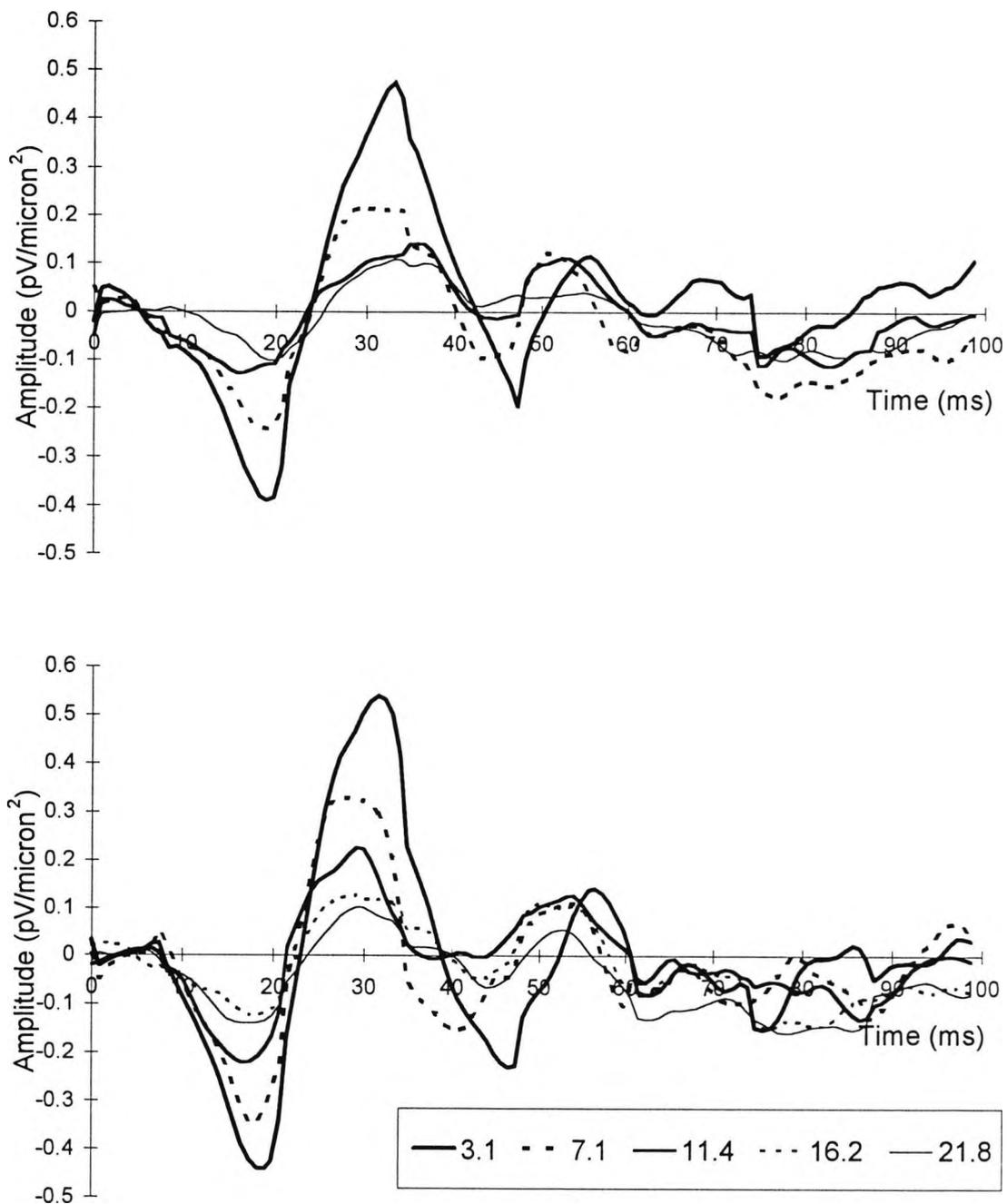
Figure 4-5   The nine linear responses, at 5 eccentricities, derived from the horizontal retinal cross-section illustrated in Figure 4-4, with the nasal hemifield responses top and the temporal hemifield responses bottom, of a young, experienced observer.
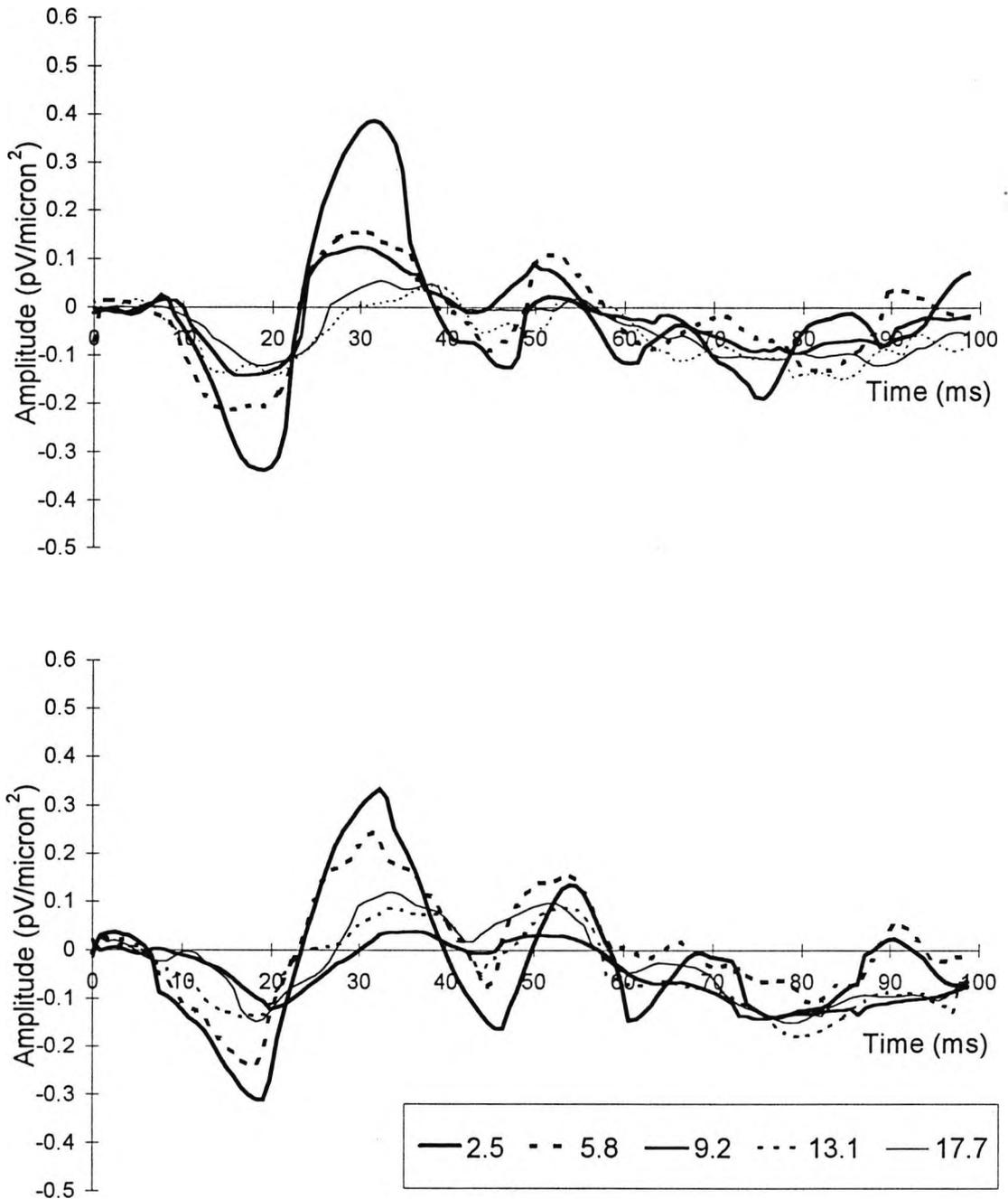
Figure 4-6   The ten linear responses, at 5 eccentricities, derived from the horizontal retinal cross-section illustrated in Figure 4-4, with the superior hemifield responses top and the inferior hemifield responses bottom, of a young experienced observer.
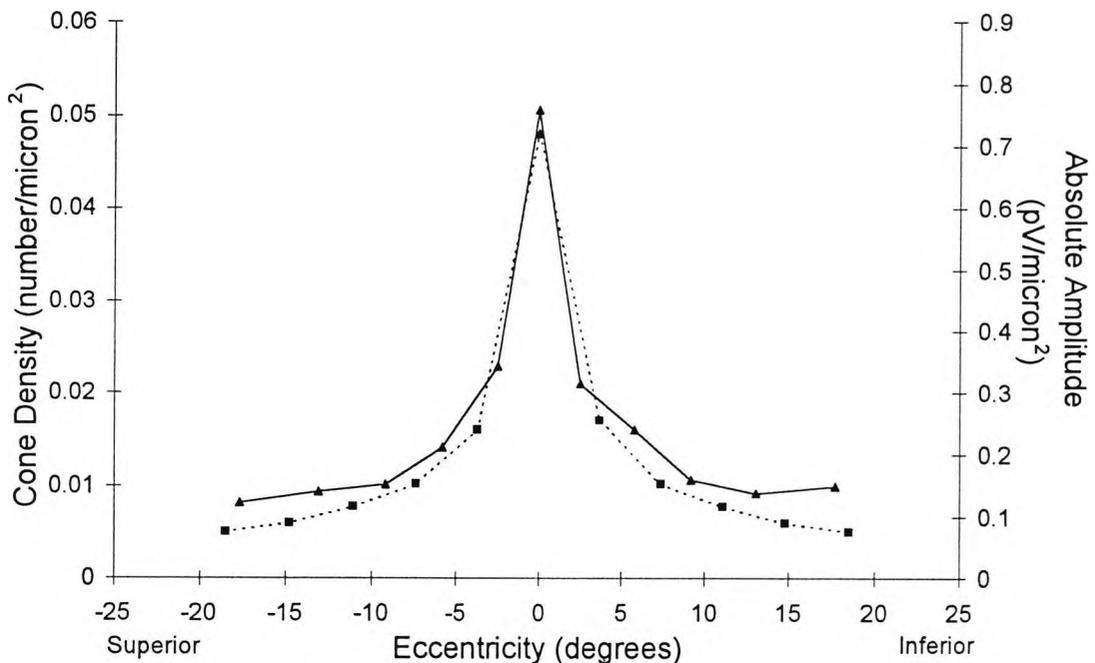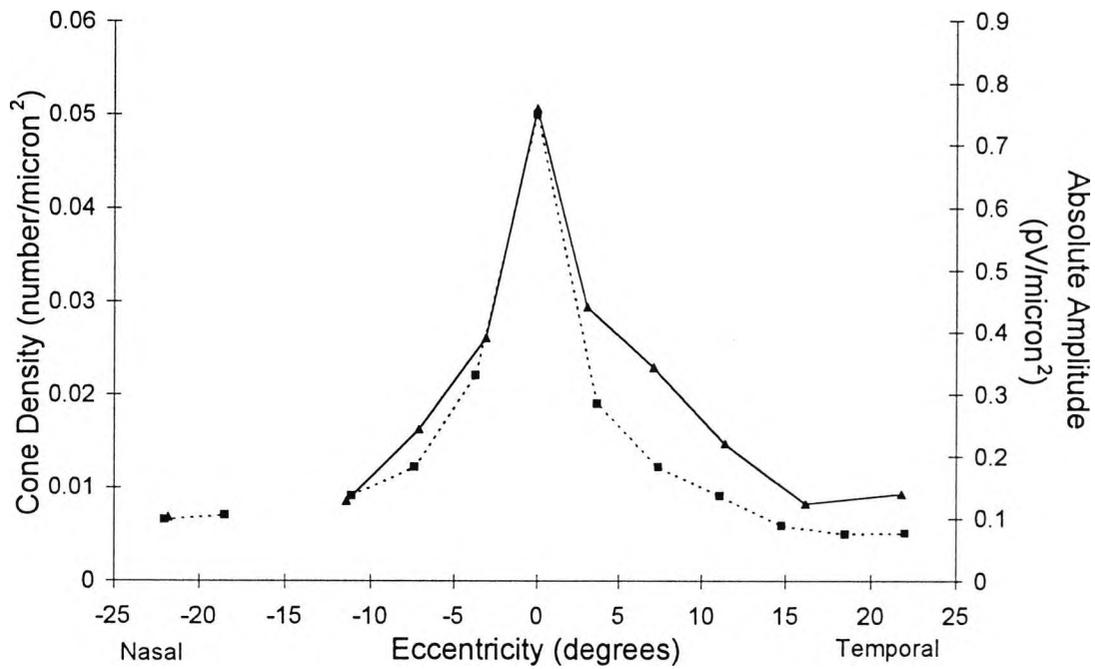
Figure 4-7 These two graphs show the cone density (dotted line and squares) and scaled a-wave amplitude (solid line and triangles) in two cross-sections: horizontal (top) and vertical (bottom). The responses have been scaled by referencing the cone density of the central retina to the scaled amplitude of the same region. In this simple comparison the agreement between the two measures fails for eccentricities greater than about three degrees. ERG amplitude densities of a young, experienced observer. Cone densities abstracted from (Curcio et al. 1990). The gap in the nasal section is due to the optic nerve head.

The effect of age-related variation has been minimised by using a subject of a similar age to the mean age of the subjects used by Curcio: the mean age of the subjects used by Curcio was 36 (1990), the age of the subject used in these experiments was 30.

4.1.1.3 Components of the linear response: a-wave amplitude.

The OFF-bipolar cell population has not been as extensively studied as the cone population and topographical maps of OFF-bipolar cell density do not exist. However, it is known that at 11 degrees eccentricity each OFF-bipolar is connected to twice as many cones as in the central retina (Kolb et al. 1992) . As the cone population density at 11 degrees is half that at 4 degrees, there will be about one quarter of the density of bipolar cells at 11 degrees that there are at 4 degrees. If the a-wave arose *exclusively* due to an OFF-bipolar cell response then the magnitude of the a-wave amplitude at 11 degrees might be expected to be about one quarter of the magnitude at 4 degrees. Inspection of Figure 4-7 illustrates that this is not the case: the a-wave at 11° is half that at 4°, so the a-wave cannot be a pure OFF bipolar cell response. Figure 4-7 shows that the scaled a-wave amplitude function shows a very close similarity with the cone density function up to about three degrees. At higher eccentricities the two waveforms appear to diverge. These results may indicate that the a-wave of the VERIS linear impulse response is the cone photoreceptor potential in the central retina, but that at eccentricities greater than about 3 degrees other responses intrude. It is also possible that the a-wave arises due to synaptic interactions. The density distribution of cone pedicles is the same

151

as the distribution of cone inner and outer segments, so a light evoked response with a topography that followed cone soma could arise in the outer plexiform layer.

4.1.1.4 Components of the linear response: a-wave latency.

Contributing responses could affect latency of the a-wave, as illustrated in Figure 4-3, where the latency of the a-wave appears to be a quite different function of eccentricity at and below 2.8 degrees than at or above 6.5 degrees. Candidates responses for intrusion into the a-wave include a rod photoreceptor response, a horizontal cell response and an OFF bipolar cell response. These electroretinographic recordings where carried out under photopic conditions known to favour cone responses. The subjects were not dark-adapted. The level of light adaption was controlled during the experiment by the amount of scattered light, which was constant because the m-sequencing always switches on the same proportion of stimulus hexagons at any one point in the stimulus cycle. Rapidly flickering stimuli are known to drive cone, but not rod, responses (Maffei and Fiorentini, 1982; Birch and Fish, 1988; Holopigian et al. 1990; Burns et al. 1992). Kondo et al. (1996) have noted the similarity between rapid (75Hz) random flash electroretinographic responses and flash 'cone' electroretinographic responses. However, focal responses from peripheral retina have not been recorded with this technique before, and a possible rod contribution to the linear response as been suggested by the results of Kondo et al. (1998) (see Section 2.6.3). If a rod response were to arise it might be expected to occur in peripheral retinal areas where rods outnumber cones (Kondo et al. 1998). The

discontinuity between the central and peripheral retina in the a-wave latency-eccentricity function that is illustrated in Figure 4-3 may be associated with a rod inclusion in the peripheral electroretinographic response. A contribution to the electroretinogram from horizontal cells and OFF bipolars has been shown to occur in photopic conditions (see 1.2.5.6). It is not possible to estimate the latency or amplitude of a horizontal cell/OFF bipolar cell contribution, but the contingency cannot be excluded.

4.1.1.5 Components of the linear response: b-wave.

The large positive deflection in the linear response will be termed the b-wave, as it has been associated with the b-wave of the photopic electroretinogram (see Section 2.6.3). It is possible that, like the a-wave, the source of the b-wave in the central retina ($\geq$2.8 degrees) may be different from the source of the b-wave in areas of the retina at or above 6.5 degrees. The marked discontinuity in the b-wave latency/eccentricity function between these two retinal areas has been illustrated in Figure 4-3. If a rod contribution to more peripheral responses exists then this might be expected to have an influence on the shape of the b-wave, as rod bipolars and third order neurons are entrained in the response.

4.1.1.6 Impedance of the retina and globe.

A further factor that must be considered is variation in the resistance of the retina and the globe. Rodieck (1973) has described an equivalent electrical circuit of retinal field potentials.

In this circuit the extracellular circuit is represented by five resistors, the length of each resistor is proportional to its ohmic value. The circuit is given in Figure 4-5, which also shows the current source within the retina, I. The resistance of the R-membrane has been quoted at round 100-200Ωcm^2, in the frog and 250Ωcm^2 in the carp (Rodieck, 1973) For comparison, the resistance of the sensory retina is about 40-50Ωcm^2 in the frog, carp, pigeon and chicken, the resistance of the vitreous humour is about 25Ωcm^2, the resistance of the choroid and the sclera is about 40Ωcm^2 (frog) (Rodieck, 1973). The resistance of the vitreous, the extra-ocular pathway and the R-membrane dominate over the resistance inherent in the sensory retina. The eccentricity of the current dipole within the retina cannot therefore be a factor in the overall resistance of the circuit. Responses derived from different hexagons can be considered as having arisen from electrical circuits with equivalent resistances.

Figure 4-8 Equivalent electrical circuit for current pathways through the eye. The lengths of the resistors are proportional to typical resistance values of the structures they represent. The current source I represents the cellular current through retinal cells. (Adapted from Rodieck, 1973).

154
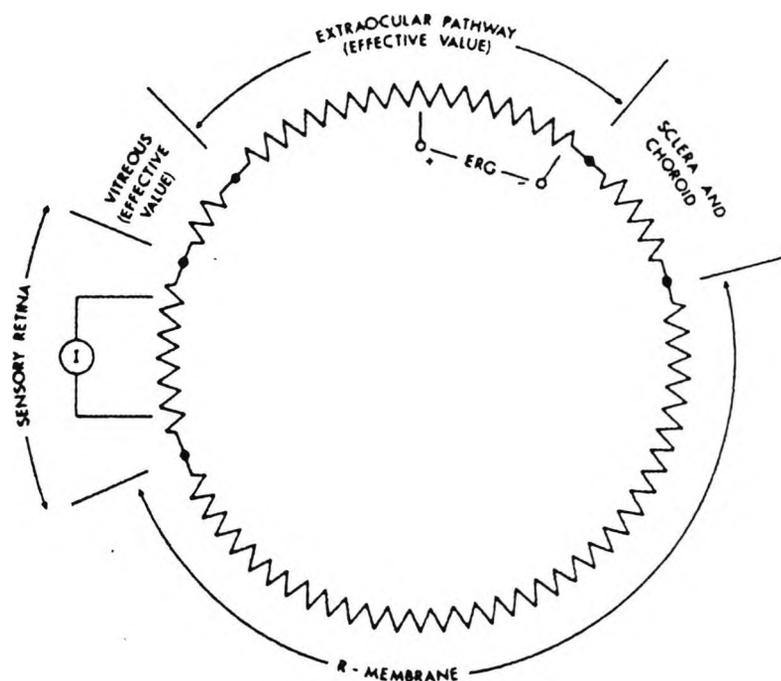
4.2 Components of the Nonlinear Response.

The response of the retina to sinusoidal inputs has been discussed in Section 2.6.   A refinement of that technique involves recording the response to the sum-of-two sinusoids.   A type of cell, or network of interconnected and interdependent cells, will respond to a stimulus consisting of the sum-of-two-sinusoids with a characteristic response.   The nonlinear response of the cells/cell networks can be probed by altering the frequencies of the sinusoids in the stimulus (Victor et al. 1977).   Different cells/cell networks will have a unique contribution to the nonlinear response of each stimulus.   A comparison of the response waveforms to different frequency sinusoids will reveal the same components, arising from the same retinal voltage generator, differing only in phase (Victor et al. 1977).   The m-sequence stimuli used by VERIS stimuli are not sinusoids, but they are binary analogues of sinusoids (see 2.3.2), and the kernel slices can be consider as responses to analogues of sum-of-two-sinusoids stimuli.   In the analogy, each kernel slice is the response to two different frequencies of sinusoids.   As in the responses to sinusoids, a comparison of the response waveforms to different kernel slices will reveal the same components, differing only in latency.

A comparison of kernel slice latencies will allow the separation of deflections from components.   Component that are manifestations of the same cells/cell networks will appear as deflections that vary in latency by the same degree, whereas deflections that are manifestations of different components will not.

155

4.2.1.1 Components of the nonlinear response: Results.

The first two slices of the VERIS second order kernel electroretinographic response are presented in Figure 4-9. The scaled average response of all the stimulus hexagons of five tests on a young, normal experienced subject is shown. A stimulus rate of 75Hz has been used. Both slices have three positive deflections and three negative deflections before 55ms, in Figure 4-9 they are indicated with filled arrow-heads for the first slice and open arrow-heads for the second slice.

In Figure 4-9 the deflections are designated in terms of their polarity and latency: in slice 1, N17, P23, N31, P38, N40, P46; in slice 2, N8, P16, N22, P27, N32, P48. Other peaks may be discernible with latencies greater than 55ms, but it is not clear whether these are true retinal responses or incursions of noise into the waveforms, and they were not analysed. The mean latency of the deflections, and the difference between those deflections, is given in Table 4-1. In Figure 4-10 the latencies of the deflections of both slices are presented together, deflections of the same component will appear as parallel lines, as the latency of the deflections will vary by the same quantity between the two slices. Deflections of different components will appear as non-parallel lines, as the latency of each deflection will vary by different degrees.

75Hz Slice 1			75Hz Slice 2			75Hz Slice1 - Slice2		
	Mean	SD		Mean	SD		Mean	SD
N17	17.10	0.455	N8	8.80	0.742	N17-N8	8.30	0.525
P23	23.07	0.371	P16	16.60	0.587	P23-P16	6.47	0.813
N31	31.37	0.371	N22	22.74	1.259	N31-N22	8.63	1.447
P38	38.01	0.371	P27	26.73	0.371	P38-P27	11.29	0.664
N40	40.50	0.371	N32	32.37	0.587	N40-N32	8.13	0.621
P46	46.48	1.017	P48	48.31	2.067	P46-P48	-1.83	1.848

Table 4-1   Mean latencies, in ms, and standard deviations of the six deflections, and the difference between those deflections, of the first two slices of the second order kernel.   75Hz stimulus rate.   N=5.

4.2.1.2 Components of the nonlinear response: Analysis.

A conceivable statistical method of kernel slice latency comparison would involve using the t-test to compare every difference in deflection latency with every other latency difference.   Whilst these comparisons ('contrasts') may be formed, calculation of multiple comparisons with t-tests can throw-up statistically significant differences by chance, if a sufficient number of comparisons is made.   If k contrasts (in this case differences in latency) are being analysed then there are $\frac{1}{2}$k(k-1) comparisons being formed. Student's t-test is only an appropriate method to analyse comparisons when such comparisons flow naturally from the plan of the experiment.   When comparisons are being formed in an exploratory way, a method of multiple comparisons is required Several methods exist, which all aim to control the overall chance of statistical significance arising to no more than the specified level (e.g. 5%).   The disadvantage is that they all, to varying degrees,

are conservative (they err on the side of non-significance), to reduce the probability of significant differences arising without an underlying trend in the population. The most conservative method is Bonferroni's, in which the P-value is multiplied by the number of contrasts being compared (6 in this case) (Altman, 1990). Two less conservative methods exist, Tukey's T-method and Scheffé S-method. Tukey's method is only appropriate for statistically independent data. Slices of the same kernel, derived from tests performed on the same subject, are not independent, so Scheffé S-method has been adopted for this study. Scheffé has shown (Scheffé, 1959) that a linear contrast L can be declared significant at the α level when the absolute value of L/SE(L) exceeds $\sqrt{[(k-1)(F_\alpha)]}$ where F is the F-distribution and is calculated on (k-1) and k(n-1) degrees of freedom and where there are k contrasts and n observations (k=6 and n=5 in this case) (Armitage and Berry, 1987). When k=2 this reduces to the t-test, but for k>2 it is noticeably conservative (Armitage and Berry, 1987).
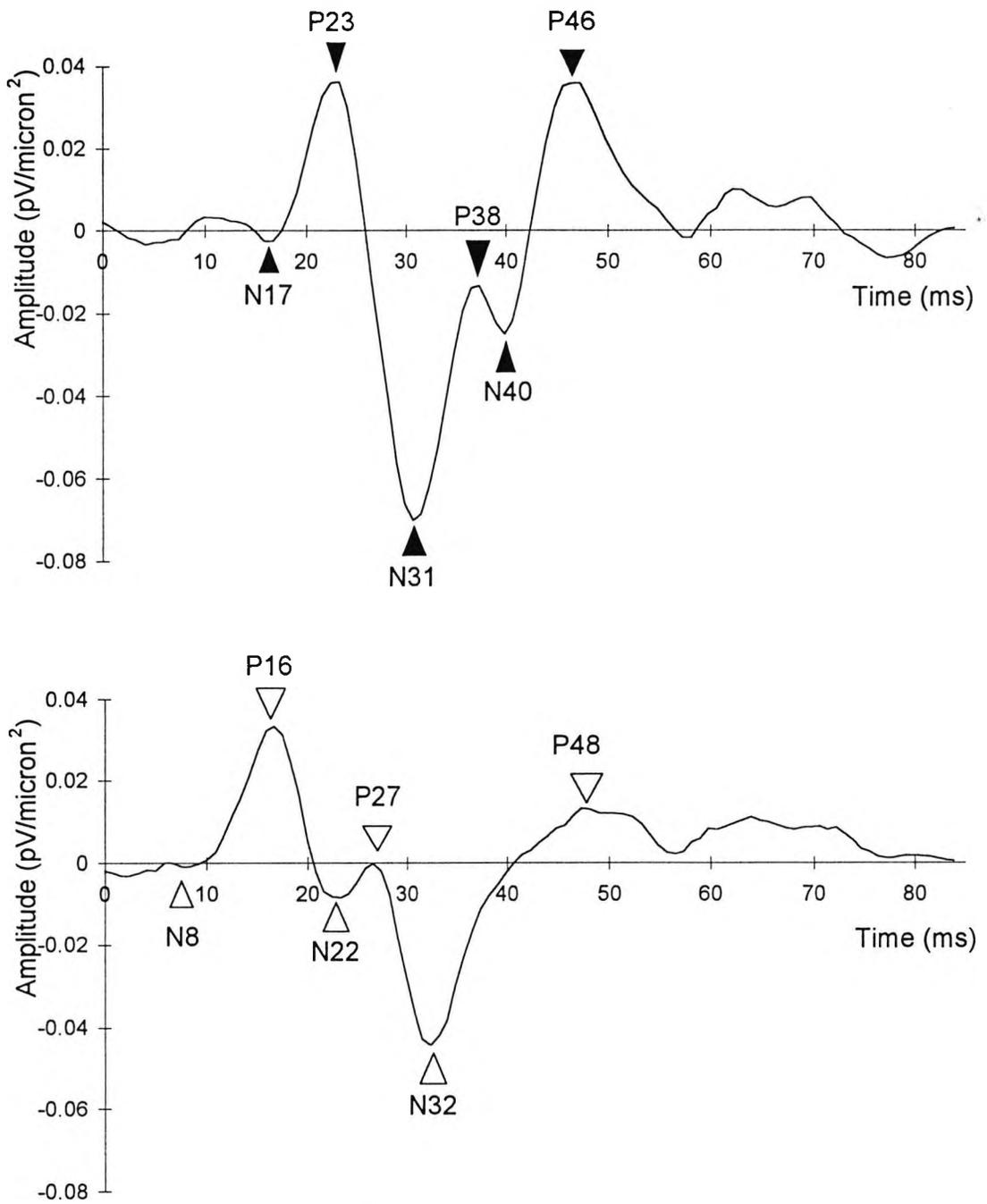
Figure 4-9. Mean response of the entire stimulus area of the first two slices of the second order kernel, the first slice is uppermost. 75Hz stimulus rate. Six deflections, in both waveforms, are indicated: in slice 1 with closed triangles, in slice 2 with open triangles.
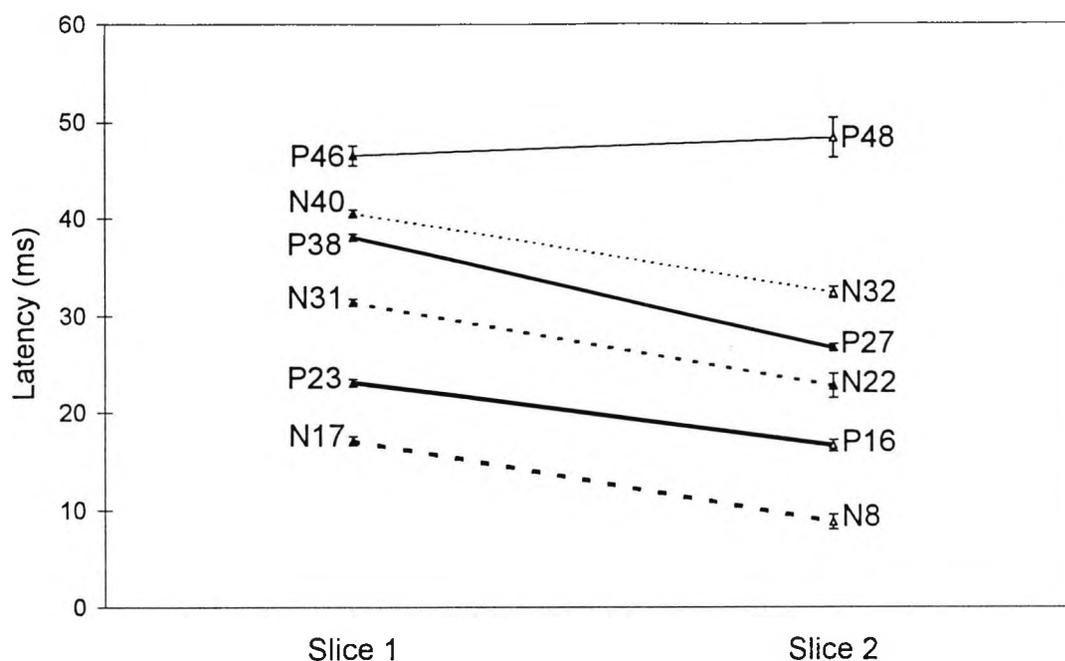
Figure 4-10.   The change in latency of the maxima and minima of six deflections of the second order kernel, 75Hz stimulus rate.   Error bars show 1 standard deviation.

	N17-N8	P23-P16	N31-N22	P38-P27	N40-N32	P46-P48
N17-N8	-					
P23-P16	**0.006**	-				
N31-N22	0.998	0.111	-			
P38-P27	**>0.001**	**>0.001**	**0.020**	-		
N40-N32	0.998	**0.025**	0.987	**>0.001**	-	
P46-P48	**>0.001**	**>0.001**	**>0.001**	**>0.001**	**>0.001**	-

Table 4-2   Results of a Scheffé method test on the difference between deflection latencies of slice 1 and slice 2 of the second order kernel, stimulus rate 75Hz.   Numbers shown are P-values, results where $P \leq 0.05$ are picked out in bold.   All the negative deflection pairs are not statistically different, indicating that they may arise from the same component of the response. With the exception of the P23-P16/N31-N22 comparison, all the positive deflection pairs are significantly different from each other and significantly different from the negative deflection pairs, suggesting that the 3 positive components derive from 3 different sources, which are different from the sources that produce the negative deflection.

A statistical analysis of the difference in deflection latency is presented in Table 4-2 using the Scheffé method. Exact P values (α levels) have been calculated so that degrees of significance can be gauged. The difference in all three negative deflections are not statistically different from each other, but are statistically significantly different from almost all of the other deflections, so it may be reasonable to conclude that they derive from the same component within the second order response. The positive deflections are statistically different from each other and (with one exception, P23-P16) different from the negative deflections, which implies that all the deflections arise from different components within the second order response. The contrast P23-P16 occupies a somewhat ambiguous position, being significantly different from N40-N32, but similar to N31-N22 which is itself different from N40-N32

Although a slightly different stimulus rate might be expected to change the relative contribution to the response from the components, the same components are expected to appear. This analysis has been repeated with responses from the same normal for a stimulus rate of 67Hz. For simplicity the same nomenclature has been used to designate the deflections, although the latencies of the features have changed slightly. Two tests have been averaged and the recordings at this stimulus rate were made before the installation of the Faraday cage, for these two reasons the responses are rather more noisy. The deflection termed N17 and N8 cannot be distinguished and the standard deviations of the deflection latencies are larger than in the 75Hz test reported above. Mean latencies of deflections of slice 1 and 2 and the difference

between those deflections are presented in Table 4-3, with standard deviations. First and second slice waveforms presented in Figure 4-11, the change in latency of five deflections in Figure 4-12.

The Scheffé method for multiple comparisons described above has been repeated on the contrast between the same deflections of the first two slices of the 67Hz, second kernel response. The results are tabulated below (Table 4-4). Although the standard deviations are larger, because n=2 and the responses themselves are more noisy, the number of comparisons is now only 5 (i.e.k=5), so the test is now somewhat less conservative. The conclusions that may be drawn are broadly in keeping with those made above for the 75Hz response. The difference in the negative deflections are not statistically different, although they are statistically different from the difference in the positive deflections, implying that the negative deflections arise from the same component and that that component does not give rise to any of the other components. Most of the positive deflections are significantly different from each other and different from the negative deflections, suggesting that they arise from different components in the second kernel response. As in the 75Hz response, the P23-P16 deflection is ambiguous. P23-P16 differs from all deflections save P46-P48, this deflection is different from both N31-N22 and P38-P27, which are, in turn, different from P23-P16.

67Hz Slice 1			67Hz Slice 2			67Hz Slice1 - Slice2		
	Mean	SD		Mean	SD		Mean	SD
N17			N8			N17-N8		
P23	26.04	0.000	P16	22.79	0.658	P23-P16	3.26	0.658
N31	36.27	0.658	N22	27.90	1.315	N31-N22	8.84	0.658
P38	42.78	1.315	P27	29.76	0.000	P38-P27	13.02	1.315
N40	45.11	0.658	N32	38.60	0.658	N40-N32	6.51	1.315
P46	56.27	1.973	P48	57.20	1.973	P46-P48	-0.93	3.946

Table 4-3   Mean latencies, in ms, and standard deviations of five deflections, and the difference between those deflections, of the first two slices of the second order kernel.   67Hz stimulus rate.   Note that although the nomenclature used in the 75Hz response has been retained, the latencies are slightly different.   N=2.   N17 and N8 are indistinguishable from noise.
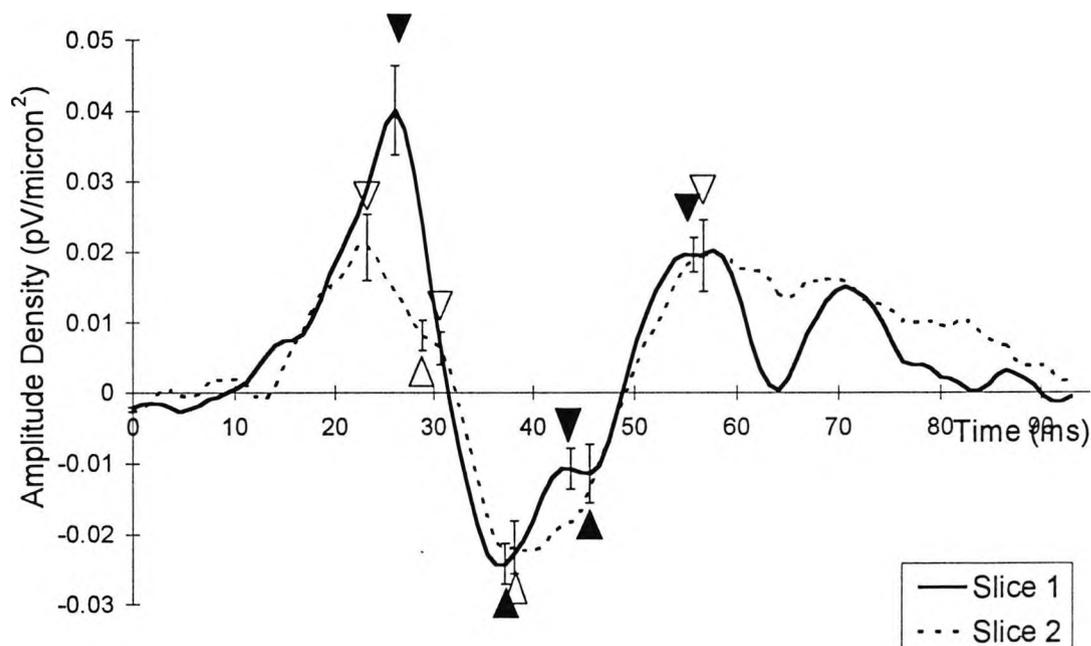
Figure 4-11.   First two slices of the second order kernel, 67Hz stimulus rate, shown on the same axis for comparison.   Maxima and minima of the first slice are indicated by filled triangles, maxima and minima of the second slice by open triangles.   Data recorded at this stimulus rate predates the Faraday Cage (see 3.1.2) and is consequently noisier, N17 and N8 cannot be identified.
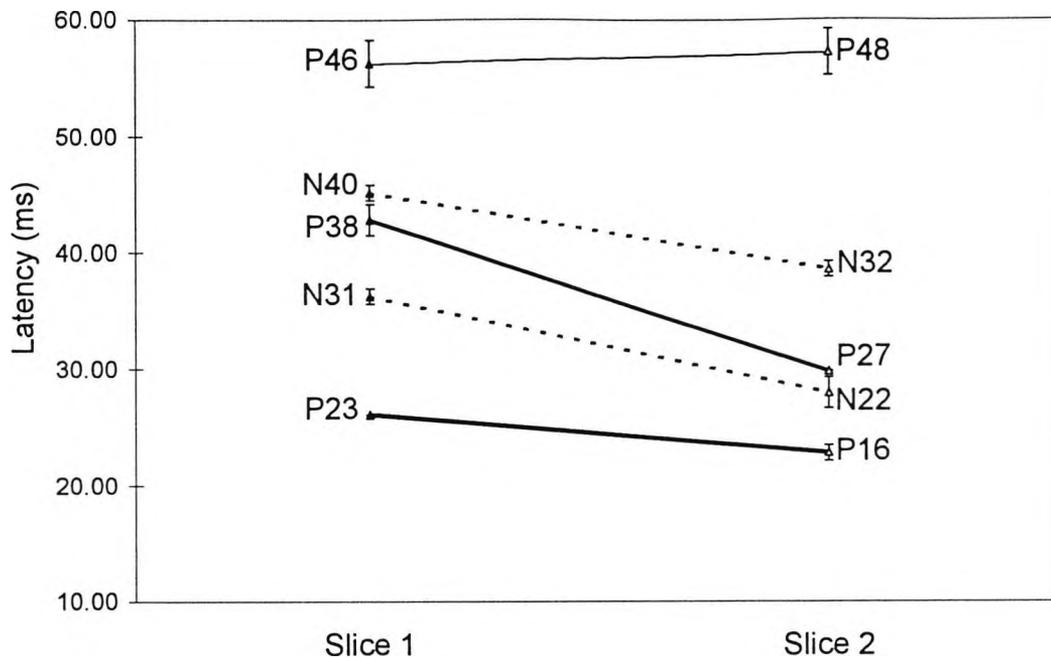
Figure 4-12   The change in latency of the maxima (solid line) and minima (dotted line) of five deflections of the second order kernel, 67Hz stimulus rate. Error bars show 1 standard deviation.

	N17-N8	P23-P16	N31-N22	P38-P27	N40-N32	P46-P48
N17-N8	-					
P23-P16	-	-				
N31-N22	-	**>0.001**	-			
P38-P27	-	**>0.001**	**0.009**	-		
N40-N32	-	**0.025**	0.090	**0.003**	-	
P46-P48	-	0.297	**0.017**	**0.004**	0.058	-

*Table 4-4   Results of a Scheffé method test on the difference between deflection latencies of slice 1 and slice 2 of the second order kernel, stimulus rate 67Hz.   Numbers shown are P-values, results where P≤0.05 are picked out in **bold**.   The negative deflections are not significantly different, although they are different from most of the positive deflections, implying, as in the 75Hz response, that they derive from the same response component and that that component is different from the component that gives rise to any of the other deflections.   The P23-P16 deflection occupies an ambiguous position.*

164

4.2.2 Modelling the Components of the Nonlinear Response.

Each slice of the nonlinear responses can be modelled as the sum of four Gaussian functions of the form:

$$R_i = A\left\{\exp\left[-\frac{1}{2}\left(\frac{n_i - \tau}{\sigma}\right)^2\right]\right\}$$

<div align="right">Equation 4-1</div>

where R_i is the response at each sampling point n_i. Each Gaussian function has a unique value of A, τ and σ, where A is the peak amplitude of the component, τ is equal to the peak latency x m-sequence step rate in Hz x sampling rate per step and σ is allowed to take any value. Values of A, τ and σ were chosen to minimise the difference between the area under the measured response and the area under the sum of the four modelled responses. Very close approximation of the measured responses can be obtained using the values of A, τ and σ given in Table 4-5. These coefficients yield three Gaussian function that are plotted in the top panels of Figure 4-13 (slice 1) and Figure 4-14 (slice 2) for the 75Hz response and Figure 4-16 (slice 1) and Figure 4-17 (slice 2) for the 67Hz response. In the bottom panels of these figures the modelled responses are plotted with their original responses, it is clear that a very accurate model of the waveforms was achieved. The four model components for each slice are presented in Figure 4-15 (75Hz) and Figure 4-18 (67Hz). Although the 75Hz component-models may appear different to the 67Hz component-models, particularly in respect of the second slice, it is not likely that such a small change in stimulus rate will radically alter the

relationship between the components in each of the slices. It is more probable that any differences may be associated with the high signal-to-noise ratio (and amplitude and latency standard deviations) that are present in the 67Hz response.

The goodness-of-fit does not mean that the underlying processes have been identified, but it does suggest that they have. Although σ has no direct physiological correlates, it is significant that the value of σ do not vary between the 75Hz and the 67Hz responses as this implies that there are common nonlinear processes underlying the two responses. The significance of t and A are clearer, being directly related to the amplitude and latency of the components. It is tempting to suggest origins for these components, although the suggestion may only be very tentative: The large downward-travelling Gaussian could be a bipolar cell response. It might then be possible that the faster Gaussian could derive from amacrine cells and be related to the oscillatory potentials (see Section 1.2.7, page 71).

Slice	1					2				
Step Rate		75		67			75		67	
Component	σ	τ	A	τ	A	σ	τ	A	τ	A
1	3.6	28	0.075	29	0.055	2.7	20	0.035	25	0.021
2	2.1	44	0.036	45	0.006	2.8	33	0.038	33	0.014
3	3.5	56	0.042	59	0.022	5.2	58	0.013	61	0.020
4	8.4	37	-0.073	38	-0.026	5.8	37	-0.052	42	-0.024

Table 4-5   The coefficients of four models of four responses, slices 1 and 2 at both 75 and 67 Hz, are presented here.   Each model is the sum of four Gaussian function (see Equation 4-1) and have three coefficients, A, τ and σ, but notice that σ is a function of slice but not of step rate.
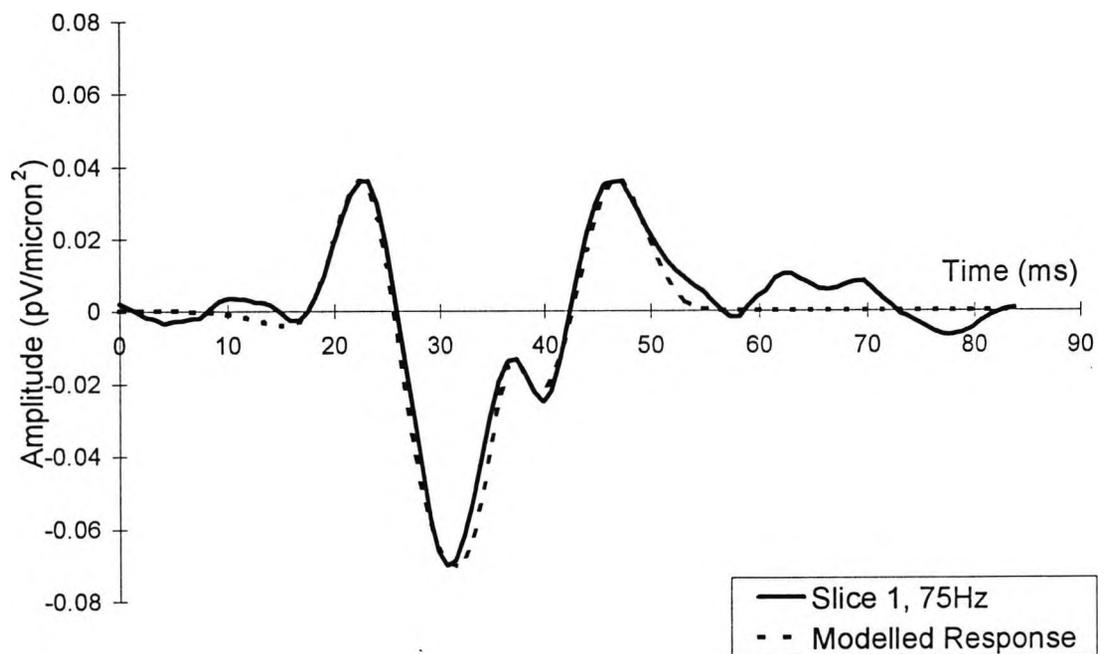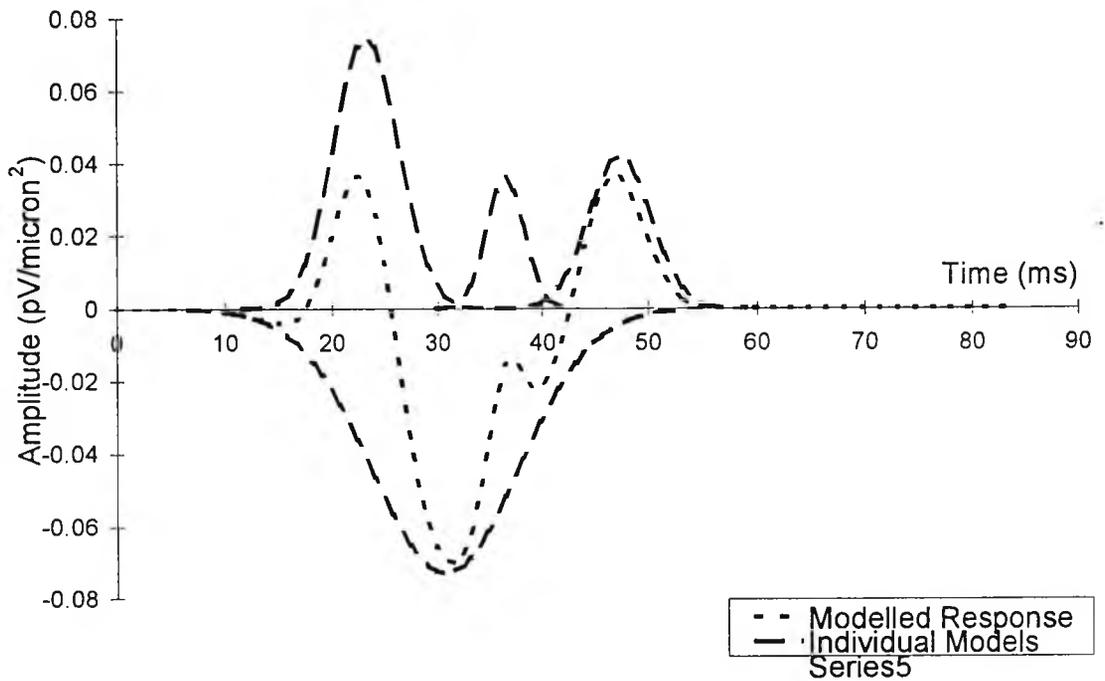
Figure 4-13   Top panel shows the four Gaussian functions (coefficients in Table 4-5) for slice 1, 75Hz, termed the individual models, with the sum of these models, termed the modelled response.   Bottom panel shows the modelled response with the original response.
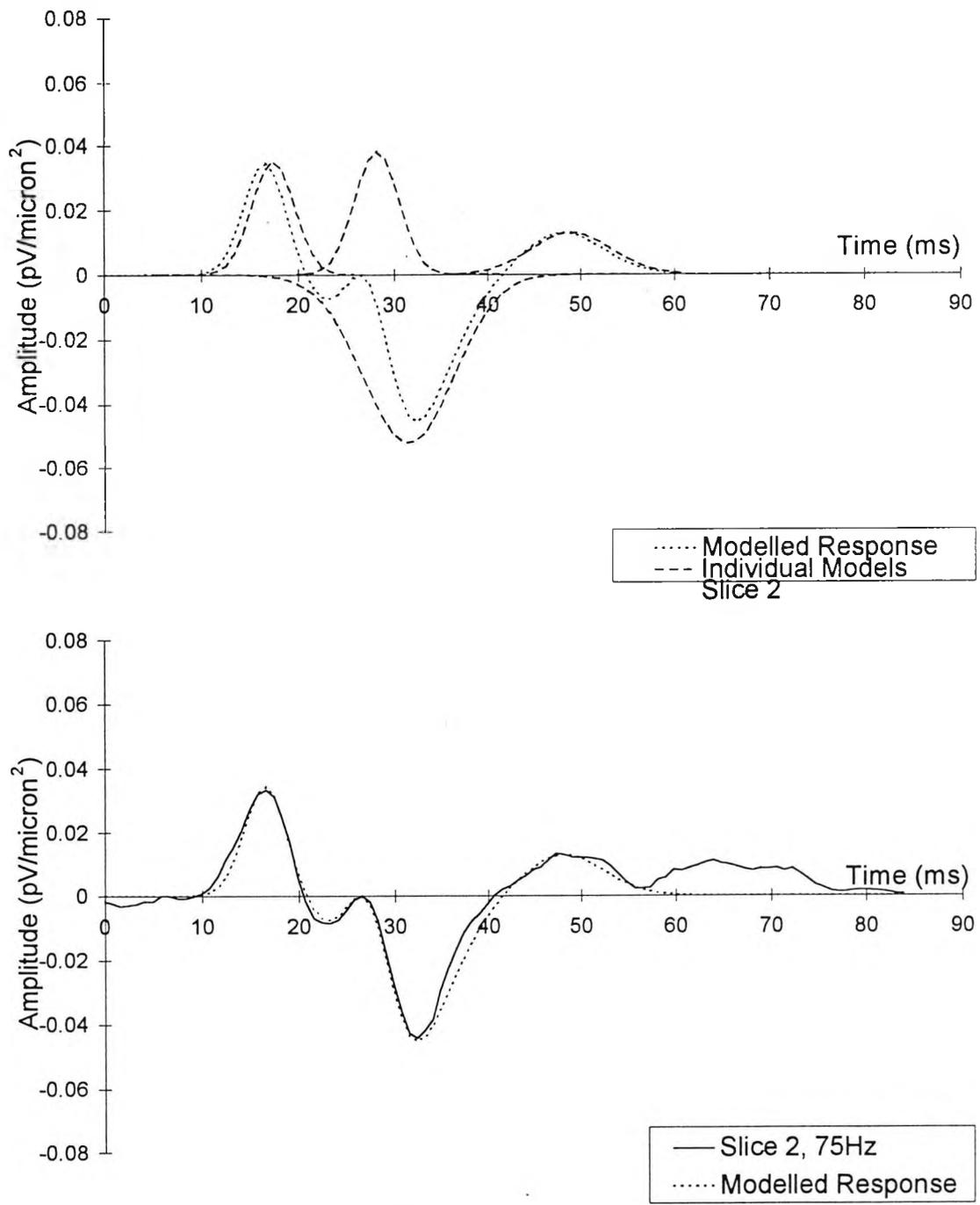
Figure 4-14   Top panel shows the four Gaussian functions (coefficients in Table 4-5) for slice 2, 75Hz, termed the individual models, with the sum of these models, termed the modelled response.   Bottom panel shows the modelled response with the original response.
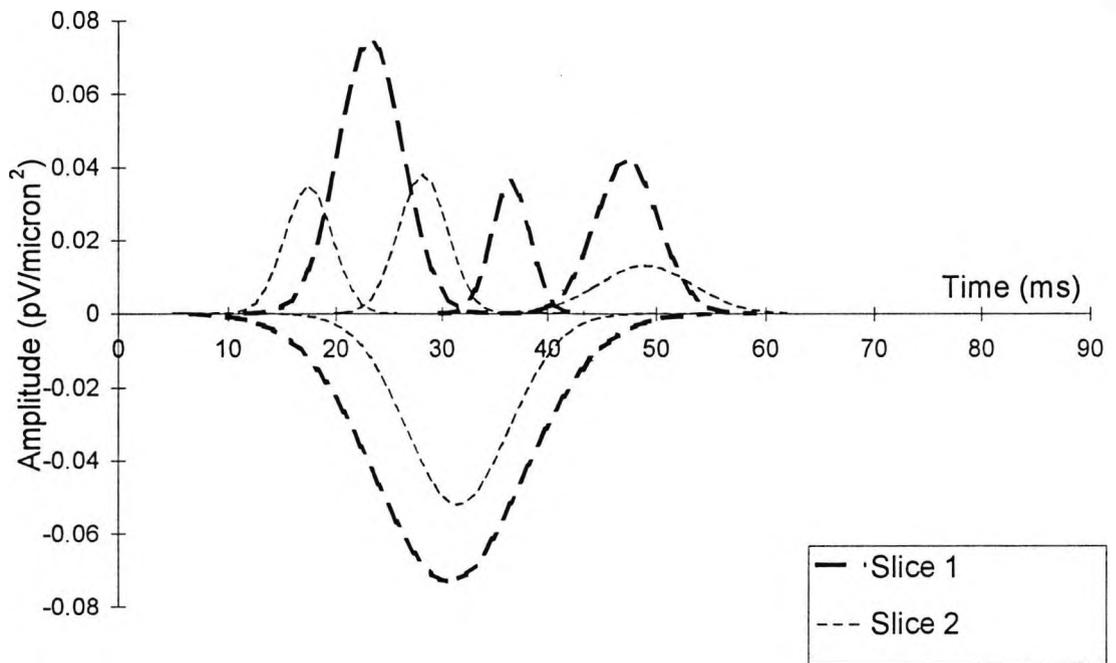
Figure 4-15   The four individual models from Figure 4-13 and Figure 4-14, slice 1 and 2 respectively, of the 75Hz response, plotted together for comparison.
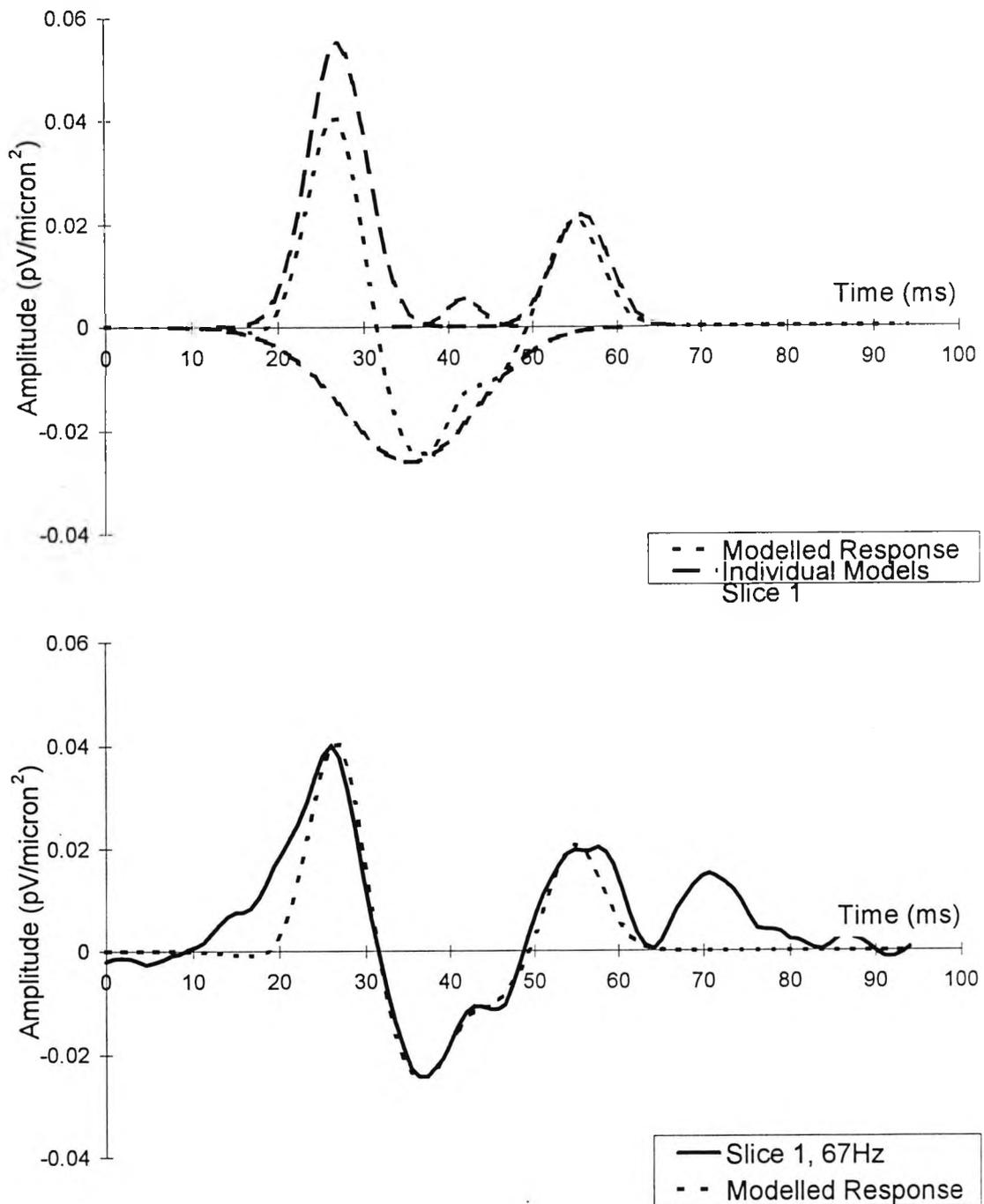
Figure 4-16   Top panel shows the four Gaussian functions (coefficients in Table 4-5) for slice 1, 67Hz, termed the individual models, with the sum of these models, termed the modelled response.   Bottom panel shows the modelled response with the original response.
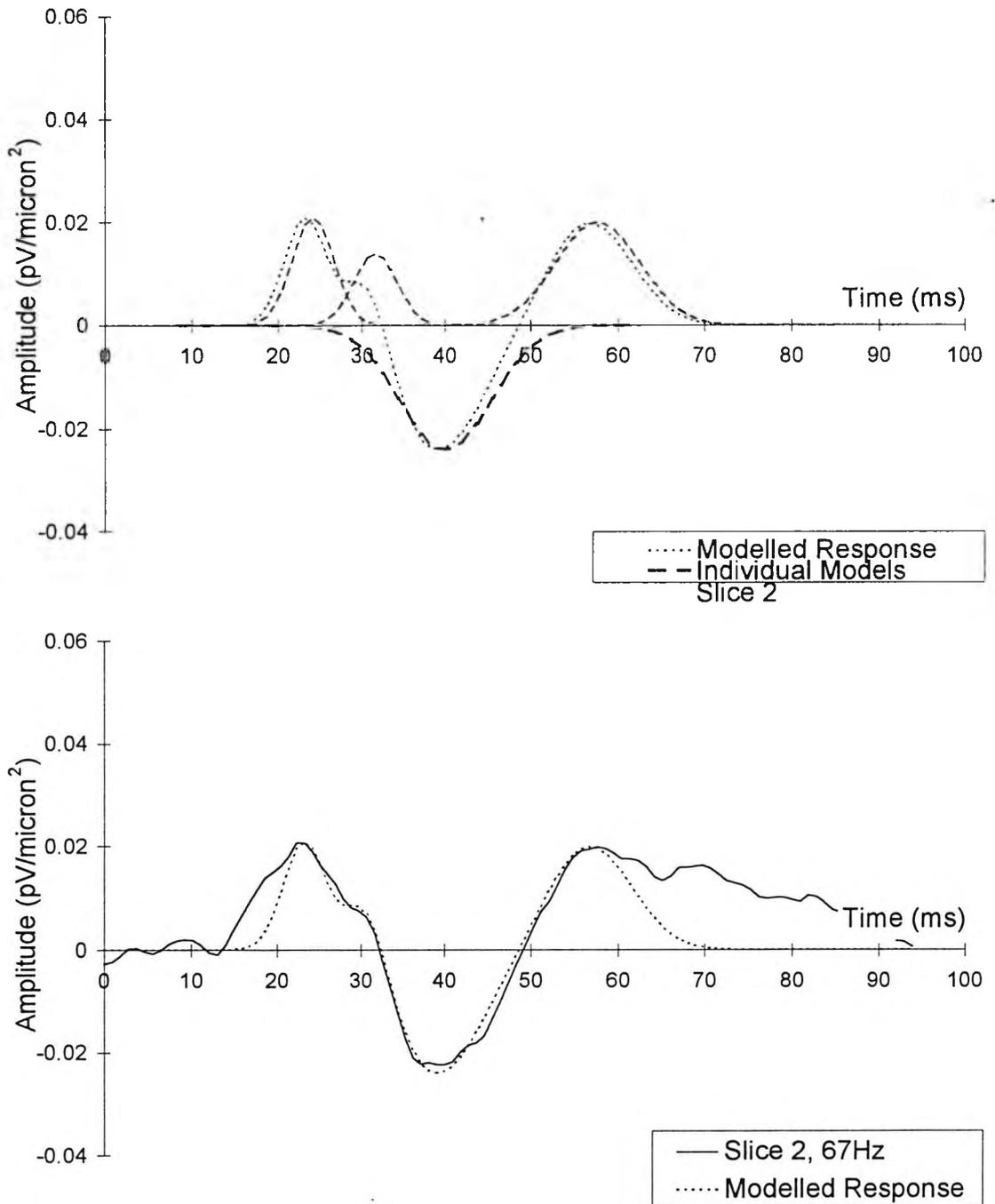
Figure 4-17 Top panel shows the four Gaussian functions (coefficients in Table 4-5) for slice 2, 67Hz, termed the individual models, with the sum of these models, termed the modelled response. Bottom panel shows the modelled response with the original response..
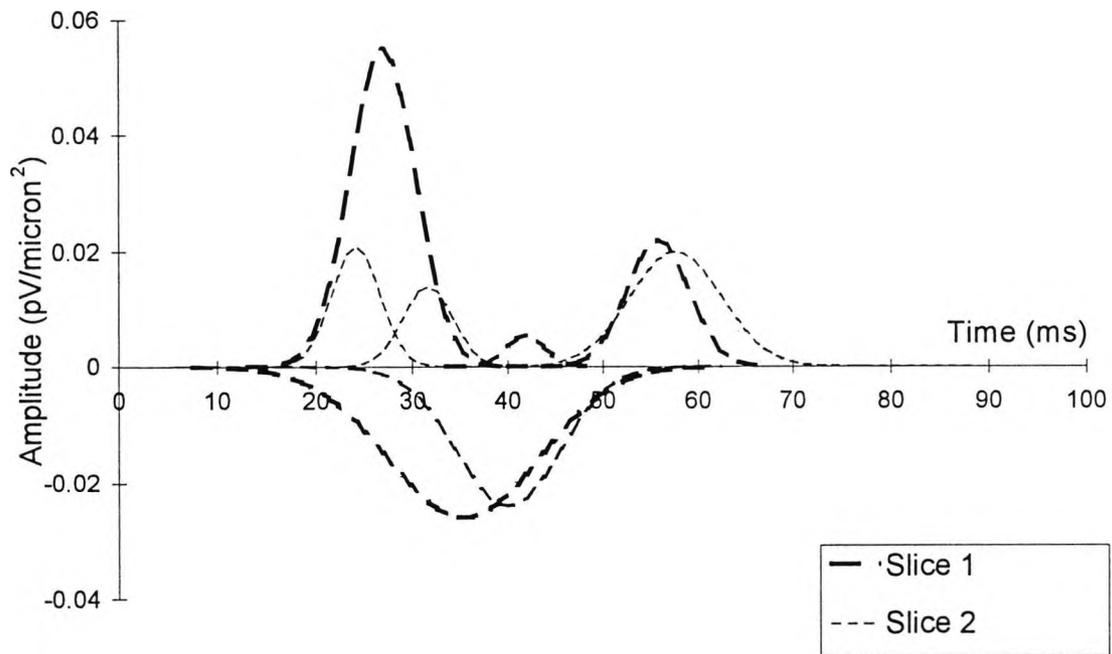
Figure 4-18   The four individual models from Figure 4-16 and Figure 4-17 slice 1 and 2 respectively, of the 67Hz response, plotted together for comparison..

4.2.3 Comparison of the topography of the nonlinear response and the rod, cone and ganglion cell population density.

The components of the second kernel that are suggested by the analysis presented in the previous section could arise from individual cell types or from groups of interconnected cells.   This question may be answered by comparing the topography of the nonlinear response with the topography of retinal neurones.   If P23 or N31 are composed entirely or almost entirely of a response from a specific cell then a similar topography might be apparent. The average response to five concentric annuli have been calculated (see Figure 4-2), and are presented in Figure 4-19.   In the next sections are compared with cone, rod and ganglion cell populations.
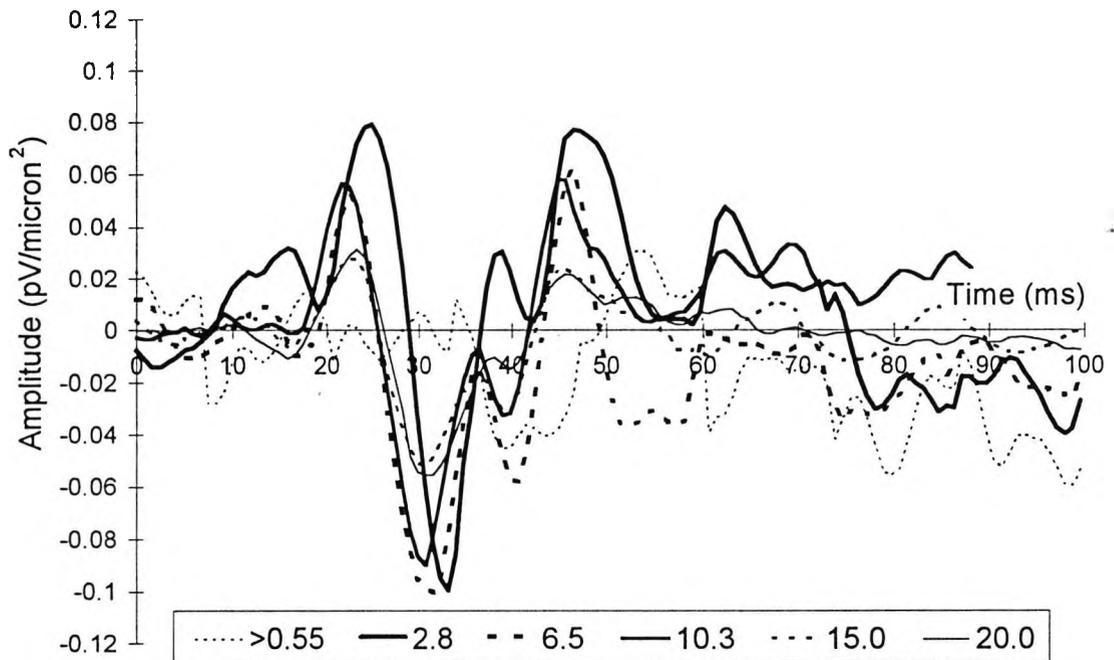
Figure 4-19   Six nonlinear responses derived from five concentric annuli and the central hexagon (scale is eccentricity in degrees).

4.2.3.1 Topography of the amplitude of P23 and N31.

Figure 4-20 illustrates the topography of the absolute amplitude of the two largest components of the first slice of the second order kernel, P23 and N31.   On the same figure the densities of the cone, rods and ganglion cells, abstracted from Curcio et al. (1990; 1990), are plotted for comparison.   By adjusting the scaling of the axes in Figure 4-20 quite different topographical comparisons can be made.   It is clear that no similarity in topography exists for any relative scaling.   However, ganglion cell size varies greatly across the retina and since ganglion cell size is related to ganglion cell receptive field size, it may be more relevant to consider the density of ganglion cell receptive fields.   In the bottom panel of Figure 4-20, the absolute amplitudes of P23 and N31 have been plotted with two functions that estimate the receptive field densities of ganglion

173

cells. One represents the receptive field size of all ganglion cells and is extrapolated from an estimate of cortical magnification, it is: $[0.0055(1+0.59\theta)]^{-2}$ (Drasdo, 1977 and 1989).
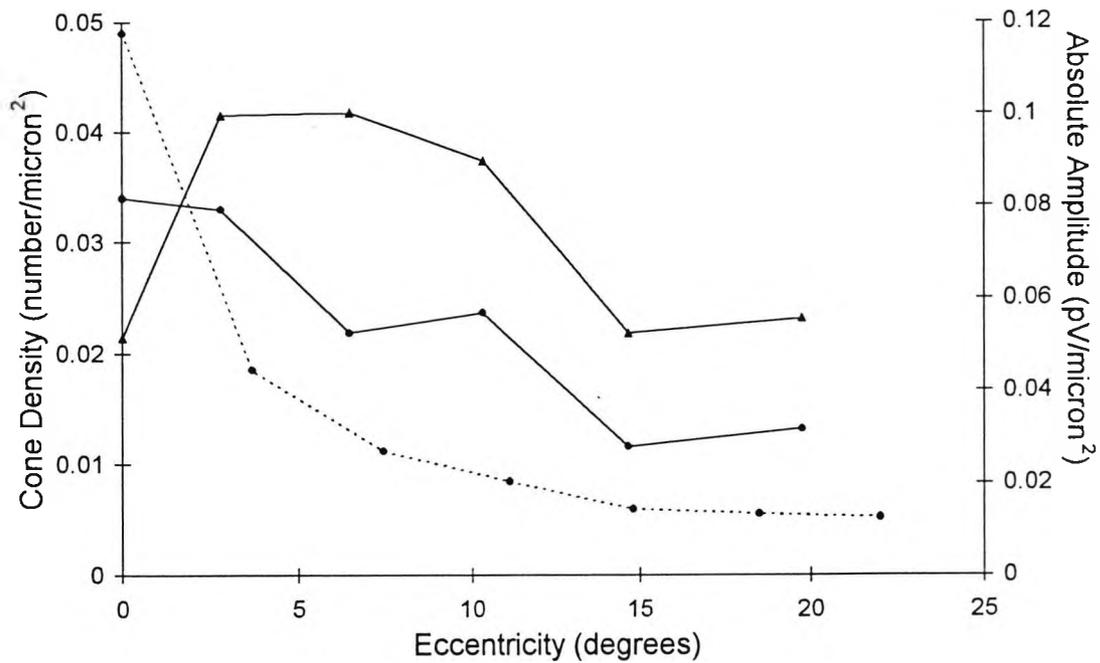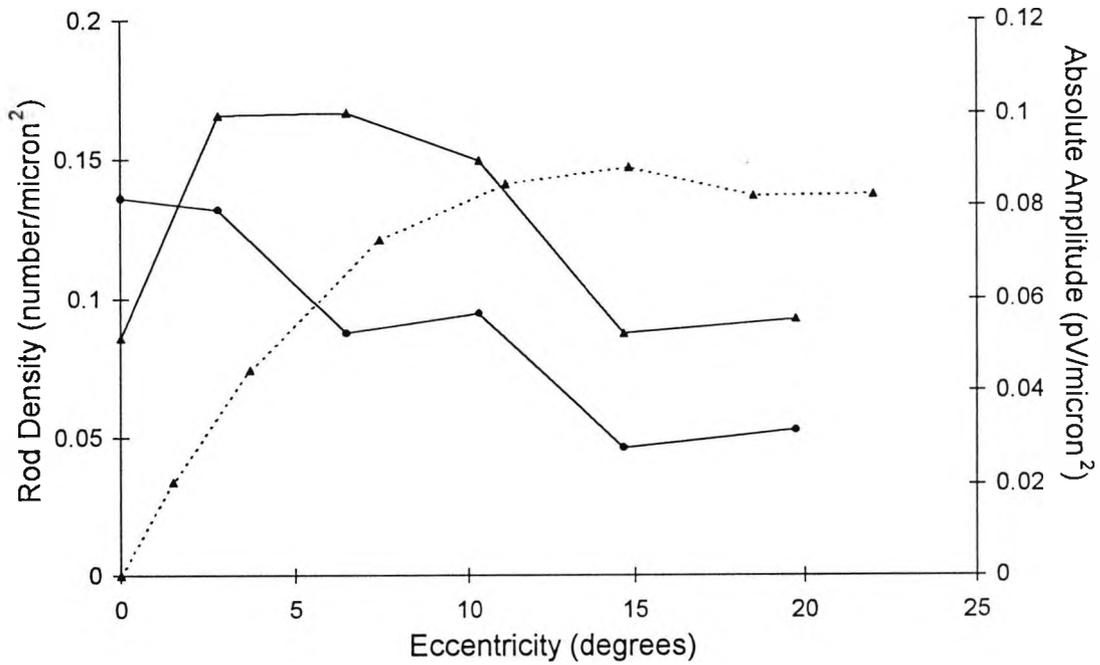
(for caption see opposite page)
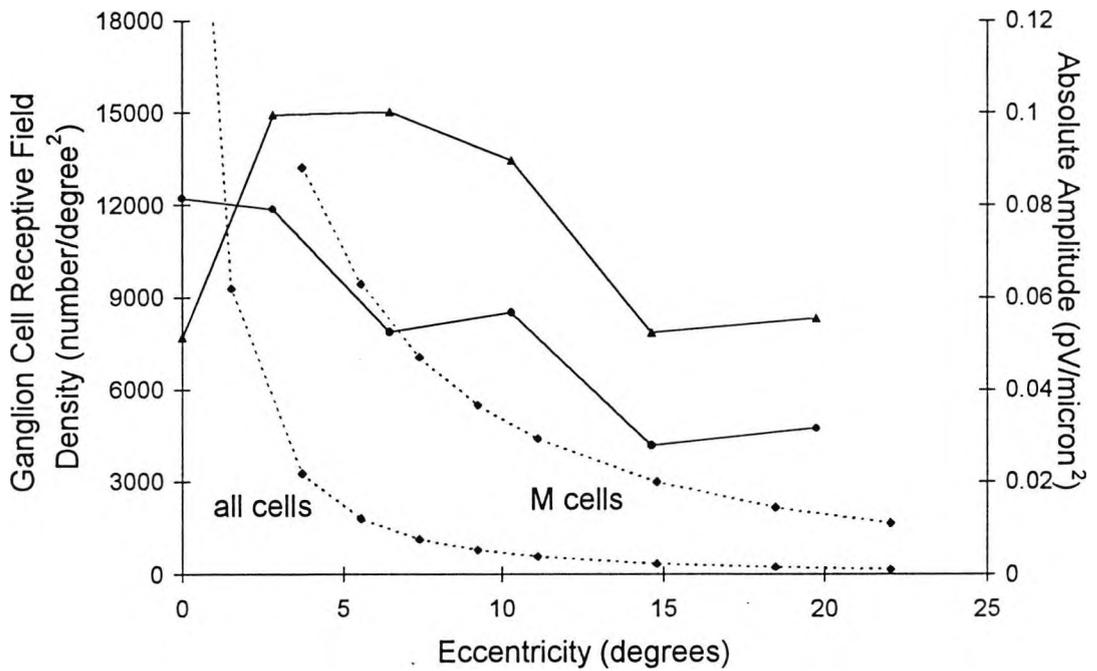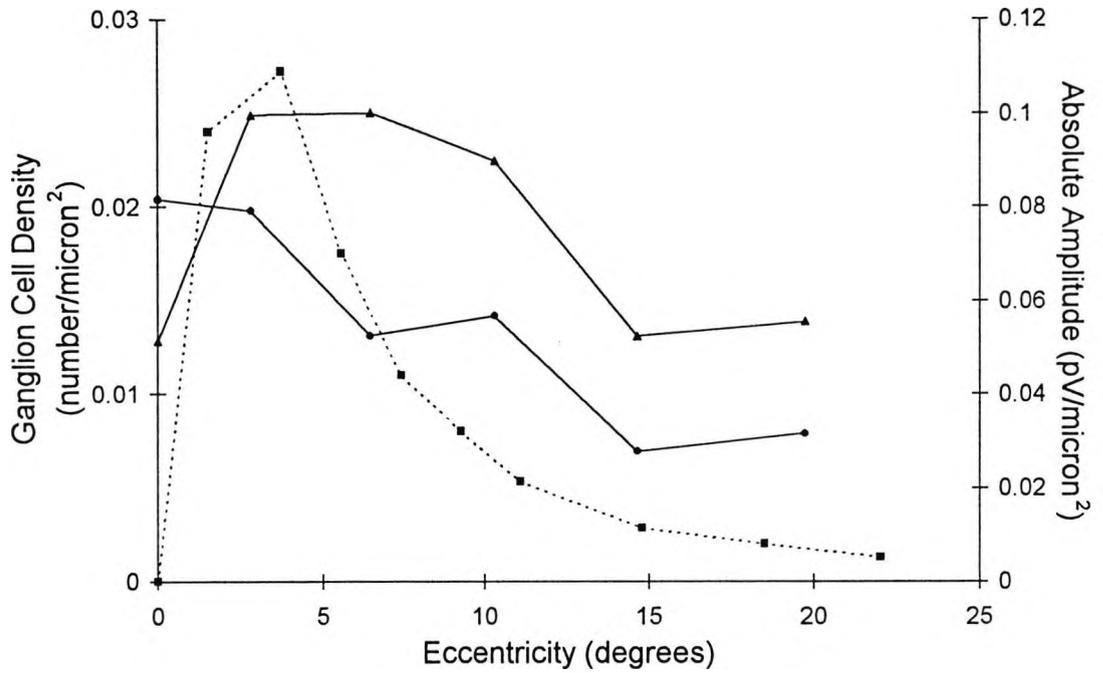
Figure 4-20   Comparison of P23 and N31 amplitude with rod (top left), cone (bottom), ganglion (top right) cell density and ganglion cell receptive field density (bottom right).

Legend:
- ⋯▲⋯ Rod Cell Density
- ⋯●⋯ Cone Cell Density
- ⋯■⋯ Ganglion Cell Density
- ⋯◆⋯ Ganglion Cell Receptive Field Density
- —— P23 Scaled Amplitude
- —— N31 Scaled Amplitude

175

The other is an estimation of the ganglion cell receptive field density of M ganglion cells only, and assumes that M-ganglion cells in the rhesus monkey form a similar proportion of all ganglion cells as they do in humans, it is: $[0.0055(1+0.157\theta)]^{-2}$ (Drasdo, 1989). The number 0.0055, found in both of these models, is proportional to the receptive field density of all ganglion cells in the fovea, but may be inaccurate for foveal M cells, because at this point in the retina P cells outnumber M cells. The value for 0 degrees eccentricity has not been plotted in Figure 4-20.

In Figure 4-20 the amplitude of P23 can be seen to approximately co-vary with M ganglion cell receptive field density. The implication is that P23 may, at least in part, have its source in the response of M-ganglion cells. If rods form a contribution to the linear response then it is plausible that rod-driven inner retinal neurones of the achromatic system, such as M ganglion cells, could contribute to the nonlinear response. The achromatic system is characterised by huge convergence in which up to 75,000 rods may have inputs on a single M ganglion cell. To serve this convergence many more inner retinal neurones are recruited to the achromatic system than to the chromatic system. For this reason the pattern electroretinographic response to chromatic stimuli is much smaller than to achromatic stimuli (Arden et al. 1982). Other neurones that contribute to the achromatic system include two types of amacrine cells - AII and A17 - that are the most numerous in the retina. A contribution to the electroretinogram from amacrine cells has already been shown: the scotopic threshold response and at least one of the oscillatory potentials have their origin in amacrine cells

(see 1.2.7 and 1.2.8). For these reasons a contribution to the nonlinear electroretinogram from amacrine cells is also possible.

4.2.3.2 Topography of the latency of P23 and N31.

Small changes in the relative latency of P23 and N31 could have a marked effect on their measured amplitudes. The difference in latency of P23 and N31, that is, the number of data points on the falling phase of the response between 23 and 31 ms, is about nine to ten data sampling points. If both of the peaks were to move by several data points in opposite directions a significant change in response amplitude could be observed without a change in the amplitude of the response of the underlying component. Figure 4-21 illustrates the topographical variation in the difference in latency of P23 and N31. It is clear that the difference in latency of both peaks does not vary greatly with topography. Topographical variation in response latency does not appear to play a role in defining response amplitude.
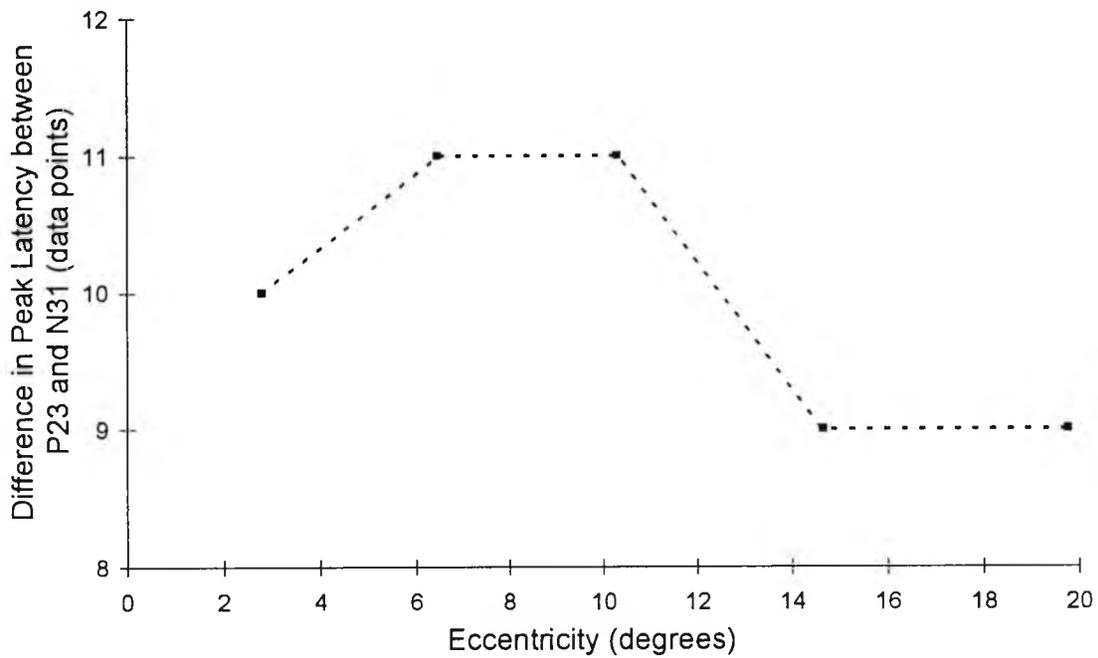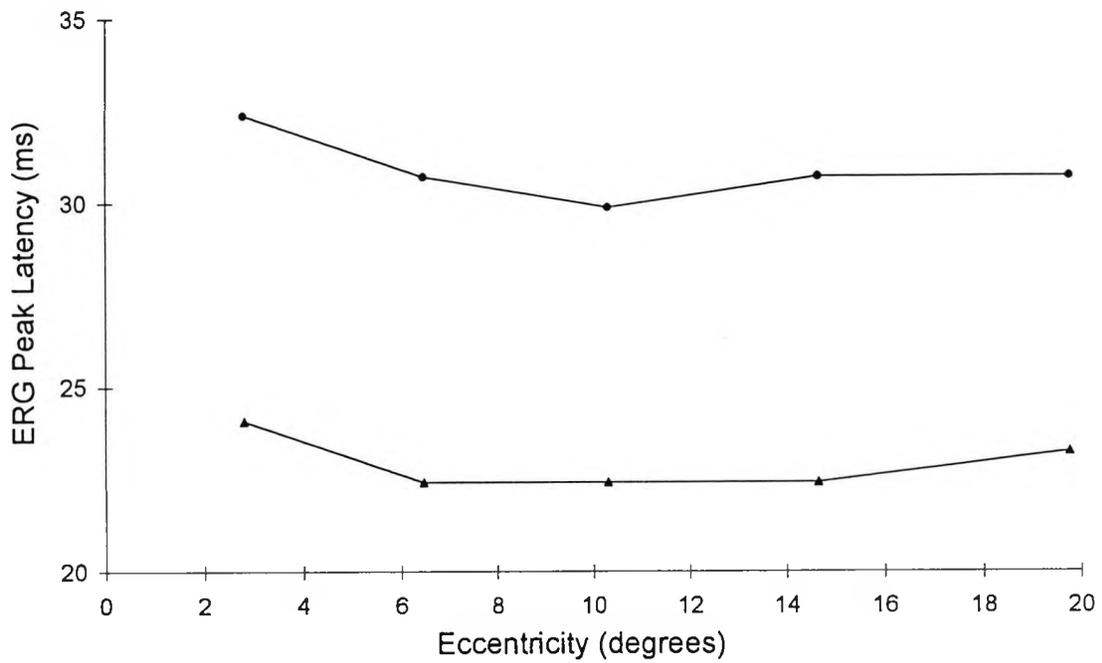
Figure 4-21   The peak latency of the P23 and the N31 features is illustrated above, and the absolute difference in latency, in data points, is illustrated below.   No variation in response latency is observable.

P23 Peak Latency
N31 Peak Latency
Latency (N31-P23)

4.2.4 The Optic Nerve Head Component.

A component of the nonlinear response has been identified in the second kernel first slice by Sutter and Bearse (1995; 1999). Using the responses of the twelve hexagons indicated in Figure 4-22, Sutter and Bearse isolated a minor component whose latency varied across the field relative to the major part of the response. The latency of the component seemed to increase with the estimated ganglion cell fibre length from the optic disk so Sutter and Bearse termed this the optic nerve head component. The rest of the response was then termed the retinal component. Other workers have been to unable repeat the experiment (Vaegan, personal communication, 1997; Keating and Parks, personal communication, 1997) or to locate the component using other techniques (Vaegan and Sanderson, 1997) and so the existence of this component has been the subject of considerable debate. However, at the 1997 ARVO meeting Bearse revealed that 16 samples per frame are required to resolve the component, and this sampling rate had not been used by the other workers. In an attempt to clear up some of the confusion the Sutter and Bearse method of component separation has been repeated here. The average of five responses of the experienced normal have been used, which were sampled 16 times per frame.

4.2.4.1 Optic Nerve Head Component: Method

The major component of the nonlinear (second kernel, first slice) response varies little from hexagon to hexagon (see Figure 4-23). However the presumed minor component has a latency which

varies in a quite different manner. Hence if the responses to the different hexagons are lined up (adjusted in time) so that the latency of the major waveform peaks become identical, the minor responses will have different timings. If these adjusted waveforms are summed, the result will be the average of the major components, but the minor components will be 'smeared out' - essentially low pass filtered. This process yields the first estimate (major).

This new estimate of the major component waveform can now be subtracted for the response to individual hexagons. The first estimate (major) must be scaled and time-shifted differently for each of the individual responses. What is left after each subtraction should be the minor component. Now, y time-shifting the minor responses so they have the same latency and averaging them, a new improved estimate of the minor response can be obtained, the first estimate (minor).

This process may now be iterated. From the crude result to each hexagon it is possible the subtract the first estimate (minor), first adjusting the latency and amplitude of the estimate. The resulting trace contains little but the major component. These are time-shifted and averaged, as before, to produce the second estimate (major) and so by similar steps the second estimate (minor).

4.2.4.2 Optic Nerve Head Component: Results and Discussion

The major component, without local variation in latency, and the minor component, with latency variation, are presented in Figure 4-

180

24; the sum of the two components are presented in Figure 4-25 with the original response. The latency of the minor component is presented in Figure 4-26 and it is clear that the latency does not simply increase linearly with distance from the optic nerve head, instead a more complicated pattern is visible.

These results suggest that Sutter and Bearse may indeed have separated the nonlinear response into two components with a different latency topographies, and suggests that Vaegan and others did fail to find the component because they were not sampling the response with sufficient frequency. Sutter and Bearse have also shown that the minor response can be enhanced by a particular siting of the reference electrode (Sutter and Bearse, 1999).

But does the minor component arise from the optic nerve head? A linear relationship between fibre length and 'optic nerve head' component latency makes no concession to inter-individual variation in ganglion cell fibre propagation velocity. There is a dispersion of fibre conduction velocities in the intraretinal nerve fibres because of varying axon diameters. The figure that Bease and Sutter site for conduction velocity, based on the cat (Stanford, 1987), might not be an accurate estimate for conduction velocity in man because cats, unlike humans, posses myelinised intraretinal nerve fibres. It is not clear why a train of nerve impulses should produce a response formed, like the minor component, of three peaks.

It is possible that the minor component may be an artefact introduced by the action of adding and subtracting waveforms after they have been time-shifted by very small measures. The entire minor component complex is only 8ms in duration, and its most sizeable portion is a negative-going spike that is only 3ms long and spans just four sampling bins. The variation in latency with hexagon spans only six time bins. Even at 16 samples per frame the technique is exploring the bottom end of temporal resolution that VERIS is capable of.
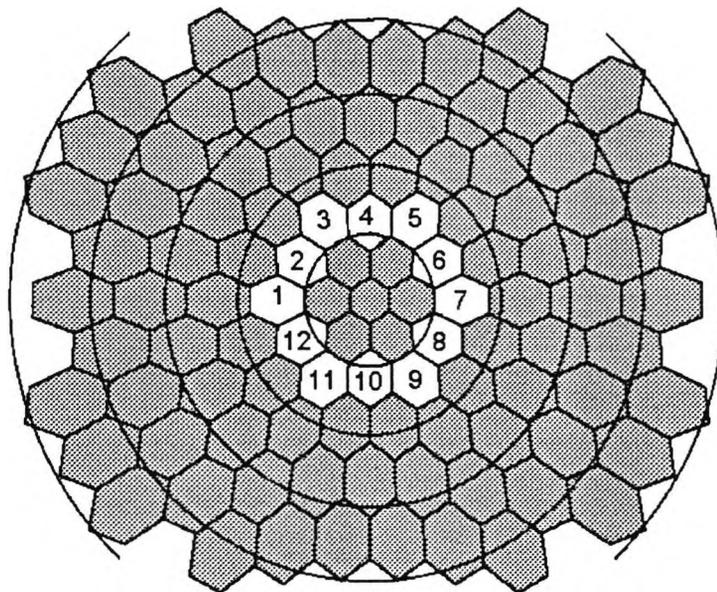
Figure 4-22   The responses of these twelve hexagons were analysed by Sutter and Bearse and in the results presented in this section.
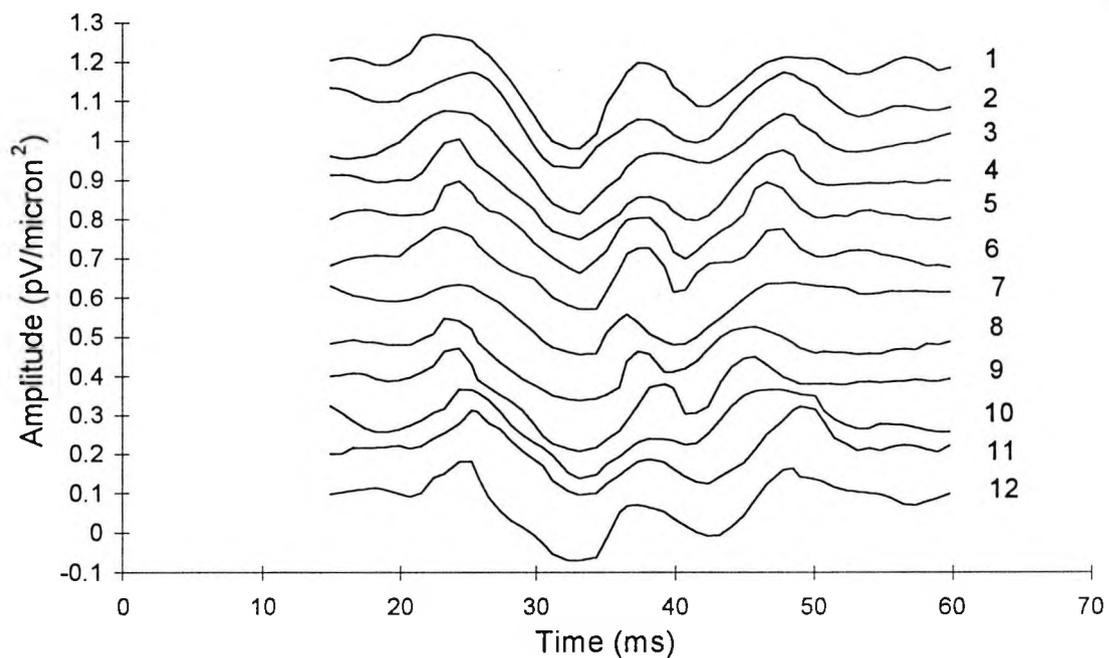
Figure 4-23   The crude responses of the twelve hexagons analysed by Sutter and Bearse and in the results presented in this section.
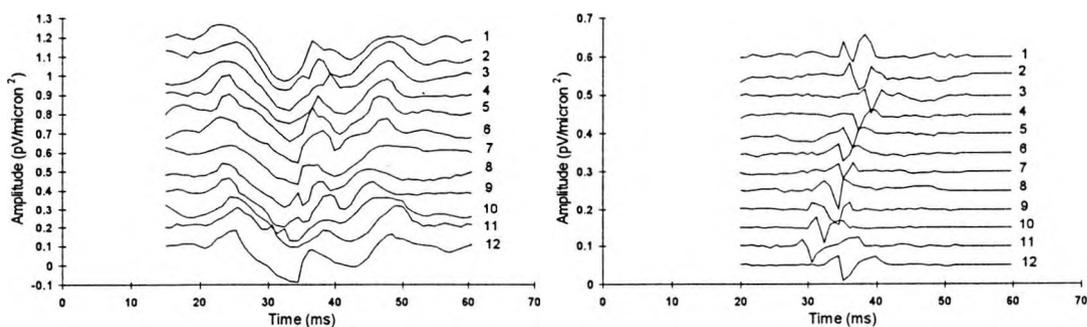
Figure 4-24   The major component (left) and minor component (right) of the second kernel first slice, hexagons are numbered with respect to scheme shown in Figure 4-22.

183
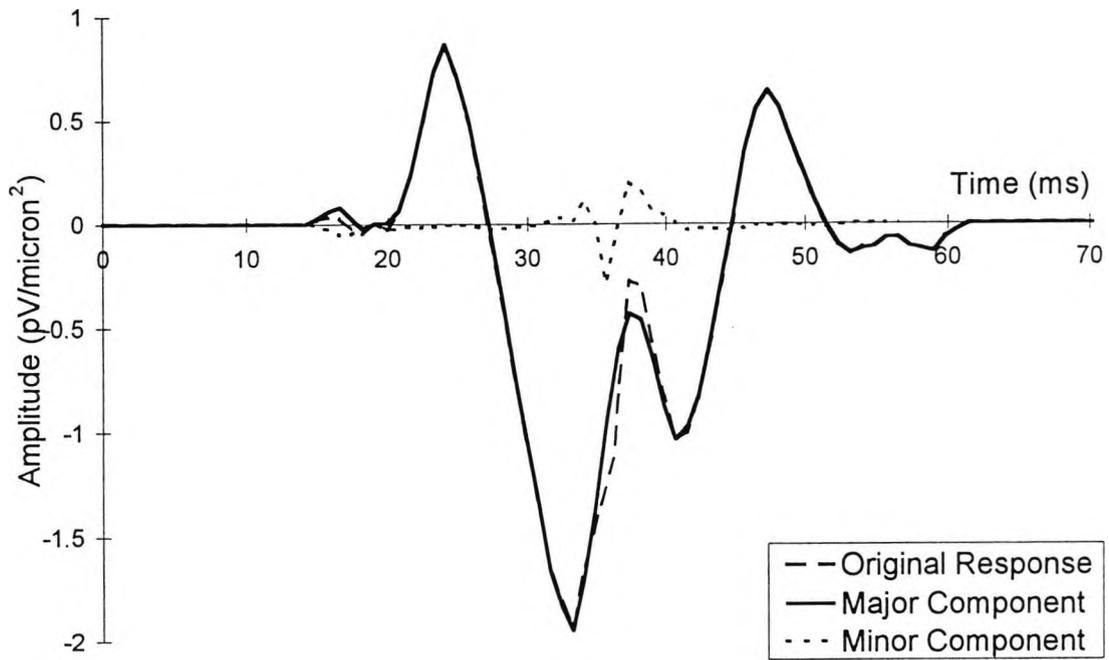
Figure 4-25   The nonlinear response (original response) with the major component and minor component of all the hexagons in the annulus.
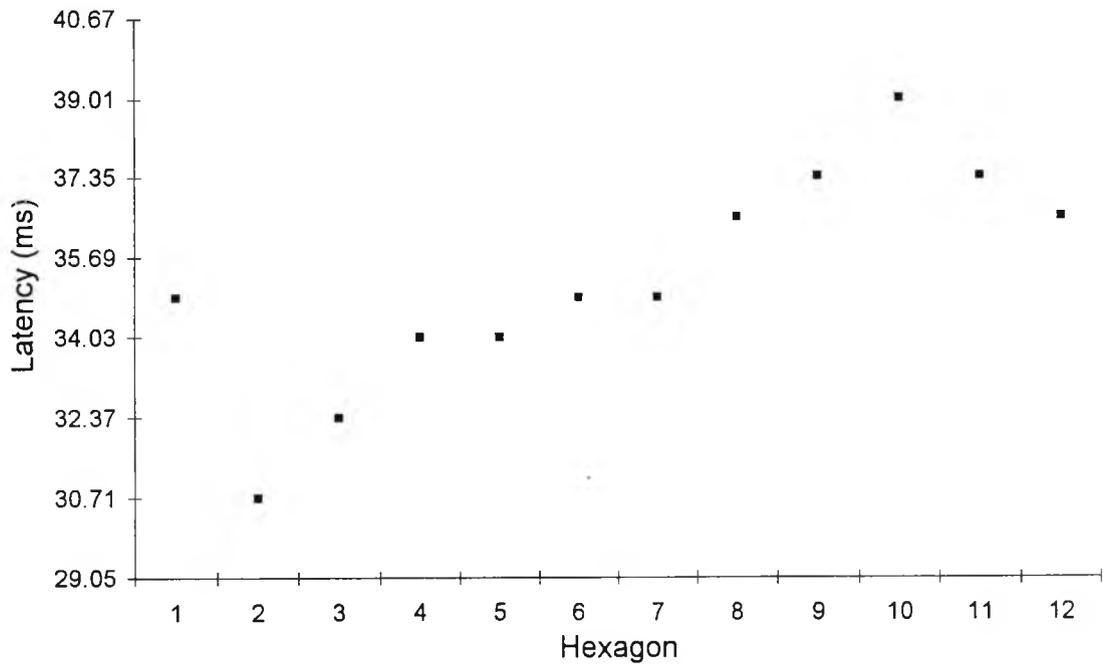
Figure 4-26   The latency to peak of the minor component, it does not follow the pattern shown in Sutter and Bearse, 1995; for key to hexagon numbering see Figure 4-22.

4.3 Topography of Age-Related Changes in the Linear and Nonlinear Electroretinographic Response of the Normal Eye.

A study was performed to investigate the topography of the effect of non-pathological ageing on the linear and nonlinear electroretinogram.

4.3.1 Age-related Changes in the Electroretinogram: Recruitment of Normals.

Normal subjects were recruited through an article in the local newspaper, or from personal contacts. Normals were given a full eye examination by a qualified optometrist in the Research Centre, unless they were colleagues from within the Research Centre (in which case ocular well-being had been demonstrated on many occasions). It was important to ensure that the normals were all free of any pathology that could confound the results. Normal volunteers who were accepted for the trial had:

- *Visual Acuity≤6/12.* Visual acuity above this level would very probably indicate a retinal pathology.
- *IOP≤21mmHg.* IOP higher than 21mmHg might indicate the presence of glaucoma.
- *No visual field defects* detectable with the Humphrey Field Analyser (24-2 programme). Visual field defects might indicate that the presence of glaucoma, or another pathology.
- *No cupping, pallor or oedema of the optic disk.* These signs might indicate the presence of glaucoma.

- *Lenticular opacities not greater than NI, CII or PI* by LOCS III (Chylack et al. 1993). A clear medium was required for multiple input stimulation.
- *No retinal disease* detectable with fundus examination. The presence of another retinal disease could confound the results by giving an abnormal ERG.
- *No colour vision anomalies* when assessed with the 100-Hue test. The presence of colour vision anomalies could confound the results by giving an abnormal ERG.

Volunteers were reimbursed £10 for inconvenience caused.

4.3.1.1 Normal subject recruitment statistics.

N=34. Age: mean=54.8, SD=15.4, range=26 to 76.

19 (55%) were female, 15 were male.

Age, sex and tested eye are given in Table 4-6, below.

4.3.2 Age-related Changes in the Electroretinogram: Method.

Linear and nonlinear (first kernel, first slice) responses were studied. In both cases the array of 103 electroretinograms from each subject were grouped into five concentric annuli (Figure 4-2) and averaged. The amplitude and latency of P23 and N31 were established in the central region and at five eccentricities corresponding to the five annuli. These twelve variables described the topographical variation in the response. Regression analysis was used to calculate the rate of change of amplitude and latency with respect to age for each component using a linear model.

Subject	Age	Sex	Eye	Subject	Age	Sex	Eye
SJC	26	F	OS	RH	60	F	OS
LM	28	F	OS	PBH	61	M	OS
JAF	29	F	OD	EAB	62	F	OS
MPC	36	F	OS	JP	63	M	OD
DRSW	47	M	OD	BA	63	M	OD
NE	32	M	OS	JBA	64	F	OS
SO	30	F	OS	DMW	65	F	OD
KTJ	30	M	OS	GAB	66	M	OD
RT	39	M	OD	MEF	66	F	OS
RW	47	F	OD	MT	68	F	OD
CPD	52	M	OS	DP	70	M	OD
PMC	53	F	OD	EEH	70	F	OD
KDY	58	M	OD	JTC	70	F	OS
JJWD	58	M	OD	GB	70	F	OS
FAEC	52	F	OD	TKOG	75	M	OS
SEAB	57	F	OS	FRB	75	M	OD
TM	47	M	OS	AB	76	F	OS

Table 4-6   Age, sex and tested-eye of all 34 normal subjects.

4.3.3 Changes in the Linear Electroretinogram due to Ageing.

The results of the analysis on the linear response are summarised in Table 4-7 (a-wave) and Table 4-8 (b-wave).   Table 4-7 shows that although the amplitude of the a-wave is not affected by age, the latency of the a-wave increases.   Both of these affects are uniform across the retina: the rate of change of a-wave latency with respect to age is between 0.040 and 0.055 ms/year.
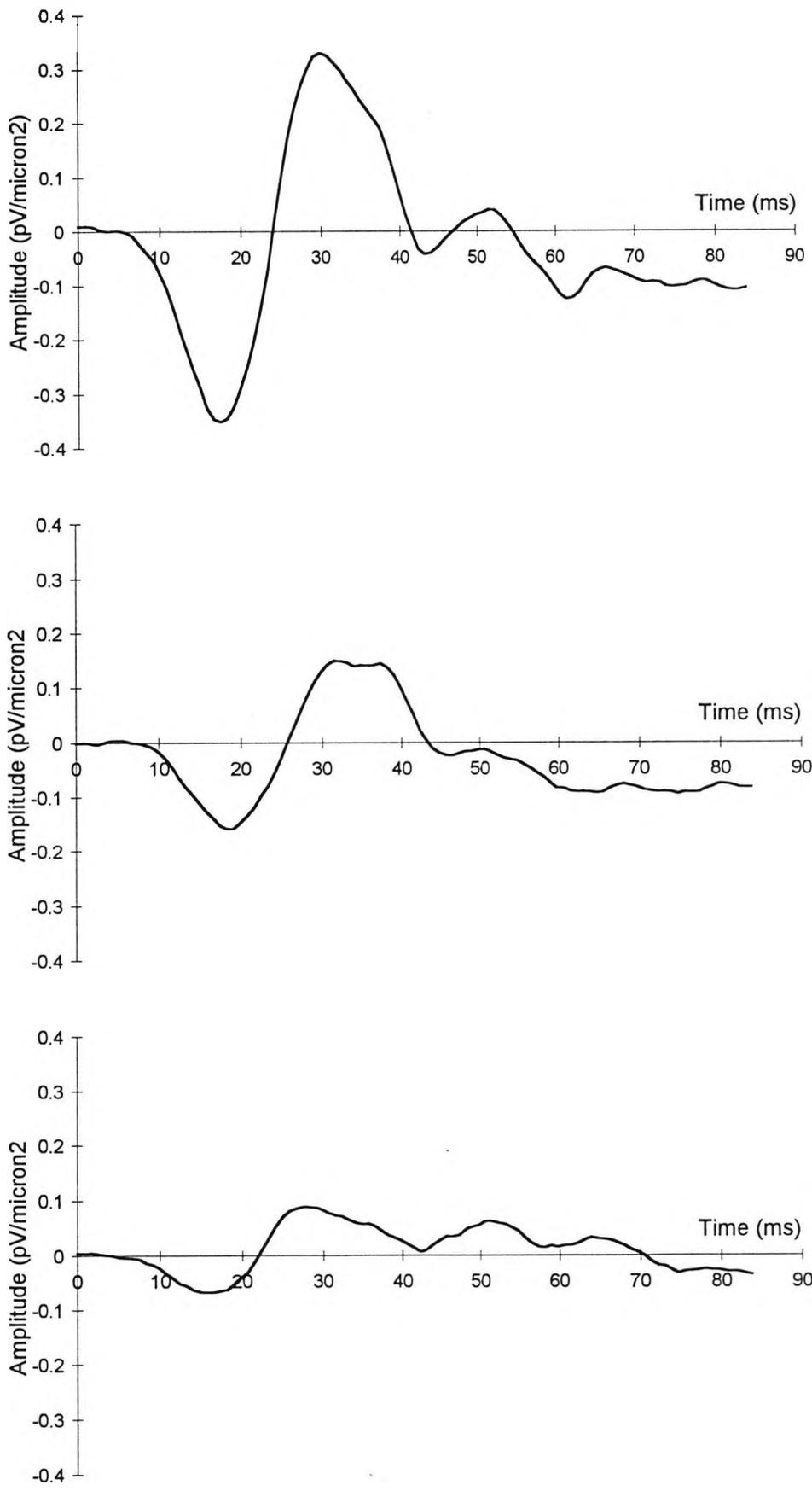
*Figure 4-27   The range in quality of the linear (left) and nonlinear (right)
responses achieved from best (top) via medium (continued next page...)*
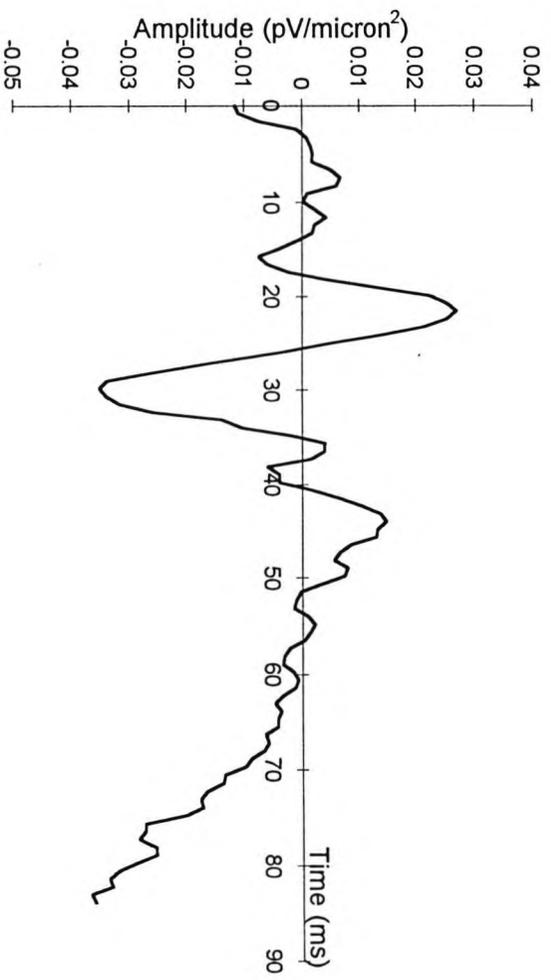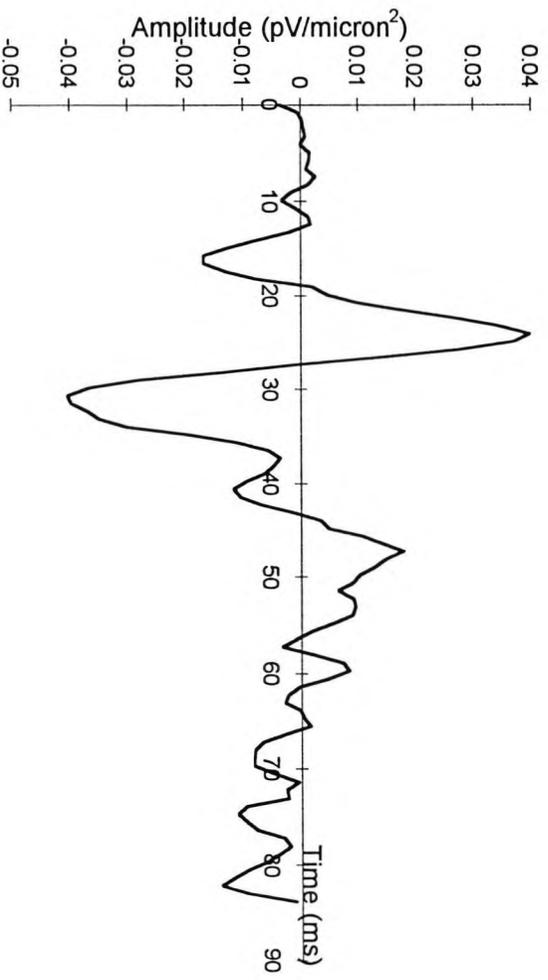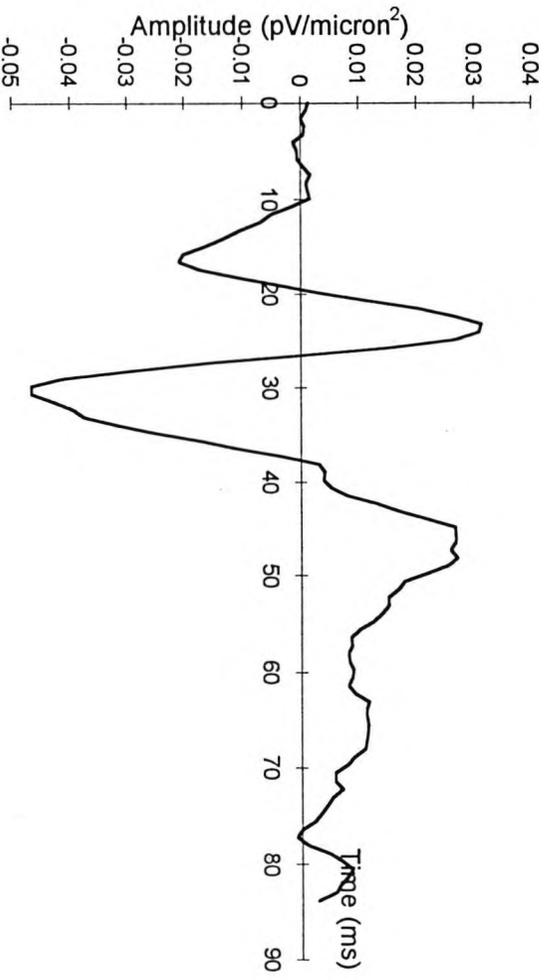
(...cont.) to worst (bottom), being subjects JAF, JTC and KTJ respectively.

189

	Linear Response, a-Wave							
	Amplitude (pv/micron^2)				Latency (ms)			
Eccentricity	Mean	r	Slope	P-Value	Mean	r	Slope	P-Value
<1.55	-0.61	0.138	0.002	NS	18.6	0.453	0.054	0.007
2.80	-0.32	0.192	0.002	NS	18.0	0.400	0.040	0.020
6.50	-0.20	0.173	0.001	NS	17.3	0.533	0.046	0.001
10.5	-0.16	0.167	0.001	NS	17.5	0.515	0.045	0.002
14.5	-0.13	0.095	0.000	NS	17.9	0.577	0.046	>0.001
20.0	-0.13	0.032	0.000	NS	18.2	0.697	0.053	>0.001

Table 4-7   Linear response, mean a-wave amplitude and latency at five eccentricities and the central area.   R value and slope are of a least squares fit to age in years.   NS = not significant, P>0.05.

Table 4-8 shows that the b-wave latency increases with age at every retinal eccentricity.   The rate of increase in latency is highest between about 11 and 15 degrees but lowest in the region below about 3 degrees.   In the central area, the rate of increase in latency of the b-wave is almost identical to the rate of increase in the latency of the a-wave (illustrated in Figure 4-28), this might conceivably imply that the change in a-wave latency is responsible for the change in b-wave latency and no other affects are being observed.   The b-wave amplitude was unchanged in ageing except in the central area, where a reduction in amplitude was observed.

The age-related changes to the linear electroretinogram of the normal retina can be summarised as an increase in a-wave latency (see Figure 4-29).   The rate of increase in latency is constant across the retina (P=0.601) (see Figure 4-30).   The latency of the b-wave and the amplitude of the a-wave is unchanged in non-pathological ageing at every retinal eccentricity, and the amplitude of the b-wave decreased only at eccentricities <1.55 degrees.

	Linear Response, b-Wave							
	Amplitude (pv/micron^2)				Latency (ms)			
Eccentricity	Mean	r	Slope	P-Value	Mean	r	Slope	P-Value
<1.55	0.83	0.342	-0.009	0.047	32.4	0.344	0.056	0.047
2.80	0.39	0.311	-0.003	NS	31.5	0.370	0.048	>0.001
6.50	0.26	0.330	-0.002	NS	30.7	0.447	0.069	0.008
10.5	0.17	0.235	-0.001	NS	30.7	0.489	0.100	0.003
14.5	0.13	0.277	-0.001	NS	32.0	0.526	0.117	0.001
20.0	0.11	0.126	0.000	NS	32.5	0.466	0.092	0.006

Table 4-8   Linear response, mean b-wave amplitude and latency at five eccentricities and the central area.   R value and slope are of linear fit to age in years.   NS = not significant, P>0.05.
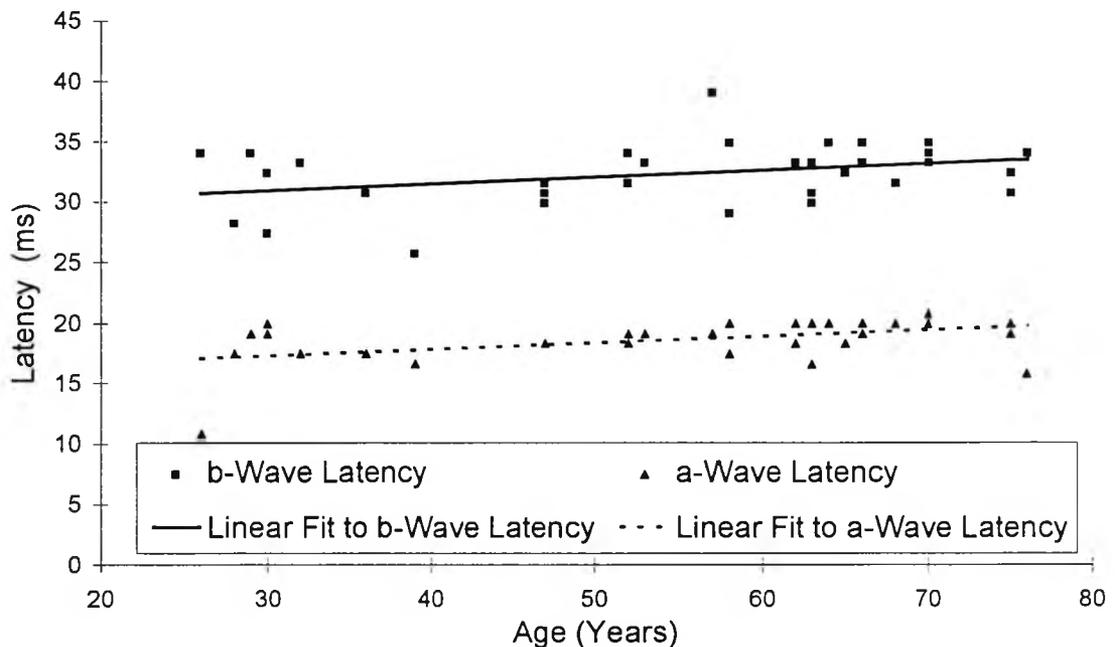
Figure 4-28   Linear response, <1.55 degrees, latency of a- and b-wave in 36 normals .   The rate of change of latency of the a-wave (0.056ms/year, P=4.7%) is identical to the rate of change of latency of the b-wave (0.054ms/year, P=0.7%).   The results of all 34 normals are presented here, some data points overlie others.
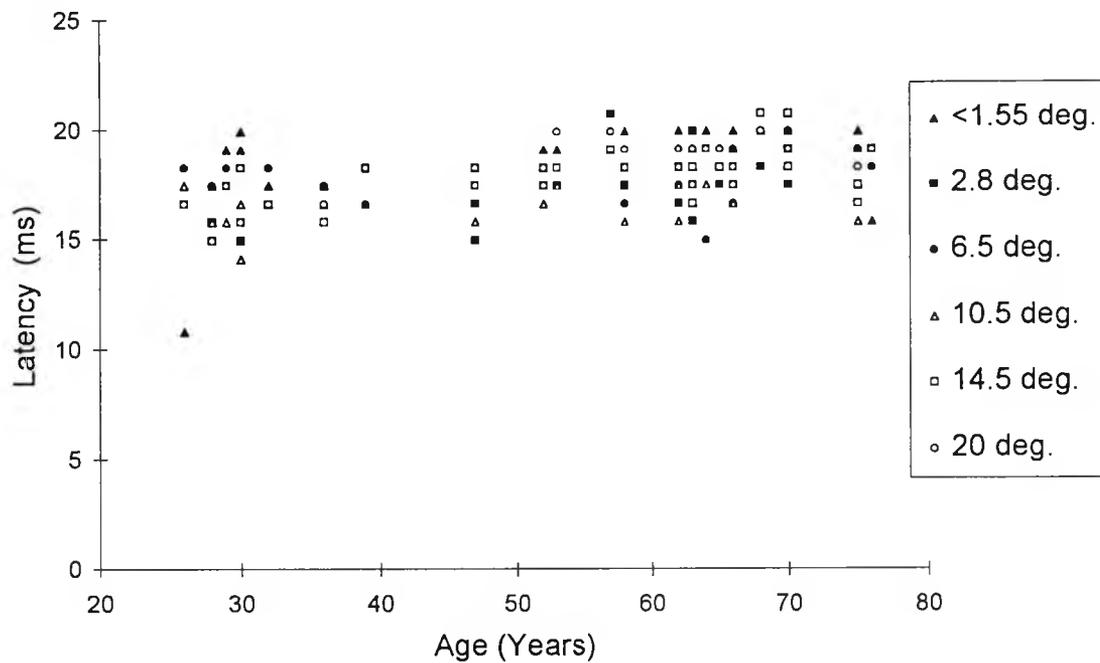
Figure 4-29   Linear response.   The latency of the a-wave of all 36 normals at the six eccentricities.   The results of all 34 normals are presented here, some data points overlie others.

Mean = 0.048 ms/year
Slope = 0.0002 ms/year/degree
$R^2 = 0.0742$
P = 0.601

Figure 4-30   Linear Response.   The rate of change of latency with respect to age.   The rate of change of latency per year with eccentricity is not statistically significantly.

4.3.3.1 Age related physiological changes in the outer retina.

Histological analysis of the age-related retina has noted a disorganisation of rod and cone outer segments, the accumulation of refractile particles and lipofuscin in cone inner segments, and displaced rod and cone nuclei (Spear, 1993). Rods are more susceptible to the deleterious affects of ageing than cones: 30% of rods may be lost from the central 30 degrees of vision by 90 years of age, but there is no significant loss of cones in the fovea or central retina before age 90 (although cones may be lost in the very far periphery, at about 60 degrees eccentricity) (Curcio and Drucker, 1993; Gao and Hollyfield, 1992). It is well established that visual acuity declines during ageing, from about 6/5 in the young to about 6/6-6/12 in 80 year olds. Two factors could bring about reduced acuity: neuronal changes and changes to the anterior eye, including a loss of transparency of the cornea, lens or vitreous and miosis. Retinal neural changes that could bring about a reduction in visual acuity include a loss of photoreceptors, bipolar cells or ganglion cells or a change in the inter-connectivity of these cells. Anatomical or physiological changes higher in the visual pathway are also conceivable and statistically significant changes in VEP amplitude and latency have been reported (Wright et al. 1985; Trick, 1987; Porciatti et al. 1992; Tomoda et al. 1991).

The decline of visual acuity with ageing cannot be attributed to a reduction in the density of cones in the fovea. A reduction in cone population density would, like media opacities, only cause a decrease in amplitude and leave the latency unaffected. The presence of disorganised cone outer segment and lipofuscins in the

inner segment indicates that phagocytotic reactions are impaired and photopigment molecules are not being replaced. A reduction in photoreceptor function, such as would be caused by defective photopigment molecules, might affect the amplitude and/or the latency of the photoreceptor potential.

Focal macular electroretinographic responses have shown a reduction in a-wave amplitude with age when evoked with checks (Bagolini et al. 1988) and flicker (Birch and Fish, 1988). Full-field photopic electroretinograms have exhibited a reduction in a- and b-wave amplitude (Weleber, 1981; Wright et al. 1985) and an increase in latency (Wright et al. 1985). All these reports have failed to control for senile miosis and media opacities, which could be responsible for the observed reductions in a- and b-wave amplitudes. Weale (1982) has shown that optical factors are insufficient to account for the visual acuity loss, and acuity continues to declines after the crystalline lens has been replaced with a prosthesis (Spear, 1993). Although cone density is maintained during ageing, it is possible that diminished cone function could play a part in reducing visual acuity. The magnitude of the visual acuity deficit increases as the luminance decreases (Spear, 1993) which might imply a reduction in the capacity of photopigments to react to low luminance levels.

4.3.3.2 The Linear Electroretinogram in Ageing: Discussion

The VERIS multifocal electroretinogram results reported here were achieved with dilated pupil and using subjects carefully screened to reduce the occurrence and severity of media opacities (see Section

194

4.3.1).   The absence of a decrease in a-wave amplitude probably reflects the absence of any age-related decline in cone population density, and no other affects.   The increased a-wave latency might be related to an alteration in cone receptor function, which can now be reported to occur uniformly at every eccentricity up to 20 degrees.   If cone function is altered due to impaired phagocytotic reactions only, then it is possible that the subsequent stages of the enzyme cascade survive the ageing process intact.   Such a result would have important implications for bipolar cells where the enzyme cascade is identical to that found in photoreceptors, only with a synapse instead of the initial stage of photopigment activation by light (Nawy and Jahr, 1990).   The amplitude of the b-wave is no smaller in the response from an aged eye than from a young eye, throughout all but the most central portion of the retina (Table 4-8), which might suggest that the enzyme cascade in bipolar cells is also unaffected by ageing.

4.3.4 Changes in the Nonlinear Electroretinogram due to Ageing.

The changes due to ageing in the amplitude and latency of the P23 and N31 features of the nonlinear electroretinogram are presented in Table 4-9 and Table 4-10.   The amplitude of the nonlinear response is remarkably resilient to age-related alteration, neither P23 or N31 undergo statistically significant change in amplitude between 20 and 80 years of age.   The latency of P23 and N31 features are more labile, and both increase significantly as age increases.   The latency of P23 is unaffected by age in an annulus up to about 2.8 degrees.   From about 2.8 degrees to the edge of the stimulated area of retina - about 20 degrees - the rate of change

of P23 latency with respect to age is about 0.06 ms/year, with a mean of between 21.8-22.5ms.

Eccentricity	Nonlinear Response, P23							
	Amplitude (pv/micron^2)				Latency (ms)			
	Mean	r	Slope	P-Value	Mean	r	Slope	P-Value
<1.55	0.258	0.286	-0.003	NS	25.4	0.002	-0.001	NS
2.80	0.085	0.239	-0.001	NS	22.3	0.272	0.061	NS
6.50	0.074	0.001	0.000	NS	22.0	0.411	0.068	0.016
10.5	0.049	0.070	0.000	NS	21.8	0.420	0.062	0.013
14.5	0.026	0.100	0.000	NS	22.2	0.435	0.064	0.010
20.0	0.026	0.176	0.000	NS	22.5	0.402	0.057	0.018

Table 4-9   Nonlinear response, mean P23 amplitude and latency at five eccentricities and the central area.   R value and slope are of linear fit to age in years.   NS = not significant, P>0.05.

Eccentricity	Nonlinear Response, N31							
	Amplitude (pv/micron^2)				Latency (ms)			
	Mean	r	Slope	P-Value	Mean	r	Slope	P-Value
<1.55	-0.153	0.223	0.003	NS	34.1	0.280	-0.131	NS
2.80	-0.099	0.184	0.001	NS	33.9	0.200	0.049	NS
6.50	-0.081	0.077	0.000	NS	31.1	0.176	0.018	NS
10.5	-0.069	0.032	0.000	NS	29.9	0.292	0.036	NS
14.5	-0.054	0.114	0.000	NS	30.8	0.084	0.008	NS
20.0	-0.046	0.184	0.000	NS	30.5	0.411	0.053	0.016

Table 4-10   Nonlinear response, mean N31 amplitude and latency at five eccentricities and the central area.   R value and slope are of linear fit to age in years.   NS = not significant, P>0.05.
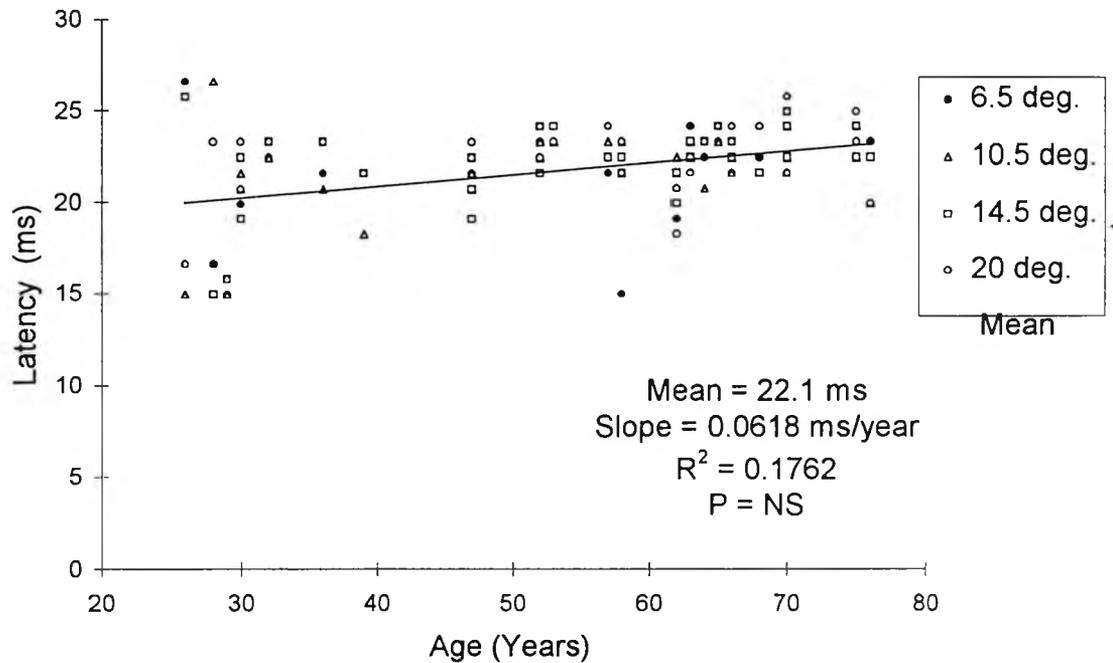
Figure 4-31   Nonlinear response.   Latency of P23 of all 34 normals at five eccentricities is presented here.   The rate of change of latency with age is the same at all these eccentricities.   The results of all 34 normals are presented here, some data points overlie others.

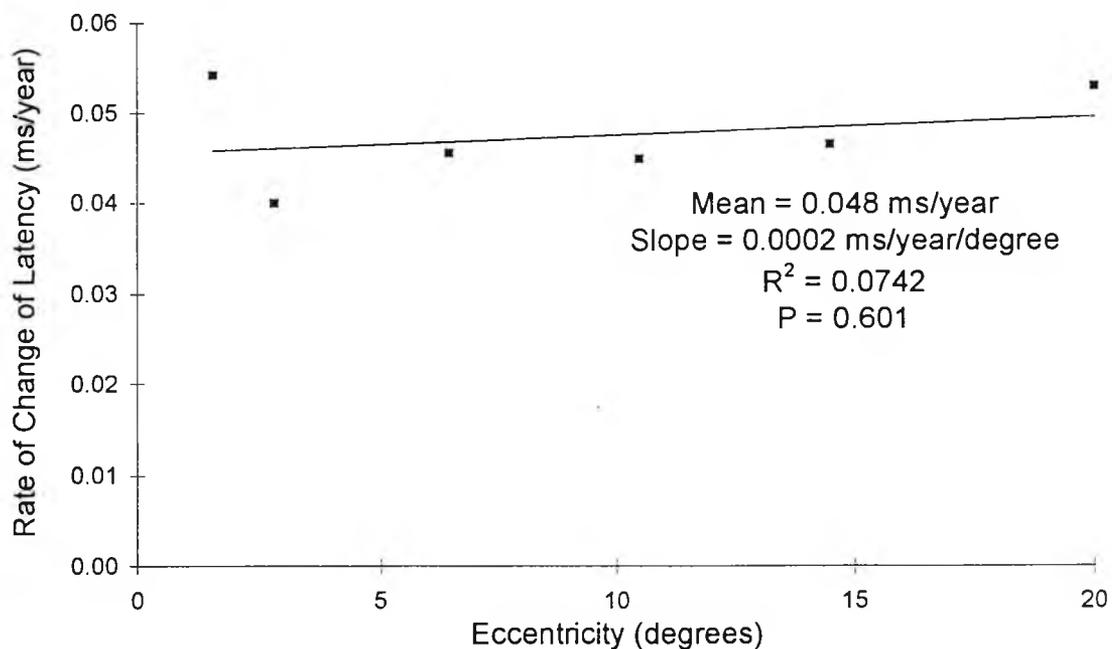The rate of change of latency with respect to age of the annulus centred at 2.8 degrees is not statistically significant, but the rate of change of latency of the more eccentric responses are statistically significant at between 1.0% and 1.8%.   Like P23, the latency of P30 is only affected by age in the periphery.   The rate of increase of latency with age varies considerably across the retina.   Only at about 20 degrees is the rate of change of latency statistically significant.

4.3.4.1 Age-related physiological changes in the inner retina.

Studies on the effect of ageing on retinal ganglion cells have employed soma and optic nerve counts as well as a histological analysis of dendritic morphology in whole-mounts.   Balaszi et al.

197

(1984) found an age-dependant statistically significant reduction in ganglion cell axon number in the optic nerve heads of 16 patients aged between 3½ and 82 years. Using linear regression Balaszi et al. found that about 5,600 axons died each year. Gao and Hollyfield (1992) found that neurones of the ganglion cell layer in the fovea decreased by 16% from the second decade to the sixth, but that this increased to 50% in the far periphery (60 degrees). Curcio and Drucker (1993) found a 29% decrease in the density of foveal ganglion cells and a 22% decrease in the mean density of ganglion cells serving the central 11 degrees of vision. Curcio and Drucker found a substantial overlap In ganglion cell density between young and old retinae and no statistically significant difference in ganglion cell density between young and old eyes in the rest of the 43 degree diameter region that they studied.

The qualitative study of senile changes in the ganglion cells of the human retina by Vrabec (1965) appears to be unique. Vrabec found that the dendritic fibres of ganglion cells in the senile eye were sometimes elongated and possessed fusiform or spherical enlargements. Occasionally the dendrites ended with these enlargements, but in other cases they sprouted fine, regular fibres. Vrabec suggested that as these changes were isolated, occurring in just one dendritic branch and not the whole neurone, the probable cause may be localised, and he suggested a loss of functional connections in the dendritic tree. Studies on the topography of photoreceptor density in ageing have found that rods are far more susceptible to age induced drop-out than cones (see 4.3.3 above). Studies on ageing in the rod-dominated retinas of rats have found complete deafferentation and degeneration of inner retinal

neurones, apparently as a result of rod loss in the outer retina (Spear, 1993). If this analysis can be carried over into human retina, then cone inputs, that are sustained throughout life, could protect proximal neurones from decay. Vrabec (1965) may indeed . have witnessed ganglion cells searching for new afferent neurones after previous synaptic neighbours have disappeared. Parts of the visual system that are dedicated to the achromatic system and receive relatively few cone inputs, for example AII amacrine cells, may not survive the ageing process as well as parts that receive a rich a supply of cone-derived inputs.

The results of studies of ageing in the human retina using pattern electroretinograms have been inconsistent. Although most reports agree that alterations in the neural elements in the retina are associated with normal ageing, they disagree as to whether such changes are apparent in latency only (Celesia et al. 1987; Tomoda et al. 1991), amplitude only (Porciatti et al. 1988), amplitude and latency but without changes to spatial frequency tuning (Trick et al. 1992; Porciatti et al. 1992), or apparent in amplitude and latency and spatial tuning (Trick et al. 1986; Trick, 1987; Korth et al. 1998; Hull and Drasdo, 1990). This confusion agrees with the anatomical findings that any age-related loss of retinal ganglion cells is quite variable. None of these papers have isolated areas of retina that may be more 'at risk' in ageing than others. All of these papers have used photopic stimuli that entrain a response from both rods and cones.

4.3.4.2 The Nonlinear Electroretinogram in Ageing: Discussion.

The analysis of the components of the nonlinear response presented in Section 4.2 suggested that neurones subserving the achromatic system may make a contribution to the nonlinear response.   The analysis of the linear response given in Section 4.1 suggested a rod contribution to responses derived from at least 12.5 degrees eccentricity.   The foregoing discussion of age related alterations in the retina has suggested that inner retinal neurones that receive rod inputs may have an enhanced susceptibility to cell loss in ageing.

In the context of nonlinear electroretinographic responses this would imply age-related alterations to peripheral retinal responses. Table 4-9 and Table 4-10 illustrate that age-related alterations in the nonlinear response do not occur in the central retina.   In the retina above 1.55 degrees, the latency of the positive P23 component is increased; at about 20 degrees the N31 component is similarly affected.   As histological studies have found that ganglion cells are rather unaffected by ageing (Gao and Hollyfield, 1992; Vrabec, 1965) and nonlinear response topography is not similar to ganglion cell topography (see Figure 4.2.3.1), these age-induced latency changes probably represent absent or defective AII or A17 amacrine cells, or other neurones that are rich in rod-derived inputs.

5. Linear and Nonlinear Electroretinographic Responses in Glaucoma.

This chapter will commence with a discussion of glaucoma, considering particularly the nature and spatial location of the visual function deficits that characterise the disease. Section 5.2 will cover the criteria that were used to recruit glaucoma patients. Section 5.3 and 5.4 will analyse the linear and nonlinear electroretinographic responses of the entire visual field and of the fovea. Further analysis of electroretinographic responses will be presented in Section 5.5 that attempts to correlate the localisation of scotomata with electroretinographic response abnormalities. In the final Section the Receiver-Operator Characteristic curve will be presented as a measure of the conceivable utility of VERIS as a clinical test.

5.1 The Aetiology, Appearance and Treatment of Glaucoma.

5.1.1 Classification of the glaucomas.

Glaucoma may be caused by the prevention of normal aqueous drainage by a narrow anterior chamber angle, in which case the glaucoma is termed *closed angle*. If the trabecular drainage is interrupted by another factor, and the anterior chamber angle is not closed, then the glaucoma is termed *open angle*. If the glaucoma is not contingent on another pathology, then the glaucoma is termed *primary*; otherwise, the glaucoma is *secondary*. Glaucoma may be classified in terms of the age at onset, that is as *infantile*, *juvenile* or *adult* glaucoma and may or may not be *congenital*

(although many glaucomas may be familial without being termed *congenital*). The time course of the disease might be *acute* (sudden and rapid), *sub-acute* (acute but also intermittent in nature) or *chronic* (symptoms slow and insidious at onset, but lasting for many years).

The scope of this thesis is limited to the glaucoma termed primary open angle glaucoma (POAG). Patients with primary open and closed angle glaucomas are the vast majority of those attending out-patient clinics, so it was not possible to recruit patients with any of the other, rarer glaucomas. Patients with closed angle glaucoma could not be tested because dilating the pupil in these patients may cause the iris to block aqueous drainage. Open angle glaucoma is sometimes called simple, quiet, noninflammatory or noncongestive and exhibits visual field defects with optic disk changes, raised IOP and an open anterior chamber angle.

Primary open angle glaucoma may be defined as a sustained increase in the intraocular pressure which the eye cannot withstand without damage to its structure or impairment of its function. Intraocular pressure (IOP) increases due to impaired drainage through the trabecular meshwork in the anterior angle (Cline et al. 1997).

5.1.2 The Optic Nerve Head in Primary Open Angle Glaucoma.

The primary site of damage to the optic nerve in primary open angle glaucoma occurs at the scleral lamina cribrosa (Quigley, 1986). The appearance of the optic nerve head associated with glaucoma

includes enlargement of the disk cup towards the disk rim, undercutting the rim tissue and deepening of the cup floor (Quigley, 1986). An optic nerve head with this appearance, a prerequisite for a diagnosis of POAG, is termed 'cupped'. Glaucomatous disks are assessed by measuring the size of the cup and the size of the disk to calculate a cup to disk ratio. It is thought that elevated intraocular pressure deforms the lamina cribrosa and causes cupping of the optic disk and an insult to the optic nerve fibres. The mechanisms of this insult might be through interrupting the axonal transport of nutrients along the nerve fibres, or might be by hindering blood supply to the optic nerve head. Axonal transport is vital for neuronal function and has been found to be interrupted in monkey eyes with chronic experimental glaucoma (Quigley, 1986).

Figure 5-1. A schematic illustration of the optic nerve head in early, middle and advanced stage glaucoma. An early glaucomatous optic nerve head is shown in a) where there is a small loss of neural tissue from the rim and compression of the lamina. In b) continued nerve fibre loss and compression of the lamina has caused a larger, deeper 'cupped' optic nerve head. Advanced glaucoma is shown in c) where little nerve tissue is left, the lamina is completely flattened and excavation under the choroid has occurred. (Quigley, 1986).
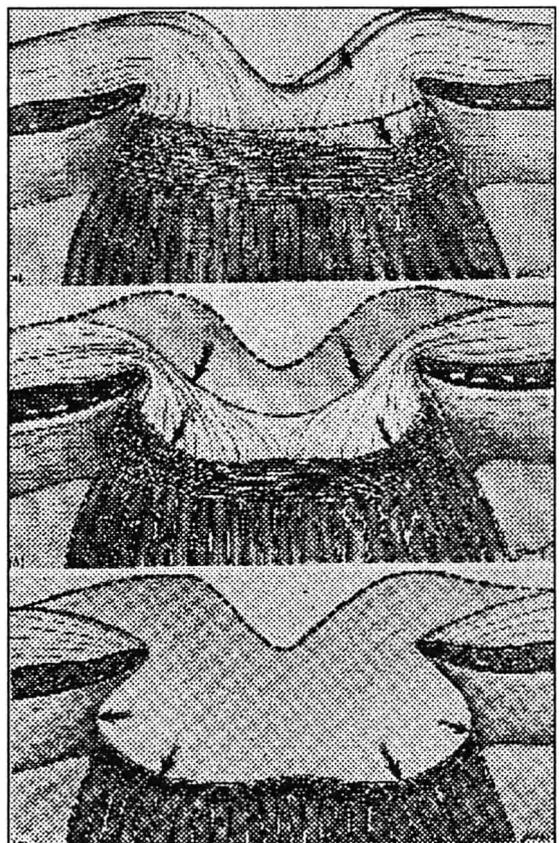
Quigley et al. (1982) have counted the number of nerve fibres passing through the optic nerve head in human glaucomatous enucleated eyes and have found that a loss of optic nerve fibres in glaucoma is directly related to optic nerve head enlargement and cupping. In another report (1987), Quigley et al. have divided the optic nerve head of monkey retinas into sixteen segments, eight central and eight peripheral, and have shown that optic nerve loss was selectively largest first in the peripheral infero-nasal sector and second in the peripheral supero-nasal sector, but smallest in the central temporal sectors. Quigley has suggested that elevated IOP acts initially to cause distortions in the lamina cribrosa that are greatest in the peripheral vertical poles of the optic nerve head, particularly at the inferior margin, and that the result is selectively greater damage to axons passing through these regions. Quigley et al. (1982) have found that although the gross number of axons was reduced in these specific zones, the axonal density (number of axons per unit area) was unchanged except in more advanced glaucoma.

5.1.3 Patterns of Ganglion Cell Loss in Primary Open Angle Glaucoma.

The location and density of nerve fibre loss in the nerve head has important corollaries for the location of retinal ganglion cell loss in glaucoma (Caprioli, 1989). Nerve fibres that enter the optic nerve head in its peripheral infero- and supero-nasal sectors belong to ganglion cells that lie in the paracentral area of the retina, within 10-20° of fixation, and it is ganglion cells in this region that are more frequently non-functional in glaucoma. Axons in the inferior portion

of the optic nerve head are more vulnerable to atrophy and they derive from ganglion cells in the inferior retina, which is more susceptible to glaucomatous damage. What is more, a reduction in the number of axons in a sector of the optic nerve head, without a significant change in axonal density, indicates focal ganglion cell loss in the retina. A reduction in optic nerve head nerve fibre density in later glaucoma indicates that diffuse ganglion cell loss follows secondarily (Quigley et al. 1982).

5.1.3.1 Retinal ganglion cell loss in glaucoma is size dependant.

In monkeys artificially made glaucomatous (Quigley et al. 1987; Glovinsky et al. 1991) and in humans (Quigley et al. 1989) the larger optic nerve fibres are selectively damaged. Size selective damage starts at an early stage and becomes more prominent with progression of the disease, but at a late stage both small and large ganglion cells are lost (Glovinsky et al. 1991). Nerve fibre size is proportional to ganglion cell size, so preferential death of large nerve cell fibres indicates an increased susceptibility of large ganglion cells to damage by optic nerve head cupping. It is not clear why large nerve fibres should have less resistance to external compressive pressure in the lamina cribrosa than small nerve fibres.

5.1.4 Visual Function Deficits in Primary Open Angle Glaucoma.

Glaucoma is commonly characterised by a visual function deficit that is termed a scotoma: a region of vision that is absent or depressed in sensitivity, in an otherwise normal visual field (Cline et

al. 1997). But there are other aspects of visual function loss in glaucoma that can be elucidated either with specific psychophysical tests that isolate aspects of particular classes of ganglion cell, or with flicker and pattern ERGs.

5.1.4.1 Perimetry in glaucoma.

Scotomata may be mapped by a perimeter, for example the Humphrey VFA. Perimeters determine the angular extent and characteristics of the visual field, peripheral to the point of fixation. The Humphrey VFA's 24-2 programme has become a clinical standard and was used in these experiments. The perimeter projects a white stimulus onto the inside of a bowl that is illuminated to a background luminance level of 31.5 apostilbs ($10cd/m^2$). The stimulus may appear in any one of 52 sites in a portion of the visual field subtending up to 25 degrees superior, inferior and temporal and 30 degrees nasal. At each of the stimulus sites the patient is tested over a range of stimulus intensities to find their sensitivity threshold, the lowest intensity stimulus that can be seen above background luminance. The Humphrey VFA plots the threshold sensitivity, in dB above the background luminance level, for each site in the visual field. It also plots the total deviation in sensitivity from an age-matched normal, and the statistical significance of this deviation, for each stimulus site. In a third plot termed pattern deviation the Humphrey VFA reports the residual deviation from an age-matched normal after the sensitivity of the entire visual field has been adjusted to account for any global reductions. Statistical significance of the pattern deviation plot is also related.

5.1.4.2 Location and progression of scotomata in Primary Open Angle Glaucoma.

The retinal location of scotomata in glaucoma directly reflect ganglion cells loss. Scotomata may be termed shallow, where threshold sensitivity increase is small, or deep, where the increase is considerable. The earliest stage of the disease is characterised by an occult loss of ganglion cells, not measurable as visual field loss with typical perimetric techniques (Hart and Becker, 1982; Quigley et al. 1989). In the next stage a scotoma is found in the paracentral area of the visual field, within 10-20° of fixation, and more commonly in the superior hemifield. Initially, the scotomata will be shallow, and may appear only transiently (Hart and Becker, 1982). As the disease progresses, adjacent nerve fibres are recruited into the degenerating region of nerve head, and the scotoma spreads to surrounding regions of retina, coalescing to form arcuate scotomata.

Later in the disease, scotomata become more common in the inferior field (Hart and Becker, 1982) which may already exhibit reduced sensitivity (Drance et al. 1987). In due course, atrophy extends to include the ganglion cells of fibres in the temporal and nasal regions of the optic nerve head (Quigley et al. 1982), which causes the development of scotomata in the nasal and temporal peripheral retina. The last nerve fibres to atrophy belong to ganglion cells in the macula, which is the last area of the visual field to be spared. Scotomata may progress in a linear, nonlinear or episodic fashion (Mikelberg et al. 1986). Typically, at least five years may be required for significant changes in the visual field to

be observed (Smith et al. 1996), and scotoma may remain localised in the superior hemifield for more than a decade (Hart and Becker, 1982).

5.1.4.3 Other visual function deficits in glaucoma.

Scotomata are not the only features of visual function loss in glaucoma. Motion detection, spatial contrast, flicker contrast and blue/yellow contrast sensitivity have all been shown to be abnormal in glaucoma (Ruben et al. 1995; Graham et al. 1996; Porciatti et al. 1997). As these aspects of visual function are associated with large ganglion cells, abnormalities correlate with findings of a selective reduction in large ganglion cell population (see Section 5.1.3).

5.1.4.4 The pattern electroretinogram and ganglion cell loss in glaucoma.

There have been a number of studies of pattern electroretinogram in patients with primary open angle glaucoma (Trick, 1992). The clear consensus is that pattern electroretinogram amplitudes are significantly reduced in glaucoma, relative to visually normal observers of a similar age (Trick, 1986; Holder, 1987; Trick, 1987; Wanger and Persson, 1987; Watanabe et al. 1989; Odom et al. 1990; Falsini et al. 1991; Bach et al. 1992; O'Donaghue et al. 1992; Graham et al. 1994; Ruben et al. 1994; Komata et al. 1995; Ruben et al. 1995; Korth et al. 1998). The diagnostic value of the pattern electroretinogram is still in dispute (Weinstein et al. 1988; Pfeiffer et al. 1993; Vaegan et al. 1995). Spatial tuning of pattern

electroretinogram losses exhibited by glaucoma patients indicates that the extent of amplitude reduction is accentuated at high spatial frequencies (0.6-0.8 degrees), but at low spatial frequencies the responses are not abnormal (Porciatti et al. 1987; Bach et al. 1988). Bach et al. (1988) have suggested that different mechanisms generate the pattern electroretinogram for small and large checks, that these mechanisms are differently affected in glaucoma, and that they may be related to large and small ganglion cell function.

5.1.4.5 Is there more than one pathomechanism in glaucoma?

Visual function deficits are not consistent between glaucoma sufferers. They may posses abnormal pattern ERGs but perform normally in psychophysical tests that isolate responses from large ganglion cells, or they may be abnormal in the psychophysical test but have normal pattern ERGs (Ruben et al. 1994). There is only a weak correlation between psychophysical tests that isolate large ganglion cells and pattern ERG responses (Ruben et al. 1995). Glaucoma patients may not perform abnormally in both psychophysical tests (Ruben et al. 1994). These results suggest that small ganglion cells as well as large can be lost at every stage in the disease and that ganglion cells may be lost diffusely, as well as focally. It has even been suggested that more than one pathomechanism may be at work in glaucoma (Ruben et al. 1994; Ruben et al. 1995). Several modes of ganglion cell atrophy may be present in POAG, affecting large and small ganglion cells differently. Some have suggested that outer as well as inner retinal function may be altered (Panda and Jonas, 1992; Mehaffey

et al. 1993; Nork et al. 1995; Toyoda et al. 1969; Janssen et al. 1986).

5.1.5 Linear and Nonlinear Multifocal Electroretinograms in Glaucoma.

Linear and nonlinear multifocal ERGs have been recorded from glaucoma sufferers using the VERIS system. There is no agreement in the results that have been reported. Some have reported that linear, first kernel responses are abnormal in glaucoma, and that the abnormalities are either diffuse (Vaegan, 1996), or focal and correlate well with the loci of defects found using perimetry (Sawada et al. 1996). Bearse et al. (1996) have found that the linear first kernel is normal but that abnormalities in a component found in the first slice of the nonlinear second order kernel that might possibly be associated with optic nerve head (Sutter and Bearse 1995, 1999) (see Section 4.2.4, page 179) is reduced in glaucoma. There is no consensus on whether a response from the ganglion cells might be found in the first order kernel, or the second order kernel. No evidence regarding the second or higher order slices of the second order kernel, or the third or higher order kernels, have been reported for any pathology.

5.1.6 Medical Treatment of Glaucoma.

The medical treatment of primary open angle glaucoma involves a course of drugs to lower IOP. First-line drugs used in the management of POAG are topical β-blockers, such as timoptol, which are believed to prevent aqueous humour formation by

blocking β_2 receptors on the ciliary epithelium. Other drugs used to lower IOP include pilocarpine, a cholinergic agonist. Cholinergic agonists are miotics, and lower IOP by stimulating muscarine receptors on the longitudinal muscle fibres of the ciliary body, producing a pull on the scleral spur which opens the trabecular meshwork and increases aqueous outflow.

5.2 Glaucoma Subject Recruitment.

5.2.1 Exclusion Criteria.

The following list of exclusion criteria was framed to avoid confounding possible abnormal electroretinographic responses due to glaucoma with abnormal electroretinographic responses due to any other pathologies.

- *Diabetes or retinitis pigmentosa.* Some reports of abnormal VERIS ERGs in diabetes (Palmowski et al. 1996; Palmowski et al. 1997) and retinitis pigmentosa (Chan and Brown, 1998) have been published.
- *Any other retinal pathologies.* The effect of other pathologies on VERIS ERGs is unknown, but could confound the results.
- *Hypertension.* Hypertension can affect electroretinographic response and retinal function by affecting blood flow through the retina.
- *Lenticular opacities $\leq$NI, CII or PI.* Correlation between the site of each input in the visual field and the site of that input in the retina could only be achieved if the ocular medium was free from opacities. NI, CII or PI by LOCS III (Chylack et al. 1993), where

211

N indicates nuclear, C cortical and P posterior, was chosen as the upper limit of acceptable opacification.

- *Visual acuity ≤6/12.* Visual acuity is not affected in glaucoma until the very last stage of the disease, when visual field defects begin to affect the macula area, but glaucoma patients are generally older than 50 years of age, and may have reduced VA for many reasons, other than glaucoma. Furthermore, a certain visual acuity is required by the VERIS test, because the subject is required to maintain fixation. Visual acuity no worse than 6/12 was accepted. This limit implied that the patient should be able to fixate properly and would help to exclude glaucoma patients who suffered from other pathologies.

5.2.2 Recruitment of Glaucoma Patients.

I attended the outpatient glaucoma clinics at St Thomas's Hospital and Moorfields Eye Hospital to recruit primary open angle glaucoma patients. The method of recruitment was the same in both hospitals.

5.2.2.1 Criteria required to identify primary open angle glaucoma patients.

Primary open angle glaucoma patients were identified as patients with:

- *Open anterior angles.* Dilation of the pupil is an important part of the experimental protocol (see 3.2.1) but is contraindicated in

212

patients who have closed anterior angles: when the pupil is dilated the iris may block aqueous drainage.

- *Intraocular pressure $\geq 22mmHg$.* POAG is identified with elevated IOP but normal IOP covers a large range and a single level at which IOP can be termed abnormal cannot be precisely identified. However, an IOP of 22mmHg is a commonly used as the upper limit or normality and has been adopted for this study. See, for example, Gaasterland et al. 1994. Treatment for glaucoma attempts to lower IOP (see 5.1.6) and is often successful. Inclusion in the study required that IOP had once been above 22mmHg for twelve consecutive months.

- *Cup/disk ratio ≥ 0.6.* Cup/disk ratios, and their relevance to the condition of the optic nerve head, have been discussed in Section 5.1.2, above. As with IOP, no unique value for glaucoma diagnosis exists, but the commonly used upper limit of normality has been adopted in this study.

- *Arcuate scotomata.* Scotomata were mapped with the Humphrey Visual Field Analyser (24-2 programme). The pattern of visual field defects had to be consistent with a diagnosis of glaucoma, as described in Section 5.1.4.2, and a scotoma, consisting of at least three adjacent sites in the visual field, was required. Furthermore, for the analysis described in Section 5.5, the scotomata had to be matched by an unaffected area of visual field, of the same shape and at the same eccentricity, in the opposite hemifield. Analyses of the progression of visual field defects in glaucoma have shown that fluctuations up to 6dB may be expected due to noise (Smith et al. 1996), but that threshold elevation of about 10dB or more may indicate that progressive visual field deterioration is

213

occurring (Fitzke et al. 1996). For inclusion in the scotomatous region a threshold of at least -9dB was required and for the matching nonscotomatous region an elevation of no more than -6dB was necessary. Thresholds given in the Pattern Deviation plot were used, because they relate localised scotomata more accurately than the Total Deviation plot (Smith et al. 1996).

5.2.2.2 Recruitment procedure.

I scrutinised patients' files after they had arrived in the clinic, but before they were examined by an ophthalmologist. Patients who had to be excluded due to criteria in Section 5.2.1 were identified at this stage. I attended the consultation of all the patients who were still possible candidates. My participation encouraged the patients to feel at ease with the notion of volunteering for the experiment, and enabled me to confirm some further aspects of the patients' suitability to do the test: patients who would be unable to move into and out of the Faraday cage, or unable to concentrate for the duration of the test, could be identified at this stage. I then interviewed the patient myself. I explained the nature of my research, and why I had identified this patient as a suitable subject. I confirmed the details of the medical history that were contained in the hospital file. I asked the patient if s/he would volunteer. Unless they felt unable to participate, I copied details of IOP measurement, C/D ratio, medication and any other medical complications from the patient's files, to supplement my own notes. In the case of patients from St Thomas' Hospital, Humphrey visual field plots (24-2 programme) were photocopied. A letter was sent immediately giving an appointment within the next ten days and

providing directions to the Research Centre. A patient's information sheet (reproduced as Appendix) was sent at the same time, giving more details of the research and what the patient was required to do.

5.2.2.3 Glaucoma subject recruitment statistics.

The total number of primary open angle glaucoma subjects that were recruited was 27. The responses of one patient were too corrupted with blinks to be used, and had to be discarded. In three cases the Humphrey field plots obtained at the Research Centre showed that the scotoma were not situated to allow matching of areas of visual field loss with areas of spared visual field in the opposite hemifield; these subjects were excluded. After these exclusions, the electroretinographic response of 23 glaucomatous eyes from 23 glaucoma subjects were analysed. Age mean was 68.4±8.3 (1SD), range was 55-82; 43% were female. Details are summarised in Table 5-1. The range in quality of responses is indicated in Figure 5-2.

5.3 Full-Field Linear and Nonlinear Responses in Primary Open Angle Glaucoma.

The simplest analysis of VERIS responses that may be achieved is to average the responses of all the hexagons to achieve a single waveform. This waveform is equivalent to the full-field response. Glaucoma is known to cause a loss of ganglion cells (see Section 5.1.3), so if a comparison between the full-field response in glaucoma and the same response in normals reveals a difference
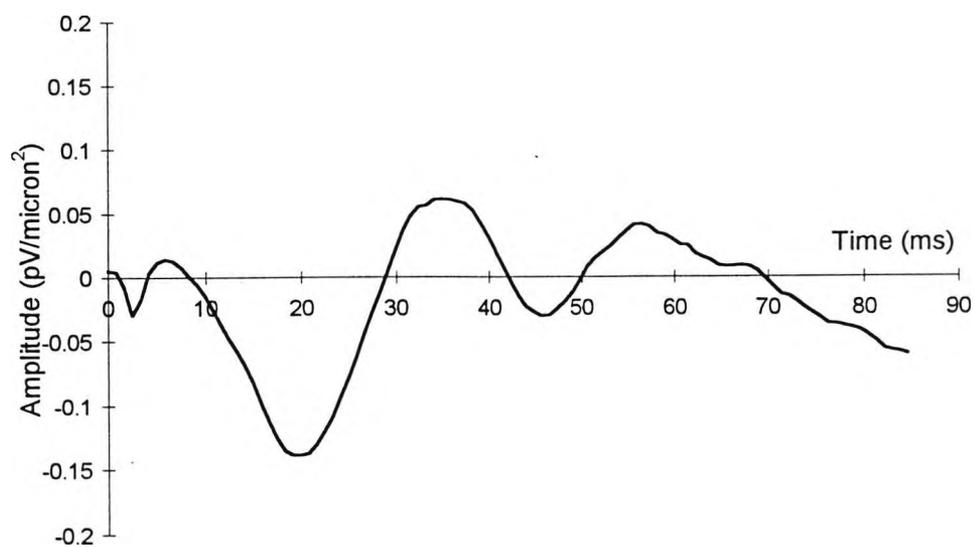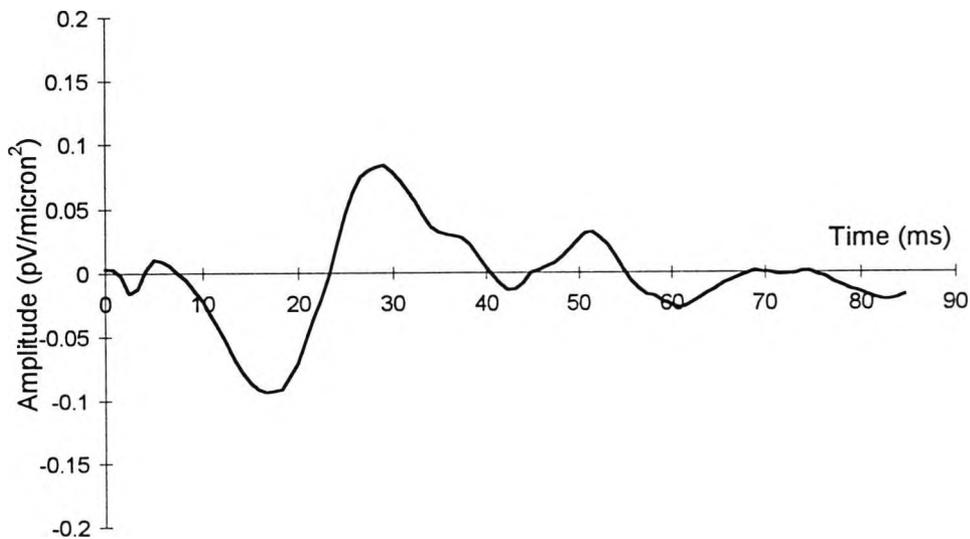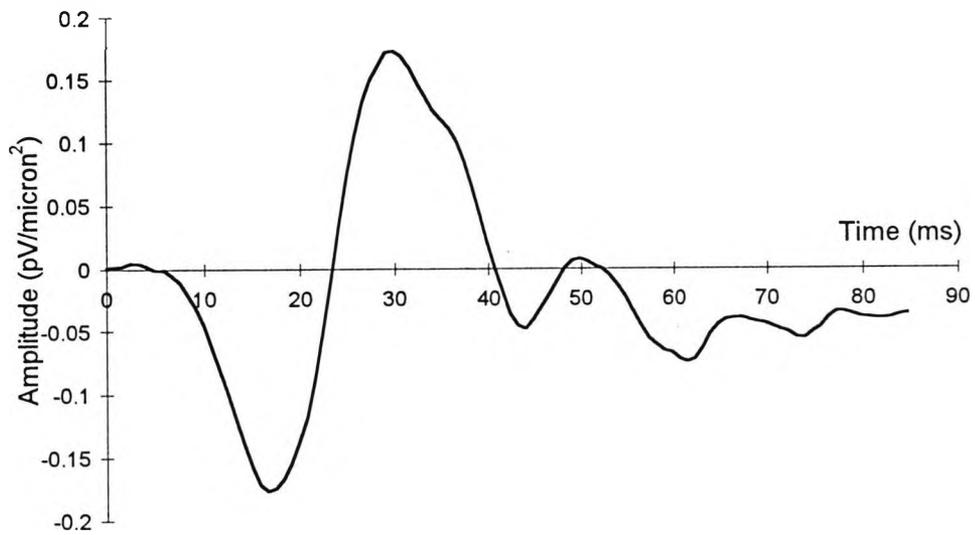
Figure 5-2   The range in quality of the linear (left) and nonlinear (right)
responses achieved from best (top) via medium (continued next page…)

216
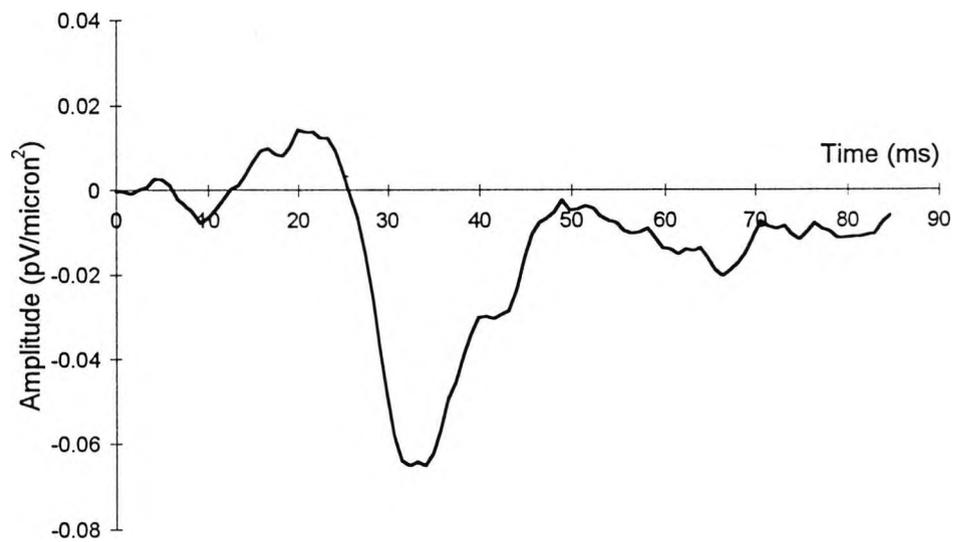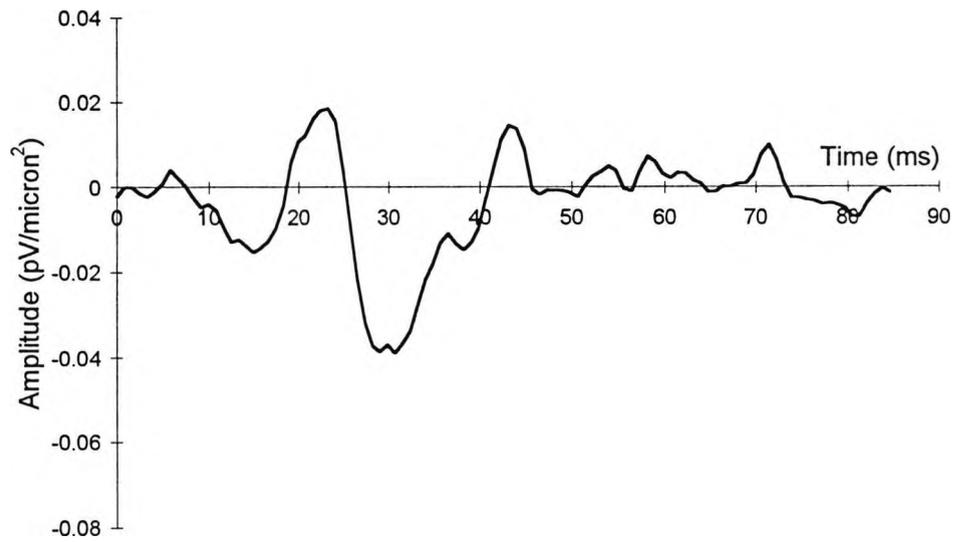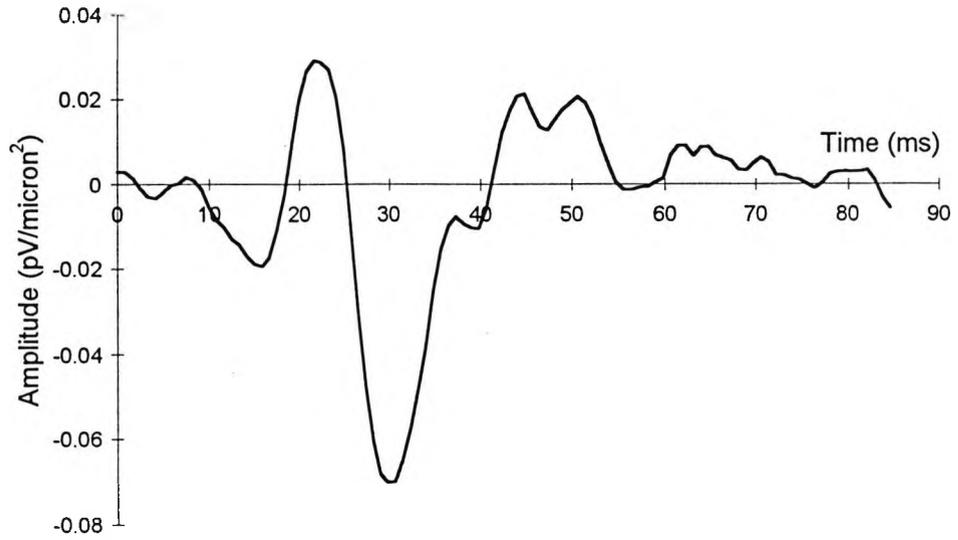
(…continued) to worst (bottom), being subjects 14,8 and 23 respectively.

Subject	Age	Sex	Eye	VA	C/D	IOP	MD	PSD
1	57	F	OS	6/6	0.9	18	-16.61	11.97
2	71	F	OS	6/12	0.6	19	-8.15	5.09
3	72	M	OD	6/9	0.7	19	-2.68	3.71
4	73	M	OD	6/6	0.8	16	-17.90	10.91
5	55	M	OD	6/5	0.9	19	-11.08	13.41
6	69	F	OS	6/12	0.9	21	-8.25	7.33
7	69	F	OD	6/9	0.8	15	-9.58	11.99
8	67	F	OD	6/6	0.7	21	-11.25	11.92
9	70	M	OS	6/9	0.7	14	-2.84	7.71
10	79	M	OD	6/12	0.8	15	-17.80	10.45
11	50	F	OD	6/6	0.8	18	-9.86	7.47
12	81	M	OS	6/9	0.6	18	-10.97	5.82
13	80	M	OD	6/9	0.8	22	-8.11	6.12
14	68	F	OD	6/9	0.6	24	-6.56	5.62
15	82	M	OD	6/6	0.8	10	-15.90	11.49
16	78	F	OS	6/9	0.8	16	-15.16	12.35
17	66	F	OS	6/9	0.8	20	-3.22	3.17
18	65	M	OS	6/5	0.9	14	-15.53	12.68
19	66	F	OD	6/9	0.9	18	-0.63	4.85
20	66	M	OD	6/9	0.9	12	-14.15	14.77
21	60	M	OS	6/9	0.7	30	-3.15	5.03
22	63	M	OD	6/9	0.6	12	-2.58	8.29
23	66	M	OD	6/9	0.7	21	-5.87	4.48

Table 5-1. Details of all 23 glaucoma subjects are given here. IOP is in mmHg; Mean Deviation (MD) and Pattern Standard Deviation (PSD) are recorded on the Humphrey VFA plots, units are decibels; patch area in mm^2, see Section 5.5.

in waveform then it may be possible to suggest that the difference has arisen due to absent ganglion cells.

5.3.1 Full-field Responses in Glaucoma: Method.

The arrays of both linear and nonlinear (second kernel, second slice) responses were averaged to achieve two response for each glaucoma subject. The responses were 'zeroed' to the baseline by averaging the first 10 data points, where the retinal response must be zero, and subtracting this number from each data point in the waveform. The waveforms were then scaled by dividing by the projected retinal area of the stimulus, in microns, to yield a response measured in $pV/micron^2$. The amplitude of prominent features in the responses of each subject were compared to the average response of all the normal subjects studies in Section 4.3. In the linear response the a- and b-wave were studied. In the nonlinear response only the two largest features, P23 and N31 were scrutinised, since it was often not possible to distinguish other features from background noise. Two-sample t-tests were performed on the difference in mean amplitude of each feature between the response in glaucoma and the normal response Exact twin tailed P-values were calculated with the routines built into 'Microsoft Excel'. As $n_{glaucoma}=n_{normal}=23$ there were 44 degrees of freedom. A one way analysis of covariance was performed on the latency of the same features, treating age as a covariate. F-statistics and exact P values were calculated using the 'SPSS' statistics package.

5.3.2 Full-field Responses in Glaucoma: Results.

The full-field linear glaucoma and normal responses are presented in Figure 5-3 and the mean amplitude and latency of the a- and b-wave in glaucoma and normals is presented in Table 5-2 and Table 5-3. The two waveforms appear identical and the statistical analysis (Table 5-2 and Table 5-3) shows that neither the amplitude nor latency of a-wave and b-wave are significantly different.
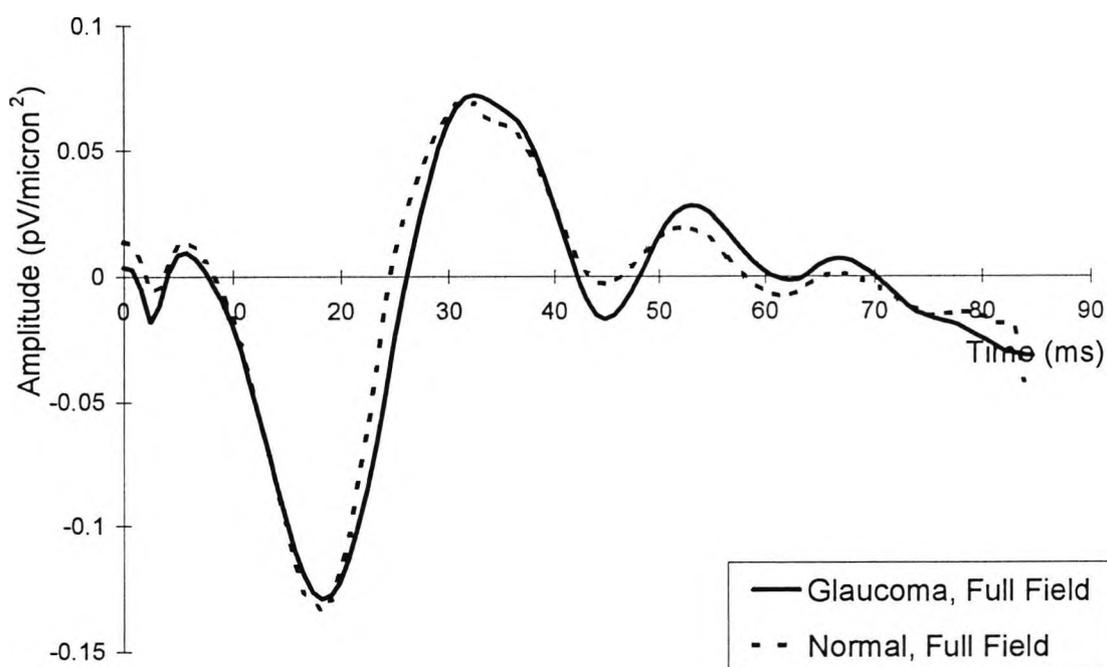
Figure 5-3   Linear Response.   Full Field.   Mean waveform in glaucoma and in normals.

	Glaucoma, n=23		Normal, n=34		two-sample	
	Mean	SD	Mean	SD	t	P
a-wave	-0.129	0.055	-0.135	0.045	0.389	NS
b-wave	0.071	0.043	0.069	0.045	0.185	NS

Table 5-2   Linear Response.   Full Field.   Amplitudes.   Mean, SD and statistical analysis (two-sample t test).   NS = not significant, P>0.05.

220

	Glaucoma, n=23		Normal, n=34		ANOVA	
	Mean	SD	Mean	SD	F	P
a-wave	18.26	1.068	18.26	0.998	0.152	NS
b-wave	33.2	0.777	32.37	0.828	0.116	NS

Table 5-3   Linear Response.   Full Field.   Latency.   Mean, SD and statistical analysis (one way ANOVA treating age as a covariate).   NS = not significant, P>0.05.

The nonlinear response waveforms are presented in Figure 5-4 and statistical analysis of the P23 and N31 features in Table 5-4 and Table 5-5.   The amplitude of the P23 feature of the glaucoma response is just significantly different from the P23 component of the normal response (P=4.6%).   The amplitude of the N31 feature and the latency of both features in glaucoma are identical to those feature in normals.
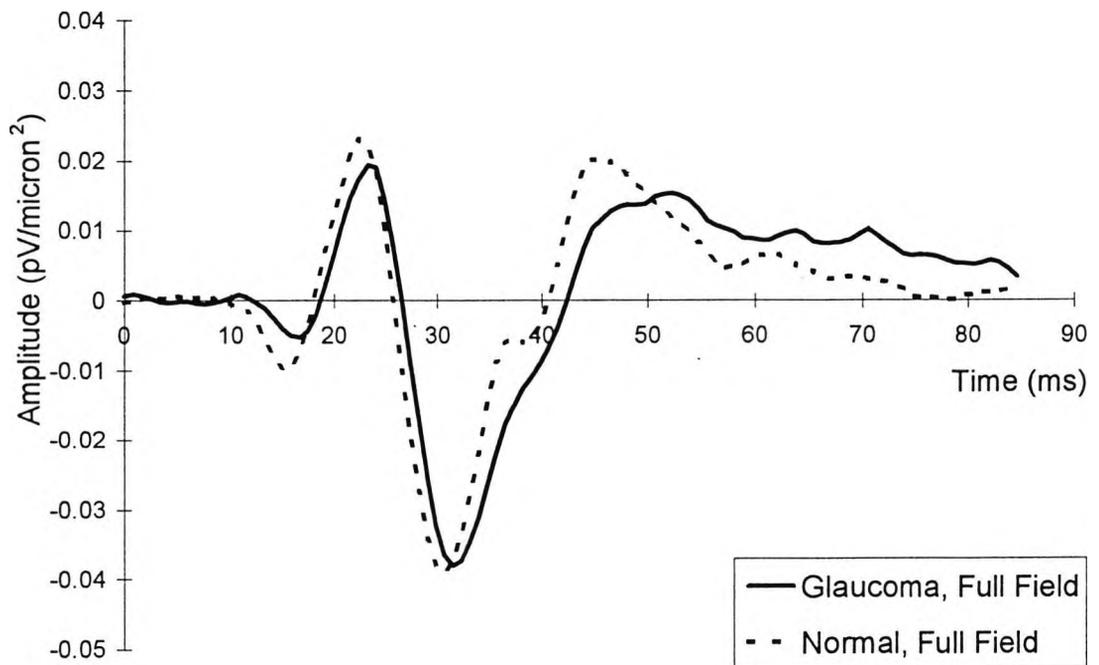
Figure 5-4   Nonlinear Response.   Full Field.   Mean waveform in glaucoma and in normals.

	Glaucoma, n=23		Normal, n=34		two-sample	
	Mean	SD	Mean	SD	t	P
P23	0.019	0.012	0.024	0.005	2.045	0.046
N31	-0.038	0.025	-0.039	0.014	0.170	NS

Table 5-4   Nonlinear Response.   Full Field.   Amplitude.   Mean, SD and statistical analysis (two-sample t test).   NS = not significant, P>0.05.

	Glaucoma, n=23		Normal, n=34		ANOVA	
	Mean	SD	Mean	SD	F	P
P23	23.24	1.090	22.41	1.038	1.392	NS
N31	31.54	0.815	30.71	1.110	1.210	NS

Table 5-5   Nonlinear Response.   Full Field.   Latency.   Mean, SD and statistical analysis (one way ANOVA treating age as a covariate).   NS = not significant, P>0.05.

5.3.3 Full-field Responses in Glaucoma: Analysis.

The linear response is unchanged in glaucoma.   Since the linear response is believed to be generated by outer retinal neurones, this suggests that the response of outer retinal neurones to high contrast stimuli are not altered by the disease.   The amplitude of the nonlinear response in glaucoma is significant different from normal.   If outer retinal neurones are normal then abnormalities in the nonlinear response can only be explained in termed of alterations to inner retinal neurones.   Glaucoma causes a reduction in ganglion cell population, so it is reasonable to suggest that absent ganglion cells have caused the abnormality in the nonlinear response.   Furthermore, the nonlinear response deviates from the normal response in the P23 feature only, N31 appears to be

unaffected. It may be possible that any ganglion cell contribution to the nonlinear response is restricted to the P23 feature alone.

5.4 Foveal Linear and Nonlinear Responses in Primary Open Angle Glaucoma

Glaucoma causes preferential drop-out of ganglion cells in the periphery. Ganglion cell drop-out does not affect the fovea until the very last stages of the disease. If the abnormality in the P23 feature of the nonlinear waveform witnessed in the full-field response is due to glaucoma then it is likely that the abnormality will not extend to the fovea. Corroboration of the suggestion that the P23 feature contains a ganglion cell response, made in the previous section, may therefore be achieved by analysing the foveal response. If the P23 feature contains a ganglion cell component then the foveal response will reveal no significant difference between normals and glaucoma.

5.4.1 Foveal Responses in Glaucoma: Method

Linear and nonlinear responses were obtained from the central hexagon (eccentricity <1.55 degrees) were analysed. The responses were 'zeroed' to the baseline and scaled to retinal area, in the same way as the full-field responses discussed above. Comparisons between normal and glaucomatous responses were formed on the amplitudes of the a-and b-wave and the P23 and N31 features of the normal and glaucomatous waveforms. The comparisons were analysed with two-sampled t-tests, and twin-tailed P-values were calculated.

223

5.4.2 Foveal Responses in Glaucoma: Results

The foveal linear and nonlinear, glaucomatous and normal responses are presented in Figure 5-5 and Figure 5-6. A statistical analysis of the a- and b-waves of the linear response is given in Table 5-6 and an identical analysis of the P23 and N31 features of nonlinear response in Table 5-8. Both glaucoma and normal waveforms appear identical in the linear and nonlinear responses. The statistical analysis shows that the amplitudes of the a- and the b-waves and the P23 and N31 features in glaucoma are not different to those amplitudes in normals.
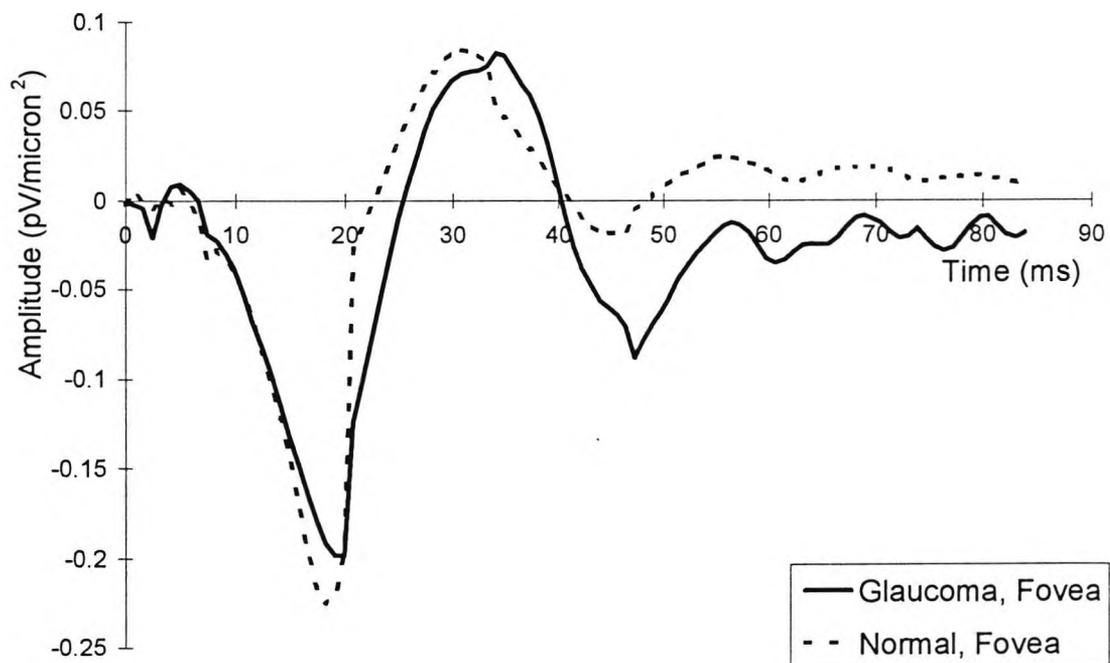
Figure 5-5   Linear Response.   Fovea.   Mean waveform in glaucoma and in normals.

	Glaucoma, n=23		Normal, n=34		two-sample	
	Mean	SD	Mean	SD	t	P
a-wave	-0.198	0.213	-0.224	0.098	0.634	NS
b-wave	0.072	0.165	0.084	0.150	0.302	NS

Table 5-6   Linear Response.   Fovea.   Amplitude.   Mean, SD and statistical analysis (two-sample t test).   NS = not significant, P>0.05.

	Glaucoma, n=23		Normal, n=34		ANOVA	
	Mean	SD	Mean	SD	F	P
a-wave	19.09	1.871	18.26	1.574	2.494	NS
b-wave	34.03	1.386	30.71	1.330	0.822	NS

Table 5-7   Linear Response.   Fovea.   Latency.   Mean, SD and statistical analysis (one way ANOVA treating age as a covariate).   NS = not significant, P>0.05.

5.4.3 Foveal Responses in Glaucoma: Analysis

The linear and nonlinear foveal responses in glaucoma are not significantly different from normal responses.   This result was entirely consistent with the idea of a contribution to the P23 feature of the nonlinear response from ganglion cells, which are not abnormal in the fovea in glaucoma.
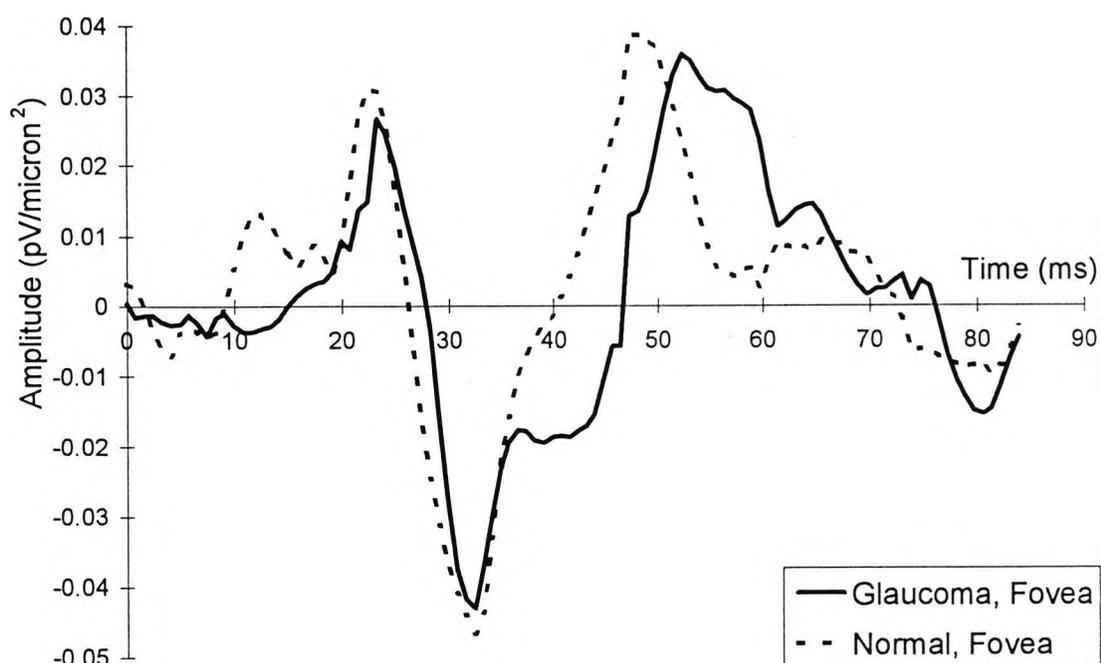
Figure 5-6   Nonlinear Response.   Fovea.   Mean waveform in glaucoma and in normals.   Difference in latency of late positive component is not consistent within the patient group.

	Glaucoma, n=23		Normal, n=34		two-sample	
	Mean	SD	Mean	SD	t	P
P23	0.027	0.056	0.031	0.055	0.287	NS
N31	-0.043	0.050	-0.047	0.045	0.287	NS

Table 5-8   Nonlinear Response.   Fovea.   Amplitude.   Mean, SD and statistical analysis (two-sample t test).   NS = not significant, P>0.05.

	Glaucoma, n=23		Normal, n=34		ANOVA	
	Mean	SD	Mean	SD	F	P
P23	23.24	1.518	22.41	1.431	0.108	NS
N31	32.37	1.700	32.37	1.632	1.018	NS

Table 5-9   Nonlinear Response.   Fovea.   Latency.   Mean, SD and statistical analysis (one way ANOVA treating age as a covariate).   NS = not significant, P>0.05.

Some ocular diseases have been shown to affect foveal VERIS electroretinographic responses, e.g. diabetes (Palmowski et al. 1996; Palmowski et al. 1997) and retinitis pigmentosa (Chan and Brown, 1998). Other ocular diseases, like cataract, affect the anterior eye and might cause abnormal foveal electroretinographic responses. As foveal responses in the patient group are normal, it confirms that these patients probably suffer from glaucoma, and no other pathology.

5.5 Linear and Nonlinear Responses of Glaucomatous Scotomata.

The results presented in Section 5.3 have suggested that the P23 feature of the nonlinear response is abnormal in glaucoma, but that other features of the nonlinear response, and the a- and b-waves of the linear response, are normal. Section 5.4 showed that the P23 feature is not abnormal in the fovea, the implication of which is that the abnormality is restricted to the peripheral retina, where glaucoma-induced ganglion cell drop-out is known to occur. The question then raised is whether the abnormality in P23 is confined to the response of areas of peripheral retina that are affected with a scotoma, or whether the abnormality is present throughout. If the abnormality in P23 is restricted to the response of areas of scotomatous retina (retina that is affected with a scotoma) then areas of nonscotomatous retina (not affected with a scotoma) will be normal. If, on the other hand, the alteration in P23 is present in responses throughout the retina then the response from nonscotomatous retina will be abnormal.

5.5.1 Responses of Glaucomatous Scotomata: Method.

A scotomatous patch of retina, in which ganglion cell loss leading to a measurable increase in sensitivity threshold had occurred, was identified for each patient. This patch of retina was paired with a nonscotomatous patch where any ganglion cell loss the retina had experienced was insufficient to cause a decrease in sensitivity threshold. The nonscotomatous patch matched the scotomatous patch in shape and eccentricity, and was always in the opposite visual field. Criteria used to identify scotomatous and nonscotomatous patches of retina have been described in Section 5.2.2.1 on page 212. The total loss of sensitivity of the scotomatous and nonscotomatous patches are for each subject in Table 5-10.

The Pattern Deviation plot was overlaid on the 103 hexagon VERIS stimulus (see Figure 5-8). The linear and nonlinear (second kernel first slice) responses derived from the hexagons lying under both patches were summed to achieve two waveforms for each glaucoma subject The responses were 'zeroed' to the baseline in the same manner as the full-field and foveal responses described above. The response was divided by the area of the patch (in microns) to achieve a scaled response waveform with amplitude units in $pV/micron^2$ that was not a function of patch area. Scaling responses to retinal patch area permitted comparisons between subject responses to be made even though no two subjects had the same sized patches. The area of the patch of each subject is given in Table 5-10.

The analysis of linear and nonlinear waveforms presented in Section 4.3 has indicated that response amplitude does not change significantly with age. It was not necessary to match the age of the patient to the age of the normals, and so a mean response array from all the normals could be used. The responses to the hexagons that had been summed to achieve the scotomatous and nonscotomatous waveforms, were summed to achieve the analogous normal waveforms for both the linear and nonlinear responses. The response analogous to the scotomatous response was termed the normal response from the same hemifield, the response analogous to the nonscotomatous response was termed the normal response from the opposite hemifield.

In most cases of POAG, scotoma are found in the superior visual field. In 19 of the 23 glaucoma subjects studied the scotomatous patch and the analogous normal patch from the same hemifield were in the superior visual field, so the nonscotomatous and normal patches from the opposite hemifield were in the inferior visual field. This situation is found in the example illustrated in Section 5.5.1.1, below. In four subjects the scotoma was found in the inferior visual field so the analogous normal patch of the same hemifield was in the inferior field and the patch of the opposite hemifield was in the superior hemifield. These subjects are indicated '*' in Table 5-10.

Subject	Total Scotomatous Sensitivity Loss (dB)	Total Nonscotomatous Sensitivity Loss (dB)	Patch Area (microns^2)
1	-527	-45	25.86
2	-103	-17	58.03
3	-36	-6	28.57
4*	-273	-21	50.07
5	-527	-29	9.20
6*	-147	-5	17.35
7	-346	-24	32.11
8	-454	-17	54.37
9	-78	-5	8.53
10*	-276	-34	30.24
11	-196	-16	26.31
12	-249	-53	36.74
13	-190	-20	25.98
14	-250	-41	49.17
15	-478	-21	61.06
16	-515	-32	62.76
17	-35	-12	12.33
18*	-304	-30	28.27
19	-57	-1	10.15
20	-370	-19	31.82
21	-66	-11	10.05
22	-82	-8	4.55
23	-82	-17	23.71

Table 5-10   Total loss of sensitivity, in dB, of the scotomatous patch and nonscotomatous patch of all 23 glaucoma subjects, and the area of the patch, in microns^2.   Subjects marked (*) have the scotomatous patch in the inferior field, the remainder have that patch in the superior field.

5.5.1.1 Example Treatment.

Figure 5-7 The method is illustrated for one example subject (number 11 in Table 5-1and Table 5-10) in this and the following three figures. Here the Humphrey Field Analyser output for the example subject is illustrated, the Pattern Deviation plot is bottom right.
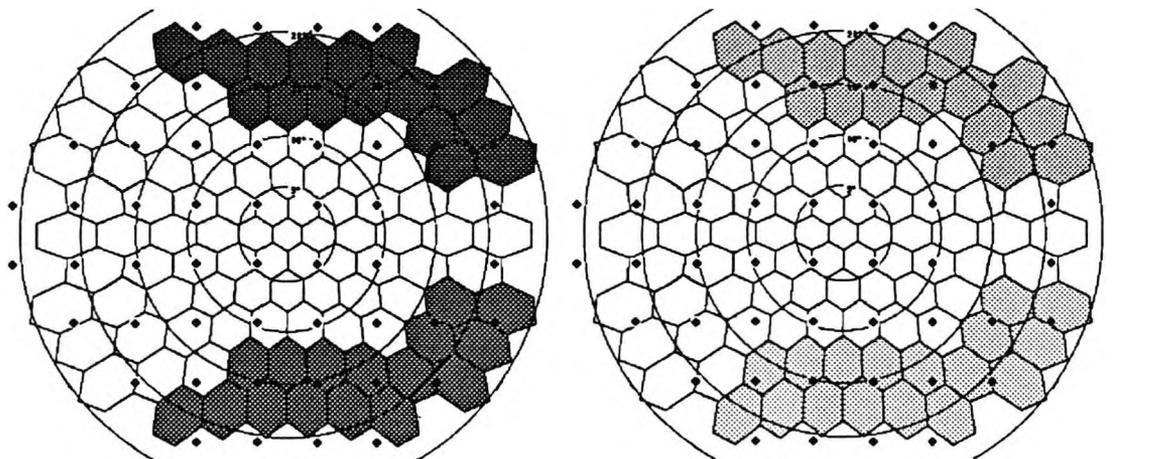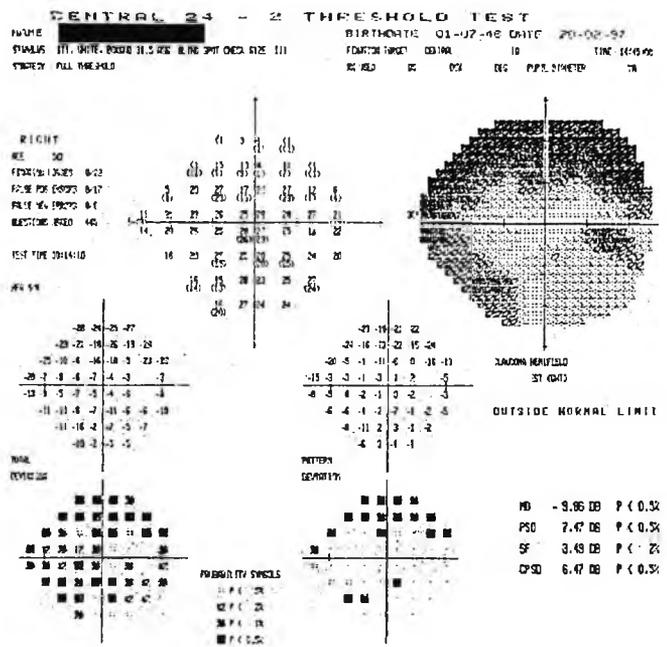
Figure 5-8 shows two VERIS 103 hexagon stimuli, overlaid with the Humphrey Field Analyser stimulation sites. The left hand side shows the scotomatous and nonscotomatous patches of retina. The right hand side shows the analogous normal patches of the same and opposite hemifields.

⬢ Scotomatous Patch

⬢ Nonscotomatous Patch

⬢ Normal, Same Hemifield Patch

⬡ Normal, Opposite Hemifield Patch
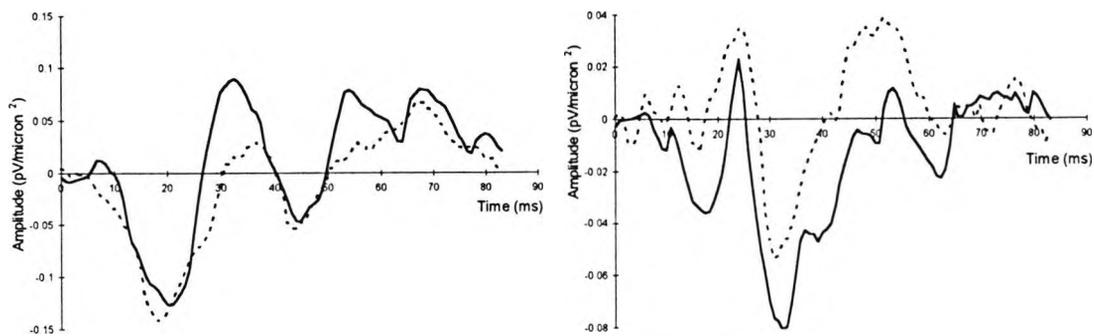
Figure 5-9 shows the linear response (left) and nonlinear response (right) of the scotomatous and nonscotomatous patches of the example subject.

——— Scotomatous Patch

- - - Nonscotomatous Patch
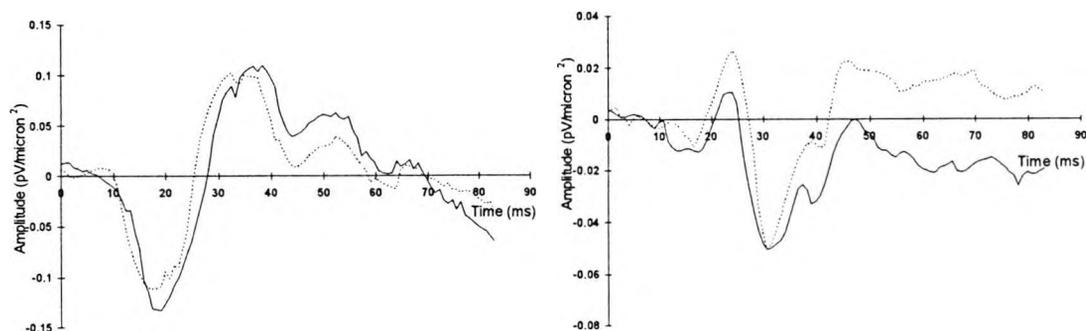
Figure 5-10 shows the linear response (left) and nonlinear response (right) for the normal same and opposite patches of the example subject.

——— Normal, Same Hemifield

- - - - - Normal, Opposite Hemifield

5.5.1.2 Statistical method.

The a- and b-wave of the linear response and P23 and N31 of the nonlinear response were analysed. Amplitudes were compared with the average response of all the normals. Latencies were compared with the mean response of the normals in the same age-decade because latency is a function of age (see Section 4.3).

When a comparison was being made on two responses from the same retina the variables were treated as a matched pair and Student's t-test was applied to the difference in amplitudes. Twin-tailed P-values were calculated, because differences in amplitude or latency could occur in either direction, using the routines built into 'Microsoft Excel'. As $n_{glaucoma}=n_{normal}=23$ there were 22 degrees of freedom.

When a comparison was being made on responses from two different retinas the variables were treated as independent variables and analysed with a two sample t-test. In each case an F-test was performed to find whether the variance of glaucomatous and normal variables were equal. The variance of the two samples was unequal ($P \geq 15\%$) in all cases so a Welch test was required, which simplified to the t-test as $n_{glaucoma}=n_{normal}$ (Armitage and Berry, 1987). Twin-tailed P-values were calculated using the routines built into 'Microsoft Excel'. As $n_{glaucoma}=n_{normal}=23$ there were 44 degrees of freedom.

5.5.2 Responses of Glaucomatous Scotomata: Results.

5.5.2.1 Linear Response.

The linear response of the scotomatous and nonscotomatous patches are plotted in Figure 5-11 and with their analogous normal responses in Figure 5-12 and Figure 5-13. Statistical analysis of the amplitudes and latencies of the a- and b-wave are presented in Table 5-11 to Table 5-16. The amplitude and latency of these features is not statistically significant from the normal response in any analysis. These results indicate that the a- and b-wave of the linear electroretinographic response, as evoked by the VERIS system, is unaffected in primary open angle glaucoma. As both the response of the scotomatous and the nonscotomatous patches are normal, it would appear that localised and diffuse visual field losses in glaucoma do not involve the retinal components from which the linear response is evoked.
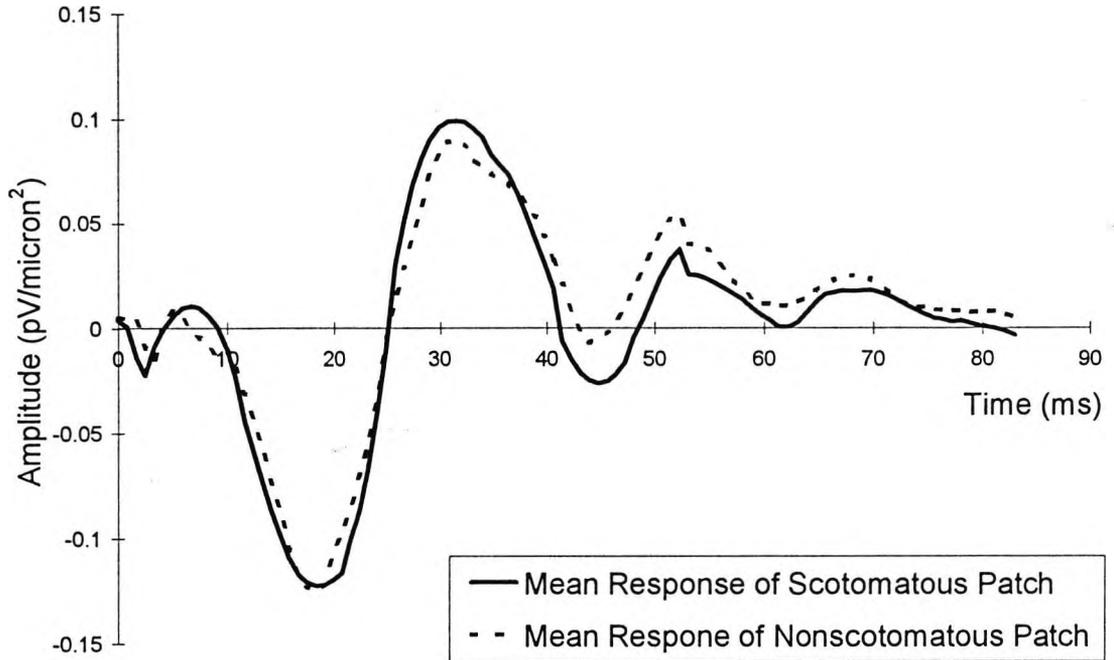
Figure 5-11   Linear response. Scotomatous response and nonscotomatous response.

Scotomatous and Nonscotomatous Response					
	Scotomatous	Nonscotomatous	Difference	SD	t	P
a-Wave	-0.122	-0.125	0.002	0.0379	0.210	NS
b-Wave	0.099	0.090	0.010	0.0392	1.111	NS

Table 5-11   Statistical analysis of the amplitudes of the linear scotomatous and nonscotomatous responses.   A paired t-test has been used.   The amplitudes of the a- and b-wave of the two waveforms are not statistically different.   Units are $pV/micron^2$; NS= not significant, P>0.05

Scotomatous and Nonscotomatous Response					
	Scotomatous	SD	Nonscotomatous	SD	t	P
a-Wave	18.26	2.310	18.26	2.975	0.753	NS
b-Wave	31.54	3.905	31.54	4.242	1.686	NS

Table 5-12   Statistical analysis of the latencies of the linear scotomatous and nonscotomatous responses.   A one-way ANOVA including age as a covariate has been used.   The latencies of the a- and b-wave of the two waveforms are not statistically different.   Units are ms, NS= not significant, P>0.05

235
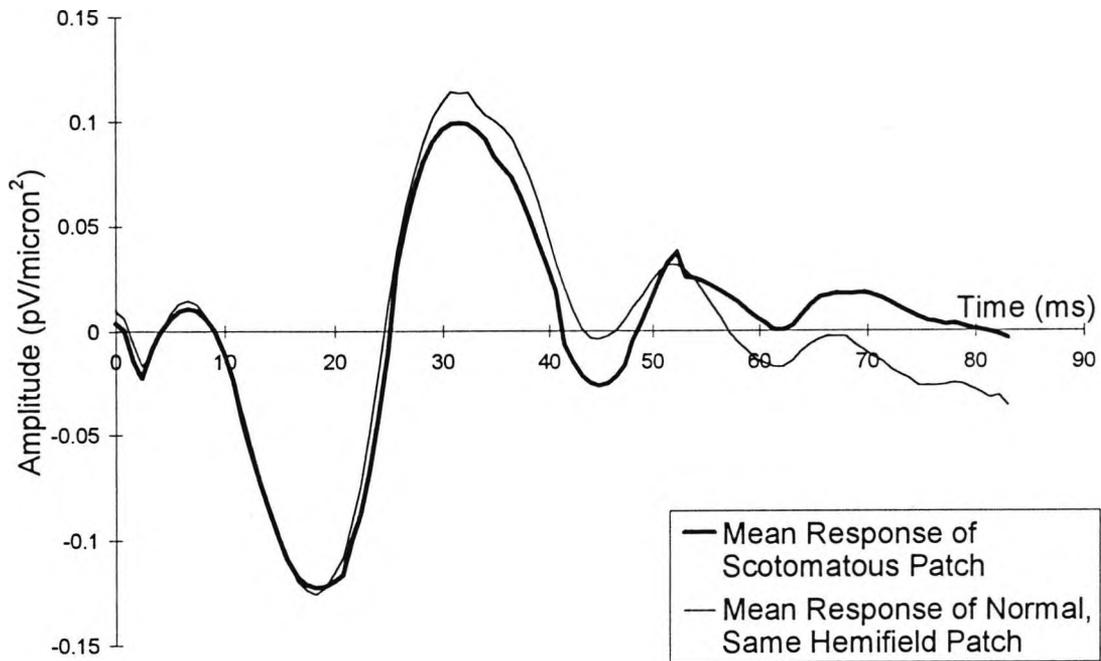
Figure 5-12 Linear response.   Scotomatous response and normal response of retina from the same hemifield.

	Scotomatous and Normal, Same Hemifield Response					
	Scotomatous		Normal		n=23	
	Mean	SD	Mean	SD	t statistic	P value
a-Wave	-0.122	-0.058	-0.126	0.026	0.304	NS
b-Wave	0.099	0.058	0.114	0.037	1.043	NS

Table 5-13   Statistical analysis of the linear scotomatous response amplitude and the normal response amplitude from the same hemifield.   The amplitudes of the a- and b-wave of the two waveforms are not statistically different.   Units are pV/micron^2; NS= not significant, P>0.05.

	Scotomatous and Normal, Same Hemifield Response					
	Scotomatous		Normal		n=23	
	Mean	SD	Mean	SD	t statistic	P value
a-Wave	18.26	2.310	18.28	0.928	0.732	NS
b-Wave	31.54	3.905	30.71	2.329	0.025	NS

Table 5-14   Statistical analysis of the linear scotomatous response latency and the normal response latency from the same hemifield.   The latencies of the a- and b-wave of the two waveforms are not statistically different.   Units are ms; NS= not significant, P>0.05.
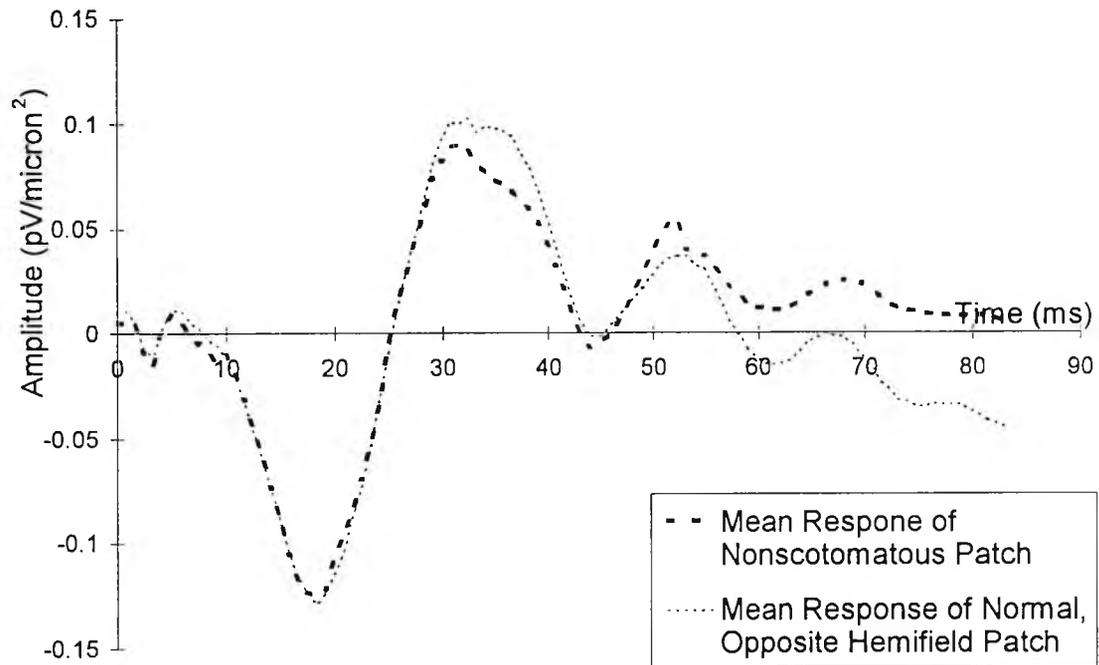
Figure 5-13   Linear Response.   Nonscotomatous response and normal response from the opposite hemifield.

Nonscotomatous and Normal, Opposite Hemifield					
Nonscotomatous		Normal		n=23	
Mean	SD	Mean	SD	t statistic	P value
a-Wave	-0.129	0.049	-0.125	0.023	0.353	NS
b-Wave	0.090	0.065	0.103	0.034	0.850	NS

Table 5-15   Statistical analysis of the linear nonscotomatous response amplitude and the normal response amplitude from the opposite hemifield. The two waveforms are statistically identical in amplitude.   Units are pV/micron^2; NS= not significant, P>0.05.

Nonscotomatous and Normal, Opposite Hemifield					
Nonscotomatous		Normal		n=23	
Mean	SD	Mean	SD	t statistic	P value
a-Wave	18.26	2.783	19.09	1.347	0.879	NS
b-Wave	31.54	1.575	32.37	0.989	1.080	NS

Table 5-16   Statistical analysis of the linear nonscotomatous response latency and the normal response latency from the opposite hemifield.   The two waveforms are statistically identical in latency.   Units are ms; NS= not significant, P>0.05.

5.5.2.2 Nonlinear Response.

Figure 5-14 illustrates the mean second kernel, first slice response from scotomatous and nonscotomatous patches of retina.   Table 5-17 illustrates that the amplitude of the P23 component of the two waveforms is significantly different, but N31 is not, Table 5-18 shows that the difference is limited to amplitude, and that latencies are unaffected.   However, Figure 5-15 and Table 5-19 show that the amplitude of the P23 component is statistically different in the normal retina (although latencies are not, see Table 5-20). A comparison must be formed between scotomatous vs. normal responses of the same hemifield and nonscotomatous responses vs. normal responses of the opposite hemifield.
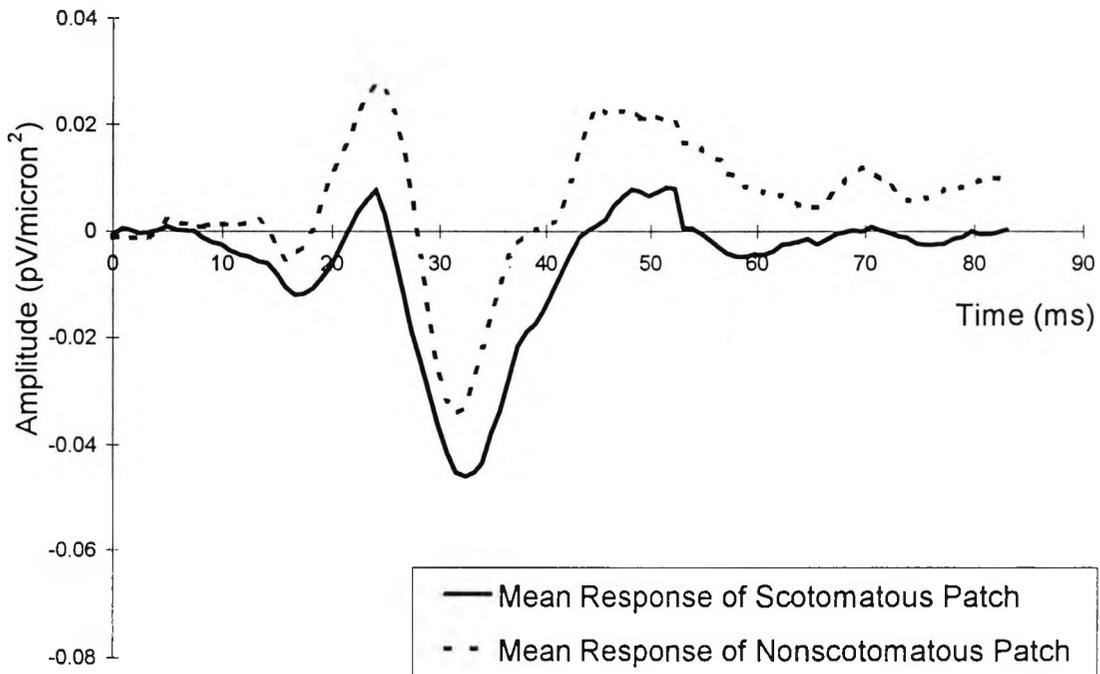
Figure 5-14 Nonlinear response. Scotomatous and nonscotomatous responses.

Scotomatous and Nonscotomatous Response					
	Scotomatous	Nonscotomatous	Difference	SD	t	P
P23	0.008	0.027	-0.019	0.022	4.065	0.0004
N31	-0.045	-0.034	-0.011	0.026	2.000	NS

Table 5-17 Statistical analysis of the amplitudes of the nonlinear scotomatous and nonscotomatous responses. The P23 feature of the two waveforms is statistically different. Units are $pV/micron^2$; NS= not significant, P>0.05.

Scotomatous and Nonscotomatous Response					
	Scotomatous	SD	Nonscotomatous	SD	t	P
P23	24.07	3.260	24.07	3.294	1.932	NS
N31	32.37	3.194	31.54	2.834	0.148	NS

Table 5-18 Statistical analysis of the latencies of the nonlinear scotomatous and nonscotomatous responses. The latencies of the two waveforms are statistically identical. Units are ms; NS= not significant, P>0.05.

240
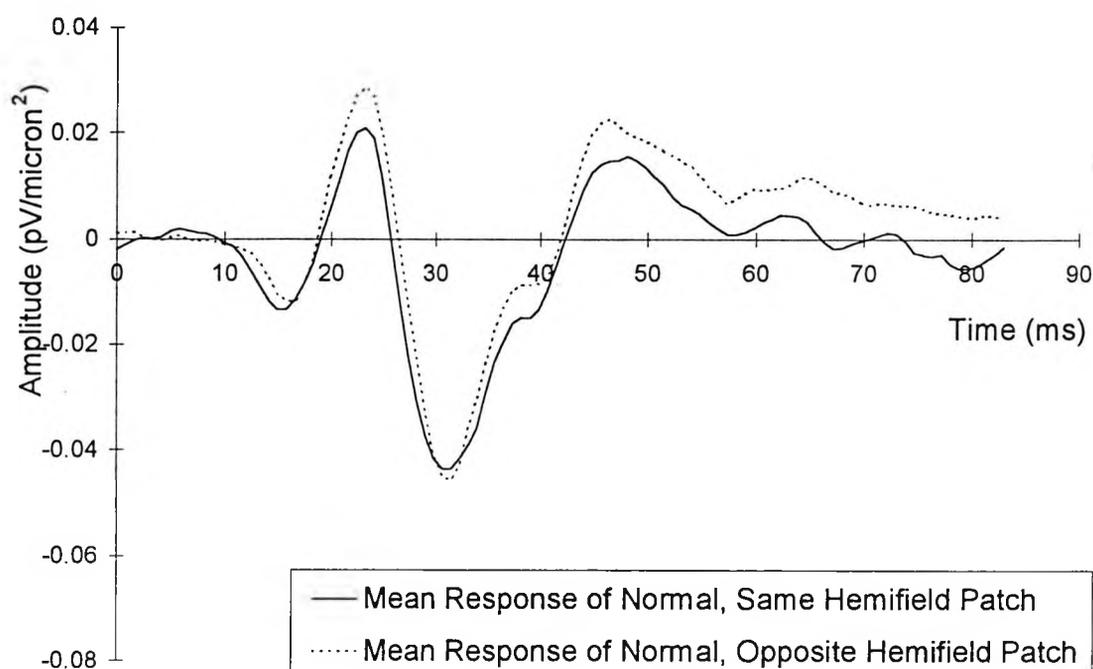
Figure 5-15   Nonlinear response.   Normal responses from the same and opposite hemifields.

Normal Same and Opposite Response					
	Same	Opposite	Difference	SD	t	P
P23	0.021	0.028	-0.007	0.011	2.804	0.009
N31	-0.044	-0.045	0.001	0.014	0.478	NS

Table 5-19   Statistical analysis of the amplitudes of the nonlinear normal same and opposite hemifield responses.   The P23 feature of the two waveforms is statistically different.   Units are $pV/micron^2$;   NS= not significant, P>0.05.

Normal Same and Opposite Response					
	Same	SD	Opposite	SD	t	P
P23	23.24	2.584	23.24	1.614	1.636	NS
N31	30.07	1.614	31.54	0.862	0.397	NS

Table 5-20   Statistical analysis of the latencies of the nonlinear normal same and opposite hemifield responses.   The two waveforms are statistically identical.   Units are ms; NS= not significant, P>0.05.

241

Figure 5-16 illustrates the mean response of the scotomatous patch of retina, plotted with the mean normal second kernel, first slice response from the same hemifield. The difference in response amplitude found in the scotomatous vs. nonscotomatous comparison, above, is repeated, and the difference in the amplitude of P23 is statistically significant (see Table 5-21). The latency of the P23 feature appears to have increased in glaucoma, but the increase in latency was not systematic throughout the sample and was not statistically significant (Table 5-22).
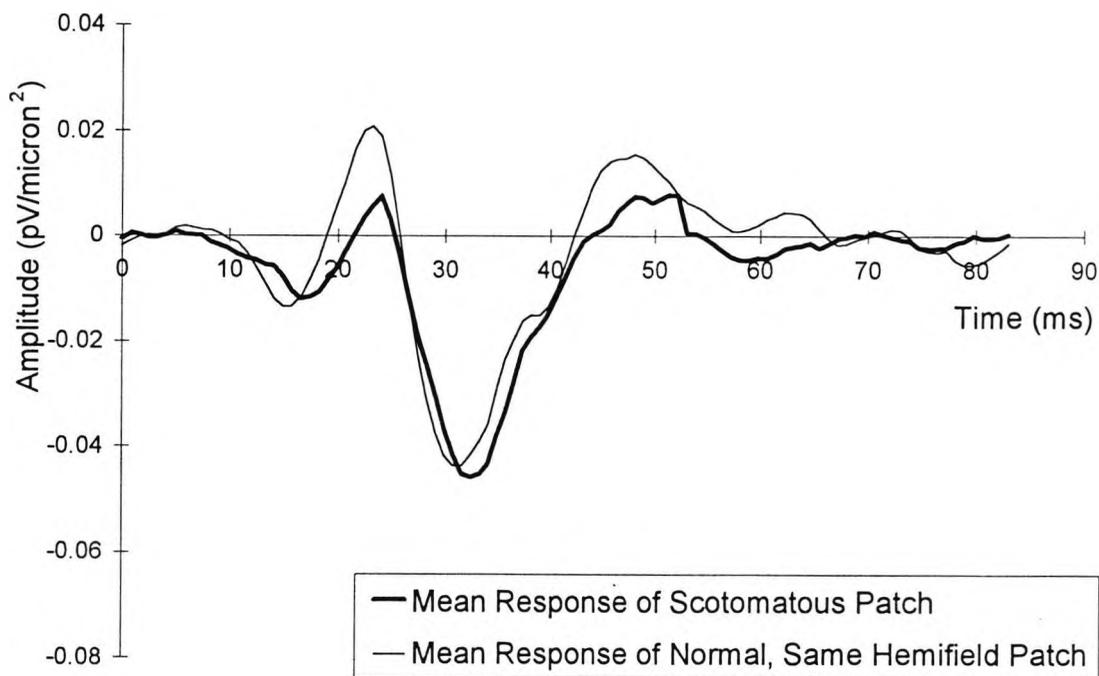
Figure 5-16   Nonlinear Response.   Scotomatous response and normal response from the same hemifield.

Scotomatous and Normal, Same Hemifield Response					
Scotomatous		Normal		n=23	
Mean	SD	Mean	SD	t statistic	P value
P23	0.007	0.015	0.021	0.011	2.072	0.044
N31	-0.046	0.030	-0.044	0.007	0.310	NS

Table 5-21   Statistical analysis of the amplitudes of the nonlinear scotomatous response and the normal response from the same hemifield. The P23 feature of the two waveforms is statistically different.   Units are pV/micron^2; NS= not significant, P>0.05.

Scotomatous and Normal, Same Hemifield Response					
Scotomatous		Normal		n=23	
Mean	SD	Mean	SD	t statistic	P value
P23	24.07	3.260	23.24	2.584	2.007	NS
N31	32.37	3.194	30.07	1.614	0.480	NS

Table 5-22   Statistical analysis of the latencies of the nonlinear scotomatous response and the normal response from the same hemifield.   The latencies of the two waveforms are statistically identical.   Units are ms; NS= not significant, P>0.05.

Figure 5-17 illustrates the mean nonscotomatous response plotted with the analogous mean normal response from the opposite hemifield.   The positive deflections of the waveforms appear identical, and statistical analysis confirms that there is no significant difference between the amplitudes of P23 (see Table 5-23).   The amplitude of the negative components of the waveform appear to be smaller in the nonscotomatous response than the normal response but this result is not significantly different.   The latencies of the features of the two waveforms are identical (see Table 5-24).
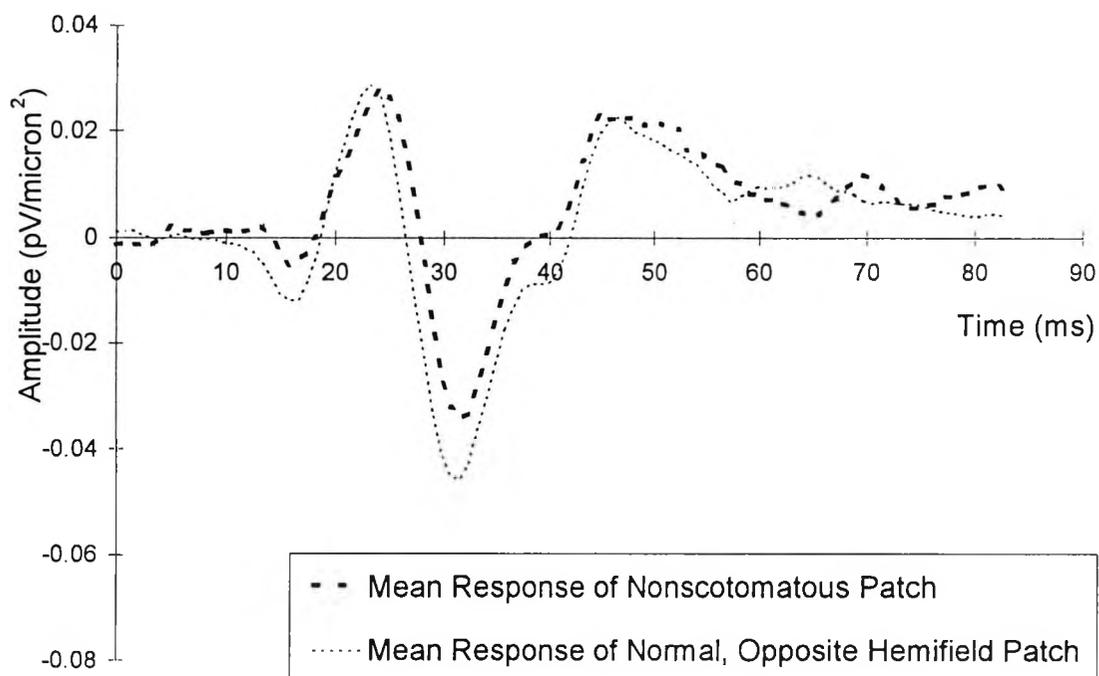
Figure 5-17 Nonlinear Response. Nonscotomatous response and normal response from the opposite hemifield.

	Nonscotomatous and Normal, Opposite Hemifield					
	Nonscotomatous		Normal		n=23	
	Mean	SD	Mean	SD	t statistic	P value
P23	0.028	0.019	0.029	0.010	0.226	NS
N31	-0.034	0.034	-0.044	0.012	1.351	NS

Table 5-23   Statistical analysis of the amplitudes of the nonlinear nonscotomatous response and the normal response from the opposite hemifield.   The amplitudes of the two waveforms are statistically identical. Units are pV/micron^2; NS= not significant, P>0.05.

	Nonscotomatous and Normal, Opposite Hemifield					
	Nonscotomatous		Normal		n=23	
	Mean	SD	Mean	SD	t statistic	P value
P23	24.07	3.294	23.24	1.614	0.181	NS
N31	31.54	2.834	31.54	0.862	0.498	NS

Table 5-24   Statistical analysis of the latencies of the nonlinear nonscotomatous response and the normal response from the opposite hemifield.   The latencies of the two waveforms are statistically identical. Units are ms; NS= not significant, P>0.05.

5.5.3 Responses of Glaucomatous Scotomata: Analysis.

The amplitude of the P23 component of the second kernel, first slice response varies between the two hemifields of the normal retina is a surprising and largely inexplicable finding.   No hemifield-related difference in rod, cone or ganglion cell population density is evident in the results of Curcio et al. (1990) and Silveira et al. (1991).   Neither has any hemifield-related difference been noted in ganglion cell number, shape, size or inter-connectivity by (Vrabec, 1965; Nelson and Kolb, 1983; Perry and Cowey, 1984; Perry and Cowey, 1985; Kolb and Dekorver, 1991; Rodieck et al. 1985; Dacey and Petersen, 1992), although these reports were not explicitly investigating this possibility.

The amplitude of the P23 component of by the second kernel, first slice response is reduced in glaucomatous scotomata, when compared to identical areas of normal retina.   As glaucomatous scotomata are known to be caused by a reduction in ganglion cell number, this result constitutes an association between a flash

nonlinear response and a response rooted in ganglion cell function. It indicates that the ganglion cell response may be located in an early positive component of the second kernel, first slice response. It is possible that the P23 component represents a ganglion cell response alone, or that ganglion cells are part of a network of interconnected cells whose combined response is the P23 component.

This result correlates with histological studies that have noted discrete areas of ganglion cell loss in peripheral retina (Quigley et al. 1982; Quigley et al. 1989). The same studies have noted that large numbers of ganglion cells may be lost, even up to 40% of the total population, before sensitivity losses occur that are measurable with perimetry. The response of areas of retina that are spared field loss in glaucoma are not significantly different from the response of the same area of a normal retina. Ganglion cell loss that is below detection threshold in the Humphrey VFA test is also undetectable in VERIS. Several explanations for this present themselves. It is possible that VERIS is not capable of detecting subtle ganglion cell loss, only gross local ganglion cell loss. The P23 component may be a coarse measure of ganglion cell function and only abnormal in the deep defects that were included in the scotomatous patches of retina.

It is also possible that the high contrast stimuli that were required to extract a measurable retinal response with VERIS are exciting a supra-threshold response that includes contributions from large and small ganglion cells. Glaucomatous ganglion cell loss may have to be very advanced before small ganglion cells are affected (Quigley

et al. 1989).   Small ganglion cells make up the majority of the ganglion cells in the human retina (Silveira and Perry, 1991) so if P23 is registering small and large ganglion cell function, glaucomatous ganglion cell loss may have to be very advanced before any change in P23 is discernible.

Retrograde degeneration of the inner retina during the advanced stages of glaucoma has been observed (Quigley, 1993) . Retrograde degeneration might bring about a loss of amacrine cells.   It is possible that the reduction in P23 amplitude may be associated with a change in amacrine cell rather than ganglion cell function.   The possibility of a contribution to the nonlinear response from amacrine cells has been discussed, and the dissimilarity between ganglion cells densities and P23 amplitude noted, in Section 4.3.4.   The absence of an alteration in the nonscotomatous response may be because although ganglion cell loss has occurred in this region, retrograde degeneration of the amacrine cells has yet to happen.

If the source of P23 may be located in ganglion or amacrine cells, what of N31?   Several alternative explanations exist.   The source of N31 may be in small ganglion cells that are unaffected in glaucoma, or it may lie in other retinal layers.   The existence of a luminance component in the pattern (Drasdo et al. 1987; Brannan et al. 1992) and flicker (Burns et al. 1992) electroretinogram hints at the possibility of outer retinal contributions to nonlinear responses. N31 may derive from outer retinal neurones themselves, although it is unlikely given the dissimilarity between N31 amplitude and the density of outer retinal neurones, presented in Section 4.2.3, and

the fact that photoreceptors and bipolar cells respond almost linearly (Sakuranaga et al. 1986; Powers and Arnett, 1981). It is more likely that N31 derives from interactions within the outer plexiform layer, as other nonlinearities have been shown to do (Shuang et al. 1995; Chang, 1993).

5.6 The VERIS Nonlinear Electroretinogram as a Clinical Test for Primary Open Angle Glaucoma.

A measure of the affectiveness of a test is the receiver-operator characteristic (ROC) curve. ROC curves have two parameters - sensitivity and specificity. Sensitivity is the proportion of patients in a sample who are defective (posses the pathology) and fail the test; it is also known as the true positive rate, the hit rate and the probability of detection. Sensitivity is expressed as:

$$\text{Sensitivity} = \frac{\text{Number of defectives failing}}{\text{Total number of defectives}}$$

Equation 5-1

Specificity is the proportion of patients in a sample who are not defective (do not posses the pathology) and do not fail the test; synonyms include the true negative rate and the correct rejection rate. Specificity is expressed as:

$$\text{Specificity} = \frac{\text{Number of normals not failing}}{\text{Total number of normals}}$$

Equation 5-2

ROC curves plot the true positive rate (sensitivity) on the ordinate axis and the false positive rate (1-specificity) on the abscissa. A

test that efficiently discriminates between defectives and normals will have a high true positive rate and a low false positive rate. A poor discriminator will manage a high true positive rate only when the false negative rate is also high. The worst kind of test will never discriminate better than a '50/50 chance' guess, in this case sensitivity and 1-specificity lie on the leading diagonal of the ROC plot.

The scotomatous and analogous normal amplitude of the P23 feature of the population of glaucoma subjects is illustrated in Figure 5-18. The ROC curve is calculated by letting a theoretical P23 amplitude threshold move across this figure. At each amplitude the points below the threshold are deemed to have failed the test, and sorted into two bins - scotomatous points that have correctly failed the test (true positives) and normal points that should have passed (false positives). The sensitivity and 1-specificity of each threshold is calculated and plotted to create the ROC curve. The ROC curve for the amplitude of P23, illustrated in Figure 5-18, is presented in Figure 5-19.
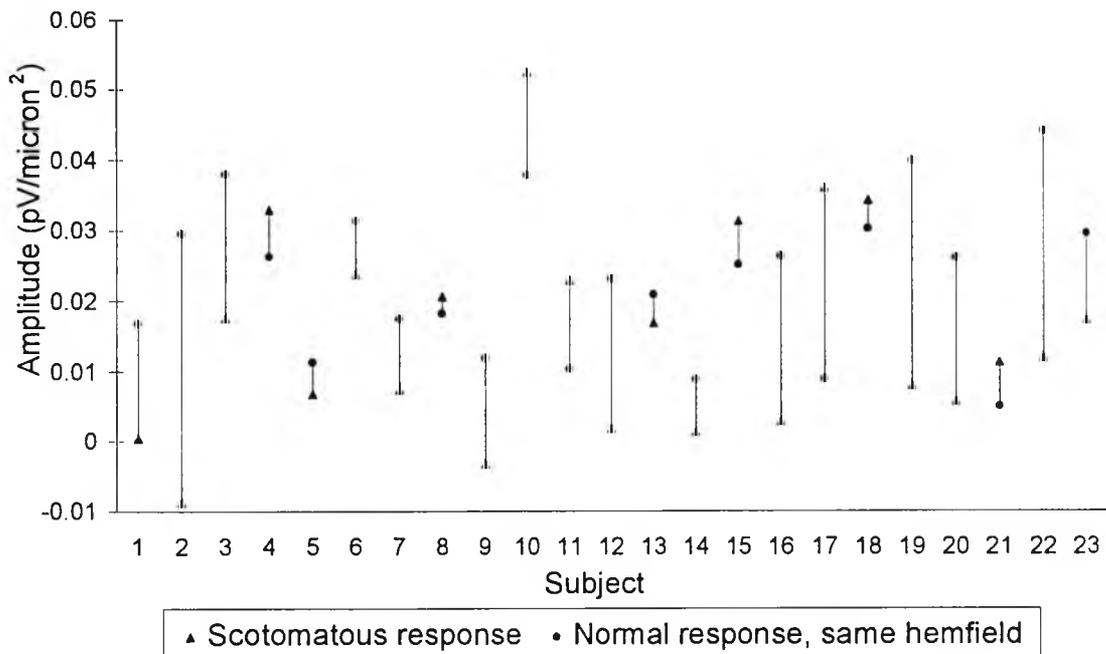
Figure 5-18   Amplitudes of P23 of the scotomatous response and the analogous normal response of all subjects.
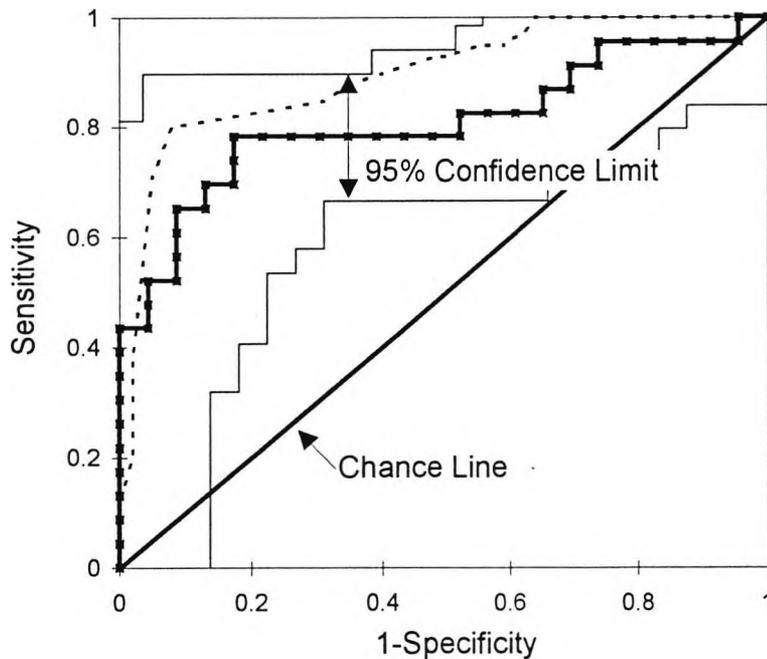
Figure 5-19   The ROC curve for the amplitude of P23 of the second kernel, first slice nonlinear response (thick line), 95% confidence limits are shown (thin line).   An example PERG test ROC curve (Graham et al. 1996) is shown (dotted line).
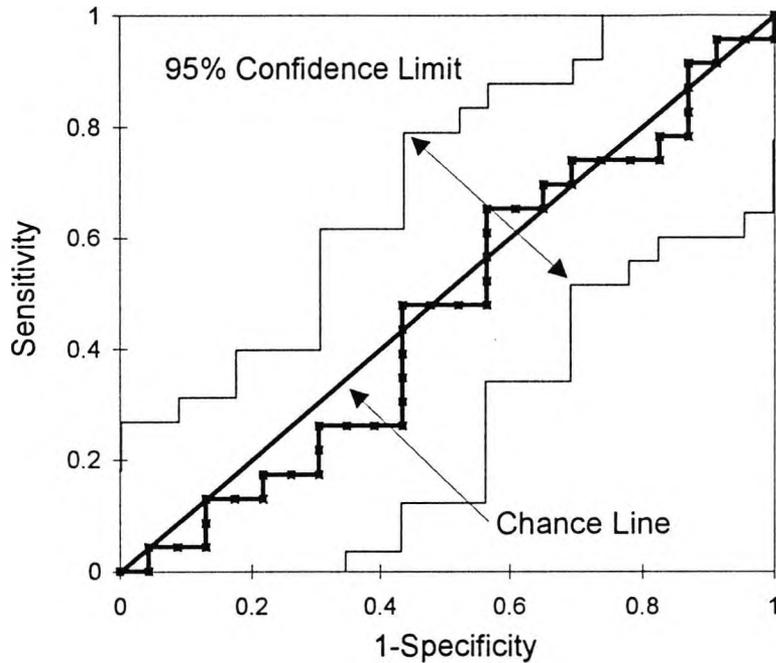
Figure 5-20   The ROC curve for the amplitude of the b-wave linear response (thick line), 95% confidence limits are shown (thin line).   The ROC curve does not deviate from the 50/50 chance line, indicating that the b-wave is not capable of discriminating scotomatous from normal retina.

The ROC plot is a nonparametric assessment of test efficiency that depends entirely on rank.   The confidence limits in Figure 5-19 and Figure 5-20 are constructed with separate (1-α) confidence intervals for each value of Sensitivity and 1-Specificity (Campbell, 1994).

Figure 5-19 shows that VERIS can be used to identify areas of glaucomatous scotomata when the amplitude of P23 of the nonlinear (second kernel, first slice) response is used.   VERIS can achieve almost 50% sensitivity for 100% specificity, and so could identify all the advanced glaucoma patients passing trough a clinic, with the penalty of misdiagnosing 50% of the normals.   In comparison, the ROC curve for the amplitude of the b-wave, linear response, is plotted in Figure 5-20.   The b-wave does not deviate

251

from the chance line and is no better at discriminating between scotomatous and normal retina than a '50/50' guess.

The subjects from which these responses were obtained had all been diagnosed with glaucoma, using the diagnostic procedures currently available: visual field analysis, IOP and C/D ratio measurement. Although VERIS could indicate which patches of retina are scotomatous, VERIS does not add to the diagnostic techniques that clinicians already possess, because these patches of retina had already been identified by the Humphrey.

Conclusion.

It is possible to record linear and nonlinear multifocal electroretinograms from human subjects using the VERIS system. .

The a-wave of the linear response has a strong contribution from cone photoreceptors, especially where the eccentricity is less than 3 degrees. Other neurone responses possibly arising from rod photoreceptors, OFF bipolar cells or horizontal cells, intrude at greater eccentricities. An increase in a-wave latency was observed in ageing, which might be caused by the build up of lipofuscins and refractile particles in cone outer segments. a-Wave latency is affected evenly across the retina and b-Wave latency is similarly altered. It is possible that the enzyme cascade, which is very similar in cones and bipolar cells, is relatively unaffected by ageing. There is no significant alteration in the amplitude of the a- wave with age, this correlates with histological observations that the density of cones is unchanged in ageing.

Temporal analysis of the second order kernel (nonlinear response) reveals that the complex waveform may be the sum of one negative and three positive components. The second order kernel may be approximated with the sum of four Gaussian functions modelled on these four components. A further component may be extracted using the method of Sutter and Bearse (1995, 1999), although the latency of this component does not possess the distinctive topographical arrangement, apparently correlated with distance from optic nerve head, found by these authors. As in the linear response, the amplitude of the nonlinear response is resistant to

age-related changes, but the latency is altered in ageing. Unlike the linear response, increases in latency in the nonlinear response are found only where the eccentricity is greater than 6.5 degrees which suggests that the neurones subserving the peripheral nonlinear response may be different to those subserving the response of the central retina. As the topography of the amplitude of features in the nonlinear response are quite different to the topography of rods, cones and ganglion cells it seems possible that the nonlinear response arises from elsewhere in the retina.

The finding that aspects of the nonlinear response are abnormal in primary open angle glaucoma, but that the linear response is unchanged, suggests that the two responses have, at least in part, different retinal origins. More specifically, the P23 component of the nonlinear response has a significantly reduced amplitude in areas of glaucomatous retina that Humphrey Visual Field Analysis reveal to have a scotomata. Other areas of retina, including the fovea, in which ganglion cell loss has yet to occur or has not met a measurable level are not significantly different from normal control responses. Response latencies are unaltered everywhere in the retina. It is conceivable that the P23 response is rooted in ganglion cell function, but it is also possible that other neurones are involved. ROC curve analysis indicates the potential clinical utility of VERIS for discriminating between scotomatous and nonscotomatous retina using the amplitude of the P23 feature.

Bibliography

Ahmed, N. and Rao, K.R. (1975) *Orthogonal Transforms for Digital Signal Processing*, Berlin: Springer-Verlag.

Altman, D.G. (1990) *Practical Statistics for Medical Research*, London: Chapman and Hall.

Ammermuller, J. and Kolb, H. (1995) Functional architecture of the turtle inner retina. *J. Comp. Neurol.* **358**, 1-34.

Arden, G.B., Carter, R.M., Hogg, C.R., Siegel, I.M. and Margolis, S. (1979) A gold foil electrode: Extending the horizons for clinical electroretinography. *Invest. Ophthalmol. Vis. Sci.* **18**, 421-426.

Arden, G.B., Vaegan and Hogg, C.R. (1982) Clinical and experimental evidence that the pattern electroretinogram (PERG) is generated in more proximal retinal layers than the focal electroretinogram (FERG). *Ann NY Acad Sci* **388**, 580-601.

Arden, G.B. and Brown, K.T. (1965) Some properties of components of the cat electroretinogram revealed by local recording under oil. *J. Physiol.* **176**, 429-461.

Arden, G.B. and Vaegan (1982) Differences between the focal and pattern electroretinogram in man. *J. Physiol.* **327**, 67-68p.(Abstract)

Arden, G.B. and Vaegan (1983) Electroretinograms evoked in man by local uniform or pattern stimulation. *J. Physiol.* **341**, 85-104.

Armitage, P. and Berry, G. (1987) *Statistical Methods in Medical Research*, 2nd edn. Oxford: Blackwell Scientific Publications.

Ashmore, J.F. and Falk, G. (1976) Absolute sensitivity of rod bipolar cells in a dark-adapted retina. *Nature* **263**, 248-249.

Asi, H., Leibu, R. and Perlman, I. (1992) Frequency-domain analysis of the human corneal electroretinogram. *Clin. Vision Sci.* **7**, 9-19.

Bach, M., Hiss, P. and Rover, J. (1988) Check-size specific changes of pattern electroretinogram in patients with early open-angle glaucoma. *Doc. Ophthalmol.* **69**, 315-322.

Bach, M., Pfeiffer, N. and Birkner-Binder, D. (1992) Pattern electroretinogram reflects diffuse retinal damage in early glaucoma. *Clin. Vision Sci.* **7**, 335-340.

Bagolini, B., Porciatti, V., Falsini, B., Scalia, G., Neroni, M. and Moretti, G. (1988) Macular electroretinogram as a function of age of subjects. *Doc. Ophthalmol.* **70**, 37-43.

Baker, C.L., Hess, R.H., Olsen, B.T. and Zrenner, E. (1988) Current source density analysis of linear and non-linear components of the primate electroretinogram. *J. Physiol.* **407**, 155-176.

Balaszi, A.G., Rootman, J., Drance, S.M., Schulzer, M. and Douglas, G.R. (1984) The effect of age on the nerve fibre population of the human optic nerve. *American Journal of*

Ophthalmology **97**, 760-766.

Baylor, D.A., Hodgkin, A.L. and Lamb, T.D. (1974) The electrical response of turtle cones to flashes and steps of light. *J. Physiol.* **242**, 685-727.

Baylor, D.A., Nunn, B.J. and Schnapp, J.L. (1984) The photocurrent, noise and spectral sensitivity of rods of the monkey *Macaca fascicularis. J. Physiol.* **357**, 575-607.

Baylor, D.A. and Fuortes, M.G.F. (1970) Electrical response of single cones in the retina of the turtle. *J. Physiol.* **207**, 77-92.

Bearse, M.A., Sutter, E.E., Smith, D.N. and Stamper, R. (1995) Ganglion cell components of the human multifocal ERG are abnormal in optic nerve atrophy and glaucoma. *Invest. Ophthal. Vis. Sci. , Supp* **36**, 2036(Abstract)

Bearse, M.A., Sim, D., Sutter, E.E., Stamper, R. and Lieberman, M. (1996) Application of the multifocal ERG to glaucoma. *Invest. Ophthal. Vis. Sci. , Supp* **37**, 2342 (Abstract)

Beauchamp, K.G. (1975) *Walsh Functions and their Applications*, London: Academic Press.

Berninger, T.A. and Arden, G.B. (1988) The pattern electroretinogram. *Eye* **2, Suppl**, S257-S283.

Birch, D.G. and Fish, G.E. (1988) Focal cone electroretinograms:

Aging and macular disease. *Doc. Ophthalmol.* **69**, 211-220.

Boycott, B.B. and Wassle, H. (1991) Morphological classification of bipolar cells of the primate retina. *Eur. J. Neurosci.* **3**, 1069-1088.

Brannan, J.R., Bodis-Wollner, I. and Storch, R.L. (1992) Evidence for two distinct nonlinear components in the human pattern ERG. *Vision Res.* **32**, 11-17.

Breton, M.E., Schueller, A.W., Lamb, T.D. and Pugh, E.N. (1994) Analysis of ERG a-wave amplification and kinetics in terms of the G-protein cascade and phototransduction. *Invest. Ophthalmol. Vis. Sci.* **35**, 295-309.

Brown, K.T. (1968) The electroretinogram: its components and their origins. *Vision Res.* **8**, 633-677.

Brown, K.T. and Murakami, M. (1964) A new receptor potential of the monkey retina with no detectable latency. *Nature* **201**, 626-628.

Brown, K.T. and Watanabe, K. (1962) Isolation and identification of a receptor potential from the pure cone fovea of the monkey retina. *Nature* **193**, 958-960.

Brown, K.T. and Wiesel, T.N. (1961a) Analysis of the intraretinal electroretinogram of the intact cat eye. *J. Physiol.* **158**, 229-256.

Brown, K.T. and Wiesel, T.N. (1961b) Localization of origins of electroretinogram components by intraretinal recording in the intact

cat eye. *J. Physiol.* **158**, 257-280.

Burkhardt, D.A. (1970) Proximal negative response in frog retina. *J. Physiol.* **33**, 405-420.

Burns, S.A., Elsner, A.E. and Kreitz, M.R. (1992) Analysis of nonlinearities in the flicker ERG. *Optom. Vis. Sci.* **69**, 95-105.

Bush, R.A. and Sieving, P.A. (1994) A proximal retinal component in the primate photopic ERG a-wave. *Invest. Ophthalmol. Vis. Sci.* **35**, 635-645.

Bush, R.A. and Sieving, P.A. (1996a) Inner retinal contributions to the primate photopic fast flicker electroretinogram. *J. Opt. Soc. Am. A* **13**, 557-565.

Bush, R.A. and Sieving, P.A. (1996b) Hyperpolarising cell contributions to the primate photopic ERG. *Vision Res.* **36**, 3313(Abstract)

Campbell, G. (1994) Advances in statistical methodology for the evaluation of diagnostic and laboratory tests. *Statistics in Medicine* **13**, 499-508.

Caprioli, J. (1989) Correlation of visual function with optic nerve and nerve fibre layer structure in glaucoma. *Surv. Ophthalmol (suppl)* **33**, 319-330.

Celesia, G.G., Kaufman, D. and Cone, S. (1987) Effects of age and

sex on pattern electroretinograms and visual evoked potentials. *EEG and Clin. Neurophys* **68**, 161-171.

Chan, H.L. and Brown, B. (1998) Investigation of retinitis pigmentosa using the multifocal electroretinogram. *Ophthal. Physiol. Opt.* **18**, 335-350.

Chang, Y. (1993) Red-green flicker photometry and nonlinearities in the flicker electroretinogram. *J. Opt. Soc. Am. A* **10**, 1413-1422.

Chylack, L.T., Wolfe, J.K., Singer, D.M., Leske, M.C., Bullimore, M.A., Bailey, I.L., Friend, J., McCarthy, D. and Wu, S. (1993) The Lens Opacificaties Classification System III. *Arch Ophthalmol* **111**, 831-836.

Cline, D., Hofstetter, H.W. and Griffin, J.R. (1997) *Dictionary of Visual Science*, 4th edn. Oxford: Butterworth-Heinemann.

Cobb, W.A. and Morton, H.B. (1954) A new component of the human electroretinogram. *J. Physiol.* **123**, 36-37.

Coleman, P.A., Massey, S.C. and Miller, R.F. (1986) Kynurenic acid distinguishes kainate and quisqualate receptors in the vertebrate retina. *Brain Res.* **381**, 172-175.

Cone, R.A. (1963) Quantum relations of the rat electroretinogram. *J. Gen. Physiol.* **46**, 1267-1286.

Curcio, C.A., Sloan, K.R., Kalina, R.E. and Hendrickson, A.E.

(1990) Human photoreceptor topography. *The Journal of Comparative Neurology* **292**, 497-523.

Curcio, C.A. and Allen, K.A. (1990) Topography of ganglion cells in human retina. *J. Comp. Neurol.* **300**, 5-25.

Curcio, C.A. and Drucker, D.N. (1993) Retinal ganglion cells in Alzheimer's disease and aging. *Ann. Neurol.* **33**, 248-257.

Dacheux, R.F. and Raviola, E. (1986) The rod pathway in the rabbit retina: A depolarising bipolar and amacrine cell. *J. Neuroscience* **6**, 331-345.

Dawson, W.W., Trick, G.L. and Litzkow, C.A. (1979) Improved electrode for electroretinography. *Invest. Ophthalmol. Vis. Sci.* **18**, 988-991.

Dick, E. and Miller, R.F. (1978) Light evoked potassium activity in mudpuppy retina: its relationship to the b-wave of the electroretinogram. *Brain Res.* **154**, 388-394.

Dowling, J.E. (1987) *The retina: an approachable part of the brain*, 1st edn. Cambridge: Harvard University Press.

Drance, S.M., Douglas, G.R., Airaksinen, P.J., Schulzer, M. and Hitchings, R.A. (1987) Diffuse visual field loss in chronic open-angle and low-tension glaucoma. *American Journal of Ophthalmology* **104**, 577-580.

Drasdo, N. (1977) Neural representation of visual space. *Nature* **266**, 554-556.

Drasdo, N. (1989) Receptive field densities of the ganglion cells of the human retina. *Vision Res.* **29**, 985-988.

Drasdo, N., Thompson, D.A., Thompson, C.M. and Edwards, L. (1987) Complementary components and local variations of the pattern electroretinogram. *Invest. Ophthalmol. Vis. Sci.* **28**, 158-162.

Esakowitz, L., Kriss, A. and Shawkat, F. (1993) A Comparison of Flash Electroretinograms Recorded from Burian-Allen, Jet, C-Glide, Gold-Foil, DTL and Skin Electrodes. *Eye* **7**, 169-171.

Evers, H.U. and Gouras, P. (1986) Three cone mechanisms in the primate electroretinogram: Two with, one without off-centre bipolar responses. *Vision Res.* **26**, 245-254.

Faber, D.S. (1969) Analysis of slow transretinal potentials in response to light. Buffalo: State University of New York. Not Available. Ph.D.

Falsini, B., Colotto, A., Porciatti, V., Buzzonetti, L., Coppe, A. and De Luca, L.A. (1991) Macular flicker- and pattern-ERGs are differently effected in ocular hypertension and glaucoma. *Clin. Vision Sci.* **6**, 423-429.

Fesenko, E.E., Stanislaw, S.K. and Lyubarsky, A.L. (1985)

Induction by cyclic GMP of cationic conductance in plasma membrane of retinal rod outer segment. *Nature* **313**, 310-313.

Fitzke, F., Hitchings, R.A., Poinoosawmy, D., McNaught, A.I. and Crabb, D.P. (1996) Analysis of visual field progression in glaucoma. *B. J. Ophthalmol.* **80**, 40-48.

Freed, M.A., Pflug, R., Kolb, H. and Nelson, R. (1996) ON-OFF amacrine cells in cat retina. *J. Comp. Neurol.* **364**, 556-566.

Frishman, L.J. and Sieving, P.A. (1995) Evidence for two sites of adaption affecting the dark-adapted ERG of cats and primates. *Vision Res.* **35**, 435-442.

Frishman, L.J. and Steinberg, R.H. (1989) Intraretinal analysis of the threshold dark-adapted ERG of cat retina. *J. Neurophysiol.* **61**, 1221-1232.

Fuortes, M.G.F. and Hodgkin, A.L. (1964) Changes in time scale and sensitivity in the ommatidia of *Limulus*. *J. Physiol.* **172**, 239-263.

Gaasterland, D.E., Ederer, F., Sullivan, E.K., Caprioli, J. and Cyrlin, M.N. (1994) Advanced glaucoma intervention study. 2) Visual field test scoring and reliability. *Ophthalmol.* **101**, 1445-1455.

Gao, H. and Hollyfield, J.G. (1992) Aging of the human retina. *Invest. Ophthalmol. Vis. Sci.* **33**, 1-17.

Gjotterberg, M. (1986) Electrodes for Electroretinography, a

comparison of four different types. *Arch Ophthalmol* **104**, 569-570.

Glovinsky, Y., Quigley, H.A. and Dunkelberger, G.R. (1991) Retinal ganglion cell loss is size dependant in experimental glaucoma. *Invest. Ophthalmol. Vis. Sci.* **32**, 484-491.

Gouras, P. (1968) Identification of cone mechanisms in monkey ganglion cells. *J. Physiol.* **199**, 533-547.

Graham, S.L., Wong, V.A.T., Drance, S.M. and Mikelberg, F.S. (1994) Pattern electroretinograms from hemifields in normal subjects and patients with glaucoma. *Invest. Ophthalmol. Vis. Sci.* **35**, 3347-3356.

Graham, S.L., Drance, S.M., Chauhan, B.C., Swindale, N.V., Hnik, P., Mikelberg, F.S. and Douglas, G.R. (1996) Comparison of psychophysical and electrophysiological testing in early glaucoma. *Invest. Ophthalmol. Vis. Sci.* **37**, 2651-2662.

Granit, R. (1933) The components of the retinal action potential in mammals and their relation to the discharge in the optic nerve. *J. Physiol.* **77**, 207-239.

Gurevitch, L. and Slaughter, M.M. (1993) Comparison of the waveforms of the ON bipolar neurone and the b-wave of the electroretinogram. *Vision Res.* **33**, 2431-2435.

Hagins, W.A., Penn, R.D. and Yoshikami, S. (1970) Dark current and photocurrent in retinal rods. *Biophys. J.* **10**, 380-413.

Hanitzsch, R., Lichtenberger, T. and Mattig, W.U. (1996) The influence of $MgCl_2$ and APB on the light-induced potassium changes and the ERG b-wave of the isolated superfused rat retina. *Vision Res.* **36**, 499-507.

Hart, W.M. and Becker, B. (1982) The onset and evolution of glaucomatous visual field defects. *Ophthalmol.* **89**, 268-279.

Hennessy, M.P. and Vaegan (1995) Amplitude scaling relationships of Burian-Allen, gold-foil and Dawson, Trick and Litzkow electrodes. *Doc. Ophthalmol.* **89**, 235-248.

Hess, R.F. and Baker, C.L. (1984) Human pattern-evoked electroretinogram. *J. Neurophysiol.* **51**, 939-951.

Heynen, H., Wachtmeister, L. and van Norren, D. (1985) Origin of the oscillatory potentials in the primate retina. *Vision Res.* **25**, 1365-1373.

Hodgkin, A.L. and O'Bryan, P.M. (1977) Internal recording of the early receptor potential in turtle cones. *J. Physiol.* **267**, 737-66.

Hogg, C.R, 1998. Personal Communication.

Holder, G.E. (1987) Significance of abnormal pattern electroretinography in anterior visual pathway dysfunction. *B. J. Ophthalmol.* **71**, 166-171.

Holopigian, K., Seiple, W., Mayron, R. and Lorenzo, M. (1990) Electrophysiological and psychological flicker sensitivity in patients with primary open-angle glaucoma and ocular hypertension. *Invest. Ophthalmol. Vis. Sci.* **31**, 1863-1868.

Hood, D.C., Seiple, W., Holopigian, K. and Greenstein, V. (1997) A comparison of the components of the multifocal and full-field ERGs. *Vis. Neurosci* **14**, 533-544.

Hood, D.C. and Birch, D.G. (1990a) The a-wave of the human electroretinogram and rod receptor function. *Invest. Ophthalmol. Vis. Sci.* **31**, 2070-2081.

Hood, D.C. and Birch, D.G. (1990b) A quantitative measure of the electrical activity of human rod photoreceptors using electroretinography. *Vis. Neurosci* **5**, 379-387.

Hood, D.C. and Birch, D.G. (1995) Phototransduction in human cones measured using the a-wave of the ERG. *Vision Res.* **35**, 2801-2810.

Hull, B.M. and Drasdo, N. (1990) The influence of age on the pattern-reversal electroretinogram. *Ophthal. Physiol. Opt.* **10**, 49-53.

Janssen, P., Naskar, R., Moore, S., Thanos, S. and Thiel, H.J. (1986) Evidence for glaucoma-induced horizontal cell alterations in the human retina. *Ger. J. Ophthalmol.* **5**, 378-385.

Karwoski, C.J. and Proenza, L.M. (1982) Light-evoked K⁺ increases in amphibian retina. *Invest. Ophthal. Vis. Sci. , Supp* -282.

Kline, R.P., Ripps, H. and Dowling, J.E. (1978) The generation of b-wave currents in the skate retina. *Proc. Natl. Acad. Sci.* **75**, 5727-5731.

Knapp, G. and Schiller, P.H. (1984) The contribution of ON bipolar cells to the electroretinogram of rabbits and monkeys: A study using 2-amino-4-phosphobutyrate (APB). *Vision Res.* **24**, 1841-1846.

Kolb, H. and Dekorver, L. (1991) Midget ganglion cells of the parafovea of the human retina: A study by electron microscopy and serial section reconstruction. *J. Comp. Neurol.* **303**, 617-636.

Kolb, H., Linberg, K.A. and Fisher, S.K. (1992) Neurons of the human retina: A Golgi study. *J. Comp. Neurol.* **318**, 147-187.

Kolb, H., Fernandez, E. and Nelson, R. (1997) www.insight.med.utah.edu/Webvision/.

Kolb, H. and Nelson, R. (1984) Neural architecture of the cat retina. *Prog. Ret. Res.* **3**, 21-60.

Komata, M., Shirao, Y., Watanabe, M. and Kawasaki, K. (1995) Delay of pattern electroretinogram peaks and its correlation to contrast threshold for motion perception in glaucoma. *Ophthalmic. Res.* **27**, 110-117. .

267

Kondo, M., Horiguchi, M., Miyake, Y., Suzuki, S. and Tanikawa, A. (1996) Effects of rapid random flash stimuli on electroretinographic responses. *Folia. Ophthalmol. Jpn.* **47**, 531-535.

Kondo, M., Miyake, Y., Horiguchi, M., Suzuki, S. and Tanikawa, A. (1998) Recording multifocal electroretinogram ON and OFF responses in humans. *Invest. Ophthalmol. Vis. Sci.* **39**, 574-580.

Korth, M., Rix, R. and Sembritzki, O. (1985) Spatial contrast transfer function of the pattern-evoked electroretinogram. *Invest. Ophthalmol. Vis. Sci.* **26**, 303-308.

Korth, M., Horn, F., Storck, B. and Jonas, J. (1998) The pattern-evoked electroretinogram (PERG): Age-related alterations and changes in glaucoma. *Graefe's Arch. Clin. Exp. Ophthalmol.* **227**, 123-130.

Lamb, T.D., McNaughton, P.A. and Yau, K.W. (1981) Spatial spread of activation and background desensitisation in toad rod outer segments. *J. Physiol.* **319**, 463-496.

Lamb, T.D. (1986) Transduction in vertebrate photoreceptors: The roles of cyclic GMP and calcium. *Trends Neurosci.* **9**, 224-228.

Lamb, T.D. and Pugh, E.N. (1992) A quantitative account of the activation steps involved in phototransduction in amphibian photoreceptors. *J. Physiol.* **449**, 719-758.

Lynn, P.A. (1982) *A Introduction to the Analysis and Processing of Signals*, 2nd edn. Hong Kong: Macmillan.

Maffei, L., Fiorentini, A., Bisti, S. and Hollander, H. (1985) Pattern ERG in the monkey after section of the optic nerve. *Exp. Brain Res.* **59**, 423-425.

Maffei, L. and Fiorentini, A. (1981) Electroretinographic responses to alternating gratings before and after section of the optical nerve. *Science* **211**, 953-955.

Maffei, L. and Fiorentini, A. (1982) Electroretinographic responses to alternating gratings in the cat. *Exp. Brain Res.* **48**, 327-334.

Masu, M., Iwakabe, H., Tagawa, Y., Miyoshi, T., Yamashita, M., Fukuda, F., Sasaki, H., Hiroi, K., Nakamura, Y., Shigemoto, R., Takada, M., Nakamura, K., Nakao, K., Katsuki, M. and Nakanishi, S. (1995) Specific deficit of the ON response in visual transmission by targeted disruption of the mGluR6 gene. *Cell* **80**, 7757-765.

Mehaffey, L., Holopigian, K. and Seiple, W. (1993) Electro-oculogram changes in patients with ocular hypertension and primary open-angle glaucoma. *Doc. Ophthalmol.* **83**, 103-110.

Mikelberg, F.S., Schulzer, M., Drance, S.M. and Lau, W. (1986) The rate of progression of scotomas in glaucoma. *American Journal of Ophthalmology* **101**, 1-6.

Miller, R.F., Frumkes, T.E., Slaughter, M.M. and Dacheux, R.F. (1981) Physiological and pharmacological basis of GABA and

glycine action on neurones of mudpuppy retina II: Amacrine and ganglion cells. *J. Neurophysiol.* **45**, 764-782.

Miller, R.F. and Dowling, J.E. (1970) Intracellular responses of the Muller (glial) cells of mudpuppy retina: their relationship to b-wave of the electroretinogram. *J. Neurophysiol.* **33**, 323-341.

Mollon, J.D. and Baker, M.R. (1995) The use of CRT displays in research on colour vision. In: Drum, B. (Ed.) *Colour Vision Deficiencies XII*, pp. 423-444. Dordrecht: Kluwer Academic Publishers]

Murakami, M. and Kaneko, A. (1966) Differentiation of PIII subcomponents in cold-blooded vertebrate retinas. *Vision Res.* **6**, 627-636.

Naka, K.I. and Rushton, W.A.H. (1967) The generation and spread of S-potentials in fish (*cyprinidae*). *J. Physiol.* **192**, 437-461.

Nawy, S. and Jahr, C.E. (1990) Suppression by glutamate of cGMP-activated conductance in retina bipolar cells. *Nature* **346**, 269-271.

Nelson, R., Famiglietti, E.V. and Kolb, H. (1978) Intracellular staining reveals different levels of stratification for ON-centre and OFF-centre ganglion cells in the cat retina. *J. Neurophysiol.* **41**, 427-483.

Nelson, R. (1982) AII amacrine cells quicken the time course of rod

signals in the cat retina. *J. Neurophysiol.* **47**, 928-947.

Nelson, R. and Kolb, H. (1983) Synaptic patterns and response properties of bipolar and ganglion cells in the cat retina. *Vision Res.* **23**, 1183-1195.

Newman, E.A. (1980) Current source-density analysis of the b-wave of frog retina. *J. Neurophysiol.* **43**, 1355-1366.

Noell, W.K. (1954) The origin of the electroretinogram. *American Journal of Ophthalmology* **38**, 78-90.

Nork, T.M., Poulsen, G.L., Vaegan and Sarks, S.H. (1995) Photoreceptor damage and loss in human eyes with primary open angle glaucoma. *Invest. Ophthal. Vis. Sci. , Supp* **36**, S331(Abstract)

O'Donaghue, E., Arden, G.B., O'Sullivan, F., Falca~o-Reis, F., Moriarty, B., Hitchings, R.A., Spilleers, W., Hogg, C.R. and Weinstein, G. (1992) The pattern electroretinogram in glaucoma and ocular hypertension. *B. J. Ophthalmol.* **76**, 387-394.

Odom, J.V., Maida, T.M. and Dawson, W.W. (1982) Pattern evoked retinal response (PERR) in human: effects of spatial frequency, temporal frequency, luminance and defocus. *Cur. Eye. Res.* **2**, 99-108.

Odom, J.V., Feghali, J.G., Jia-chi, J. and Weinstein, G.W. (1990) Visual function deficits in glaucoma. Electroretinogram pattern and

luminance nonlinearities. *Arch Ophthalmol* **108**, 222-227.

Odom, J.V., Reits, D., Burgers, N. and Riemslag, F.C.C. (1992) Flicker electroretinograms: a systems analytic approach. *Optom. Vis. Sci.* **69**, 106-116.

Ogden, T.E. (1973) The oscillatory waves of primate electroretinogram. *Vision Res.* **13**, 1059-1074.

Osterberg, G. (1935) Topography of the layer of rods and cones. *Acta Ophthalmol.* **6**, 1-103.

Palmowski, A.M., Bearse, M.A. and Sutter, E.E. (1996) Nonlinear interactions in diabetic retinopathy. *Invest. Ophthal. Vis. Sci. , Supp* **73**, 4478

Palmowski, A.M., Sutter, E.E., Bearse, M.A. and Fung, W. (1997) Mapping of retinal function in diabetic retinopathy using the multifocal electroretinogram. *Invest. Ophthalmol. Vis. Sci.* **38**, 2589-2596.

Panda, S. and Jonas, J.B. (1992) Decreased photoreceptor count in human eyes with secondary angle-closure glaucoma. *Invest. Ophthalmol. Vis. Sci.* **33**, 2532-2536.

Peachey, N.S., Roveri, L., Messing, A. and McCall, M.A. (1997) Functional consequences of oncogene-induced horizontal cell degeneration in the retinas of transgenic mouse. *Vis. Neurosci* **14**, 627-632.

Penn, R.D. and Hagins, W.A. (1972) Kinetics of photocurrent in retinal rods. *Biophys. J.* **12**, 1073-1094.

Perry, V.H. and Cowey, A. (1984) Retinal ganglion cells that project to the superior collicus and pretectum in the Macaque monkey. *Neuroscience* **12**, 1125-1137.

Perry, V.H. and Cowey, A. (1985) The ganglion cell and cone distribution in the monkey retina: Implications for central magnification factors. *Vision Res.* **25**, 1795-1810.

Pfeiffer, N., Tillmon, B. and Bach, M. (1993) Predictive value of the pattern electroretinogram in high-risk ocular hypertension. *Invest. Ophthalmol. Vis. Sci.* **34**, 1710-1715.

Polyak, S. (1957) *The vertebrate visual system*, 1st edn. Chicago: University of Chicago Press.

Porciatti, V. (1987) Non-linearities in the focal ERG evoked by pattern and uniform-field stimulation. *Invest. Ophthalmol. Vis. Sci.* **28**, 1306-1313.

Porciatti, V., Falsini, B., Brunori, S., Colotto, A. and Moretti, G. (1987) Pattern electroretinogram as a function of spatial frequency in ocular hypertension and early glaucoma. *Doc. Ophthalmol.* **65**, 349-355.

Porciatti, V., Falsini, B., Scalia, G., Fadda, A. and Fontanesi, G.

(1988) The pattern electroretinogram by skin electrodes: Effect of spatial frequency and age. *Doc. Ophthalmol.* **70**, 117-122.

Porciatti, V., Burr, D.C., Morrone, C. and Fiorentini, A. (1992) The effect of ageing on the pattern electroretinogram and visual evoked potential in humans. *Vision Res.* **32**, 1199-1209.

Porciatti, V., Di Bartolo, E., Marco Nardi, M. and Fiorentini, A. (1997) Response to chromatic and luminance contrast in glaucoma: A psychophysical and electrophysiological study. *Vision Res.* **37**, 1975-1987.

Powers, R.L. and Arnett, D.W. (1981) Spatio-temporal cross-correlation analysis of catfish retinal neurons. *Biol. Cybern.* **41**, 179-196.

Pugh, E.N. and Cobbs, W.H. (1986) Visual transduction in vertebrate rods and cones: A tale of two transmitters, calcium and cyclic GMP. *Vision Res.* **26**, 1613-1643.

Quigley, H.A. (1993) Open-Angle Glaucoma. *Med. Prog.* **328**, 1097-1106.

Quigley, H.A., Addicks, E.M. and Green, W.R. (1982) Optic nerve damage in glaucoma III. Quantitative correlation of nerve fibre loss and visual field defect in glaucoma, ischemic neuropathy, papillodema and toxic neuropathy. *Arch Ophthalmol* **100**, 135-146.

Quigley, H.A. (1986) Pathophysiology of the optic nerve in

glaucoma. In: McAllister, J.A. and Wilson, R.P. (Eds.) *Glaucoma*, pp. 30-53. London: Butterworth and Co.]

Quigley, H.A., Sanchez, R.M., Dunkelberger, G.R., L'Hernault, N.L. and Baginski, T.A. (1987) Chronic glaucoma selectively damages large optic nerve fibres. *Invest. Ophthalmol. Vis. Sci.* **28**, 913-920.

Quigley, H.A., Dunkelberger, G.R. and Green, W.R. (1989) Retinal ganglion cell atrophy correlated with automated perimetry in human eyes with glaucoma. *American Journal of Ophthalmology* **107**, 453-464.

Rodieck, R.W., Binmoeller, K.F. and Dineen, J. (1985) Parasol and midget ganglion cells of the human retina. *J. Comp. Neurol.* **233**, 115-132.

Riggs, L.A., Johnson, E.P. and Schick, A.M.L. (1964) Electrical responses of the human eye to moving stimulus patterns. *Science* **144**, 567

Robson, J.G. and Frishman, L.J. (1995) Response linearity and kinetics of the cat retina: The bipolar cell component of the dark-adapted electroretinogram. *Vis. Neurosci* **12**, 837-850.

Robson, J.G. and Frishman, L.J. (1996) Photoreceptor and bipolar-cell contributions to the cat electroretinogram: A kinetic model for the early part of the flash response. *J. Opt. Soc. Am. A* **13**, 613-622.

Rodieck, R.W. (1973) *The Vertebrate Retina*, New York: W.H.

Freeman.

Ruben, S.T., Hitchings, R.A., Fitzke, F. and Arden, G.B. (1994) Electrophysiology and psychophysics in ocular hypertension and glaucoma: Evidence for different pathomechanisms in early glaucoma. *Eye* **8**, 516-520.

Ruben, S.T., Arden, G.B., O'Sullivan, F. and Hitchings, R.A. (1995) Pattern electroretinogram and peripheral colour contrast thresholds in ocular hypertension and glaucoma: Comparison and correlation of results. *B. J. Ophthalmol.* **79**, 326-331.

Sakuranaga, M., Sato, S., Hida, E. and Naka, K. (1986) Nonlinear analysis: Mathematical theory and biological applications. *CRC Critical Reviews in Biomedical Engineering* **14**, 127-184.

Sawada, A., Nakazaki, S., Nao-i, N., Nagatomo, A. and Arai, M. (1996) Retinal topography using multifocal electroretinogram in open-angle glaucoma. *Invest. Ophthal. Vis. Sci., Supp* **37**, 2345(Abstract)

Scheffé, H. (1959) *The Analysis of Variance*, New York: Wiley.

Shuang, W., Burns, S.A. and Elsner, A.E. (1995) Effects of flicker adaption and temporal gain control on the flicker ERG. *Vision Res.* **35**, 2943-2953.

Sieving, P.A., Frishman, L.J. and Steinberg, R.H. (1986) Scotopic threshold response of proximal retina in cat. *J. Neurophysiol.* **56**,

1049-1061.

Sieving, P.A. (1993) Photopic ON- and OFF-pathway abnormalities in retinal dystrophies. *Trans. Am. Ophthalmol. Soc.* **LXXXXI**, 701-773.

Sieving, P.A., Murayama, K. and Naarendorp, F. (1994) Push-pull model of the primate electroretinogram: a role for hyperpolarising neurons in shaping the b-wave. *Vis. Neurosci* **11**, 519-532.

Sillman, A.J., Ito, H. and Tomita, T. (1969) Studies on the mass receptor potential of the isolated frog retina. II. On the basis of the ionic mechanism. *Vision Res.* **9**, 1443-1451.

Silveira, L.C.L. and Perry, V.H. (1991) The topography of magnocellular projecting ganglion cells in the primate retina. *Neuroscience* **40**, 217-237.

Slaughter, M.M. and Miller, R.F. (1981) 2-amino-4-phosphonobutyric acid: a new pharmacological tool for retinal research. *Science* **211**, 182-185.

Slaughter, M.M. and Miller, R.F. (1983a) An excitatory amino acid antagonist blocks cone input to sign-conserving second-order retinal neurones. *Science* **219**, 1230-1232.

Slaughter, M.M. and Miller, R.F. (1983b) The role of excitatory amino acid transmitters in the mudpuppy retina: an analysis with kainic acid and *N*-methyl aspartate. *J. Neuroscience* **3**, 1701-1711.

Slaughter, M.M. and Miller, R.F. (1985) Characterisation on an extended glutamate receptor of the ON bipolar neurone in the vertebrate retina. *J. Neuroscience* **5**, 224-233.

Smith III, E.L., Harwerth, R.S., Crawford, M.L.J. and Duncan, G.C. (1989) Contribution of the retinal ON channels to scotopic and photopic spectral sensitivity. *Vis. Neurosci.* **3**, 225-239.

Smith, R.G., Freed, M.A. and Sterling, P. (1986) Microcircuitry of the dark-adapted cat retina: Functional architecture of the rod-cone network. *J. Neuroscience* **6**, 3505-3517.

Smith, S.D., Katz, J. and Quigley, H.A. (1996) Analysis of progressive change in automated visual fields in glaucoma. *Invest. Ophthalmol. Vis. Sci.* **37**, 1419-1428.

Spear, P.D. (1993) Neural bases of visual deficits during aging. *Vision Res.* **33**, 2589-2609.

Spekreijse, H., Estevez, O. and van der Tweel, H. (1973) Luminance response to pattern reversal. *Doc. Ophthalmol. Proc. Ser.* **2**, 205-211.

Speros, P. and Price, J. (1981) Oscillatory potentials. History, techniques and potential use in the evaluation of disturbances of retinal circulation. *Surv. Ophthalmol.* **25**, 237-252.

Stanford, L.R. (1987) Conduction velocity variations minimize conduction time differences among retinal ganglion cells. *Science* **238**, 358-360.

Stockton, R.A. and Slaughter, M.M. (1989) B-wave of the electroretinogram: a reflection of ON bipolar activity. *J. Gen. Physiol.* **93**, 101-122.

Stryer, L. (1986) Cyclic GMP cascade of vision. *Ann. Rev. Neurosci.* **9**, 87-119.

Sutter, E.E. (1991) The fast m-transform: A fast computation of cross-correlations with binary m-sequences. *SIAM Journal of Computing* **20**, 686-694.

Sutter, E.E. (1992) A deterministic approach to nonlinear systems analysis. In: Pinker, R.B. (Ed.) *Nonlinear Vision: Determination of neural receptive fields, functions and networks*, pp. 171-220. Bahram Nabet: CRC Press]

Sutter, E.E. and Bearse, M.A. (1995) Extraction of a ganglion cell component from the corneal response. *Vision Science and its Applications, 1995 OSA Technical Digest Series* **1**, 310-313.

Sutter, E.E. and Bearse, M.A. (1999) The optic nerve head component of the human ERG. *Vision Res.* **39**, 419-436.

Sutter, E.E. and Vaegan (1990) Lateral interaction component and local luminance nonlinearities in the human pattern reversal ERG.

Vision Res. **30**, 659-671.

Thompson, D.A. and Drasdo, N. (1987) Computation of the luminance and pattern components of the bar pattern electroretinogram. *Doc. Ophthalmol.* **66**, 233-244.

Thornton, E. (1991) *Electrical Interference and Protection*, New York: Ellis Horwood.

Tian, N. and Slaughter, M.M. (1995) Correlation of dynamic response in the ON bipolar neurone and the b-wave of the electroretinogram. *Vision Res.* **35**, 1359-1364.

Tomita, T., Kaneko, A., Murakami, M. and Pautler, E.L. (1967) Spectral response curves of single cones in the carp. *Vision Res.* **7**, 519-531.

Tomita, T. (1970) Electrical activity of vertebrate photoreceptors. *Quarterly Review of Biophysics* **3**, 179-222.

Tomoda, H., Celesia, G.G., Bridgell, M.G. and Toleikis, S. (1991) The effects of age on steady-state pattern electroretinograms and visual evoked potiential. *Doc. Ophthalmol.* **77**, 201-211.

Toyoda, J., Nosaki, H. and Tomita, T. (1969) Light-induced resistance changes in single photoreceptors of *necturus* and *gekko*. *Vision Res.* **9**, 453-463.

Trick, G.L. (1986) PRRP abnormalities in glaucoma and ocular

hypertension. *Invest. Ophthalmol. Vis. Sci.* **27**, 1730-1736.

Trick, G.L., Trick, L.R. and Haywood, K.M. (1986) Altered pattern evoked retinal and cortical potentials associated with human senescence. *Cur. Eye. Res.* **5**, 717-724.

Trick, G.L. (1987) Pattern reversal retinal potential in ocular hypertensives at high and low risk of developing glaucoma. *Doc. Ophthalmol.* **65**, 79-85.

Trick, G.L. (1992) Pattern Electroretinogram: An electrophysiological technique applicable to primary open-angle glaucoma and ocular hypertension. *J. Glaucoma* **1**, 271-279.

Trick, G.L., Nesher, R., Cooper, D.G. and Shields, S.M. (1992) The human pattern ERG: Alteration of response properties with aging. *Optom. Vis. Sci.* **69**, 122-128.

Trick, L.R. (1987) Age-related alterations in retinal function. *Doc. Ophthalmol.* **65**, 35-43.

Vaegan, Graham, S.L., Goldberg, I., Buckland, L. and Hollows, F.C. (1995) Flash and pattern electroretinogram changes with optic atrophy and glaucoma. *Experimental Eye Research* **60**, 697-706.

Vaegan (1996) The spatial distribution of ERG losses across the posterior pole of glaucomatous eyes in multifocal recordings. *Australian and New Zealand Journal of Ophthalmology* **24**, 28-31.

Vaegan and Sanderson, G. (1997) Multifocal flash ERG kernels do not contain a spatially tuned local component or one generated at the disk. *Invest. Ophthal. Vis. Sci. , Supp* **38**, 4123(Abstract)

Vaegan and Sutter, E.E. (1990) Fundamental differences between the nonlinearities of pattern and focal electroretinograms. *Doc. Ophthalmol.* **76**, 13-25.

Victor, J.D., Shapley, R.M. and Knight, B.W. (1977) Nonlinear analysis of cat retinal ganglion cells in the frequency domain. *Proc. Natl. Acad. Sci.* **74**, 3068-3072.

Volterra (1938) *Theory of Functionals*, London: Blackie and Son.

Vrabec, F. (1965) Senile changes in the ganglion cells of the human retina. *B. J. Ophthalmol.* **49**, 561-572.

Wachtmeister, L. and Dowling, J.E. (1978) The oscillatory potentials of the mudpuppy retina. *Invest. Ophthalmol. Vis. Sci.* **17**, 1176-1188.

Wanger, P. and Persson, H.E. (1987) Pattern-reversal electroretinograms and high-pass resolution perimetry in suspected or early glaucoma. *Ophthalmol.* **94**, 1098-1103.

Watanabe, I., Iijima, H. and Tsukahara, S. (1989) The pattern electroretinogram in glaucoma: an evaluation by relative amplitude from the Bjerrum area. *B. J. Ophthalmol.* **73**, 131-135.

Weale, R.A. (1982) Senile ocular changes, cell death, and vision. In: Sekuler, R., Kline, D. and Dismukes, K. (Eds.) *Aging and human visual function*, pp. 161-171. New York: Alan R. Liss]

Weinstein, G.W., Arden, G.B., Hitchings, R.A., Ryan, S., Calthorpe, C.M. and Odom, J.V. (1988) The pattern electroretinogram (PERG) in ocular hypertension and glaucoma. *Arch Ophthalmol* **106**, 923-928.

Weleber, R.G. (1981) The effect of age on human cone and rod ganzfield electroretinograms. *Invest. Ophthalmol. Vis. Sci.* **30**, 392-399.

Williams, L.W. (1995) *Gray's Anatomy*, 38th edn. London: Churchill Livingstone.

Wright, C.E., Williams, D.E., Drasdo, N. and Harding, G.F.A. (1985) The influence of age on the electroretinogram and visual evoked potential. *Doc. Ophthalmol.* **59**, 365-384.

Xu, X. and Karwoski, C.J. (1994a) Current source density (CSD) analysis of retinal field potentials I. Methodological considerations and depth profiles. *J. Neurophysiol.* **72**, 84-95.

Xu, X. and Karwoski, C.J. (1994b) Current source density analysis of retinal field potentials II. Pharmacological analysis of the b-wave and M-wave. *J. Neurophysiol.* **72**, 96-105.

Yamashita, E. (1959) Some analyses of slow potentials of toad's

retina. *Tokohu J. exp. Med.* **70**, 221-233.

Yoshikami, S. and Hagins, W.A. (1970) Ionic basis of dark current and photocurrent of retinal rods. *Biophys. J.* **10**, 60a

Appendix: Patient's Information Sheet.

Multifocal ERG Trial

Explanation to the Patient

Background

A new electrical test of the eye has been invented which can produce a map of the activity of the back of the eye, and may be better and easier than the field test which you have already had.

Purpose of Study

We want to find out if this laboratory test will in fact work in hospital conditions, with real patients. To do this we need to produce these electrical maps and compare them with the ordinary maps of the visual field. Then we can decide if all the defects can be picked up by the new test.

Procedures

You have been approached because we feel that your condition is ideal for us to gain a better understanding of this new technique. If you agree to participate, you will be asked to attend a clinic at The Applied Vision Research Centre at City University. We will send you a letter with directions, this could be at any time that suits your convenience (we can pay travelling expenses).

The test is similar to other electrical test that have been in use for some time. We will record the electricity which is generated by the nerve cells at the back of one of your eyes. The stimulus is a very complicated honeycomb pattern which flickers on a TV screen. You have to watch this steadily for about 20 seconds at a time. This is repeated about 30 times, because only a small amount of electricity is produced. We place fine wires around the eye to record the electricity, this is not uncomfortable. We also need to put a standard eye drop into your eye, to make the iris expand. This will rapidly wear off, but for up to 3 hours you will notice things look brighter and slightly blurred with that eye. The test is carried out in a special booth made of wire mesh, which is effectively transparent, the purpose of this is to shield you (and the wires) from any other source of electricity in nearby rooms.

Consequences of the Procedures

After the eye drops have worn off, no adverse affects of the test are anticipated.

Benefits

We hope that a realistic assessment of the utility of this technique will be possible, allowing better management and earlier diagnosis of the condition from which you suffer, and of a range of others. However, no specific benefits for your case can be guaranteed.

Termination

You are free to terminate your involvement in the trial at any stage. It will not effect your treatment in any way.

Confidentiality

Normal standards of medical confidentiality will be maintained during this study. Standard Data Protection Procedures will be adhered to.

Voluntary Participation

If you do not wish to participate in this study, you will not be at a disadvantage and you will continue to receive normal clinical management. If you do wish to participate, your general practitioner will be informed that you have agreed to take part.

Contact Names and Telephone Numbers

This study is being led by Professor Geoffrey Arden, Applied Vision Research Centre, City University Department of Optometry and Visual Science, 321-311 Goswell Road, London EC1V 7DD. He may be contacted on 0171 477 8000 ext. 4345.